JSCSEN 88(2)113–221(2023)

ISSN 1820-7421(Online)

Journal of the Serbian Chemical Society

Electronic version

VOLUME 88

No 2

BELGRADE 2023

Available on line at

www.shd.org.rs/JSCS/

The full search of JSCS is available through

DOAJ DIRECTORY OF OPEN ACCESS JOURNALS

www.doaj.org

The **Journal of the Serbian Chemical Society** (formerly Glasnik Hemijskog društva Beograd), one volume (12 issues) per year, publishes articles from the fields of chemistry. The **Journal** is financially supported by the **Ministry of Education, Science and Technological Development of the Republic of Serbia.**

Articles published in the **Journal** are indexed in **Clarivate Analytics products: Science Citation Index-Expanded™** – accessed *via* **Web of Science®** and **Journal Citation Reports®**.

Impact Factor announced 2022: **1.100; 5-year Impact Factor**: **1.175**.

Articles appearing in the **Journal** are also abstracted by: **Scopus, Chemical Abstracts Plus (CAplus℠), Directory of Open Access Journals, Referativnii Zhurnal (VINITI), RSC Analytical Abstracts, EuroPub, Pro Quest** and **Asian Digital Library.**

Publisher:	**Serbian Chemical Society**, Karnegijeva 4/III, P. O. Box 36, 1120 Belgrade 35, Serbia tel./fax: +381–11–3370–467, E-mails: **Society** – shd@shd.org.rs; **Journal** – jscs@shd.org.rs Home Pages: **Society** – http://www.shd.org.rs/, **Journal** – http://www.shd.org.rs/JSCS/
Internet Service:	Contents, Abstracts and full papers (from Vol 64, No. 1, 1999) are available in the electronic form at the Web Site of the **Journal** (http://www.shd.org.rs/JSCS/).
Former Editors:	**Nikola A. Pušin** (1930–1947), **Aleksandar M. Leko** (1948–1954), **Panta S. Tutundžić** (1955–1961), **Miloš K. Mladenović** (1962–1964), **Đorđe M. Dimitrijević** (1965–1969), **Aleksandar R. Despić** (1969–1975), **Slobodan V. Ribnikar** (1975–1985), **Dragutin M. Dražić** (1986–2006).
Editor-in-Chief:	BRANISLAV Ž. **NIKOLIĆ**, Serbian Chemical Society (E-mail: jscs-ed@shd.org.rs)
Deputy Editor:	DUŠAN **SLADIĆ**, Faculty of Chemistry, University of Belgrade
Sub editors:	
Organic Chemistry	DEJAN **OPSENICA**, Institute of Chemistry, Technology and Metallurgy, University of Belgrade JÁNOS **CSANÁDI**, Faculty of Science, University of Novi Sad
Biochemistry and Biotechnology	OLGICA **NEDIĆ**, INEP – Institute for the Application of Nuclear Energy, University of Belgrade
Inorganic Chemistry	MILOŠ **ĐURAN**, Serbian Chemical Society
Theoretical Chemistry	IVAN **JURANIĆ**, Serbian Chemical Society
Physical Chemistry	LJILJANA **DAMJANOVIĆ-VASILIĆ**, Faculty of Physical Chemistry, University of Belgrade
Electrochemistry	SNEŽANA **GOJKOVIĆ**, Faculty of Technology and Metallurgy, University of Belgrade
Analytical Chemistry	SLAVICA **RAŽIĆ**, Faculty of Pharmacy, University of Belgrade
Polymers	BRANKO **DUNJIĆ**, Faculty of Technology and Metallurgy, University of Belgrade
Thermodynamics	MIRJANA **KIJEVČANIN**, Faculty of Technology and Metallurgy, University of Belgrade
Chemical Engineering	TATJANA **KALUĐEROVIĆ RADOIČIĆ**, Faculty of Technology and Metallurgy, University of Belgrade
Materials	RADA **PETROVIĆ**, Faculty of Technology and Metallurgy, University of Belgrade
Metallic Materials and Metallurgy	ANA **KOSTOV**, Mining and Metallurgy Institute Bor, University of Belgrade
Environmental and Geochemistry	VESNA **ANTIĆ**, Faculty of Agriculture, University of Belgrade
History of and Education in Chemistry	DRAGICA **TRIVIĆ**, Faculty of Chemistry, University of Belgrade
English Language Editors:	LYNNE **KATSIKAS**, Serbian Chemical Society VLATKA **VAJS**, Serbian Chemical Society JASMINA **NIKOLIĆ**, Faculty of Technology and Metallurgy, University of Belgrade
Technical Editors:	VLADIMIR **PANIĆ**, ALEKSANDAR **DEKANSKI**, VUK **FILIPOVIĆ**, Institute of Chemistry, Technology and Metallurgy, University of Belgrade
Journal Manager & Web Master:	ALEKSANDAR **DEKANSKI,** Institute of Chemistry, Technology and Metallurgy, University of Belgrade
Office:	VERA **ĆUŠIĆ**, Serbian Chemical Society

Editorial Board

From abroad: **R. Adžić**, Brookhaven National Laboratory (USA); **A. Casini**, University of Groningen (The Netherlands); **G. Cobb**, Baylor University (USA); **D. Douglas**, University of British Columbia (Canada); **G. Inzelt**, Etvos Lorand University (Hungary); **J. Kenny**, University of Perugia (Italy); **Ya. I. Korenman**, Voronezh Academy of Technology (Russian Federation); **M. D. Lechner**, University of Osnabrueck (Germany); **S. Macura**, Mayo Clinic (USA); **M. Spiteller**, INFU, Technical University Dortmund (Germany); **M. Stratakis**, University of Crete (Grecce); **M. Swart**, University de Girona (Cataluna, Spain); **G. Vunjak-Novaković**, Columbia University (USA); **P. Worsfold**, University of Plymouth (UK); **J. Zagal**, Universidad de Santiago de Chile (Chile).

From Serbia: **B. Abramović**, **V. Antić**, **V. Beškoski**, **J. Csanadi**, **Lj. Damjanović-Vasilić**, **A. Dekanski**, **V. Dondur**, **B. Dunjić**, **M. Đuran, S. Gojković**, **I. Gutman**, **B. Jovančićević**, **I. Juranić**, **T. Kaluđerović Radioičić**, **L. Katsikas**, **M. Kijevčanin**, **A. Kostov**, **V. Leovac**, **S. Milonjić**, **V.B. Mišković-Stanković**, **O. Nedić**, **B. Nikolić**, **J. Nikolić**, **D. Opsenica**, **V. Panić**, **M. Petkovska**, **R. Petrović**, **I. Popović**, **B. Radak**, **S. Ražić**, **D. Sladić**, **S. Sovilj**, **S. Šerbanović**, **B. Šolaja**, **Ž. Tešić**, **D. Trivić**, **V. Vajs**.

Subscription: The annual subscription rate is **150.00 €** including postage (surface mail) and handling. For Society members from abroad rate is **50.00 €**. For the proforma invoice with the instruction for bank payment contact the Society Office (E-mail: shd@shd.org.rs) or see JSCS Web Site: http://www.shd.org.rs/JSCS/, option Subscription.

Godišnja pretplata: Za članove SHD: **2.500,00 RSD**, za penzionere i studente: **1000,00 RSD**, a za ostale: **3.500,00 RSD**:za organizacije i ustanove: **16.000,00 RSD**. Uplate se vrše na tekući račun Društva: **205-13815-62**, poziv na broj **320**, sa naznakom "pretplata za JSCS".

Nota: Radovi čiji su svi autori članovi SHD prioritetno se publikuju.

Odlukom Odbora za hemiju Republičkog fonda za nauku Srbije, br. 66788/1 od 22.11.1990. godine, koja je kasnije potvrđena odlukom Saveta Fonda, časopis je uvršten u kategoriju međunarodnih časopisa (**M-23**). Takođe, aktom Ministarstva za nauku i tehnologiju Republike Srbije, 413-00-247/2000-01 od 15.06.2000. godine, ovaj časopis je proglašen za publikaciju od posebnog interesa za nauku. **Impact Factor** časopisa objavljen 2022. godini iznosi **1,100**, a petogodišnji **Impact Factor 1,175**.

INSTRUCTIONS FOR AUTHORS (2021)

GENERAL

The *Journal of the Serbian Chemical Society* (the *Journal* in further text) is an international journal publishing papers from all fields of chemistry and related disciplines. Twelve issues are published annually. The Editorial Board expects the editors, reviewers, and authors to respect the well-known standard of professional ethics.

Types of Contributions

Original scientific papers	(up to 15 typewritten pages, including Figures, Tables and References) report original research which must not have been previously published.
Short communications	(up to 8 pages) report unpublished preliminary results of sufficient importance to merit rapid publication.
Notes	(up to 5 pages) report unpublished results of short, but complete, original research
Authors' reviews	(up to 40 pages) present an overview of the author's current research with comparison to data of other scientists working in the field
Reviews[a]	(up to 40 pages) present a concise and critical survey of a specific research area. Generally, these are prepared at the invitation of the Editor
Surveys	(about 25 pages) communicate a short review of a specific research area.
Book and Web site reviews	(1 - 2 pages)
Extended abstracts	(about 4 pages) of Lectures given at meetings of the Serbian Chemical Society Divisions
Letters to the Editor	report miscellaneous topics directed directly to the Editor

[a]Generally, Authors' reviews, Reviews and Surveys are prepared at the invitation of the Editor.

Research Data Policy

The Journal of the Serbian Chemical Society (JSCS) encourages that all supporting data sets and the results, which were used for discussion and making conclusions in the presented paper, should be available to readers. We strongly support authors to deposits their datasets in free available repositories. Read more at https://www.shd-pub.org.rs/index.php/JSCS/DataPolicy.

PrePrint Policy

Authors are allowed to store a preprint version of their manuscript on a recognized preprint server such as ChemRxiv, arXiv, or on any repository that provides a public identifier (e.g. DOI) prior to submission. Read more at https://www.shd-pub.org.rs/index.php/JSCS/Preprint.

ORCID

The journal requires from corresponding authors to submit ORCID upon registration, while co-authors are forwarded an ORCID attribution request upon manuscript submission, and upon potential acceptance of the paper for publication. Read more at https://www.shd-pub.org.rs/index.php/JSCS/Orcid.

Submission of manuscripts

Manuscripts should be submitted using the **OnLine Submission Form**, available on the JSCS Web Site (**http://www.shd-pub.org.rs/index.php/JSCS**). The manuscript must be uploaded as a Word.doc or .rtf file, with tables and figures (including the corresponding captions – above Tables and below Figures), placed within the text to follow the paragraph in which they were mentioned for the first time.

Please note that **Full Names (**First Name, Last Name), **Full Affiliation** and **Country** (from drop down menu) of **ALL OF AUTHORS** (written in accordance with English spelling rules - the first letter capitalized) must be entered in the manuscript Submission Form (Step 3). Manuscript Title, authors' names and affiliations, as well as the Abstract, **WILL APPEAR** in the article listing, as well as in **BIBLIOGRAPHIC DATABASES (WoS, SCOPUS...)**, in the form and in the order entered in the author details

Graphical abstract

Graphical abstract is a one-image file containing the main depiction of the authors work and/or conclusion and must be supplied along with the manuscript. It must enable readers to quickly gain the main message of the paper and to encourage browsing, help readers identify which papers are most relevant to their research interests. Authors must provide an image that clearly represents the research described in the paper. The most relevant figure from the work, which summarizes the content, can also be submitted. The image should be submitted as a separate file in **Online Submission Form - Step 2**.

Specifications: The graphical abstract should have a clear start and end, reading from top to bottom or left to right. Please omit unnecessary distractions as much as possible.

- **Image size:** minimum of 500×800 pixels (W×H) and a minimum resolution of 300 dpi. If a larger image is sent, then please use the same ratio: 16 wide × 9 high. Please note that your image will be scaled proportionally to fit in the available window in TOC; a 150x240 pixel rectangle. Please be sure that the quality of an image cannot be increased by changing the resolution from lower to higher, but only by rescanning or exporting the image with a higher resolution, which can be set in usual "settings" option.
- **Font:** Please use Calibri and Symbol font with a large enough font size, so it is readable even from the image of a smaller size (150 × 240 px) in TOC.
- **File type:** JPG and PNG only.

No additional text, outline or synopsis should be included. Please do not use white space or any heading within the image.

Cover Letter

Manuscripts must be accompanied by a cover letter (strictly uploaded in **Online Submission Step 2**) in which the type of the submitted manuscript and a warranty as given below are given. The Author(s) has(have) to warranty that the manuscript submitted to the *Journal* for review is original, has been written by the stated author(s) and has not been published elsewhere; is currently not being considered for publication by any other journal and will not be submitted for such a review while under review by the *Journal*; the manuscript contains no libellous or other unlawful statements and does not contain any materials that violate any personal or proprietary rights of any other person or entity. All manuscripts will be acknowledged on receipt (by e-mail).

Illustrations

Illustrations (Figs, schemes, photos…) in TIF or EPS format (JPG format is acceptable for colour and greyscale photos, only), must be additionally uploaded (Online Submission Step 2) as a separate file or one archived (.zip, .rar or .arj) file. Figures and/or Schemes should be prepared according to the **Artwork Instructions -** http://www.shd.org.rs/JSCS/jscs-pdf/Artwork_Instructions.pdf!

For any difficulties and questions related to **OnLine Submission Form -** https://www.shd-pub.org.rs/index.php/JSCS/submission/wizard, please refer to **User Guide -** https://openjournal-systems.com/ojs-3-user-guide/ , Chapter **Submitting an Article -** https://openjournalsystems.com/ojs-3-user-guide/submitting-an-article/. If difficulties still persist, please contact JSCS Editorial Office at **JSCS@shd.org.rs**

A manuscript not prepared according to these instructions will be returned for resubmission without being assigned a reference number.

Conflict-of-Interest Statement*: Public trust in the peer review process and the credibility of published articles depend in part on how well a conflict of interest is handled during writing, peer review, and editorial decision making. A conflict of interest exists when an author (or the author's institution), reviewer, or editor has financial or personal relationships that inappropriately influence (bias) his or her actions (such relationships are also known as dual commitments, competing interests, or competing loyalties). These relationships vary from those with negligible potential to those with great potential to influence judgment, and not all relationships represent true conflict of interest. The potential for a conflict of interest can exist whether or not an individual believes that the relationship affects his or her scientific judgment. Financial relationships (such as employment, consultancies, stock ownership, honoraria, paid expert testimony) are the most easily identifiable conflicts of interest and the most likely to undermine the credibility of the journal, the authors, and of science itself. However, conflicts can occur for other reasons, such as personal relationships, academic competition, and intellectual passion.

Informed Consent Statement*: Patients have a right to privacy that should not be infringed without informed consent. Identifying information, including patients' names, initials, or hospital numbers, should not be published in written descriptions, photographs, and pedigrees unless the information is essential for

*International Committee of Medical Journal Editors ("Uniform Requirements for Manuscripts Submitted to Biomedical Journals"), February 2006

scientific purposes and the patient (or parent or guardian) gives written informed consent for publication. Informed consent for this purpose requires that a patient who is identifiable be shown the manuscript to be published. Authors should identify Individuals who provide writing assistance and disclose the funding source for this assistance. Identifying details should be omitted if they are not essential. Complete anonymity is difficult to achieve, however, and informed consent should be obtained if there is any doubt. For example, masking the eye region in photographs of patients is inadequate protection of anonymity. If identifying characteristics are altered to protect anonymity, such as in genetic pedigrees, authors should provide assurance that alterations do not distort scientific meaning and editors should so note. The requirement for informed consent should be included in the journal's instructions for authors. When informed consent has been obtained it should be indicated in the published article.

Human and Animal Rights Statement* When reporting experiments on human subjects, authors should indicate whether the procedures followed were in accordance with the ethical standards of the responsible committee on human experimentation (institutional and national) and with the Helsinki Declaration of 1975, as revised in 2000 (5). If doubt exists whether the research was conducted in accordance with the Helsinki Declaration, the authors must explain the rationale for their approach, and demonstrate that the institutional review body explicitly approved the doubtful aspects of the study. When reporting experiments on animals, authors should be asked to indicate whether the institutional and national guide for the care and use of laboratory animals was followed.

PROCEDURE

All contributions will be peer reviewed and only those deemed worthy and suitable will be accepted for publication. The Editor has the final decision. To facilitate the reviewing process, authors are encouraged to suggest up to three persons competent to review their manuscript. Such suggestions will be taken into consideration but not always accepted. If authors would prefer a specific person not be a reviewer, this should be announced. The Cover Letter must be accompanied by these suggestions. Manuscripts requiring revision should be returned according to the requirement of the Editor, within 60 days upon reception of the reviewing comments by e-mail.

The *Journal* maintains its policy and takes the liberty of correcting the English as well as false content of manuscripts **provisionally accepted** for publication in the first stage of reviewing process. In this second stage of manuscript preparation by JSCS Editorial Office, the author(s) may be required to supply some **additional clarifications and corrections**. This procedure will be executed during copyediting actions, with a demand to author(s) to perform corrections of unclear parts before the manuscript would be published OnLine as **finally accepted manuscript (OLF Section of the JSCS website)**. Please note that the manuscript can receive the status of **final rejection** if the author's corrections would not be satisfactory.

When finally accepted manuscript is ready for printing, the corresponding author will receive a request for proof reading, which should be performed within 2 days. Failure to do so will be taken as the authors agree with any alteration which may have occurred during the preparation of the manuscript for printing.

Accepted manuscripts of active members of the Serbian Chemical Society (all authors) have publishing priority.

MANUSCRIPT PRESENTATION

Manuscripts should be typed in English (either standard British or American English, but consistent throughout) with 1.5 spacing (12 points Times New Roman; Greek letters in the character font Symbol) in A4 format leaving 2.5 cm for margins. For Regional specific, non-standard characters that may appear in the text, save documents with Embed fonts Word option: *Save as -> (Tools) -> Save Options… -> Embed fonts in the text.*

The authors are requested to seek the assistance of competent English language expert, if necessary, to ensure their English is of a reasonable standard. The Serbian Chemical Society can provide this service in advance of submission of the manuscript. If this service is required, please contact the office of the Society by e-mail (jscs-info@shd.org.rs).

Tables, figures and/or schemes must be embedded in the main text of the manuscript and should follow the paragraph in which they are mentioned for the first time. **Tables** must be prepared with the aid of the **WORD table function**, without vertical lines. The minimum size of the font in the tables should be **10 pt**. Table columns must not be formatted using multiple spaces. Table rows must not be formatted using any returns (enter key; ↵ key) and are **limited to 12 cm width**. Tables should not be incorporated as graphical objects. **Footnotes to Tables** should follow them and are to be indicated consequently (in a single line) in superscript letters and separated by semi-column.

Table caption must be placed above corresponding Table, while **Captions of the Illustrations** (Figs. Schemes...) must follow the corresponding item. **The captions, either for Tables or Illustrations**, should make the items comprehensible without reading of the main text (but clearly referenced in), must follow numerical order (Roman for Tables, Arabic for Illustrations), and should not be provided on separate sheets or as separate files.

High resolution Illustrations (named as Fig. 1, Fig. 2… and/or Scheme 1, Scheme 2…) in **TIF or EPS format** (JPG format is acceptable for photos, only) **must be additionally uploaded as a separate files or one archived (.zip, .rar) file.**

Illustrations should be prepared according to the ARTWORK INSTRUCTIONS - http://www.shd.org.rs/JSCS/jscs-pdf/Artwork_Instructions.pdf. **!**

All pages of the manuscript must be numbered continuously.

DESIGNATION OF PHYSICAL QUANTITIES AND UNITS

IUPAC recommendations for the naming of compounds should be followed. SI units, or other permissible units, should be employed. The designation of physical quantities must be in italic throughout the text (including figures, tables and equations), whereas the units and indexes (except for indexes having the meaning of physical quantities) are in upright letters. They should be in Times New Roman font. In graphs and tables, a slash should be used to separate the designation of a physical quantity from the unit (example: p / kPa, j / mA cm^{-2}, t / °C, T_0 / K, τ / h, ln (j / mA cm^{-2})…). Designations such as: p (kPa), t [min]…, are not acceptable. However, if the full name of a physical quantity is unavoidable, it should be given in upright letters and separated from the unit by a comma (example: Pressure, kPa; Temperature, K; Current density, mA cm^{-2}…). Please do not use the axes of graphs for additional explanations; these should be mentioned in the figure captions and/or the manuscript (example: "pressure at the inlet of the system, kPa" should be avoided). The axis name should follow the direction of the axis (the name of y-axis should be rotated by 90°). Top and right axes should be avoided in diagrams, unless they are absolutely necessary.

Latin words, as well as the names of species, should be in *italic*, as for example: *i.e.*, *e.g.*, *in vivo*, *ibid*, *Calendula officinalis* L., *etc*. The branching of organic compound should also be indicated in *italic*, for example, *n*-butanol, *tert*-butanol, *etc*.

Decimal numbers must have decimal points and not commas in the text (except in the Serbian abstract), tables and axis labels in graphical presentations of results. Thousands are separated, if at all, by a comma and not a point.

Mathematical and chemical equations should be given in separate lines and must be numbered, Arabic numbers, consecutively in parenthesis at the end of the line. All equations should be embedded in the text Complex equations (fractions, integrals, matrix…) should be prepared with the aid of the **Microsoft Equation 3.0** (or higher) or **MathType** (Do not use them to create simple equations and labels). **Using the Insert -> Equation option, integrated in MS Office 2010 and MS Office 2013, as well as insertion of equation objects within paragraph text IS NOT ALLOWED.**

ARTICLE STRUCTURE

- TITLE PAGE
- MAIN TEXT – including Tables and Illustrations with corresponding captions
- SUPPLEMENTARY MATERIAL (optional**)**

Title page

- **Title** in bold letters, should be clear and concise, preferably 12 words or less. The use of non-standard abbreviations, symbols and formulae is discouraged.
- AUTHORS' NAMES in capital letters with the full first name, initials of further names separated by a space and surname. Commas should separate the author's names except for the last two names when 'and' is to be used. In multi-affiliation manuscripts, the author's affiliation should be indicated by an Arabic number placed in superscript after the name and before the affiliation. Use * to denote the corresponding author(s).
- *Affiliations* should be written in italic. The e-mail address of the corresponding author should be given after the affiliation(s).

- *Abstract:* A one-paragraph abstract written of 150 – 200 words in an impersonal form indicating the aims of the work, the main results and conclusions should be given and clearly set off from the text. Domestic authors should also submit, on a separate page, an Abstract - Izvod, the author's name(s) and affiliation(s) in Serbian (Cyrillic letters). (Домаћи аутори морају доставити Извод (укључујући имена аутора и афилијацију) на српском језику, исписане ћирилицом, иза Захвалнице, а пре списка референци.) For authors outside Serbia, the Editorial Board will provide a Serbian translation of their English abstract.
- *Keywords:* Up to 6 keywords should be given. Do not use words appearing in the manuscript title
- RUNNING TITLE: A one line (maximum five words) short title in capital letters should be provided.

Main text – should have the form:

- **INTRODUCTION,**
- **EXPERIMENTAL (RESULTS AND DISCUSSION),**
- **RESULTS AND DISCUSSION (EXPERIMENTAL),**
- **CONCLUSIONS,**
- **NOMENCLATURE (optional) and**
- ***Acknowledgements*: If any.**
- REFERENCES (Citation of recent papers published in chemistry journals that highlight the significance of work to the general readership is encouraged.)

The sections should be arranged in a sequence generally accepted for publication in the respective fields. They subtitles should be in capital letters, centred and NOT numbered.

- The INTRODUCTION should include the aim of the research and a concise description of background information and related studies directly connected to the paper.
- The EXPERIMENTAL section should give the purity and source of all employed materials, as well as details of the instruments used. The employed methods should be described in sufficient detail to enable experienced persons to repeat them. Standard procedures should be referenced and only modifications described in detail. On no account should results be included in the experimental section.

Chemistry

Detailed information about instruments and general experimental techniques should be given in all necessary details. If special treatment for solvents or chemical purification were applied that must be emphasized.

Example: Melting points were determined on a Boetius PMHK or a Mel-Temp apparatus and were not corrected. Optical rotations were measured on a Rudolph Research Analytical automatic polarimeter, Autopol IV in dichloromethane (DCM) or methanol (MeOH) as solvent. IR spectra were recorded on a Perkin-Elmer spectrophotometer FT-IR 1725X. ^{1}H and ^{13}C NMR spectra were recorded on a Varian Gemini-200 spectrometer (at 200 and 50 MHz, respectively), and on a Bruker Ultrashield Advance III spectrometer (at 500 and 125 MHz, respectively) employing indicated solvents (*vide infra*) using TMS as the internal standard. Chemical shifts are expressed in ppm (δ / ppm) values and coupling constants in Hz (J / Hz). ESI-MS spectra were recorded on Agilent Technologies 6210 Time-Of-Flight LC-MS instrument in positive ion mode with CH_3CN/H_2O 1/1 with 0.2 % HCOOH as the carrying solvent solution. Samples were dissolved in CH_3CN or MeOH (HPLC grade purity). The selected values were as follows: capillary voltage = 4 kV, gas temperature = 350 °C, drying gas flow 12 L min^{-1}, nebulizer pressure = 310 kPa, fragmentator voltage = 70 V.The elemental analysis was performed on the Vario EL III- C,H,N,S/O Elemental Analyzer (Elementar Analysensysteme GmbH, Hanau-Germany). Thin-layer chromatography (TLC) was performed on precoated Merck silica gel 60 F254 and RP-18 F254 plates. Column chromatography was performed on Lobar LichroPrep Si 60 (40-63 μm), RP-18 (40-63 µm) columns coupled to a Waters RI 401 detector, and on Biotage SP1 system with UV detector and FLASH 12+, FLASH 25+ or FLASH 40+ columns pre packed with KP-SIL [40-63 µm, pore diameter 6 nm (60 Å)], KP-C18-HS (40-63 µm, pore diameter 9 nm (90 Å) or KP-NH [40-63 µm, pore diameter 10 nm (100 Å)] as adsorbent. Compounds were analyzed for purity (HPLC) using a Waters 1525 HPLC dual pump system equipped with an Alltech, Select degasser system, and dual λ 2487 UV-VIS detector. For data processing, Empower software was used (methods A and B). Methods C and D: Agylent Technologies 1260 Liquid Chromatograph equipped with Quat Pump (G1311B), Injector (G1329B) 1260 ALS, TCC 1260 (G1316A) and Detector 1260 DAD VL+ (G1315C). For data processing, LC OpenLab CDS ChemStation software was used. For details, see Supporting Information.

1. Synthesis experiments

Each paragraph describing a synthesis experiment should begin with the name of the product and any structure number assigned to the compound in the Results and Discussions section. Thereafter, the compound should be identified by its structure number. Use of standard abbreviations or unambiguous molecular formulas for reagents and solvents, and of structure numbers rather than chemical names to identify starting materials and intermediates, is encouraged.

When a new or improved synthetic method is described, the yields reported in key experimental examples, and yields used for comparison with existing methods, should represent amounts of isolated and purified products, rather than chromategraphically or spectroscopically determined yields. Reactant quantities should be reported in weight and molar units and for product yields should be reported in weight units; percentage yields should only be reported for materials of demonstrated purity. When chromatography is used for product purification, both the support and solvent should be identified.

2. Microwave experiments

Reports of syntheses conducted in microwave reactors must clearly indicate whether sealed or open reaction vessels were used and must document the manufacturer and model of the reactor, the method of monitoring the reaction mixture temperature, and the temperature-time profile. Reporting a wattage rating or power setting is not an acceptable alternative to providing temperature data. Manuscripts describing work done with domestic (kitchen) microwave ovens will not be accepted except for studies where the unit is used for heating reaction mixtures at atmospheric pressure.

3. Compound characterization

The Journal upholds a high standard for compound characterization to ensure that substances being added to the chemical literature have been correctly identified and can be synthesized in known yield and purity by the reported preparation and isolation methods. For **all new** compounds, evidence adequate to establish both **identity** and **degree of purity** (homogeneity) must be provided.

Identity *- Melting point.* All homogeneous solid products (*e.g.* not mixtures of isomers) should be characterized by melting or decomposition points. The colors and morphologies of the products should also be noted.

Specific rotations. Specific rotations based on the equation $[\alpha]^{t};D = (100\ \alpha) / (l\ c)$ should be reported as unitless numbers as in the following example: $[\alpha]^{20}$; D = -25.4 (c 1.93, $CHCl_3$), where c / g mL^{-1} is concentration and l / dm is path length. The units of the specific rotation, (deg mL) / (g dm), are implicit and are not included with the reported value.

Spectra/*Spectral Data.* Important IR adsorptions should be given.

For all new diamagnetic substances, NMR data should be reported (^1H, ^{13}C, and relevant heteronuclei). ^1H NMR chemical shifts should be given with two digits after the decimal point. Include the number of protons represented by the signal, signal multiplicity, and coupling constants as needed (*J* italicized, reported with up to one digit after the decimal). The number of bonds through which the coupling is operative, ^{x}J, may be specified by the author if known with a high degree of certainty. ^{13}C NMR signal shifts should be rounded to the nearest 0.01 ppm unless greater precision is needed to distinguish closely spaced signals. Field strength should be noted for each spectrum, not as a comment in the general experimental section. Hydrogen multiplicity (C, CH, CH_2, CH_3) information obtained from routine DEPT spectra should be included. If detailed signal assignments are made, the type of NOESY or COSY methods used to establish atom connectivity and spatial relationships should be identified in the Supporting Information. Copies of spectra should also be included where structure assignments of complex molecules depend heavily on NMR interpretation. Numbering system used for assignments of signals should be given in the Supporting Information with corresponding general structural formula of named derivative.

HPLC/LCMS can be substituted for biochemistry papers where the main focus is not on compound synthesis.

HRMS/*elemental analysis.* To support the molecular formula assignment, HRMS data accurate within 5 ppm, or combustion elemental analysis [carbon and hydrogen (and nitrogen, if present)] data accurate within 0.5 %, should be reported for new compounds. HRMS data should be given in format as is usually given for combustion analysis: calculated mass for given formula following with observed mass: (+)ESI-HRMS *m*/*z*: [molecular formula + H]$^+$ calculated mass, observed mass. Example: (+)ESI-HRMS *m*/*z*: calculated for [$C_{13}H_8BrCl_2N$ + H^+] 327.92899, observed 327.92792.

NOTE: in certain cases, a crystal structure may be an acceptable substitute for HRMS/elemental analysis.

Biomacromolecules. The structures of biomacromolecules may be established by providing evidence about sequence and mass. Sequences may be inferred from the experimental order of amino acid, saccharide, or nucleotide coupling, from known sequences of templates in enzyme-mediated syntheses, or through standard sequencing techniques. Typically, a sequence will be accompanied by MS data that establish the molecular weight.

Example: Product was isolated upon column chromatography [dry flash (SiO_2, eluent EA, EA/MeOH gradient 95/5 → 9/1, EA/MeOH/NH_3 gradient 18/0.5/0.5 → 9/1/1, and flash chromatography (Biotage SP1, RP column, eluent MeOH/H_2O gradient 75/25 → 95/5, N-H column, eluent EA/Hex gradient 6/3 → EA). was obtained after flash column chromatography (Biotage SP NH column, eluent hexane/EA 4:6 → 2:6). Yield 968.4 mg (95 %). Colorless foam softens at 96-101 °C. $[\alpha]^{20}$; D = +0,163 (c =2.0×10^{-3} g/mL, CH_2Cl_2). IR (ATR): 3376w, 2949m, 2868w, 2802w, 1731s, 1611w, 1581s, 1528m, 1452m, 1374s, 1331w, 1246s, 1171m, 1063w, 1023m, 965w, 940w, 881w, 850w, 807w, cm^{-1}. ^{1}H NMR (500 MHz, $CDCl_3$, δ): 8.46 (*d*, 1H, J = 5.4, H-2'), 7.89 (*s*, 1H, J = 2.0, H-8'), 7.71 (*d*, 1H, J = 8.9, H-5'), 7.30 (*dd*, 1H, J_1 = 8.8, J_2 = 2.1, H-6'), 6.33 (*d*, 1H, J = 5.4, H-3'), 6.07 (*s*, HN-Boc, exchangeable with D_2O), 5.06 (*s*, 1H, H-12), 4.92-4.88 (*m*, 1H, H-7), 4.42 (*bs*, H-3), 3.45 (*s*,CH_3-N), 3.33 (*bs*, H-9'), 3.05-2.95 (*m*, 2H, H-11'), 2.70-2.43 (*m*, 2H, H-24) and HN, exchangeable with D_2O), 2.07 (*s*, CH_3COO), 2.04 (*s*, CH_3COO), 1.42 (*s*, 9H, $(CH_3)_3$C-N(Boc)), 0.88 (*s*, 3H, CH_3-10), 0.79 (*d*, 3H,J = 6.6, CH_3-20), 0.68 (*s*, 3H, CH_3-13). ^{13}C NMR (125 MHz, $CDCl_3$, δ): 170.34, 170.27, 151.80, 149.92, 148.87, 134.77, 128.36, 125.11, 121.43, 117.29, 99.98, 75.41, 70.82, 50.43, 49.66, 47.60, 47.33, 44.97, 43.30, 41.83, 41.48, 37.65, 36.35, 35.44, 34.89, 34.19, 33.23, 31.24, 28.79, 28.35, 27.25, 26.45, 25.45, 22.74, 22.63, 21.57, 21.31, 17.85, 12.15. (+)ESI-HRMS (*m*/*z*): calculated for $[C_{45}H_{67}ClN_4O_6 + H]^+$ 795.48219, observed 795.48185. Combustion analysis for $C_{45}H_{67}ClN_4O_6$: Calculated. C 67.94, H 8.49, N 7.04; found C 67.72, H 8.63, N 6.75. HPLC purity: method A: RT 1.994, area 99.12 %; method C: RT 9.936, area 98.20 %.

Purity - Evidence for documenting compound purity should include one or more of the following:

a) Well-resolved high field 1D ^{1}H NMR spectrum showing at most only trace peaks not attributable to the assigned structure and a standard 1D proton-decoupled ^{13}C NMR spectrum. Copies of the spectra should be included as figures in the Supporting Information.
b) Quantitative gas chromatographic analytical data for distilled or vacuum-transferred samples, or quantitative HPLC analytical data for materials isolated by column chromatography or separation from a solid support. HPLC analyses should be performed in two diverse systems. The stationary phase, solvents (HPLC), detector type, and percentage of total chromatogram integration should be reported; a copy of the chromatograms may be included as a figure in the Supporting Information.
c) Electrophoretic analytical data obtained under conditions that permit observing impurities present at the 5 % level.

HRMS data may be used to support a molecular formula assignment **but cannot be used as a criterion of purity**.

4. Biological Data

Quantitative biological data are required for all tested compounds. Biological test methods must be referenced or described in sufficient detail to permit the experiments to be repeated by others. Detailed descriptions of biological methods should be placed in the experimental section. Standard compounds or established drugs should be tested in the same system for comparison. Data may be presented as numerical expressions or in graphical form; biological data for extensive series of compounds should be presented in tabular form. Tables consisting primarily of negative data will not usually be accepted; however, for purposes of documentation they may be submitted as supporting information. Active compounds obtained from combinatorial syntheses should be resynthesized and retested to verify that the biology conforms to the initial observation.

Statistical limits (statistical significance) for the biological data are usually required. If statistical limits cannot be provided, the number of determinations and some indication of the variability and reliability of the results should be given. References to statistical methods of calculation should be included. Doses and concentrations should be expressed as molar quantities (*e.g.*, mol/kg, μmol/kg, M, mM). The routes of administration of test compounds and vehicles used should be indicated, and any salt forms used (hydrochlorides, sulfates, *etc.*) should be noted. The physical state of the compound dosed (crystalline, amorphous; solution, suspension) and the formulation for dosing (micronized, jet-milled, nanoparticles) should be indicated. For those compounds found to be inactive, the highest concentration (*in vitro*) or dose level (*in vivo*) tested should be indicated.

- The RESULTS AND DISCUSSION should include concisely presented results and there significance discussed and compared to relevant literature data. The results and discussion may be combined or kept separate.
- The inclusion of a CONCLUSION section, which briefly summarizes the principal conclusions, is recommended.
- NOMENCLATURE is optional but, if the authors wish, a list of employed symbols may be included.
- REFERENCES should be numbered sequentially as they appear in the text. Please note that any reference numbers appearing in the Illustrations and/or Tables and corresponding captions must follow the numbering sequence of the paragraph in which they appear for the first time. When cited, the reference number should be superscripted in Font 12, following any punctuation mark. In the reference list, they should be in normal position followed by a full stop. Reference entry must not be formatted using Carriage returns (enter key; ↵ key) or multiple space key. The formatting of references to published work should follow the *Journal*'s style as follows:

Journals[a]:	A. B. Surname1, C. D. Surname2, *J. Serb. Chem. Soc.* **Vol** (Year) first page Number (https://doi.org/doi)[b]
Books:	A. B. Surname1, C. D. Surname2, *Name of Book*, Publisher, City, Year, pp. 100-101 (https://doi.org/doi)[b]
Compilations:	A. B. Surname1, C. D. Surname2, in *Name of Compilation*, A. Editor1, C. Editor2, Ed(s)., Publisher, City, Year, p. 100 (https://doi.org/doi)[b]
Proceedings:	A. B. Surname1, C. D. Surname2, in *Proceedings of Name of the Conference or Symposium*, (Year), Place of the Conference, Country, *Title of the Proceeding*, Publisher, City, Year, p. or Abstract No. 100
Patents:	A. B. Inventor1, C. D. Inventor2, (Holder), Country Code and patent number (registration year)
Chemical Abstracts:	A. B. Surname1, C. D. Surname2, *Chem. Abstr*. CA 234 567a; For non-readily available literature, the Chemical Abstracts reference should be given in square brackets: [C.A. 139/2003 357348t] after the reference
Standards:	EN ISO 250: *Name of the Standard* (Year)
Websites:	Title of the website, URL in full (date accessed)

[a] When citing Journals, the International Library Journal abbreviation is required. Please consult, *e.g.*, https://images.webofknowledge.com/WOK46/help/WOS/A_abrvjt.html

[b] doi should be replaced by doi number of the Article, for example: http://dx.doi.org/10.2298/JSC161212085B (as active link). If doi do not exist, provide the link to the online version of the publication.

Only the last entry in the reference list should end with a full stop.

The names of all authors should be given in the list of references; the abbreviation *et al.* may only be used in the text. The original journal title is to be retained in the case of publications published in any language other than English (please denote the language in parenthesis after the reference). Titles of publications in non-Latin alphabets should be transliterated. Russian references are to be transliterated using the following transcriptions:

ж→zh, х→kh, ц→ts, ч→ch, ш→sh, щ→shch, ы→y, ю→yu, я→ya, э→e, й→i, ь→'.

Supplementary material

Authors are encouraged to presentthe information and results non-essential to the understanding of their paper as SUPPLEMENTARY MATERIAL (can be uploaded inStep 4 of Online Submission). This material may include as a rule, but is not limited to, the presentation of analytical and spectral data demonstrating the identity and purity of synthesized compounds, tables containing raw data on which calculations were based, series of figures where one example would remain in the main text, etc. The Editorial Board retain the right to assign such information and results to the Supplementary material when deemed fit. Supplementary material does not appear in printed form but can be downloaded from the web site of the JSCS.

Mathematical and chemical equations should be given in separate lines and must be numbered, Arabic numbers, consecutively in parenthesis at the end of the line. All equations should be embedded in the text Complex equations (fractions, integrals, matrix…) should be prepared with the aid of the

Microsoft Equation 3.0 (or higher) or MathType (Do not use them to create simple equations and labels). Using the Insert -> Equation option, integrated in MS Office 2010 and MS Office 2013, as well as insertion of equation objects within paragraph text IS NOT ALLOWED.

Deposition of crystallographic data

Prior to submission, the crystallographic data included in a manuscript presenting such data should be deposited at the appropriate database. Crystallographic data associated with organic and metal-organic structures should be deposited at the Cambridge Crystallographic Data Centre (CCDC) by e-mail to **deposit@ccdc.cam.ac.uk**

Crystallographic data associated with inorganic structures should be deposited with the Fachinformationszentrum Karlsruhe (FIZ) by e-mail to **crysdata@fiz-karlsruhe.de**. A deposition number will then be provided, which should be added to the reference section of the manuscript.

For detailed instructions please visit the JSCS website:
https://www.shd-pub.org.rs/index.php/JSCS/Instructions

ARTWORK INSTRUCTIONS

JSCS accepts only **TIFF** or **EPS** formats, as well as **JPEG** format (only for colour and greyscale photographs) for electronic artwork and graphic files. **MS files** (Word, PowerPoint, Excel, Visio) **NOT acceptable**. Generally, scanned instrument data sheets should be avoided. Authors are responsible for the quality of their submitted artwork. Every single Figure or Scheme, as well as any part of the Figure (A, B, C…) should be prepared according to following instructions (every part of the figure, A, B, C…, must be submitted as an independent single graphic file):

TIFF

Virtually all common artwork and graphic creation software is capable of saving files in TIFF format. This 'option' can normally be found under 'the 'Save As...' or 'Export...' commands in the 'File' menu.

TIFF (Tagged Image File Format) is the recommended file format for bitmap, greyscale and colour images.

- Colour images should be in the RGB mode
- When supplying TIFF files, please ensure that the files are supplied at the correct resolution:
    1. Line artwork: minimum of 1000 dpi
    2. RGB image: minimum of 300 dpi
    3. Greyscale image: minimum of 300 dpi
    4. Combination artwork (line/greyscale/RGB): minimum of 500 dpi
- Images should be tightly cropped, without frame and any caption.
- If applicable please re-label artwork with a font supported by JSCS (Arial, Helvetica, Times, Symbol) and ensure it is of an appropriate font size.
- Save an image in TIFF format with LZW compression applied.
- It is recommended to remove Alpha channels before submitting TIFF files.
- It is recommended to flatten layers before submitting TIFF files.

Please be sure that quality of an image cannot be increased by changing the resolution from lower to higher, but only by rescanning or exporting the image with higher resolution, which can be set in usual "settings" facilities.

EPS

Virtually all common artwork creation software, such as Canvas, ChemDraw, CorelDraw, SigmaPlot, Origin Lab…, are capable of saving files in EPS format. This 'option' can normally be found under the 'Save As...' or 'Export...' commands in the 'File' menu.

For vector graphics, EPS (Encapsulated PostScript) files are the preferred format as long as they are provided in accordance with the following conditions:

- when they contain bitmap images, the bitmaps should be of good resolution (see instructions for TIFF files)
- when colour is involved, it should be encoded as RGB
- an 8-bit preview/header at a resolution of 72 dpi should always be included
- embed fonts should always included and only the following fonts should be used in artwork: Arial, Helvetica, Times, Symbol
- the vertical space between the parts of an illustration should be limited to the bare necessity for visual clarity
- no data should be present outside the actual illustration area
- line weights should range from 0.35 pt to 1.5 pt
- when using layers, they should be reduced to one layer before saving the image (Flatten Artwork)

JPEG

Virtually all common artwork and graphic creation software is capable of saving files in JPEG format. This 'option' can normally be found under 'the 'Save As...' or 'Export...' commands in the 'File' menu.

JPEG (Joint Photographic Experts Group) is the acceptable file format **only for colour and greyscale photographs**. JPEG can be created with respect to photo quality (low, medium, high; from 1 to 10), ensuring file sizes are kept to a minimum to aid easy file transfer. Images should have a minimum resolution of 300 dpi. Image width: minimum 3.0 cm; maximum 12.0 cm.

Please be sure that quality of an image cannot be increased by changing the resolution from lower to higher, but only by rescanning or exporting the image with higher resolution, which can be set in usual "settings" facilities.

SIZING OF ARTWORK

- JSCS aspires to have a uniform look for all artwork contained in a single article. Hence, it is important to be aware of the style of the journal.
- Figures should be submitted in black and white or, if required, colour (charged). If coloured figures or photographs are required, this must be stated in the cover letter and arrangements made for payment through the office of the Serbian Chemical Society.
- As a general rule, the lettering on an artwork should have a finished, printed size of 11 pt for normal text and no smaller than 7 pt for subscript and superscript characters. Smaller lettering will yield a text that is barely legible. This is a rule-of-thumb rather than a strict rule. There are instances where other factors in the artwork, (for example, tints and shadings) dictate a finished size of perhaps 10 pt. Lines should be of at least 1 pt thickness.
- When deciding on the size of a line art graphic, in addition to the lettering, there are several other factors to address. These all have a bearing on the reproducibility/readability of the final artwork. Tints and shadings have to be printable at the finished size. All relevant detail in the illustration, the graph symbols (squares, triangles, circles, *etc*.) and a key to the diagram (to explain the explanation of the graph symbols used) must be discernible.
- The sizing of halftones (photographs, micrographs,...) normally causes more problems than line art. It is sometimes difficult to know what an author is trying to emphasize on a photograph, so you can help us by identifying the important parts of the image, perhaps by highlighting the relevant areas on a photocopy. The best advice that can be given to graphics suppliers is not to over-reduce halftones. Attention should also be paid to magnification factors or scale bars on the artwork and they should be compared with the details inside. If a set of artwork contains more than one halftone, again please ensure that there is consistency in size between similar diagrams.

General sizing of illustrations which can be used for the Journal of the Serbian Chemical Society:

- Minimum fig. size: 30 mm width
- Small fig. size - 60 mm width
- Large fig. size - 90 mm width
- Maximum fig. size - 120 mm width

Pixel requirements (width) per print size and resolution for bitmap images:

	Image width	A	B	C
Minimal size	30 mm	**354**	**591**	**1181**
Small size	60 mm	**709**	**1181**	**2362**
Large size	90 mm	**1063**	**1772**	**3543**
Maximal size	120 mm	**1417**	**2362**	**4724**

A: 300 dpi > RGB or Greyscale image
B: 500 dpi > Combination artwork (line/greyscale/RGB)
C: 1000 dpi> Line artwork

The designation of physical quantities and graphs formatting

The designation of physical quantities on figures must be in italic, whereas the units are in upright letters. They should be in Times New Roman font. In graphs a slash should be used to separate the designation of a physical quantity from the unit (example: p / kPa, t °C, T_0 / K, τ / h, ln (j / mA cm^{-2})…). Designations such as: p (kPa), t [min]…, are not acceptable. However, if the full name of a physical quantity is unavoiable, it should be given in upright letters and separated from the unit by a comma (example: Pressure, kPa, Temperature, K…). Please do not use the axes of graphs for additional explanations; these should be mentioned in the figure captions and/or the manuscript (example: "pressure at the inlet of the system, kPa" should be avoided). The axis name should follow the direction of the axis (the name of y-axis should be rotated by 90°). Top and right axes should be avoided in diagrams, unless they are absolutely necessary. Decimal numbers must have decimal points and not commas in the axis labels in graphical presentations of results. Thousands are separated, if at all, by a comma and not a point.

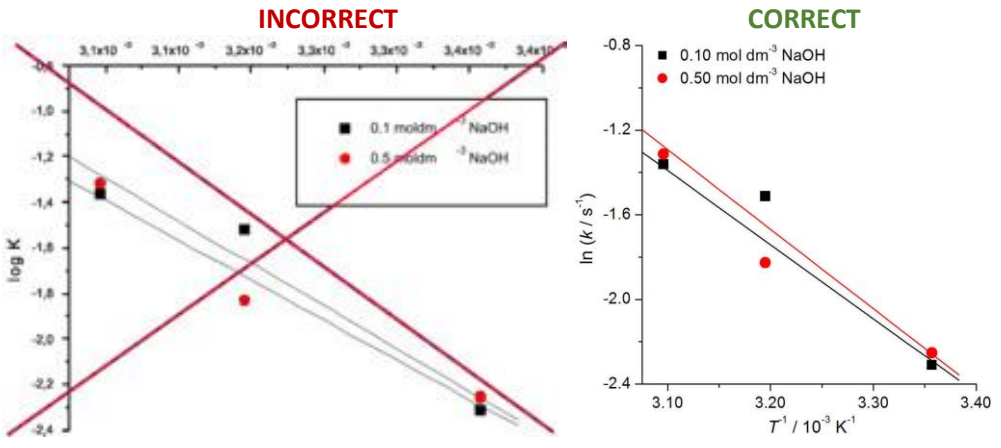

Journal of the Serbian Chemical Society
JSCS-info@shd.org.rs • www.shd.org.rs/JSCS

J. Serb. Chem. Soc. Vol. 88, No. 2 (2023)

CONTENTS*

Published by the Serbian Chemical Society
Karnegijeva 4/III, P.O. Box 36, 11120 Belgrade, Serbia
Printed by the Faculty of Technology and Metallurgy
Karnegijeva 4, P.O. Box 35-03, 11120 Belgrade, Serbia

* For colored figures in this issue please see electronic version at the Journal Home Page: http://www.shd.org.rs/JSCS/

Journal of the Serbian Chemical Society
JSCS@tmf.bg.ac.rs • www.shd.org.rs/JSCS
J. Serb. Chem. Soc. *88* (2) 113–121 (2023)
JSCS–5614
Original scientific paper
Published 18 November 2022

Divergent synthesis and antitumour activity of novel conformationally constrained (–)-muricatacin analogues

SLAĐANA M. STANISAVLJEVIĆ[1], BOJANA M. SREĆO ZELENOVIĆ[1]*#, MIRJANA POPSAVIN[1#], MARKO V. RODIĆ[1], VELIMIR POPSAVIN[1,2#] and VESNA V. KOJIĆ[3]

[1]University of Novi Sad, Faculty of Sciences, Department of Chemistry, Biochemistry and Environmental Protection, Trg Dositeja Obradovića 3, 21000 Novi Sad, Serbia, [2]Serbian Academy of Sciences and Arts, Kneza Mihaila 35, 11000 Belgrade, Serbia and [3]University of Novi Sad, Faculty of Medicine, Oncology Institute of Vojvodina, Put dr Goldmana 4, 21204 Sremska Kamenica, Serbia

(Received 13 June, revised 5 August, accepted 18 August 2022)

Abstract: Four novel conformationally restricted (–)-muricatacin analogues, bearing a methoxy group at the C-5 position and with an alkoxymethyl group as the C-7 side chain, have been synthesised and their *in vitro* antiproliferative activity was evaluated against a panel of seven human tumour cell lines, as well as a single normal cell line. All analogues (**9**–**12**) showed diverse antiproliferative effects against all tested human malignant cell lines, but were devoid of any significant cytotoxicity towards the normal foetal lung fibroblasts (MRC-5). A structure–activity relationship study reveals that the introduction of tetrahydrofuran ring, the replacement of C-8 methylene group in the side chain of muricatacin analogues with the O-8 ether functionality, as well as the length of side chain may be beneficial for the antiproliferative effects of these lactones. All novel analogues were more potent than lead compound, (–)-muricatacin, against HL-60 cell line.

Keywords: D-glucose; antitumour agents; muricatacin mimics; furanolactones; cytotoxicity; SAR analysis.

INTRODUCTION

(–)-Muricatacin (**1**) is a naturally occurring acetogenin derivative, which has been isolated by McLaughlin and co-workers[1] from the seeds of *Annona muricata L.* together with its enantiomer (+)-muricatacin (*ent*-**1**). Both natural products (**1** and *ent*-**1**) have received a great deal of attention due to their similar biological profiles: remarkable antiproliferative activities towards various human tumour cells,[2,3] antimalarial as well as pesticidal activities.[1]

* Corresponding author. E-mail: bojana.sreco@dh.uns.ac.rs
# Serbian Chemical Society member.
https://doi.org/10.2298/JSC220613069S

Many syntheses of **1** from various precursors have been reported.[4–16] Also, several muricatacin analogues have been synthesised[3,7,17–20] and some of them were evaluated for their antitumour activity.[7,19,20]

As a part of our ongoing program in the synthesis of oxygenated lactones as potential antitumour agents from abundant monosaccharides, the synthesis of four novel 8-oxa analogues of (–)-muricatacin (**9**–**12**, Fig. 1) with furano-furanone ring system and methoxy group at the C-5 position was achieved from D--glucose. These molecules represent conformationally constrained oxa-analogues of lactone **1**, with methoxy group at the C-5 position. Analogue **9** is a heteroannelated mimic of **1** with the restricted geometry of the C_4–C_6 segment, due to the presence of the tetrahydrofuran (THF) ring. The molecule **10** represents a one-carbon lower homologue of **9**, while the molecules **11** and **12** are two- and three-carbon lower homologues of lactone **9**.

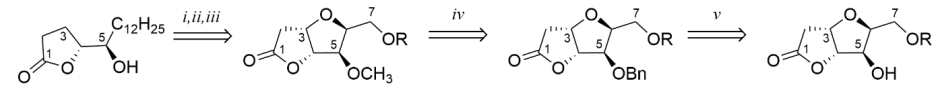

(–)-Muricatacin (**1**)

9 R = C_9H_{19}
10 R = C_8H_{17}
11 R = C_7H_{15}
12 R = C_6H_{13}

13 R = C_9H_{19}
14 R = C_8H_{17}
15 R = C_7H_{15}
16 R = C_6H_{13}

17 R = C_9H_{19}
18 R = C_8H_{17}
19 R = C_7H_{15}
20 R = C_6H_{13}

Fig. 1. Design of (–)-muricatacin analogues with a methoxy group (**9**–**12**), a benzyl group (**13**–**16**) and with a hydroxyl group at C-5 position (**17**–**20**): *i*) THF-ring closure; *ii*) 5-*O*-methylation; *iii*) exchange of C_8 methylene group with O_8 ether function; *iv*) substitution of methyl with benzyl group at C-5; *v*) debenzylation at C-5.

Our recent results on the antiproliferative activity of analogues **17**–**20** showed that they exhibit moderate to submicromolar cytotoxicity.[21] That led us to prepare C-5 methoxy derivatives **9**–**12**, and to examine their cytotoxic activity, as well as the cytotoxicity of previously synthesised analogues **13**–**16**,[21] for a detailed structure–activity relationship (SAR) analysis.

EXPERIMENTAL

General procedures

Melting points were determined on Büchi 510, or on hot stage microscope Nagema PHMK 05 apparatus and were not corrected. Optical rotations were measured on Autopol IV (Rudolph Research) automatic polarimeter. IR spectra were recorded with a FTIR Nexus 670 (Thermo-Nicolet) spectrophotometer. NMR spectra were recorded on a Bruker AC 250 E or a Bruker Avance III 400 MHz instrument and chemical shifts are expressed in ppm downfield from tetramethylsilane. Low resolution mass spectra were recorded on Finnigan-MAT 8230 (CI) mass spectrometer. High-resolution mass spectra were taken on a Micromass LCT KA111 spectrometer or on LTQ OrbitrapXL (Thermo Fisher Scientific Inc.) mass spectrometer. TLC was performed on DC Alufolien Kieselgel 60 F254 (E. Merck). Flash column chromatography was performed using Kieselgel 60 (0.040–0.063, E. Merck). All organic ext-

racts were dried with anhydrous Na_2SO_4. Organic solutions were concentrated in a rotary evaporator under reduced pressure at a bath temperature below 35 °C.

Synthesis procedures

*Methyl (Z)- (**4**) and (E)-3-O-methyl-5,6-dideoxy-1,2-O-isopropylidene-α-D-xylo-hept-5--enofuranuronate (**5**)*. To a solution of compound **2** (1.923 g, 7.01 mmol), in dry EtOAc (193 mL), H_5IO_6 (2.008 g, 8.76 mmol) was added. The mixture was stirred at room temperature for 3 h, then filtered and evaporated to afford crude aldehyde **3**. To a stirred and cooled (0 °C) solution of **3** (1.530 g, 7.56 mmol) in dry MeOH (35 mL) MCMP (2.558 g, 7.56 mmol) was added and the mixture was stirred for 0.5 h at 0 °C and then for 2.5 h at room temperature. The reaction mixture was evaporated and the residue was purified by flash chromatography (3:2 light petroleum/Et_2O). The pure product **4** (1.240 g, 69 %) was first eluted, isolated as a colourless oil. Further elution gave compound **5** which was additionally purified (1:1 $^iPr_2O$/ /light petroleum) to give the pure *E*-olefin **5** (0.133 g, 7 %).

*Dimethylacetal 2,5-Anhydro-6-deoxy-3-O-methyl-L-ido-hepturono-4,7-lactone (**6**)*. A solution of **4** (0.245 g, 0.95 mmol) in dry MeOH (7 mL) which contains 2.5 % H_2SO_4, was refluxed for 2 h. The mixture was cooled to 35 °C and alkalized (pH 9) by adding solid $NaHCO_3$ (0.917 g, 10.92 mmol, 11.5 eq) in three portions every 5 min. After adding the entire amount of base, the suspension was stirred at 35 °C for 1 h, then filtered and evaporated. The residue was purified by flash column chromatography (3:2 cyclohexane/EtOAc) to give pure **6** (0.174 g, 79 %).

*3,6-Anhydro-2-deoxy-5-O-methyl-L-ido-heptono-1,4-lactone (**8**)*. Dimethylacetal **6** (0.769 g, 3.31 mmol) was dissolved in 9:1 TFA/H_2O (15.5 mL) and stirred at room temperature for 1 h. After completion of the reaction, the solution was evaporated by co-distillation with toluene. The crude aldehyde **7** was dissolved in dry MeOH (39 mL) and treated with a first portion of $NaBH_4$ (0.094 g, 2.49 mmol, 3 eq). After stirring the mixture at room temperature for 0.5 h, an additional amount of $NaBH_4$ (0.063 g, 1.67 mmol, 2 eq) was added. The mixture was stirred at room temperature for additional hour. The reaction mixture was neutralized with AcOH and evaporated. The residue was purified by flash chromatography (4:1 CH_2Cl_2/EtOAc) to give pure alcohol **8** (0.399 g, 64 %).

*General procedure for the synthesis of analogues **9**–**12***

To a solution of compound **8** (1 equiv.) in dry Et_2O (2 mL) Ag_2O (2.5 equiv.), AgOTf (0.3 eq) and the corresponding alkyl bromide RBr (2.5 equiv.) were added. The mixture was stirred under reflux for 16–27 h (Table I). After completion of the reaction, which was detected by thin layer chromatography (TLC), the mixture was purified by flash column chromatography (7:3 light petroleum/Et_2O).

The characterization data for all synthesised compounds (**4**–**6** and **8**–**12**) are given in the Supplementary material to this paper.

TABLE I. Preparation of final products **9**–**12**

Entry	R	Reaction time, h	Product	Yield, %
1	C_9H_{19}	22.5	9	72
2	C_8H_{17}	16	10	86
3	C_7H_{15}	23	11	80
4	C_6H_{13}	27	12	73

Cytotoxic activity

Test cells. The *in vitro* cytotoxicity of test compounds was evaluated against seven human malignant cell lines: myelogenous leukaemia (K562), promyelocytic leukaemia (HL-60), T cell leukaemia (Jurkat), Burkitt's lymphoma (Raji), ER^+ breast adenocarcinoma (MCF-7), ER^- breast adenocarcinoma (MDA-MB 231) and cervix carcinoma (HeLa). Cytotoxic activity against normal foetal lung fibroblasts (MRC-5) was also estimated.

MTT test. Cytotoxic activity was evaluated by using standard MTT assay,[22] after exposure of cells to the tested compounds for 72 h.

RESULTS AND DISCUSSION

Chemistry

The syntheses of (–)-muricatacin analogues **9**–**12** are presented in Scheme 1. Starting compound **2** was prepared from D-glucose in two synthetic steps as previously reported by us.[23] Methyl derivative **2** was treated with periodic acid in dry ethyl acetate and the crude aldehyde **3** was obtained. Compound **3** reacted with stabilized ylide, $Ph_3P{=}CHCO_2Me$, in anhydrous MeOH and gave the expected *Z*-olefin **4** (69 %) as the major product of the Wittig olefination. A minor amount of corresponding *E*-olefin **5** (7 %) was also obtained in this reaction.

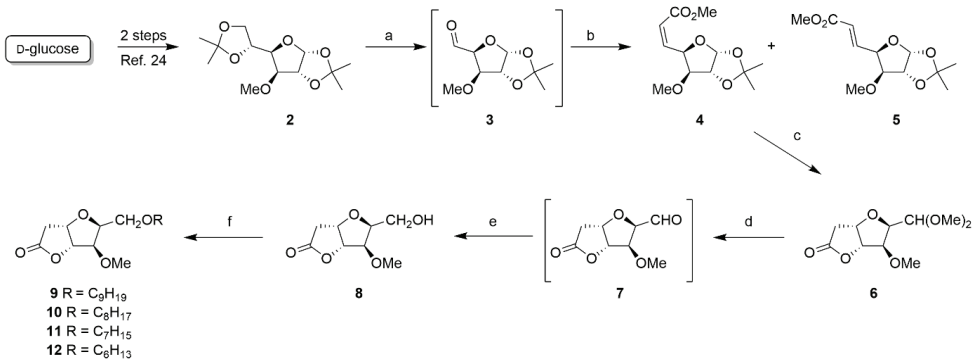

Scheme 1. Reagents and conditions: a) H_5IO_6, EtOAc, rt, 3 h; b) $Ph_3P{=}CHCO_2Me$, MeOH, 0 °C, 0.5 h, then rt 1.5 h, 69 % for **4**, 7 % for **5** (from **2**); c) 2.5 % H_2SO_4/MeOH, reflux, 2 h, $NaHCO_3$, rt, 1 h, 79 %; d) 9:1 TFA/H_2O, rt, 1 h; e) $NaBH_4$, MeOH, rt, 1.5 h, 64 % (from **6**); f) $C_9H_{19}Br$ for **9**, $C_8H_{17}Br$ for **10**, $C_7H_{15}Br$ for **11**, $C_6H_{13}Br$ for **12**, Ag_2O, AgOTf, CH_2Cl_2, reflux, 22.5 h (for **9**), 16 h (for **10**), 23 h (for **11**), 27 h (for **12**), 72 % (for **9**), 86 % (for **10**), 80 % (for **11**), 73 % (for **12**).

An acid-catalyzed methanolysis of **4**, in the presence of a catalytic amount of sulphuric acid gave furano-lactone **6** in 79 % yield. Hydrolytic removal of the dimethyl acetal protective group in **6** followed by a subsequent $NaBH_4$ reduction of the resulting aldehyde **7** gave the corresponding primary alcohol **8** in 64 % yield.

The stereochemistry of compound **8** was confirmed by single crystal X-ray diffraction analysis (for selected crystallographic and refinement details see the

Table S-II of the Supplementary material). The molecular structure of **8** is depicted in Fig. 2. All structural parameters of the molecule are within limits found in structures with similar fragments. The furano-lactone ring core is fused in *cis* manner and both five-membered rings are puckered, details of which are analysed by Cremer–Pople formalism.[24] The furanose ring (counting clockwise O3→C3→C4→C5→C6) is moderately puckered (q_2 = 36.05(17) pm), and its conformation is close to twisted at C5–C6 bond. The pseudorotational phase angle φ_2 = 130.5(3)° indicates its deformation towards the envelope form, as the ring formally traversed 25 % along ${}^6T_5 \rightarrow {}^6E$ pseudorotational pathway. Ring substituents C2 (δ = 29.58(13)°), O4 (δ = 16.44(11)°), and O5 (δ = 9.82(11)°) can be classified as axial, while C7 (δ = 65.96(13)°) is equatorial; δ is the angle subtended between Cremer–Pople ring mean plane normal and substituent bond vector.[25] The lactone ring (counting clockwise O4→C1→C2→C3→C4) is less puckered (q_2 = 14.0(2) pm) and its conformation is closer to the envelope form, with C3 as the flap. Its exact conformation is determined by φ_2 = 130.5(3)°, which means that the ring formally traversed 37 % along $E_4 \rightarrow {}^3T_4$ pseudorotational pathway.

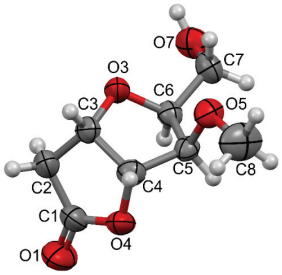

Fig. 2. Molecular structure of **8** determined by single crystal X-ray diffraction. Ellipsoids are drawn at 50 % probability level. Hydrogen atoms are shown as spheres of arbitrary radii.

The key intermediate, alcohol **8**, readily reacted with an excess of nonyl bromide in ether, in the presence of silver(I)-oxide and a catalytic amount of silver(I)-triflate, to give the expected 7-*O*-nonyl derivative **9** in 72 % yield. Under similar experimental conditions, the primary alcohol **8** reacted with different alkyl bromides (C_8–C_6) to afford the corresponding ether derivatives **10**––**12** in good yields (Scheme 1).

In vitro *antiproliferative activity*

After completion of the synthesis, analogues **9**–**12** were evaluated for their *in vitro* cytotoxicity against a panel of seven human tumour cell lines (human myelogenous leukaemia, K562, promyelocytic leukaemia, HL-60, T cell leukaemia, Jurkat, Burkitt's lymphoma, Raji, ER^+ breast adenocarcinoma, MCF-7, ER^- breast adenocarcinoma, MDA-MB 231, and cervix carcinoma, HeLa) and one normal cell line (foetal lung fibroblasts, MRC-5). Cell growth inhibition was evaluated after 72 h of cells treatment by using the MTT test.[22] (–)-Muricatacin (**1**)

and the commercial antitumour agent doxorubicin (DOX) were used as positive controls in this assay.

According to the recorded IC_{50} (Table II), all tumour cell lines were sensitive to all of the synthesised analogues (**9**–**12**). All four (–)-muricatacin mimics (**9**–**12**) demonstrated diverse antiproliferative effects toward MDA-MB 231 and Jurkat cells, in contrast to the lead **1**, which was completely inactive against these cell lines.

TABLE II. *In vitro* cytotoxicity (IC_{50}* / μM) of (–)-muricatacin (**1**), DOX and analogues **9**–**20** after 72 h

Compound	Cell line							
	K562	HL-60	Jurkat	Raji	MCF-7	MDA-MB 231	HeLa	MRC-5
1	0.04	25.85	>100	0.1	21.35	>100	0.17	>100
9	10.25	17.70	15.40	21.75	4.85	11.32	13.50	>100
10	18.12	13.68	7.36	35.84	1.11	28.33	9.12	>100
11	5.60	24.54	22.97	28.49	12.31	25.33	11.51	>100
12	7.69	21.18	25.34	27.03	18.33	15.81	15.22	>100
13	8.76	6.12	9.71	15.95	22.18	39.48	68.32	>100
14	9.09	13.92	5.47	16.85	18.77	28.26	18.02	>100
15	8.87	5.67	8.86	17.33	22.87	34.59	10.90	>100
16	5.65	7.42	5.25	11.82	25.31	8.50	33.79	>100
17[a]	5.66	4.75	6.97	7.25	>100	>100	6.39	>100
18[a]	0.74	0.68	19.78	4.25	0.34	28.70	3.41	>100
19[a]	1.02	1.10	11.53	5.98	2.38	9.76	0.56	>100
20[a]	0.70	4.91	8.87	1.11	12.34	15.62	3.54	>100
DOX	0.25	0.92	0.03	2.98	0.20	0.09	0.07	0.10

[a]Taken from reference[21]

Also, all novel analogues (**9**–**12**) were more potent than lead **1** against HL-60 cell line.

The most active compound against the MCF-7 cells was analogue **10**. This molecule exhibited strong cytotoxicity (IC_{50} = 1.11 μM) although its potency was 5.5 times lower than the activity of DOX (IC_{50} = 0.20 μM), but 19 times higher than that of the control compound **1** (IC_{50} = 21.35 μM). The analogue **9** also showed very good activity (IC_{50} = 4.85 μM) against this cell line, which was 4 times higher than that of lead **1**.

The conformationally restricted benzyl analogues of **1**, compounds **13**–**16**, exhibited cytotoxic activity against all seven malignant cell lines. Against the HL-60 cell line the previously synthesised analogues **13**–**16** showed from 1.85

* IC_{50} is the concentration of compound required to inhibit the cell growth by 50 % compared to an untreated control. Values are means of three independent experiments. Coefficients of variation were less than 10 %.

times (analogue **14**, IC_{50} = 13.92 μM) to 4.5 times (analogue **15**, IC_{50} = 4.85 μM) better cytotoxicity than natural product **1** (IC_{50} = 25.85 μM).

Against Jurkat cell line benzyl derivatives **13**–**16** exhibited strong antiproliferative effects (IC_{50} values in the range of 5.25−9.71 μM). However, the parent compound **1** was completely inactive against this cell line.

Against the MCF-7 cell line analogues **13**–**16** demonstrated similar cytotoxicity (IC_{50}: 18.77−25.31 μM) as parent compound **1** (IC_{50} = 21.35 μM).

All synthesised compounds showed diverse growth inhibitory effects against the tested malignant cells, but were devoid of any significant cytotoxicity toward the normal foetal lung fibroblasts (MRC-5), as well as the natural product **1**, in contrast to the commercial antitumour agent doxorubicin (DOX) that exhibited potent cytotoxic activity (IC_{50} = 0.10 μM) against this cell line.

SAR analysis

Our previous findings showed that the introduction of an oxygen atom in the side chain of (–)-muricatacin analogues increases the antiproliferative activity.[21] In this work we compared (–)-muricatacin analogues with this structural feature and the changes were based on the position C-5, so we compared three series of analogues: with OMe-group (**9**–**12**), with OBn-group (**13**–**16**) and with OH-group (**17**–**20**) at that position.

Analogues **9**–**12** demonstrated better cytotoxicity than the parent compound **1** against most of the cell lines tested in this study (Fig. S-17A of the Supplementary material). The corresponding benzyl derivatives (**13**–**16**) performed better antiproliferative effects in comparison to the analogues **9**–**12** (Fig. S-17B). Finally, the analogues with OH-group at C-5 position (**17**–**20**) were more potent than benzyl analogues (**13**–**16**, Fig. S-17C). So, our further work will be focused on the preparation of a larger number of similar analogues and then we will be able to make a reliable conclusion that the free OH-group at position C-5 increases the cytotoxic activity of conformationally restricted (–)-muricatacin analogues.

CONCLUSION

In conclusion, four novel (−)-muricatacin analogues (**9**–**12**) were designed and synthesised from D-glucose as a starting compound. The newly synthesised molecules, as well as the previously synthesised benzyl analogues (**13**–**16**), were evaluated for their *in vitro* cytotoxic activity against seven human malignant cell lines. A SAR study showed that the presence of additional tetrahydrofuran ring, O-8 ether functionality, as well as the length of alkyl chain, may improve the cytotoxicity of analogues toward the majority of cell lines under evaluation.

All synthesised compounds demonstrated diverse antiproliferative effects against the human malignant cell lines but were devoid of any significant cytotoxicity towards the normal foetal lung fibroblasts (MRC-5). Hence, we believe

that this approach may be of use in the search for novel, more potent and selective anticancer agents, derived from the natural product **1**.

SUPPLEMENTARY MATERIAL

Additional data and information are available electronically at the pages of journal website: https://www.shd-pub.org.rs/index.php/JSCS/article/view/11924, or from the corresponding author on request.

Acknowledgements. This work was supported by research grants from the Ministry of Education, Science and Technological Development of the Republic of Serbia (Contract No. 451-03-68/2020-14/200125). This work has also received funding from the Serbian Academy of Sciences and Arts under the strategic projects programme (Grant agreement No. 01-2019--F65), as well as from a research project from the same institution (Grant No. F-130).

И З В О Д

ДИВЕРГЕНТНА СИНТЕЗА И АНТИТУМОРСКА АКТИВНОСТ НОВИХ КОНФОРМАЦИОНО КРУТИХ АНАЛОГА (−)-МУРИКАТАЦИНА

СЛАЂАНА М. СТАНИСАВЉЕВИЋ[1], БОЈАНА М. СРЕЋО ЗЕЛЕНОВИЋ[1], МИРЈАНА ПОПСАВИН[1], МАРКО В. РОДИЋ[1], ВЕЛИМИР ПОПСАВИН[1,2] и ВЕСНА В. КОЈИЋ[3]

[1]Универзитет у Новом Саду, Природно–математички факултет, Департман за хемију, биохемију и заштиту животне средине, Трг Доситеја Обрадовића 3, 21000 Нови Сад, [2]Српска академија наука и уметности, Кнеза Михаила 35, 11000 Београд и [3]Универзитет у Новом Саду, Медицински факултет, Онколошки институт Војводине, Пут др Голдмана 4, 21204 Сремска Каменица

Синтетизована су четири нова конформационо крута аналога (−)-мурикатацина са метокси-групом у положају C-5 и са алкоксиметил-групом у бочном низу и испитана је њихова *in vitro* антипролиферативна активност према седам хуманих туморских и једној здравој ћелијској линији. Сви аналози (**9–12**) су показали различите антипролиферативне ефекте према свим испитиваним малигним ћелијским линијама, а изостала је цитотоксична активност према ћелијској линији нормалних феталних фибробласта плућа (MRC-5). SAR анализа показује да увођење тетрахидрофуранског прстена, замена C-8 метиленске групе са етарском функцијом у бочном низу, као и дужина бочног ланца, могу бити од значаја за цитотоксичне ефекте ових лактона. Сви новодобијени аналози су били потентнији од водећег једињења (−)-мурикатацина према HL-60 ћелијској линији..

(Примљено 13. јуна, ревидирано 5. августа, прихваћено 18. августа 2022)

REFERENCES

1. M. J. Rieser, J. F. Kozlowski, K. V. Wood, J. L. McLaughlin, *Tetrahedron Lett.* **32** (1991) 1137 (https://doi.org/10.1016/S0040-4039(00)92027-6)
2. C.-C. Liaw, F.-R. Chang, S.-L. Chen, C.-C. Wu, K.-H. Lee, Y. C. Wu, *Bioorg. Med. Chem.* **13** (2005) 4767 (https://doi.org/10.1016/j.bmc.2005.05.008)
3. A. Cavé, C. Chaboche, B. Figadère, J. C. Harmange, A. Laurens, J. F. Peyrat, M. Pichon, M. Szlosek, J. Cotte-Lafitte, A. M. Quéro, *Eur. J. Med. Chem.* **32** (1997) 617 (https://doi.org/10.1016/S0223-5234(97)83287-4)
4. M. Chandrasekhar, K. L. Chandra, V. K. Singh, *ARKIVOC* **VII** (2002) 34 (https://doi.org/10.3998/ark.5550190.0003.705)

5. K. J. Quinn, A. K. Isaacs, R. A. Arvary, *Org. Lett.* **6** (2004) 4143 (https://doi.org/10.1021/ol040047f)
6. B. Dhotare, A. Chattopadhyay, *Tetrahedron Lett.* **46** (2005) 3103 (https://doi.org/10.1016/j.tetlet.2005.03.002)
7. V. Popsavin, B. Srećo, G. Benedeković, M. Popsavin, J. Francuz, V. Kojić, G. Bogdanović, *Bioorg. Med. Chem. Lett.* **18** (2008) 5182 (https://doi.org/10.1016/j.bmcl.2008.08.097)
8. M. T. Barros, M. A. J. Charmier, C. D. Maycock, T. Michaud, *Tetrahedron* **65** (2009) 396 (https://doi.org/10.1016/j.tet.2008.10.020)
9. M. González, Z. Gándara, B. Covelo, G. Gómez, Y. Fall, *Tetrahedron Lett.* **52** (2011) 5983 (https://doi.org/10.1016/j.tetlet.2011.08.160)
10. Y.-F. Tsai, C.-C. Huang, S.-H. Lin, P.-M. Su, Y.-J. Chen, T.-Y. Wu, *Heterocycles* **85** (2012) 299 (https://doi.org/10.3987/COM-11-12397)
11. M. González, Z. Gándara, Z. Pazos, G. Gómez, Y. Fall, *Synthesis* (2013) 625 (https://doi.org/10.1055/s-0032-1318113)
12. S. Chatterjee, A. Manna, T. Bhaumik, *Tetrahedron: Asymmetry* **25** (2014) 1624 (https://doi.org/10.1016/j.tetasy.2014.11.001)
13. D. A. Chaudhari, A. B. Ingle, R. A. Fernandes, *Tetrahedron: Asymmetry* **27** (2016) 114 (https://doi.org/10.1016/j.tetasy.2016.01.003)
14. S. Yaragorla, R. Muthyala, *ARKIVOC* (2010) 178 (https://doi.org/10.3998/ark.5550190.0011.a15)
15. C. R. Reddy, D. Suman, N. N. Rao, *Helv. Chim. Acta* **98** (2015) 967 (https://doi.org/10.1002/hlca.201400356)
16. C. Cooze, A. Manchoju, S. V. Pansare, *Synlett* (2017) 2928 (https://doi.org/10.1055/s-0036-1590858)
17. S. H. Tsai, P. C. Hsieh, L. L. Wei, H. F. Chiu, Y. C. Wu, M. J. Wu, *Tetrahedron Lett.* **40** (1999) 1975 (https://doi.org/10.1002/chin.199923295)
18. J. M. Andres, N. de Elena, R. Pedrosa, A. Pérez-Encabo, *Tetrahedron: Asymmetry* **12** (2001) 1503 (https://doi.org/10.1016/S0957-4166(01)00044-1)
19. V. Popsavin, I. Krstić, M. Popsavin, B. Srećo, G. Benedeković, V. Kojić, G. Bogdanović *Tetrahedron* **62** (2006) 11044 (https://doi.org/10.1016/j.tet.2006.09.054)
20. B. Srećo, G. Benedeković, M. Popsavin, P. Hadžić, V. Kojić, G. Bogdanović, V. Divjaković, V. Popsavin, *Tetrahedron* **67** (2011) 9358 (https://doi.org/10.1016/j.tet.2011.09.132)
21. B. Srećo Zelenović, S. Kekezović, M. Popsavin, V. Kojić, G. Benedeković, V. Popsavin, *J. Serb. Chem. Soc.* **84** (2019) 1345 (https://doi.org/10.2298/JSC190912104S)
22. D. A. Scudiero, R. H. Shoemaker, K. D. Paull, A. Monks, S. Tierney, T. H. Nofziger, M. J. Currens, D. Seniff, M. R. Boyd, *Cancer. Res.* **48** (1988) 4827 (https://pdfs.semanticscholar.org/3299/2997d7d34c82c2ce34937b25c5a770dbd735.pdf)
23. J. Francuz, M. Popsavin, S. Djokić, V. Kojić, T. Srdić-Rajić, M. Rodić, D. Jakimov, V. Popsavin, *Med. Chem. Commun.* **9** (2018) 2017 (https://doi.org/10.1039/C8MD00431E)
24. D. Cremer, J. A. Pople, *J. Am. Chem. Soc.* **97** (1975) 1354 (https://dx.doi.org/10.1021/ja00839a011)
25. D. Cremer, *Isr. J. Chem.* **20** (1980) 12 (https://dx.doi.org/https://doi.org/10.1002/ijch.198000048).

Journal of the Serbian Chemical Society
JSCS@tmf.bg.ac.rs • www.shd.org.rs/JSCS
J. Serb. Chem. Soc. 88 (2) S35–S50 (2023) *Supplementary material*

SUPPLEMENTARY MATERIAL TO

Divergent synthesis and antitumour activity of novel conformationally constrained (–)-muricatacin analogues

SLAĐANA M. STANISAVLJEVIĆ[1], BOJANA M. SREĆO ZELENOVIĆ[1]*, MIRJANA POPSAVIN[1], MARKO V. RODIĆ[1], VELIMIR POPSAVIN[1,2] and VESNA V. KOJIĆ[3]

[1]University of Novi Sad, Faculty of Sciences, Department of Chemistry, Biochemistry and Environmental Protection, Trg Dositeja Obradovića 3, 21000 Novi Sad, Serbia, [2]Serbian Academy of Sciences and Arts, Kneza Mihaila 35, 11000 Belgrade, Serbia and [3]University of Novi Sad, Faculty of Medicine, Oncology Institute of Vojvodina, Put dr Goldmana 4, 21204 Sremska Kamenica, Serbia

J. Serb. Chem. Soc. 88 (2) (2023) 113–121

PHYSICAL AND SPECTRAL DATA OF SYNTHESIZED COMPOUNDS

*Methyl-(Z)-3-O-methyl-5,6-dideoxy-1,2-O-isopropylidene-α-d-xylo-hept-5-enofuranuronate (**4**)*

Colourless oil $[\alpha]_D$=−143 (*c* 0.5, MeOH), R_f=0.31 (3:2 PE/Et_2O). IR ($CHCl_3$): ν_{max} 1721 (C=O), 1165 (O-C, ester). ^{1}H NMR (400 MHz, $CDCl_3$): δ 1.20 and 1.39 (2 × s, 3 H each, C*Me*$_2$), 3.22 (s, 3 H, OCH_3), 3.61 (s, 3 H, CO_2CH_3), 3.92 (d, 1 H, $J_{3,4}$=3.3 Hz, H-3), 4.48 (d, 1 H, $J_{1,2}$=3.9 Hz, H-2), 5.51 (ddd, 1 H, $J_{4,5}$=6.9, $J_{3,4}$=3.3, $J_{4,6}$=1.6 Hz, H-4), 5.82 (dd, 1 H, $J_{5,6}$=11.8, $J_{4,6}$=1.7 Hz, H-6), 5.82 (d, 1 H, $J_{1,2}$=3.9 Hz, H-1), 6.19 (dd, 1 H, $J_{5,6}$=11.8, $J_{4,5}$=6.9 Hz, H-5). ^{13}C NMR (100 MHz, $CDCl_3$): δ 26.2 and 26.8 (2×CH_3-isopropylidene), 51.3 (CO_2CH_3), 58.0 (OCH_3), 77.6 (C-4), 82.2 (C-2), 86.2 (C-3), 104.9 (C-1), 111.5 (Me_2C), 120.6 (C-6), 145.2 (C-5), 165.8 (CO_2CH_3). HRMS-Heated ESI-Orbitrap: *m/z* 281.09908 (M^++Na), calcd. for $C_{12}H_{18}NaO_6$: 281.10011; *m/z* 297.07278 (M^++K), calcd. for $C_{12}H_{18}KO_6$: 297.07404.

*Methyl-(E)-3-O-methyl-5,6-dideoxy-1,2-O-isopropylidene-α-d-xylo-hept-5-enofuranuronate (**5**)*

White crystals, mp 47 ºC (Et_2O/hexane), $[\alpha]_D$=−59.6 (*c* 0.5, $CHCl_3$), R_f =0.20 (3:2 PE/Et_2O). IR ($CHCl_3$): ν_{max} 1724 (C=O), 1166.8 (O-C, ester). ^{1}H NMR (400 MHz, $CDCl_3$): δ 1.34 and 1.51 (2 × s, 3 H each, C*Me*$_2$), 3.39 (s, 3 H, OCH_3), 3.75 (s, 3 H, CO_2CH_3), 3.78 (d, 1 H, $J_{3,4}$=3.2 Hz, H-3), 4.62 (d, 1 H, $J_{1,2}$=3.8 Hz, H-2), 4.80 (ddd, 1 H, $J_{4,5}$=4.9, $J_{3,4}$=3.0, $J_{4,6}$=1.7 Hz, H-4), 5.96 (d,1 H, $J_{1,2}$=3.8

* Corresponding author. E-mail: bojana.sreco@dh.uns.ac.rs

Hz, H-1), 6.18 (dd, 1 H, $J_{5,6}$=15.7, $J_{4,6}$=1.7 Hz, H-6), 6.97 (dd, 1 H, $J_{5,6}$=15.7, $J_{4,5}$=4.9 Hz, H-5). ^{13}C NMR (100 MHz, $CDCl_3$): δ 26.1 and 26.8 (CMe_2), 51.6 (CO_2CH_3), 58.2 (OCH_3), 79.3 (C-4), 81.9 (C-2), 85.6 (C-3), 104.8 (C-1), 111.8 (Me_2C), 122.7 (C-6), 141.4 (C-5), 166.4 (-CO_2CH_3). HRMS-Heated ESI-Orbitrap: *m/z* 281.09931 (M^++Na), calcd. for $C_{12}H_{18}NaO_6$: 281.10011; *m/z* 297.0735 (M^++K), calcld. for $C_{12}H_{18}KO_6$: 297.07404.

*Dimethylacetal 2,5-anhydro-6-deoxy-3-O-methyl-l-ido-hepturono-4,7-lactone (**6**)*

Colorless oil; $[\alpha]_D$=−11 (*c* 0.5, $CHCl_3$), R_f=0.26 (4:1 $CHCl_3$/EtOAc). IR ($CHCl_3$): ν_{max} 1789 (C=O). ^{1}H NMR (400 MHz, $CDCl_3$): δ 2.70 (d, 1 H, $J_{6a,6b}$=18.8 Hz, H-6a), 2.74 (dd, 1 H, $J_{6a,6b}$=18.8, $J_{5,6b}$=4.2 Hz, H-6b), 3.42 (s, 3 H, OCH_3, C-3), 3.44 i 3.47 (2 × s, 3 H each, OCH_3), 3.99 (d, 1 H, $J_{2,3}$=3.6 Hz, H-3), 4.06 (dd, 1 H, $J_{1,2}$=7.3, $J_{2,3}$=3.7 Hz, H-2), 4.57 (d, 1 H, $J_{1,2}$=7.3 Hz, H-1), 4.90 (d, 1 H, $J_{4,5}$=4.5 Hz, H-4), 4.97 (m, 1 H, $J_{4,5}$=4.5, $J_{5,6b}$=4.3 Hz, H-5).^{13}C NMR (100 MHz, $CDCl_3$): δ 36.0 (C-6), 53.6 and 55.2 (2 × OCH_3), 58.6 (OCH_3 C-3), 77.5 (C-5), 79.6 (C-2), 83.4 (C-3), 84.5 (C-4), 102.0 (C-1), 175.2 (C=O). HRMS-Heated ESI-Orbitrap: *m/z* 255.08469 (M^++Na), calcd. for $C_{10}H_{16}NaO_6$: 255.08446.

*3,6-Anhydro-2-deoxy-5-O-methyl-l-ido-heptono-1,4-lactone (**8**)*

White, needle-like crystals, mp 78−80 °C (EtOAc/hexane), $[\alpha]_D$=−10.2, (*c* 0.5, $CHCl_3$), R_f= 0.2 (3:2 CH_2Cl_2/EtOAc). IR ($CHCl_3$) ν_{max} 3455 (OH), 1781 (C=O). ^{1}H NMR (400 MHz, $CDCl_3$): δ 2.14 (bs, 1 H, OH), 2.68 (dd, 1 H, $J_{2a,2b}$=18.8, $J_{2a,3}$=1.2 Hz, H-2a), 2.76 (dd, 1 H, $J_{2a,2b}$=18.8, $J_{2b,3}$=5.7 Hz, H-2b), 3.51 (s, 3 H, OCH_3), 3.82 (dd, 1 H, $J_{7a,7b}$=12.1, $J_{6,7a}$=4.4 Hz, H-7a), 3.88 (dd, 1 H, $J_{7a,7b}$ =12.1, $J_{6,7b}$=4.8 Hz, H-7b), 4.11 (d, 1 H, $J_{5,6}$=4.9 Hz, H-5), 4.23 (q, 1 H, $J_{5,6}$=4.7, $J_{6,7}$=4.7, $J_{6,7b}$=4.7 Hz, H-6), 4.95 (d, 1 H, $J_{3,4}$=4.7 Hz, H-4), 5.01 (m, 1 H, $J_{2a,3}$=1.2, $J_{2b,3}$=5.8, $J_{3,4}$=4.7 Hz, H-3). ^{13}C NMR (100 MHz, $CDCl_3$): δ 36.0 (C-2), 58.6 (-OMe), 61.5 (C-7), 76.9 (C-3), 80.5 (C-6), 85.1 (C-5), 85.3 (C-4), 175.2 (C=O). HRMS-Heated ESI-Orbitrap: *m/z* 211.05787 (M^++Na), calcd. for $C_8H_{12}NaO_5$: 211.05824.

*3,6-Anhydro-2-deoxy-5-O-metyl-7-O-nonyl-l-ido-heptono-1,4-lactone (**9**)*

Colorless, glassy crystals, mp 38–41 ºC (CH_2Cl_2/hexane), $[\alpha]_D$ = –12.8 (*c* 0.45, $CHCl_3$); R_f=0.23 (1:1 PE/Et_2O). IR ($CHCl_3$): ν_{max} 1787.89 (C=O). ^{1}H NMR (400 MHz, $CDCl_3$): δ 0.89 (t, 3 H, *J* = 6.9 Hz, CH_3 from side chain), 1.24–1.33 (m, 12 H, 6 × CH_2 from side chain), 1.59 (m, 2 H, $OCH_2CH_2(CH_2)_6CH_3$), 2.70 (dd, 1 H, $J_{2a,2b}$=19.0, $J_{2a,3}$=2.3 Hz, H-2a), 2.76 (dd, 1 H, $J_{2a,2b}$=18.8, $J_{2b,3}$=4.9 Hz, H-2b), 3.40–3.54 (m, 5 H, OCH_3 and $OCH_2(CH_2)_7CH_3$), 3.60 (dd, 1 H, $J_{7a,7b}$=10.3, $J_{6,7a}$= 6.3 Hz, H-7a), 3.65 (dd, 1 H, $J_{7a,7b}$=10.3, $J_{6,7b}$=4.7 Hz, H-7b), 4.00 (bd, 1 H, $J_{5,6}$=4.1 Hz, H-5), 4.25 (dt, 1 H, $J_{5,6}$=4.4, $J_{6,7b}$=4.5, $J_{6,7a}$=6.3 Hz, H-6), 4.94 (dd, 1 H, $J_{3,4}$=4.8, $J_{4,5}$=0.8 Hz, H-4), 4.97 (m, 1 H, $J_{2a,3}$=2.3, $J_{2b,3}$=4.8,

$J_{3,4}$=4.8 Hz, H-3). ^{13}C NMR (100 MHz, $CDCl_3$): δ 14.1 (CH_3), 22.7, 26.1, 29.3, 29.5, 29.6, 29.6, 31.9 (7×CH_2 from side chain), 36.0 (C-2), 58.6 (OCH_3), 68.4 (C-7), 71.8 ($OCH_2(CH_2)_7CH_3$), 76.7 (C-3), 79.6 (C-6), 83.9 (C-5), 84.9 (C-4), 175.4 (C=O). HRMS-Heated ESI-Orbitrap: *m/z* 337.19785 (M^+ + Na), calcd. for $C_{17}H_{30}NaO_5$: 337.19854.

*3,6-Anhydro-2-deoxy-5-O-metyl-7-O-octyl-l-ido-heptono-1,4-lactone (**10**)*

White cristals, mp 37–39 °C (Et_2O/hexane), $[\alpha]_D$ = –17.2 (*c* 0.5, $CHCl_3$); R_f=0.15 (7:3 PE/Et_2O). IR ($CHCl_3$): ν_{max} 1791.06 (C=O). ^{1}H NMR (400 MHz, $CDCl_3$): δ 0.89 (t, 3 H, *J*=6.9 Hz, CH_3), 1.22–1.36 (m, 10 H, 5 × CH_2 from side chain), 1.52–1.64 (m, 2 H, $OCH_2CH_2(CH_2)_5CH_3$), 2.70 (dd, 1 H, $J_{2a,2b}$=18.9, $J_{2a,3}$=2.1 Hz, H-2a), 2.78 (dd, 1 H, $J_{2a,2b}$=18.9, $J_{2b,3}$ = 4.9 Hz, H-2b), 3.39–3.53 (m, 2 H, $OCH_2(CH_2)_6CH_3$), 3.47 (s, 3 H, CH_3 from OCH_3), 3.59 (dd, 1 H, $J_{7a,7b}$=10.3, $J_{6,7a}$ =6.4 Hz, H-7a), 3.64 (dd, 1 H, $J_{7a,7b}$=10.3, $J_{6,7b}$=4.8 Hz, H-7b), 3.99 (bd, 1 H, $J_{5,6}$=4.0 Hz, H-5), 4.25 (dt, 1 H, $J_{6,7a}$=6.3, $J_{6,7b}$=4.6, $J_{5,6}$=4.4 Hz, H-6), 4.94 (dd, 1 H, $J_{3,4}$=4.8, $J_{4,5}$=0.8 Hz, H-4), 4.97 (td, 1 H, $J_{2a,3}$=2.2, $J_{2b,3}$=4.9, $J_{3,4}$=4.9 Hz, H-3).^{13}C NMR (100 MHz, $CDCl_3$): 14.1 (CH_3), 22.6, 26.1, 29.2, 29.4, 29.6, 31.8 (6 × CH_2 from side chain), 36.0 (C-2), 58.6 (OMe), 68.4 (C-7), 71.8 [$OCH_2(CH_2)_6CH_3$], 76.8 (C-3), 79.6 (C-6), 83.9 (C-5), 84.9 (C-4); 175.4 (C=O). HRMS-Heated ESI-Orbitrap: *m/z* 323.18393 (M^+ + Na), calcd. for $C_{16}H_{28}NaO_5$: 323.18289.

*3,6-Anhydro-2-deoxy-7-O-heptyl-5-O-metyl-l-ido-heptono-1,4-lactone (**11**)*

White, needle-like cristals, mp 44−45 °C (Et_2O/hexane), $[\alpha]_D$=−10.0 (*c* 0.5, $CHCl_3$), R_f=0.16 (3:2 PE/Et_2O). IR ($CHCl_3$) ν_{max} 1791 (C=O).^{1}H NMR (400 MHz, $CDCl_3$): δ 0.86 (t, 3 H, *J*=6.9 Hz, CH_3 from side chain), 1.22−1.33 (m, 8 H, 4×CH_2 from side chain), 1.56 (m, 2 H, $OCH_2CH_2(CH_2)_4CH_3$), 2.66 (dd, 1 H, $J_{2a,2b}$=18.8, $J_{2a,3}$=1.6 Hz, H-2a), 2.73 (dd, 1 H, $J_{2a,2b}$=18.8, $J_{2b,3}$=5.3 Hz, H-2b), 3.37−3.55 (m, 2 H, $OCH_2(CH_2)_5CH_3$), 3.46 (s, 3 H, OCH_3), 3.56 (dd, 1 H, $J_{7a,7b}$=10.3, $J_{6,7a}$=6.4 Hz, H-7a), 3.61 (dd, 1 H, $J_{7a,7b}$=10.3, $J_{6,7b}$=4.8 Hz, H-7b), 3.96 (d, 1 H, $J_{5,6}$=4.0 Hz, H-5), 4.22 (dt, 1 H, $J_{5,6}$=4.4, $J_{7b,6}$=4.5, $J_{6,7a}$=6.3 Hz, H-6), 4.91 (d, 1 H, $J_{3,4}$=5.0 Hz, H-4), 4.94 (m, 1 H, $J_{2a,3}$=1.8, $J_{2b,3}$=5.0, $J_{3,4}$=5.0 Hz, H-3).^{13}C NMR (100 MHz, $CDCl_3$): δ 14.1 (CH_3), 22.6, 26.0, 29.1, 29.6, 31.8 (5 × CH_2 from side chain), 36.0 (C-2), 58.6 (OCH_3), 68.4 (C-7), 71.8 [$OCH_2(CH_2)_5CH_3$], 76.8 (C-3), 79.5 (C-6), 83.9 (C-5), 84.9 (C-4), 175.4 (C=O). HRMS-Heated ESI-Orbitrap: *m/z* 309.16716 (M^++Na), calcd. for $C_{15}H_{26}NaO_5$: 309.16779.

*3,6-Anhydro-2-deoxy-7-O-hexyl-5-O-metyl-l-ido-hexyl-1,4-lactone (**12**)*

White crystals, mp 55 °C, (Et_2O/hexane); $[\alpha]_D$=−13.2 (*c* 0.5, $CHCl_3$), R_f=0.26 (7:3 PE/Et_2O). IR ($CHCl_3$) ν_{max} 1790 (C=O). ^{1}H NMR (400 MHz, $CDCl_3$): δ 0.90 (t, 3 H, *J*=6.9 Hz, CH_3 from side chain), 1.23–1.39 (m, 6 H, 3 ×

CH_2 from side chain), 1.60 (m, 2 H, $OCH_2CH_2(CH_2)_3CH_3$), 2.71 (dd, 1 H, $J_{2a,2b}$=18.8, $J_{2a,3}$=2.2 Hz, H-2a), 2.76 (dd, 1 H, $J_{2a,2b}$=18.8, $J_{2b,3}$=4.9 Hz, H-2b), 3.41-3.54 (m, 5 H, OCH_3 i $OCH_2(CH_2)_4CH_3$), 3.60 (dd, 1 H, $J_{7a,7b}$=10.3, $J_{6,7a}$=6.3 Hz, H-7a), 3.65 (dd, 1 H, $J_{7a,7b}$=10.3, $J_{6,7b}$=4.8 Hz, H-7b), 4.00 (d, 1 H, $J_{5,6}$=4.0 Hz, H-5), 4.22 (dt, 1 H, $J_{5,6}$=4.4, $J_{6,7b}$=4.5, $J_{6,7a}$=6.3 Hz, H-6), 4.92 (d, 1 H, $J_{3,4}$=4.8 Hz, H-4), 4.94 (m, 1 H, $J_{2a,3}$=2.2, $J_{2b,3}$=4.8, $J_{3,4}$=4.7 Hz, H-3). ^{13}C NMR (100 MHz, $CDCl_3$): δ 14.0 (CH_3), 22.6, 25.7, 29.5, 31.6 (4 × CH_2 from side chain), 36.0 (C-2), 58.5 (OCH_3), 68.4 (C-7), 71.8 [$OCH_2(CH_2)_5CH_3$], 76.8 (C-3), 79.5 (C-6), 83.8 (C-5), 84.9 (C-4), 175.4 (C=O). HRMS-Heated ESI-Orbitrap: *m/z* 273.17019 (M^++H), calcd. for $C_{14}H_{25}O_5$: 273.1702; *m/z* 295.15213 (M^++Na), calcld. for $C_{14}H_{24}NaO_5$: 295.15214.

NMR SPECTRA OF FINAL PRODUCTS

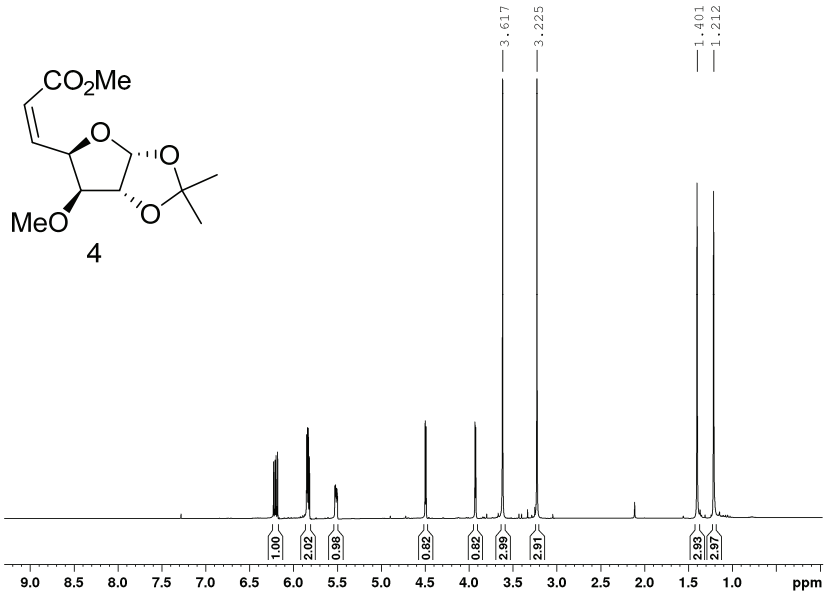

Fig. S-1. ^{1}H-NMR spectrum of **4** (400 MHz, $CDCl_3$).

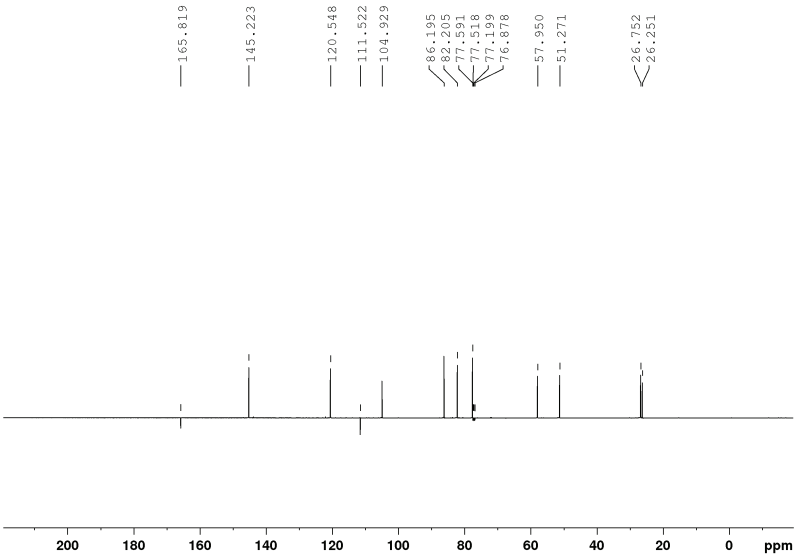

Fig. S-2. ^{13}C-NMR spectrum of **4** (100 MHz, $CDCl_3$).

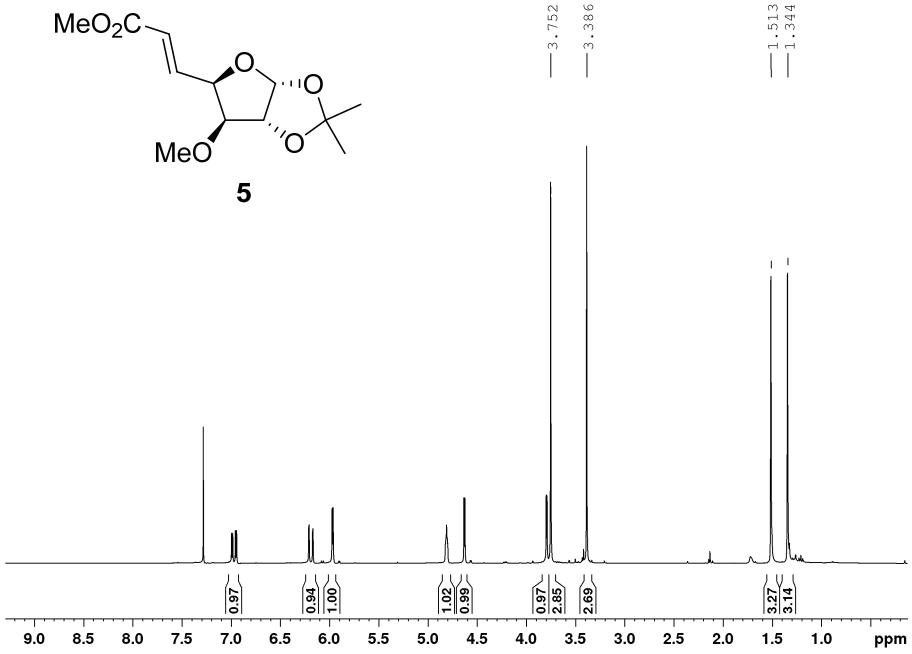

Fig. S-3. ^{1}H-NMR spectrum of **5** (400 MHz, $CDCl_3$).

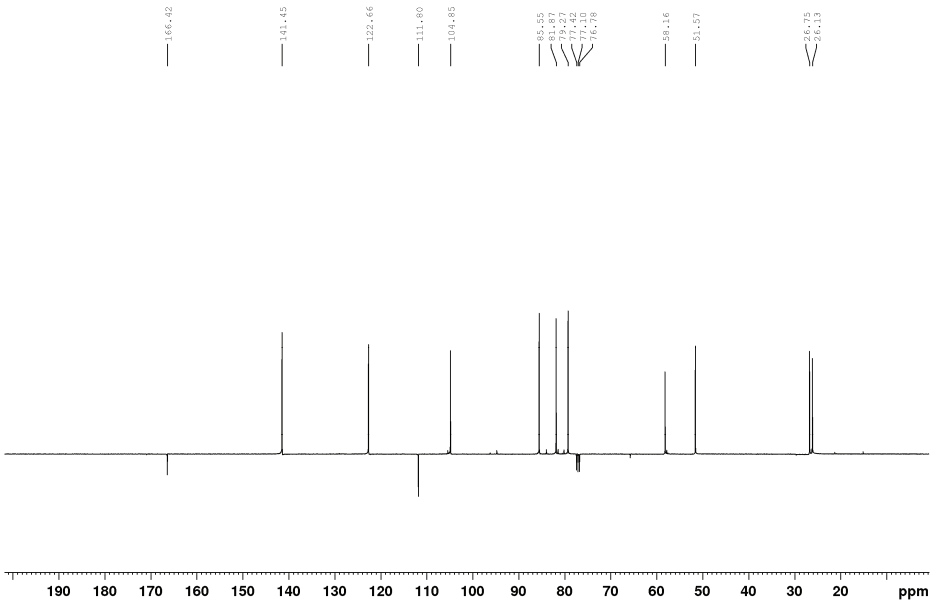

Fig. S-4. ^{13}C-NMR spectrum of **5** (100 MHz, $CDCl_3$).

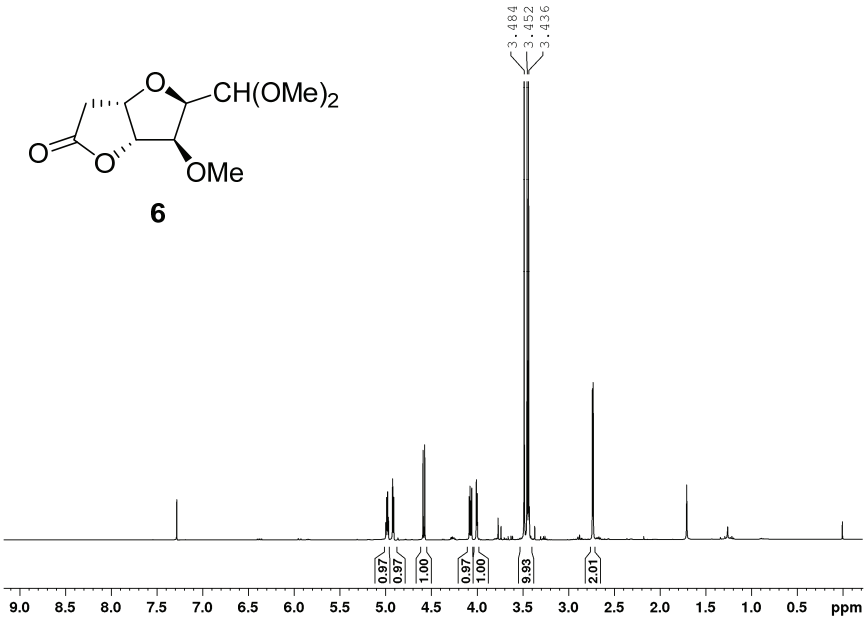

Fig. S-5. ^{1}H-NMR spectrum of **6** (400 MHz, $CDCl_3$).

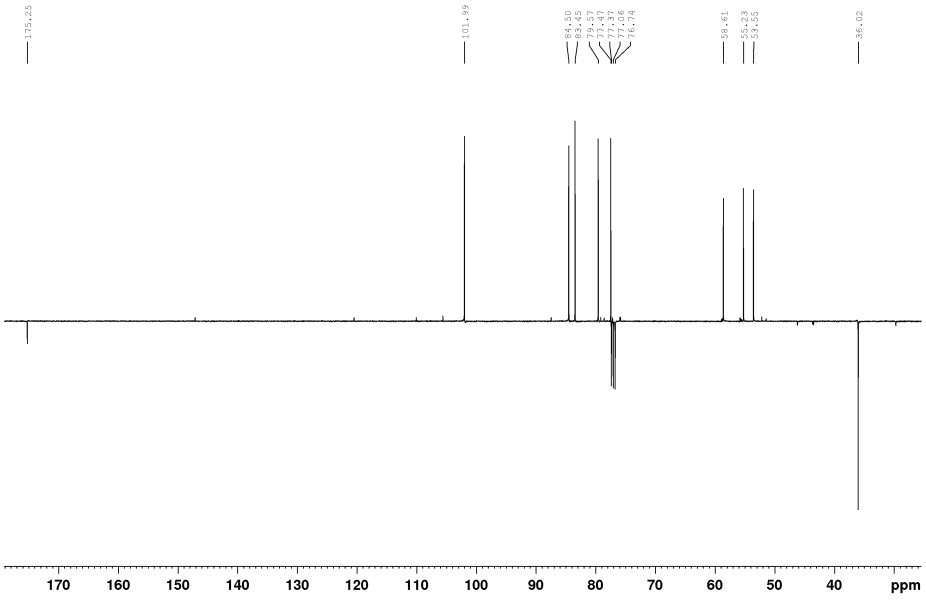

Fig. S-6. ^{13}C-NMR spectrum of **6** (100 MHz, $CDCl_3$).

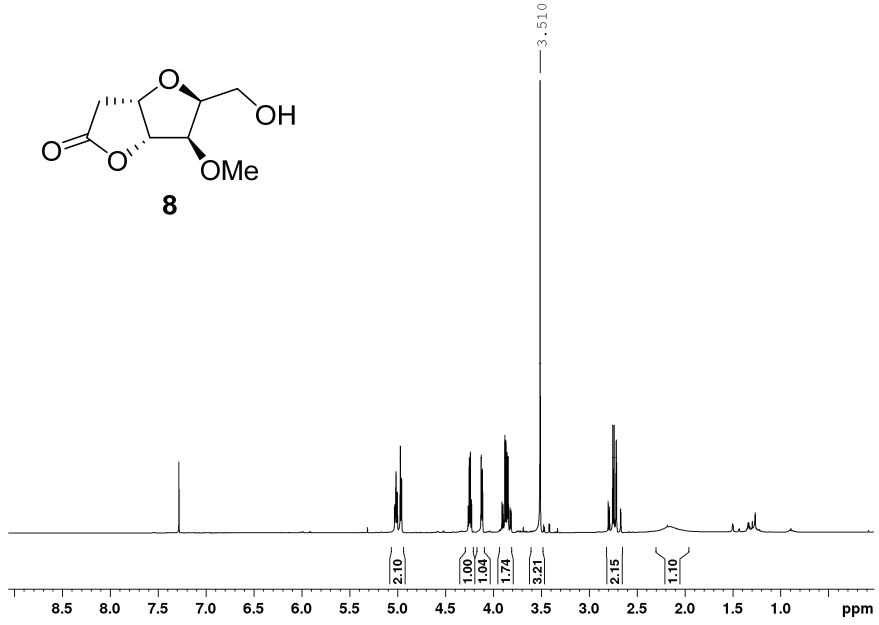

Fig. S-7. ^{1}H-NMR spectrum of **8** (400 MHz, $CDCl_3$).

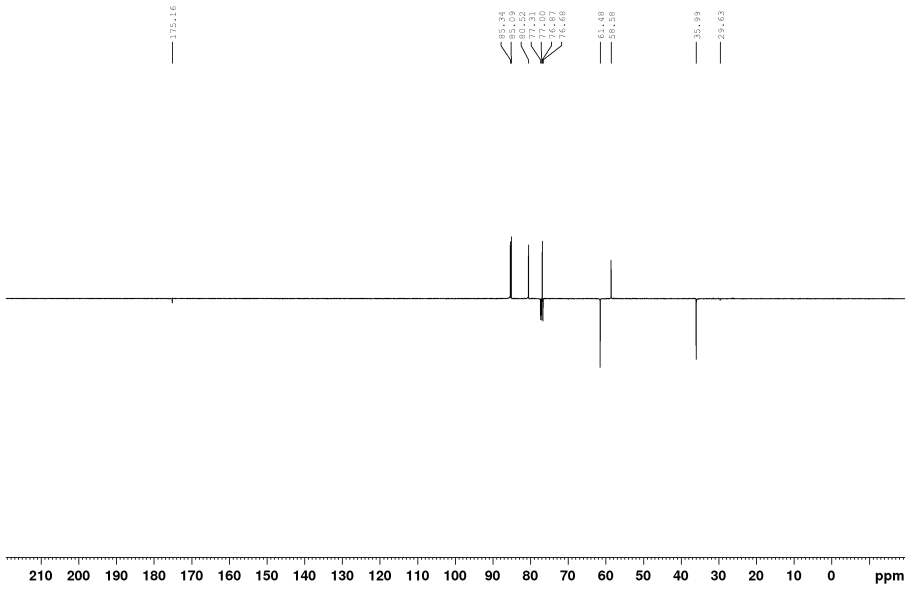

Fig. S-8. ^{13}C-NMR spectrum of **8** (100 MHz, $CDCl_3$).

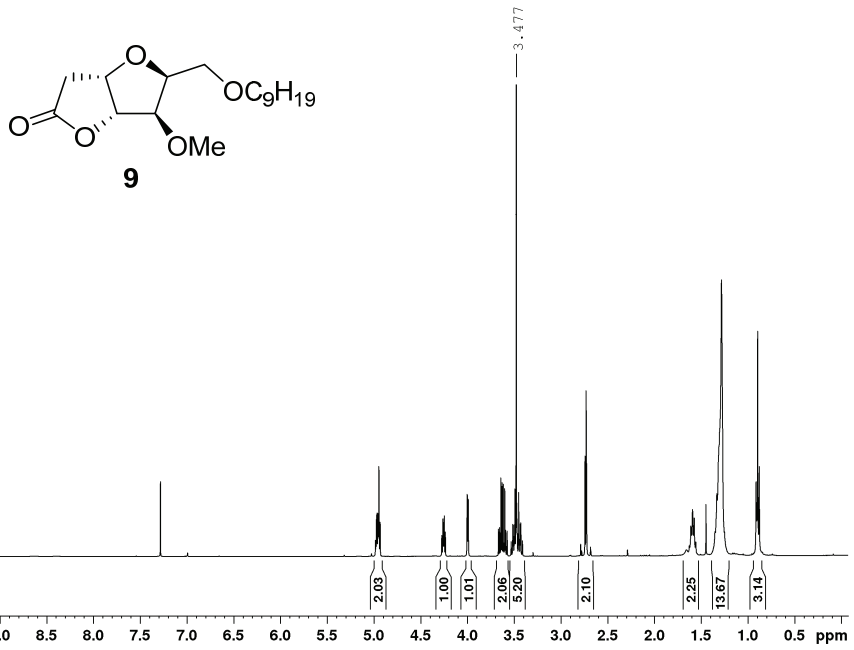

Fig. S-9. ^{1}H-NMR spectrum of **9** (400 MHz, $CDCl_3$).

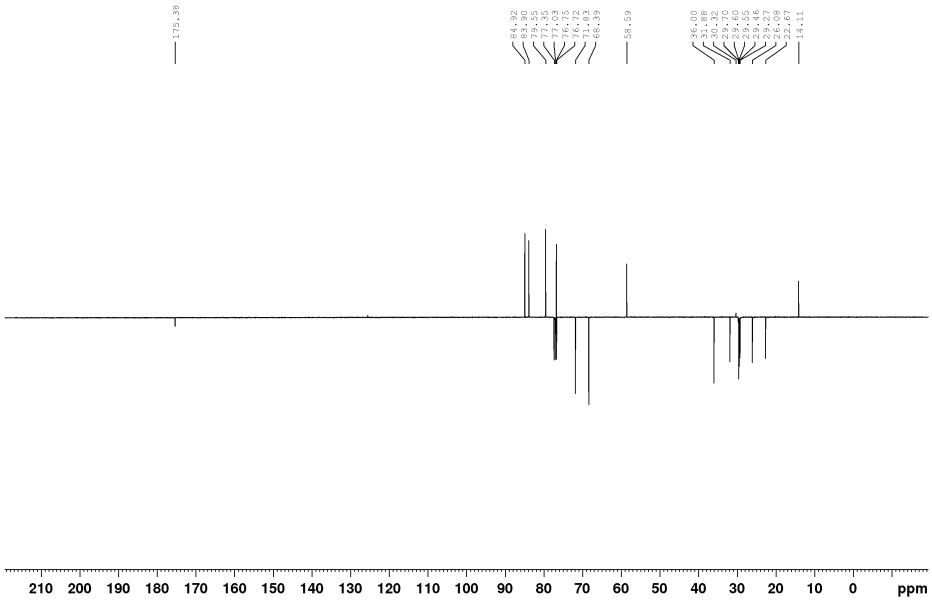

Fig. S-10. ^{13}C-NMR spectrum of **9** (100 MHz, $CDCl_3$).

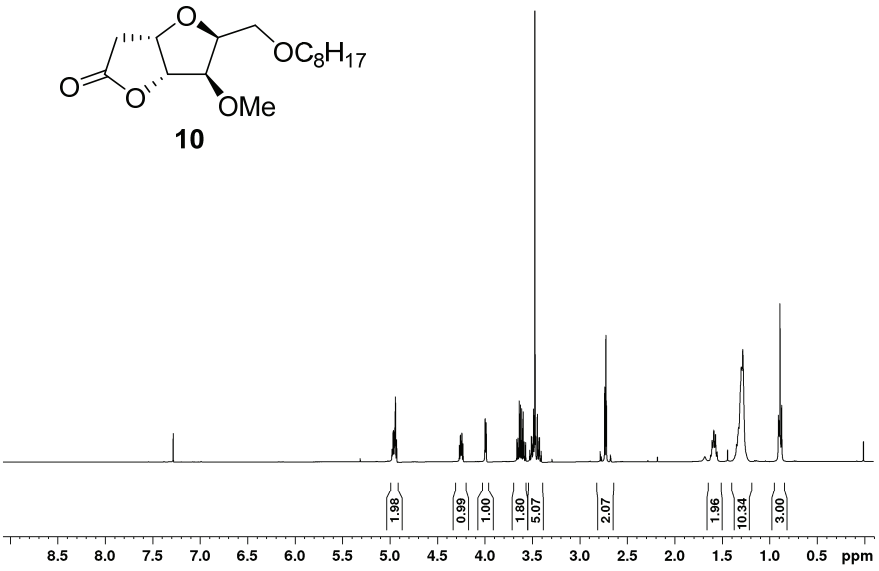

Fig. S-11. ^{1}H-NMR spectrum of **10** (400 MHz, $CDCl_3$).

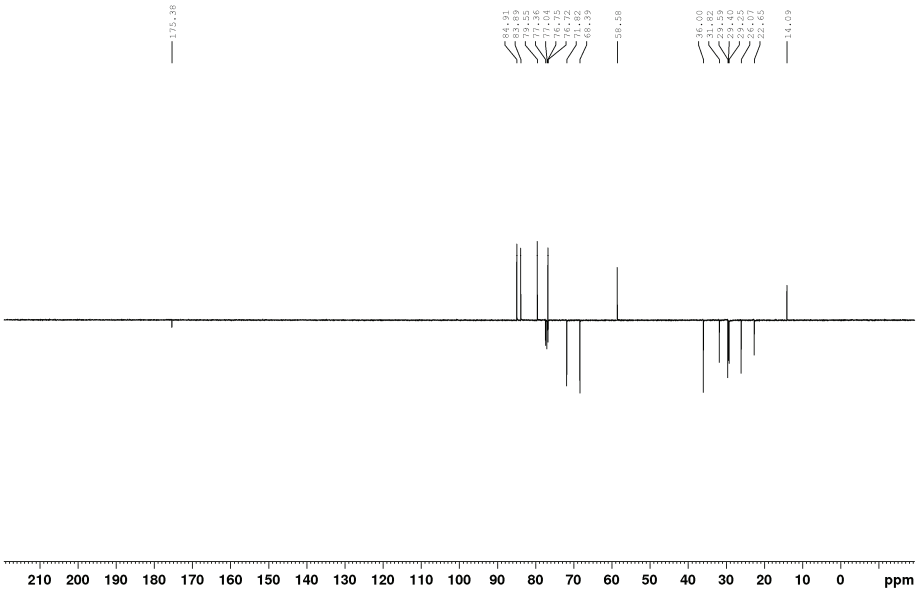

Fig. S-12. ^{13}C-NMR spectrum of **10** (100 MHz, $CDCl_3$).

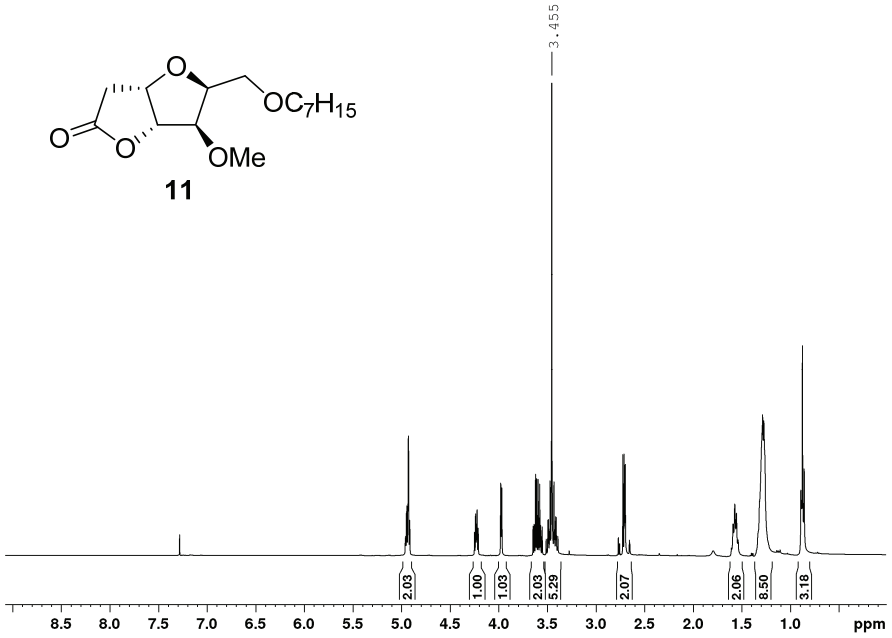

Fig. S-13. ^{1}H-NMR spectrum of **11** (400 MHz, $CDCl_3$).

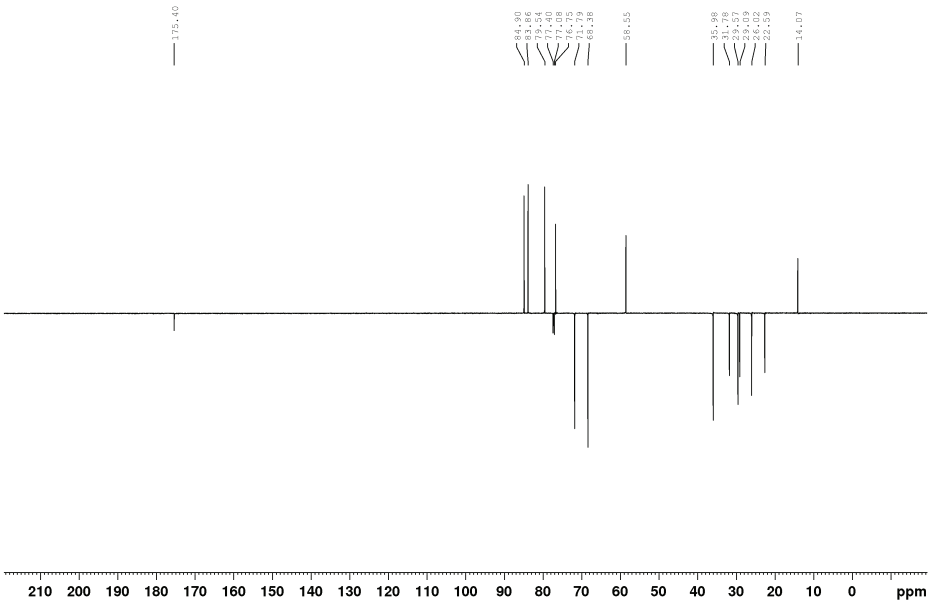

Fig. S-14. ^{13}C-NMR spectrum of **11** (100 MHz, $CDCl_3$).

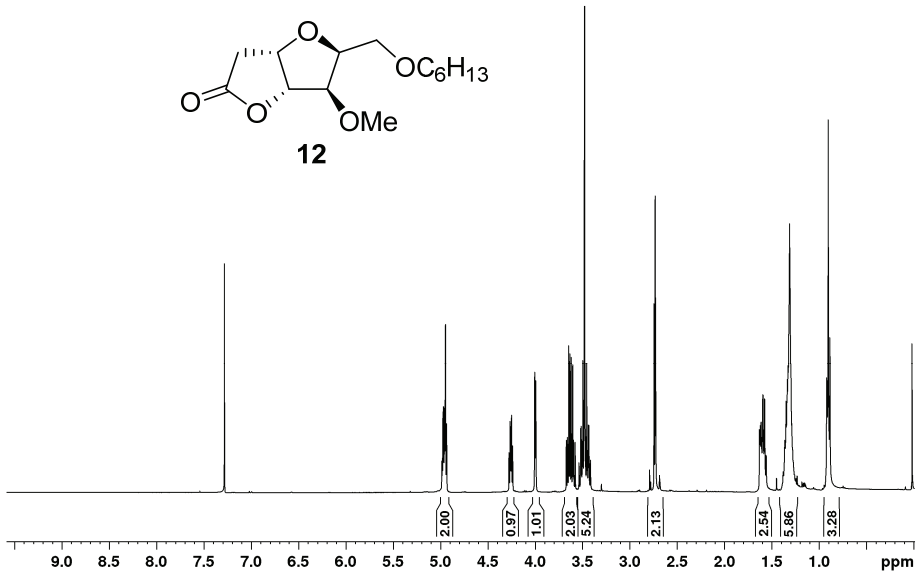

Fig. S-15. ^{1}H-NMR spectrum of **12** (400 MHz, $CDCl_3$).

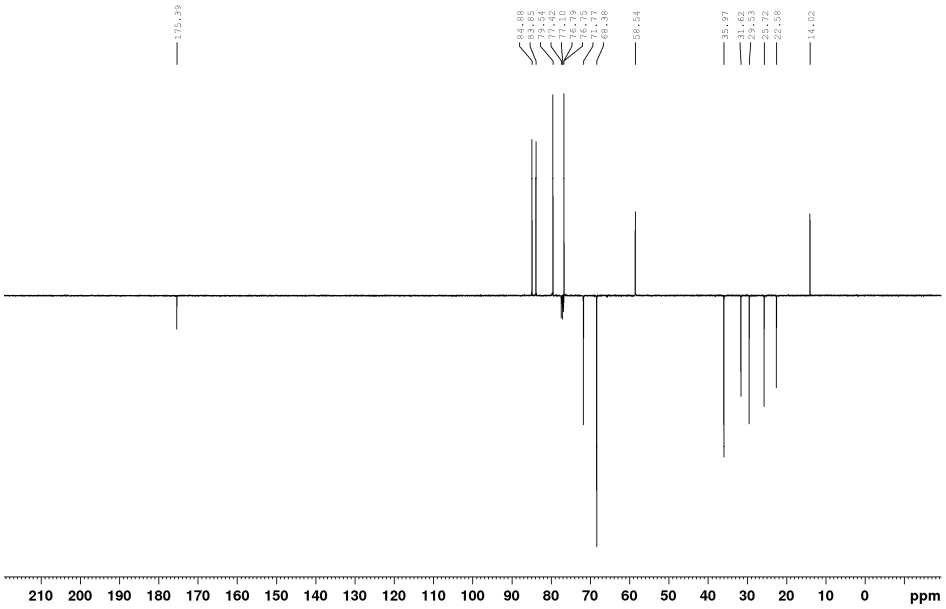

Fig. S-16. ^{13}C-NMR spectrum of **12** (100 MHz, $CDCl_3$).

SAR ANALYSIS

TABLE S-I. Cytotoxicity data for SAR analysis

Compound	K562	HL60	Jurkat	Raji	MCF-7	MDA-MB 231	HeLa
1	**0.04**	**25.85**	**100**	**0.1**	**21.35**	**100**	**0.17**
9	10.25	17.7	15.4	21.75	4.85	11.32	13.5
10	18.12	13.68	7.36	35.84	1.11	28.33	9.12
11	5.6	24.54	22.97	28.49	12.31	25.33	11.51
12	7.69	21.18	25.34	27.03	18.33	15.81	15.22
13	8.76	6.12	9.71	15.95	22.18	39.48	68.32
14	9.09	13.92	5.47	16.85	18.77	28.26	18.02
15	8.87	5.67	8.86	17.33	22.87	34.59	10.9
16	5.65	7.42	5.25	11.82	25.31	8.5	33.79
17[b]	5.66	4.75	6.97	7.25	102.36	296.78	6.39
18[b]	0.74	0.68	19.78	4.25	0.34	28.7	3.41
19[b]	1.02	1.1	11.53	5.98	2.38	9.76	0.56
20[b]	0.7	4.91	8.87	1.11	12.34	15.62	3.54

[a]IC_{50} is the concentration of compound required to inhibit the cell growth by 50% compared to an untreated control. Values are means of three independent experiments. Coefficients of variation were less than 10 %.
[b]Taken from reference[1]

The structure-activity relationships were accessed as follows: the IC_{50} values of two compounds were compared, and the Δ log IC_{50} was calculated (Δ log IC_{50} is a difference between the log IC_{50} values of an analogue and the corresponding control compound). Positive Δ log IC_{50} values show a decrease of antipro-

liferative activity, whereas negative values indicate an increase in the activity upon the structural modification being considered. The results are presented in Figure S-17.

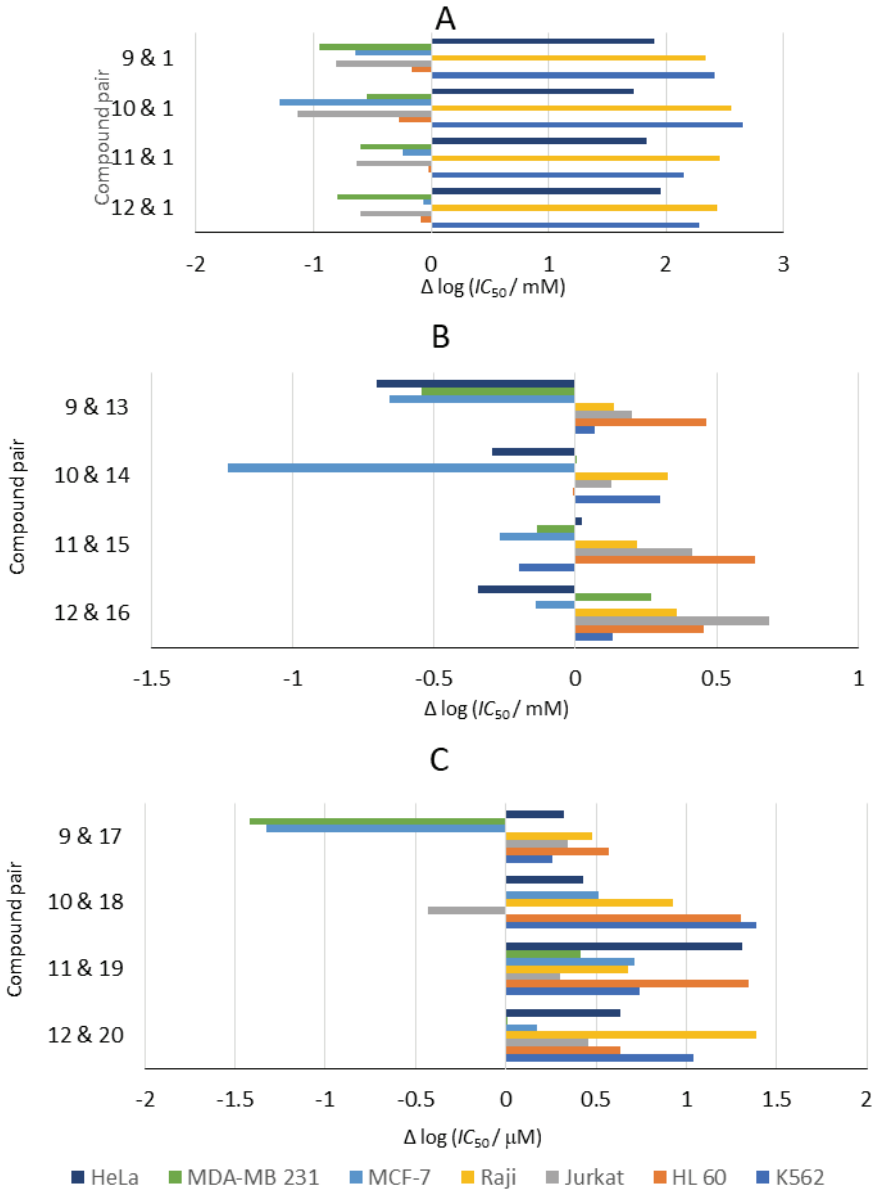

Fig. S-17. SAR Analysis. Influence of: (A) THF-ring closure, exchange of C_8 methylene group with O_8 ether function, 5-*O*-methylation; (B) substitution of methyl with benzyl group at C-5; (C) demethylation at C-5.

CRYSTAL STRUCTURE DETERMINATION

Diffraction experiments were performed on a Gemini S diffractometer. Data collection and reduction procedures were computed with CrysAlisPro.[2] Crystal structure was solved with SHEXLT,[3] and refined with SHEXL,[4] utilizing ShelXle[5] as a graphical user interface. The structure was validated internally by PLATON[6] and externally against Cambridge Structural Database[7] data by MOGUL[8] utility within Mercury CSD.[9] Crystallographic and refinement details are deposited in the Cambridge Crystallographic Data Centre under CCDC 2164235, obtainable free of charge from https://www.ccdc.cam.ac.uk/structures/. Selected crystallographic and refinement details are listed in Table S-II.

Table S-II. Pertinent crystallographic and refinement details of compound **8**

Crystal data	
Chemical formula	$C_8H_{12}O_5$
M_r	188.18
Crystal system	Orthorhombic
Space group	$P2_12_12_1$
Temperature, K	295
a / Å	7.4251 (2)
b / Å	7.7715 (2)
c / Å	16.2624 (5)
V / Å^3	938.41 (5)
Z	4
Radiation type	Mo $K\alpha$
μ / mm^{-1}	0.11
Crystal size, mm	0.58 × 0.36 × 0.28
Data collection	
Diffractometer	Gemini S (Oxford Diffraction)
Absorption correction	Multi-scan
T_{min}, T_{max}	0.918, 1.000
No. of measured	8304
No. of independent	2259
No. of observed [$I > 2\sigma(I)$] reflections	1989
R_{int}	0.021
$(\sin \theta / \lambda)_{max}$ / Å^{-1}	0.687
Refinement	
$R[F^2 > 2\sigma(F^2)]$	0.036
$wR(F^2)$	0.087
S	1.07
No. of reflections	2259
No. of parameters	123
H-atom treatment	Mixed
$\Delta\rho_{max}$, $\Delta\rho_{min}$ / e Å^{-3}	0.12, −0.18
Absolute structure parameter	Meaningless

REFERENCES

1. B. Srećo Zelenović, S. Kekezović, M. Popsavin, V. Kojić, G. Benedeković, V. Popsavin, *J. Serb. Chem. Soc.* **84** (2019) 1345 (https://doi.org/10.2298/JSC190912104S)
2. Rigaku Oxford Diffraction, *CrysAlisPro Software system*, Rigaku Corporation, Wroclaw, Poland, 2021 https://www.rigaku.com/products/crystallography/crysalis
3. G. M. Sheldrick, *Acta Crystallogr. A* **71** (2015) 3 (https://dx.doi.org/10.1107/S2053273314026370)
4. G. M. Sheldrick, *Acta Crystallogr. C* **71** (2015) 3 (https://dx.doi.org/10.1107/S2053229614024218)
5. C. B. Hübschle, G. M. Sheldrick, B. Dittrich, *J. Appl. Crystallogr.* **44** (2011) 1281 (https://dx.doi.org/10.1107/S0021889811043202)
6. A. L. Spek, A*cta Crystallogr. D* 65 (2009) **148** (https://dx.doi.org/10.1107/S090744490804362X)
7. C. R. Groom, I. J. Bruno, M. P. Lightfoot, S. C. Ward, A*cta Crystallogr B* **72** (2016) 171 (https://dx.doi.org/10.1107/S2052520616003954)
8. I. J. Bruno, J. C. Cole, M. Kessler, J. Luo, W. D. Sam Motherwell, L. H. Purkis, B. R. Smith, R. Taylor, R. I. Cooper, S. E. Harris, A. Guy Orpen, *J. Chem. Inf. Comput. Sci.* **44** (2004) 2133 (https://dx.doi.org/10.1021/CI049780B)
9. C. F. Macrae, I. J. Bruno, J. A. Chisholm, P. R. Edgington, P. McCabe, E. Pidcock, L. Rodriguez-Monge, R. Taylor, J. van de Streek, P. A. Wood, *J. Appl. Crystallogr.* **41** (2008) 466 (https://dx.doi.org/10.1107/S0021889807067908).

Journal of the Serbian Chemical Society
JSCS@tmf.bg.ac.rs • www.shd.org.rs/JSCS
J. Serb. Chem. Soc. *88* (2) 123–139 (2023)
JSCS–5615
Original scientific paper
Published 14 December 2022

Screening the binding affinity of bile acid derivatives for the glucocorticoid receptor ligand-binding domain

SRĐAN BJEDOV[1]*#, SOFIJA BEKIĆ[2#], MAJA MARINOVIĆ[2], DUŠAN ŠKORIĆ[1#], KSENIJA PAVLOVIĆ[1#], ANĐELKA ĆELIĆ[2], EDWARD PETRI[2] and MARIJA SAKAČ[1#]

[1]*Department of Chemistry, Biochemistry and Environmental Protection, Faculty of Sciences, University of Novi Sad, Trg Dositeja Obradovića 3, 21000, Novi Sad, Serbia and* [2]*Department of Biology and Ecology, Faculty of Sciences, University of Novi Sad, Trg Dositeja Obradovića 2, 21000, Novi Sad, Serbia*

(Received 12 September, revised 22 September, accepted 28 September 2022)

Abstract: The necessity of anti-inflammatory drugs such as glucocorticoids has been evident during the COVID-19 pandemic. Glucocorticoids, are the standard therapy for the treatment of moderate and severe COVID-19 patients. However, serious side effects limit the use of these drugs, and anti-inflammatory drugs with better pharmacological properties are urgently required. Bile acids are of interest, because of their anti-inflammatory and immunomodulatory properties, facilitated through an unclear mechanism involving transmembrane and nuclear receptors. In this work, we screened the binding activity of a number of bile acid derivatives, for the ligand-binding domain of glucocorticoid receptor (GR-LBD), the most important receptor for anti-inflammatory processes. Tested compounds include oximes, lactones, lactams, tetrazoles, dienones, C-24 alcohols and cholic acid amides. Cholic acid oxime, deoxycholic acid dienone, 3-keto-24-cholic alcohol and cholic acid amide showed best binding affinities for GR-LBD among tested compounds. The in silico molecular docking explanation is provided. SAR analysis showed that expansion of B and C steroid rings or attachment of heterocycle to C ring is not beneficial for binding; side chain should contain hydrogen donor group; the GR-LBD tolerate well different functionalities on C-3 position. These results provide valuable information toward synthesis of the new glucocorticoids based on bile acids.

Keywords: organic synthesis; docking studies; molecular modelling.

INTRODUCTION

Glucocorticoids (GCs) are a class of steroid hormones that are among the most commonly prescribed drugs used for the treatment of allergic, inflam-

* Corresponding author. E-mail: srdjan.bjedov@dh.uns.ac.rs
# Serbian Chemical Society member.
https://doi.org/10.2298/JSC220912078B

matory, and immune disorders such as rheumatoid arthritis, asthma, brain edema, shock, and various blood cancers.[1,2] More recently, they were also the first drugs shown to reduce deaths from COVID19.[3] GCs are the most effective, cost-efficient, and necessary anti-inflammatory and immunomodulatory drugs available. However, the use of GCs is limited by serious adverse effects, such as diabetes, osteoporosis, muscle wasting, hypertension, and glaucoma. Also, certain groups of patients do not respond well to GC therapy.[4] Thus, there is an urgent medical need for new molecules with both enhanced GC therapeutic activities, and fewer or less severe side effects. GCs mediate their effects via the glucocorticoid receptor (GR), a ligand-activated transcription factor. GC activated GR performs its anti-inflammatory functions through a number of mechanisms, among which the most important are transrepression and transactivation.[5,6]

As steroid molecules, bile acids (BAs) play important roles as hormones that regulate a large number of metabolic processes, including inflammation. BAs are enzymatically synthesized in hepatocytes from cholesterol, conjugated with glycine or taurine, and stored in the gallbladder. When food is ingested, liver-synthesized primary BAs are secreted in the small intestine where they emulsify dietary lipids and lipid-soluble vitamins, enabling their absorption. A fraction of primary BAs is converted to secondary BAs by intestinal microbiota. Secreted BAs are reabsorbed and returned to the liver by a very efficient process known as enterohepatic circulation. The hormonal role of BAs is mediated through the BA--activated nuclear receptor farnesoid X receptor (FXR), which controls gene transcription in BA homeostasis and *via* G-protein coupled receptor TGR5. TGR5 is broadly expressed in humans and is involved in various physiological and pathological processes, including energy expenditure, glucose homeostasis, obesity, and bile acid homeostasis.[7]

The anti-inflammatory properties of BAs were reported by Hench in the 1930s. He observed alleviation of rheumatic symptoms in patients with the onset of severe jaundice, a side effect associated with increased BA serum concentrations.[8] BAs were first used as starting compounds for the synthesis of cortisol, which resulted in the 1950 Nobel Prize in Physiology or Medicine for Hench, Kendall and Reichstein.[9] FXR is involved in the pathophysiology of several inflammatory diseases, including non-alcoholic fatty liver diseases, inflammatory bowel disease and atherosclerosis.[10,11] Activation of TGR5 in macrophages and monocytes suppresses lipopolysaccharide-induced production of cytokines and prevents liver damage. The beneficial effects of TRG5 activation were noticed in multiple inflammatory diseases, including diet-induced obesity, atherosclerosis, colitis and steatohepatitis. More information about TGR5 and immunometabolism can be found in an excellent review by Perino and Schoonjans.[12]

Although the hormonal and anti-inflammatory activity of BAs *via* FXR and TGR5 pathways is well established, there is reasonable evidence that some of the

anti-inflammatory activities of BAs is also mediated through GRs. It was found that 5*β*-cholanic acid can bind to GR and modulate GR signaling in cell models of Parkinson's disease.[13] Taurochenodeoxycholic acid also exhibited anti-inflammatory and immunomodulatory properties by inhibiting transcription and expression of AP-1 *via* stimulation of the GR.[14] Ursodeoxycholic acid exerts immune-suppressive effects by reducing IFN-*γ* production by liver lymphocytes, such as NK and NKT cells, in a GR-dependent manner, which may be an important immunological mechanism.[15]

The promiscuity of bile acids for FXR, TGR5 and GR could be exploited in an anti-inflammatory and immunomodulatory manner. In the present work, we explored the GR binding affinity of BA derivatives as a screen for unexplored BA structural features that may be important for GR binding. This work is aimed at the development of anti-inflammatory compounds that could lead to drugs with fewer side effects than current GCs.

EXPERIMENTAL

General synthetic methods

^{1}H- and ^{13}C-NMR spectra were recorded on a Bruker Avance III HD 400 (400 MHz 1H, 101 MHz 13C) apparatus using tetramethylsilane as an internal standard. HRMS spectra (TOF) were recorded on a 6210 time-of-flight LC/MS Agilent Technologies (ESI+) instrument. IR spectra were recorded on a Perkin Elmer Spectrum Two FT-IR spectrometer, and Thermo Nexus 670 FT-IR spectrometer, and melting points were determined on Stuart MP-10 apparatus. Flash chromatography was performed on silica gel 60 (0.04–0.063 mm, Merck). Synthesis of compounds **28** and **29** was done according to a procedure described in our earlier publication,[16] and compound **27** was obtained following the Iqbal and Elliott protocol.[17] For synthesis of **25**, we used a different route then Leppik,[18] and **1** was obtained by a method described by Hüttenrauch.[19]

Spectral data of the compounds are given in the Supplementary material to this paper.

*(3*EZ*, 7*Z*, 12*Z*)-3,7,12-Trioximino-5*β*-cholan-24-oic acid (**1**)*

NaOAc (1.09 g, 13.3 mmol) and $NH_2OH{\times}HCl$ (0.45 g, 7.09 mmol) were added to a suspension of dehydrocholic acid (DCA, 0.63 g, 1.6 mmol) in MeOH (20 mL). The mixture was refluxed for 40 min, and the resulting suspension filtered and washed with cold water. Compound **1** was obtained as a pure mixture of geometric isomers, as a white powder with a yield of 0.6541 g (91 %; thermal decomposition before melting started at 240 °C).

*Methyl (7*Z*,12*Z*)-3,3-dimethoxy-7,12-dioximino-5*β*-cholan-24-oate (**2**)*

NaOAc (0.80 g, 9.8 mmol) and $NH_2OH{\times}HCl$ (0.25 g, 3.9 mmol) were added to a solution of **3** (0.44 g, 1 mmol) in MeOH (20 mL). The mixture was refluxed for 1 h, and the resulting suspension filtered and washed with cold water and dried. Pure compound **2** was obtained as a white powder at a yield of 0.35 g (72 %; thermal decomposition before melting started at 240 °C).

*Methyl 3,3-dimethoxy-7,12-dioxo-5*β*-cholan-24-oate (**3**)*

TsOH (0.16 g, 0.9 mmol) and 2,2-dimethoxypropane (7 mL, 57 mmol) were added to a solution of DCA (1 g, 2.5 mmol) in MeOH (50 mL). The mixture was refluxed for 3 h, evaporated under vacuum, dissolved in EtOAc, washed with cold water (2×15 mL) and dried.

Pure compound **3** was obtained as a white powder at a yield of 1.1 g (93 %; thermal decomposition before melting started at 225 °C).

*12α-Hydroxy-3-oxo-5β-chola-4,6-dien-24-oic acid (**25**)*

Compound **27** (0.4985 g; 1.05 mmol) was dissolved in methanolic KOH (1 g; 17.8 mmol in 50 mL MeOH) and refluxed for 30 min. After reaction completion, the reaction mixture was poured into water (200 mL) and acidified with HCl (1:2) to pH 1. The resulting precipitate was filtered, washed with brine to neutral pH and dried. The raw mixture was purified by flash chromatography (CH_2Cl_2/EtOAc 94:6). Compound **25** was obtained as white needle-like crystals (after recrystallisation from acetone) at a yield of 0.3642 g (90 %); mp 251 °C, mp lit.[20] 249–252 °C.

*12α-Hydroxy-3-oxo-5β-chola-4,6-dien-24-oic acid (**25**) and ethyl 12α-hydroxy-3-oxo-5β--chola-4,6-dien-24-oate (**26**)*

Compound **27** (0.4872 g; 1.02 mmol) was dissolved in ethanolic KOH (0.19 g; 3.4 mmol in 70 mL EtOH) and refluxed for 1 h. After reaction completion, reaction mixture was poured in water (200 mL) and acidified with HCl (1:2) to pH 1. The resulting precipitate was filtered, washed with brine to neutral pH and dried. The raw mixture was purified by flash chromatography (CH_2Cl_2/EtOAc 94:6). Compound **25** was obtained at a yield of 0.1116 g (28 %) and compound **26** (mp 136 °C) at a yield of 0.2872 g (67 %).

2-(5β-Chol-3-ene-7α,12α,24-triol)-N-*(1-hydroxy-2-methylpropan-2-yl)acetamide (**30**)*

Triethylamine (0.3 mL), 2-amino-2-methyl-1-propanol (0.2 mL, 1.1 mmol) and EEDQ (0.23 g, 0.9 mmol) were added to a suspension of compound **29** (0.299 g, 0.69 mmol) in EtOAc (10 mL). The reaction mixture was refluxed for 5 h. After cooling to room temperature, the reaction mixture was washed successively with 3 M HCl (2×4 mL), H_2O (4 mL), 10 % $NaHCO_3$ (2×10 mL) and then with water to neutrality (3×5 mL). The organic layer was dried and evaporated in vacuum to give an oily residue, which was further purified by flash column chromatography (CH_2Cl_2/MeOH 96:4). Pure **30** was obtained at a yield of 0.2612 g (75 %).

Fluorescent assay in yeast

A yeast-based fluorescent screen was applied for testing the relative binding affinities of BA derivatives **1**, **2**, **4**–**23** and **25**–**31** for the GR ligand binding domain (LBD). Assays were conducted following our previously published procedure; optimized for identification of steroidal ligands of the GR.[21,13] *Saccharomyces cerevisiae* FY250 strain (MATα, ura3-52, his32Δ00, leu2Δ1, trp1Δ6) and expression vector pRF4-6-rGR LBD-EYFP were kindly provided by Dr. Blake Peterson from The University of Kansas.[22] Yeast cells were transformed with plasmid DNA by treatment with lithium acetate and polyethylene glycol, to improve the efficiency of exogenous DNA uptake, following the procedure of Gietz *et al.*[23] Transformed yeast cells were then incubated at 30 °C until the appearance of transformant colonies on agar plates. Selection medium supplemented with 2 % raffinose was then inoculated with recombinant yeast cells grown to saturation in a Biosan orbital shaker-incubator ES-20/60. Saturated yeast cells were diluted in fresh medium and grown to mid-logarithmic phase ($OD_{600\,nm} \approx$ 0.5), monitored using a Nicolet Evolution 100 UV–Vis spectrophotometer. Protein expression was induced by addition of galactose to a final concentration of 2 %. Bile acid derivatives, prednisolone or estradiol (high- and low-affinity GR ligands) were added to a final concentration of 100 μM. Stock solutions of all tested compounds were freshly prepared in DMSO. Incubation was continued for 15 h at 25 °C. Resulting fluorescence intensity was detected by

fluorimeter (Fluoroskan Ascent FL) and fluorescence microscopy (Olympus BX51) using a FITC filter. For fluorimetry, 150 μL of cell suspension was added to a microplate in triplicate and fluorescence was recorded using an excitation and emission filter set of 485 and 538 nm. Growth medium without cells served as a blank. To normalize fluorescence intensity to cell number, the optical density of yeast cells was measured at 600 nm using a Thermo Lab systems Multiscan EX spectrophotometer. Ligand binding affinity was calculated as the fold fluorescence change between cells exposed to test compounds and those treated with negative control ligand, estradiol. Histograms showing the relative binding affinity of bile acid derivatives and control ligands for GR-LBD were created in Origin Pro 8 with included error bars, obtained by propagation of standard error of the mean. Additionally, the fluorescence intensity distribution of recombinant yeast cells expressing GR LBD-YFP treated with bile acid derivatives or control compounds, was visualized by fluorescence microscopy.

Molecular docking

Coordinates for the GR-LBD receptor were converted to PDBQT format in the program VegaZZ using the available "receptor.c" script.[24] Structural coordinates for compounds **1**, **25**, **28** and **31** were created in the program Avogadro 1.0.3;[25] Avogadro: an open-source molecular builder and visualization tool based on the structure of dexamethasone, taken from PDB 1M2Z.[26] Ligand geometries were optimized in Avogadro 1.0.3 using an MMFF94 force field and 500 steps of conjugate gradient minimization with a convergence setting of 10e-7. Non-polar hydrogens were merged and gasteiger partial charges added in VEGAZZ 3.1.0,[27] using the "ligand.c" script, and resulting ligand coordinates were converted to PDBQT format for Autodock. Grid maps for atoms present in the tested compounds were created using the program AutoGrid, with a grid center of 31.04, 7.76, 12.52, grid spacing of 0.0375 nm and dielectric of –0.1465. Docking simulations in Autodock 4.2,[29] were conducted using the Lamarckian genetic algorithm with the following parameters: GA population size 150. GA num evaluations 250000. GA num generations 27000. AutoGrid calculations and Autodock simulations were conducted using the PyRx virtual screening tool (version 0.8).[27] Results were visualized in the program PyMol (v0.99).[28]

RESULTS AND DISCUSSION

Chemistry

Compounds used in the present study were chosen to examine the influence of easy-to-achieve modifications of the BA molecule on GR binding affinity. Structures of compounds investigated in the present work can be categorized into roughly seven categories: oximes, lactones, lactams, tetrazoles, dienones, C-24 alcohols and cholic acid amides.

Structures of oxime derivatives are shown in Fig. 1.

Synthesis of oximes **1** and **2** is shown in Scheme 1. The reaction of dehydrocholic acid (DCA) with hydroxylamine hydrochloride afforded a mixture of geometric isomers **1**, at the C-3 oxime group. The mixture of isomers **1** was obtained with a yield of 91 % and individual isomers were not separated. The isomer ratio of **1** could be speculated to be 3:2 based on the intensity of C-3 signals (156.87 and 156.67 ppm) present in ^{13}C-NMR spectra. Compound **2** was obtained in a two-step sequence. First, the carbonyl group at C-3 was regioselectively trans-

formed into acetal, while the carboxyl group was esterified which afforded **3** in excellent yield (93 %). This reaction represents a very good way for regioselective protection of the C-3 bile acid carbonyl group. Next, C-7 and C-12 carbonyl groups were converted into oxime to obtain dioxime **2**.

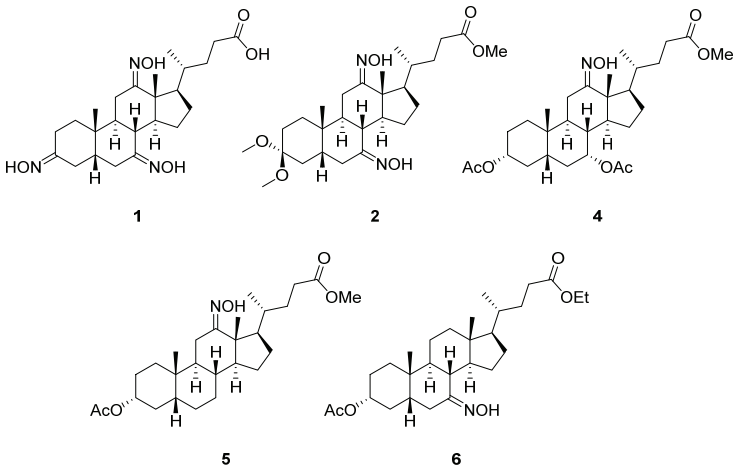

Fig. 1. Structures of oximes.

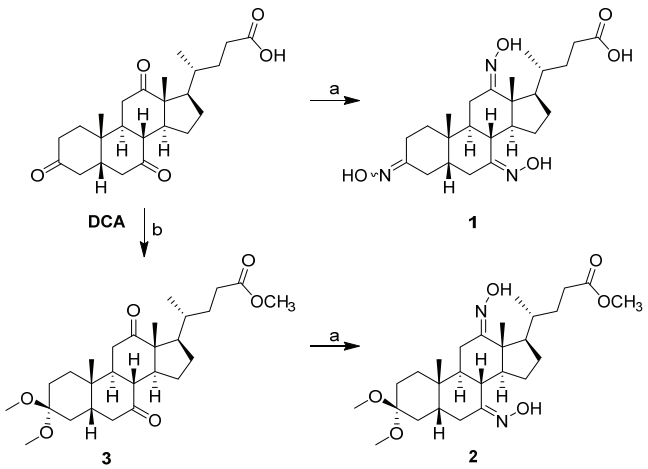

Scheme 1. Reagents and conditions: a) $NH_2OH \times HCl$, NaOAc, MeOH, 40 min, reflux; b) MeOH, 2,2-dimethoxypropane, TsOH, 3 h, reflux.

Unlike **1**, compound **2** was obtained as a stereochemically pure compound. The stereochemistry of oxime groups at C-7 and C-12 was determined as *Z*-based on the absence of cross-peaks in NOESY NMR spectra that originate from, the through space, interaction of oxime hydrogens with any steroid skeleton hydrogens. Only the *Z* configuration for the oxime groups could provide enough dis-

tance to explain the lack of NOE interactions. Stereochemistry could be explained by the larger volume available for hydroxyl groups if the oximes have a *Z* configuration (Fig. 2). Oximes **4**,[29] **5**[30] and **6**[31] were prepared by procedures found in the corresponding literature.

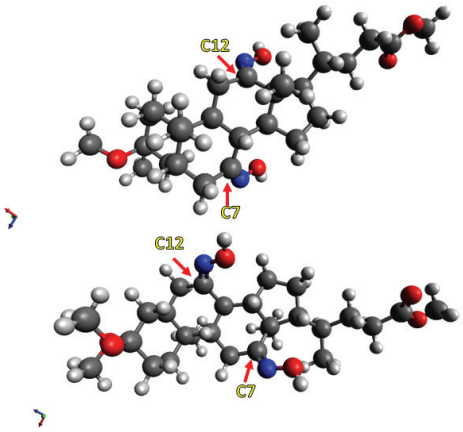

Fig. 2. Different perspectives of **2** show the available space for Z-oriented oxime groups at C-7 and C-12.

Bile acid derivatives with a lactone or lactam moiety in B or C steroid ring (Fig. 3) **7**–**14** were synthesized according to published procedures,[31–33] while the stereochemistry and physicochemical properties of these compounds were described by Poša *et al.*[34]

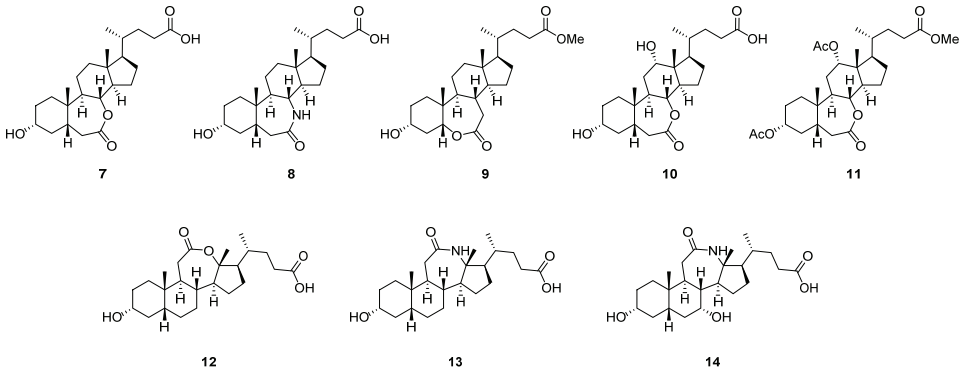

Fig. 3. Structures of bile acid lactone and lactam derivatives **7**–**14**.

The structures of tetrazoles **15**–**23** used in the present work are shown in Fig. 4. Tetrazole rings are fused on B and C steroid rings.

The general synthesis of tetrazole compounds is shown in Scheme 2, using the synthesis of **16** as an example. Bile acid derivative **24**, with C-3 acetoxy, C-24 ethoxycarbonyl groups, and a carbonyl group at C-12, was subjected to Schmidt reaction condition (Scheme 2) with trimethylsilyl azide as an azide source and tri-

methylsilyl trifluoromethanesulfonate as an amide intermediate activator. Details of the synthesis of the tetrazole compounds used in the present study have been published by our group.[35]

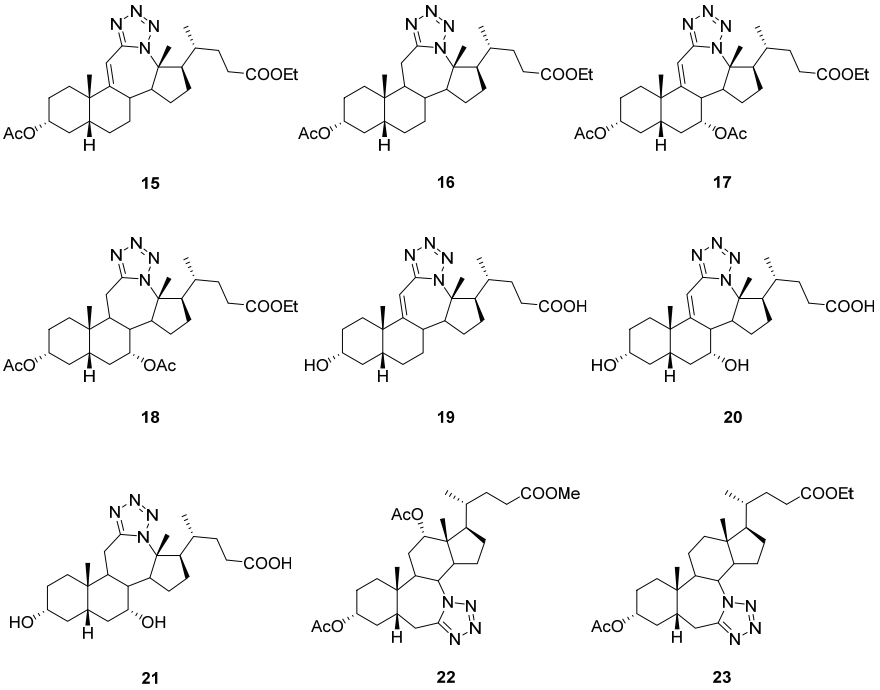

Fig. 4. Structures of the bile acid tetrazole derivatives **15**–**23**.

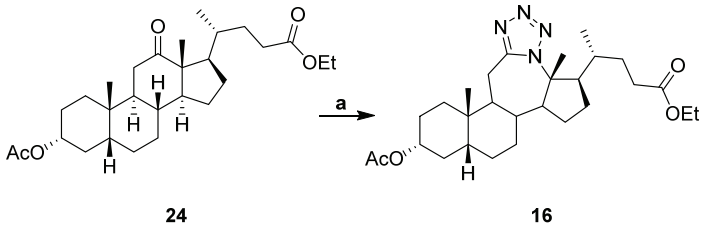

Scheme 2. The general synthesis of tetrazole compounds **15**–**23** is illustrated using the synthesis of **16** as an example. Reagents and conditions: $TMSN_3$, TMSOTf, ACN, rt, 3 h (a).

Structures of dienones **25** and **26**, alcohols **28** and **29** and amides **30** and **31** are shown in Fig. 5.

Dienones **25** and **26** were obtained by the following procedures: when compound **27** (Scheme 3) was refluxed in methanolic potassium hydroxide solution, elimination and hydrolysis occurred to afford **25** at a yield of 90 % (78 % reported by Leppik *et. al.*[18]). Reaction samples were collected every 5 min and since

only one product was detectable by TLC, it appears that both elimination and hydrolysis reactions occur simultaneously. The same result was obtained upon treatment of **27** with methanolic KOH solution for five days at room temperature, or 2 M NaOH solution for five hours at room temperature, or by reflux with HCl solution (1:3) in water/acetone 5/7 for five hours. When ethanol was used instead of methanol, in addition to **25** (28 %), transesterification occurs to afford ethyl ester **26** (67 %). Signals corresponding to vinylic protons in **25** are easily visible by ^{1}H-NMR as overlapping singlet peaks of H-4 and H-6 at 6.16 ppm, and a singlet from H-7 at 5.61 ppm. An additional quartet at 4.03 and a triplet at 1.16 in the ^{1}H-NMR of **26** suggests the presence of an esterified carboxyl group.

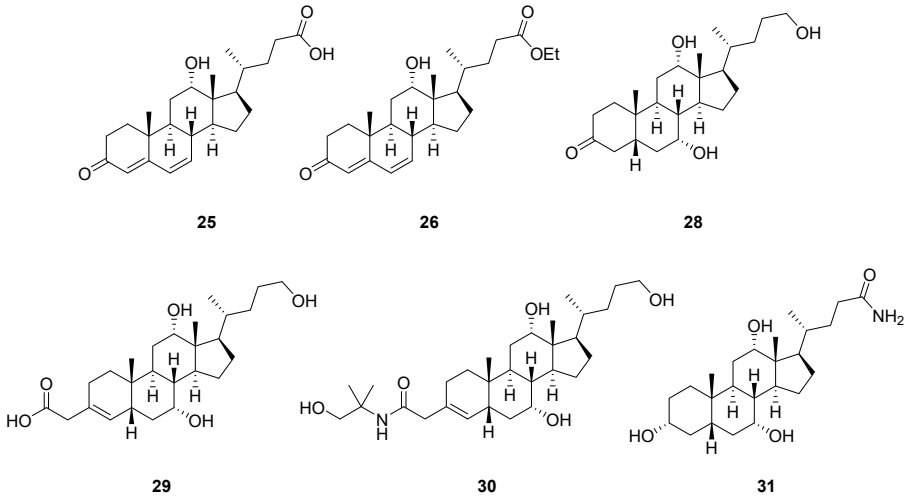

Fig. 5. Structures of dienone, alcohol and amide derivatives **25**, **26**, **28**–**31**.

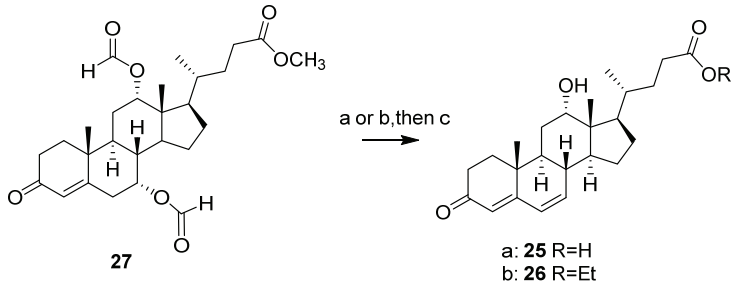

Scheme 3. Reagents and conditions: a) KOH, MeOH, 0.5 h, reflux; b) KOH, EtOH, 1 h, reflux; c) HCl, H_2O.

Easily obtainable and well-known 3-dehydrocholic acid (3DCA) was transformed into the bile alcohol **28** using acetal protection as seen in **3**, and subsequent reduction (Scheme 4). The same bile alcohol **28** was transformed into **29**

using a Wittig–Horner–Emmons reaction. Details concerning the synthesis of **28** and **29** are available in our previous publication.[16]

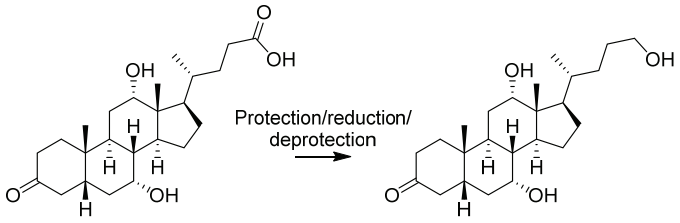

3DCA **28**

Scheme 4. Synthesis of bile alcohol **28**.

Compound **30** was obtained in the good yield (75 %) by reaction of **29** with 2-amino-2-methyl-1-propanol using EEDQ as a coupling agent (Scheme 5).

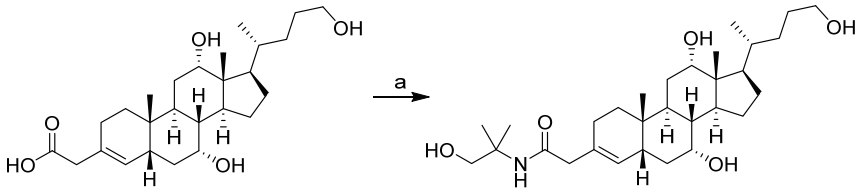

29 **30**

Scheme 5. Reagents and conditions: 2-Amino-2-methyl-1-propanol, EEDQ, TEA, EtOAc, 5 h, reflux (a).

The cholic acid amide **31** (Fig. 5) was synthesized according to a procedure reported by Miljković *et al.*[36]

Fluorescent assay in yeast

In order to test the relative binding affinities of the synthesized BA derivatives, we used a yeast-based fluorescent screen that is optimized for identification of steroidal ligands of the glucocorticoid receptor, as previously described.[13,21] Briefly, the fluorescence intensity of yeast cells expressing the ligand-binding domain (LBD) of the glucocorticoid receptor (GR) fused to a yellow fluorescent protein (YFP) has been shown to respond in a dose-dependent manner to treatment with GR agonists such as prednisolone.[13,21] Because the assay is measured in yeast, the concentration of ligand required to elicit a response may not necessarily be the same concentration that would affect GR activity *in vivo*. During optimization of the assay, we measured dose response for a positive control ligand (prednisolone, Fig. S-1 of the Supplementary material). As assay sensitivity was highest at a final prednisolone concentration of 100 μM, bile acid derivatives were tested at 100 μM. In the present study, bile acid derivatives **1**, **2**, **4**–**23** and **25**–**31** were tested against GR-LBD, by mea-

suring fold fluorescence changes between cells exposed to test compounds compared with those treated with a negative control ligand, E2 (estradiol), or a positive control GR agonist (prednisolone). It can be seen in Fig. 6, that bile acid derivatives **1**, **25**, **28** and **31** displayed fold fluorescence changes indicative of moderate binding affinity for GR-LBD compared with prednisolone or estradiol.

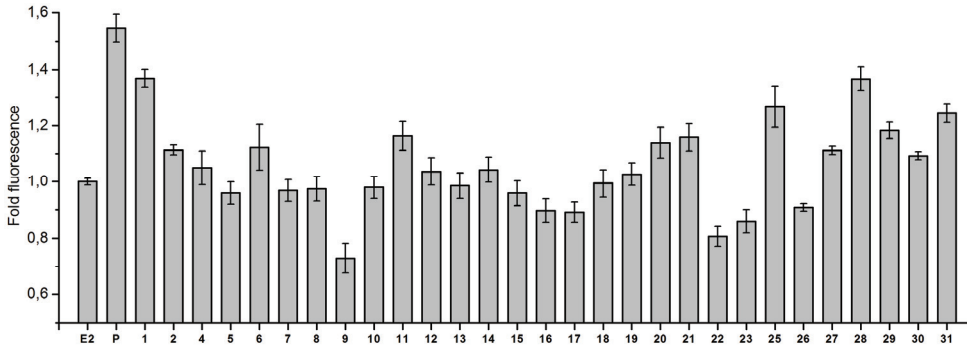

Fig. 6. Bile acid derivatives **1**, **25**, **28** and **31** showed fold fluorescence changes consistent with moderate binding affinity for GR-LBD-YFP based on a fluorescent screen in yeast following 15 h exposure at a final concentration of 100 μM. Ligand binding affinity was calculated as the fold fluorescence change between cells exposed to test compounds compared with those treated with negative control ligand, E2 (estradiol), measured by fluorimetry. Prednisolone (P) was tested as a positive control GR agonist.

To validate these results, yeast cells treated with the same compounds were also visualized by fluorescence microscopy. As can be seen in Fig. 7, treatment of recombinant yeast expressing GR-LBD-YFP with the GR agonist prednisolone resulted in a strong increase and relocalization of fluorescence intensity, while treatment with compounds **1**, **25**, **28** and **31** resulted in a more moderate increase in overall fluorescence intensity compared to cells treated with negative control estradiol.

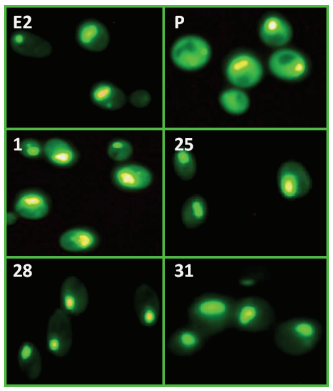

Fig. 7. Recombinant yeast cells expressing GR-LBD-YFP treated with 100 μM estradiol (E2, negative control GR ligand), prednisolone (P, positive control GR ligand) or test BA derivatives **1, 25**, **28** and **31** for 15 h, visualized using a fluorescence microscope. The intensity of cell fluorescence is proportional to GR ligand binding affinity.

Molecular docking

Based on fluorescent screening in yeast, compounds **1**, **25**, **28** and **31** have moderate binding affinity for GR-LBD compared with prednisolone, a strong GR agonist. To visualize these results in a molecular framework, binding poses and binding energies were predicted for compounds **1**, **25**, **28** and **31** by molecular docking in the program Autodock.[37] Because the structure of GR in complex with prednisolone has not been published, coordinates for GR-LBD in complex with another GR agonist, dexamethasone (PDB 1M2Z), were used as 'receptor' for docking.[26] For all docking simulations, the receptor was kept rigid and the ligand was allowed to rotate around flexible bonds. To validate the Autodock protocol for our system, control redocking simulations were conducted using dexamethasone as a positive control "ligand". Autodock correctly reproduced the X-ray structure with an *RMSD* of < 0.06 nm^2 and a strong binding energy of –57.20 kJ/mol. Based on the X-ray structure, dexamethasone (DEX) is in part held oriented in the GR ligand binding site via polar contacts with arginine 611, glutamine 570 and asparagine 564. As can be seen in Fig. 8, very similar binding poses and intermolecular contacts are formed by test compounds **28**, **25** and **31**.

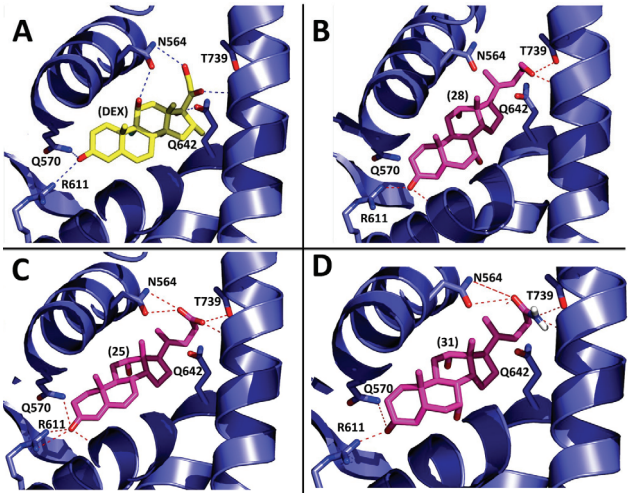

Fig. 8. Molecular docking poses and predicted binding affinities for test compounds **25**, **28** and **31** compared with dexamethasone (DEX), a positive control GR ligand. The X-ray structure of GR ligand binding domain in complex with dexamethasone (PDB 1M2Z) was used as receptor for Autodock simulations. Top ranking poses for the following compounds are shown: A) dexamethasone, B) **28**, C) **25** and D) **31**.

All three compounds bind in the same orientation, forming interactions with Asn564, Thr739 and Gln642 from the D-ring side, and Arg611 and Gln570 from the A-ring side of these BA derivatives. Consistent with experimental results, moderate binding energies of <−41.84 kJ/mol were predicted for each of these

test compounds: for compound **25**, −46.36 kJ/mol; compound **28** −45.94 kJ/mol, and compound **31** −42.16 kJ/mol. None of the test compounds had a predicted binding affinity greater than prednisolone, as expected. Interestingly, although compounds **1** displayed moderate affinity for GR-LBD in fluorescence experiments, docking of C-3 *Z*-isomer of **1** failed to predict binding to GR under the simulation conditions used. In general, Autodock is capable of correctly predicting the binding affinity and geometry for a set of compounds if ligand binding is not associated with significant backbone and side chain conformational changes.[37] Thus, binding by compound **1** likely induces conformational changes to the GR active site that are different from the GR conformation present in complex with dexamethasone, preventing Autodock from correctly estimating the binding pose and affinity for compound **1**. For compounds **25**, **28** and **31**, molecular docking results could be used in future studies as a starting point to design molecules with increased binding affinity, and/or specificity for GR-LBD.

CONCLUSION

Compounds used in the present work were designed to examine the influence of specific functionality modifications of BAs on their GR binding properties. Bile acids have a suitably functionalized steroid skeleton for modification in strategic regions for GR interactions. Our glucocorticoid receptor binding assay provided insight into structural features important for binding of the tested molecules to GR. The results of the SAR analysis are shown in Fig. 9.

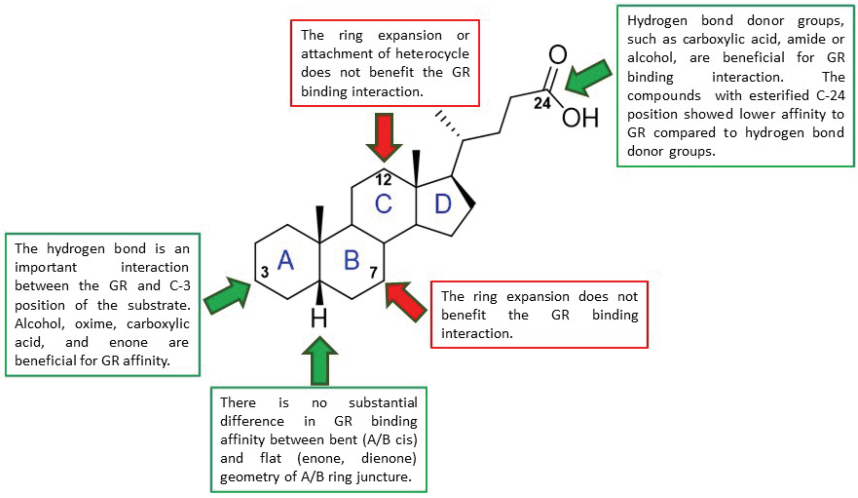

Fig. 9. Results of SAR analysis.

Four differently functionalized compounds **1**, **25**, **28** and **31** showed moderate binding affinity for GR-LBD compared with prednisolone or estradiol. The oxime geometric isomers in **1** showed the best relative binding affinity, not just among

tested oximes but among all tested compounds. Although we were not able to separate the geometric isomers in mixture **1** and molecular docking did not enable prediction of possible interactions with the enzyme, binding affinity could be attributed to the C-24 carboxylic group and oxime groups. The hydroxyl group at C-11 with β orientation (11β-OH) has been previously shown to be very important for GR-glucocorticoid interactions,[38] and the relative binding affinities measured for **1** suggest that the C-12 oxime group could be exploited as an alternative hydrogen bond donor to the 11β-OH group. Lactone, lactam, and tetrazole derivatives did not show any significant binding affinity. It seems that the B or C steroid ring expansion or attachment of heterocycle at the C ring is not beneficial for binding affinities. Compounds **28**, **25** and **26** have a keto or enone moiety, which is known to be involved in anchoring steroids in the receptor pocket.[39] However, it seems that the hydrogen bond donating group at C-24 is very important for binding to GR. This was observed for all of the tested compounds. Ethyl ester **26** has a much smaller GR binding affinity compared to free acid **25**. Compound **28** with the C-3 keto and C-24 hydroxyl group has a GR binding affinity similar to **1**, among the best of the tested compounds. There is a degree of plasticity in the GR-LBD for the steroid A-ring and C-3 functional groups, since compounds **1** with C-3 oxime *E* and *Z* groups; **29**, with carboxymethyl group at C-3, and even compound **30** with the corresponding amide at C-3 have moderate or less than moderate GR-LBD binding affinity. This work gives important insight into structural modification of bile acid steroid skeleton that could be used for development of new small molecule drug for treatment of inflammatory diseases.

SUPPLEMENTARY MATERIAL

Additional data and information are available electronically at the pages of journal website: https://www.shd-pub.org.rs/index.php/JSCS/article/view/12062, or from the corresponding author on request.

Acknowledgements. The authors acknowledge financial support from the Ministry of Education, Science and Technological Development of the Republic of Serbia (Grant No. 451-03-9/2021-14/ 200125).

ИЗВОД

ИСПИТИВАЊЕ АФИНИТЕТА ДЕРИВАТА ЖУЧНИХ КИСЕЛИНА ЗА ВЕЗИВАЊЕ ЗА ЛИГАНД-ВЕЗУЈУЋИ ДОМЕН ГЛУКОКОРТИКОИДНОГ РЕЦЕПТОРА

СРЂАН БЈЕДОВ[1], СОФИЈА БЕКИЋ[2], МАЈА МАРИНОВИЋ[2], ДУШАН ШКОРИЋ[1], КСЕНИЈА ПАВЛОВИЋ[1], АНЂЕЛКА ЋЕЛИЋ[2], ЕДВАРД ПЕТРИ[2] и МАРИЈА САКАЧ[1]

[1]*Департман за хемију, биохемију и заштиту животне средине, Природно–математички факултет, Универзитет у Новом Саду, Трг Доситеја Обрадовића 3, 21000, Нови Сад и* [2]*Департман за биологију и екологију, Природно–математички факултет, Универзитет у Новом Саду, Трг Доситеја Обрадовића 3, 21000, Нови Сад*

Антиинфламаторни лекови као што су глукокортикоиди били су неопходни током пандемије COVID-19 за лечење пацијената са умереним и тешким облицима COVID-19. Међутим, озбиљни нежељени ефекти ограничавају употребу ових лекова и хитно су пот-

ребни антиинфламаторни лекови са бољим фармаколошким својствима. Жучне киселине привлаче све више интереса, због својих антиинфламаторних и имуномодулаторних својстава, испољених засад нејасним механизмом који укључује трансмембранске и нуклеарне рецепторе. У овом раду смо испитали афинитет везивања низа деривата жучних киселина за лиганд-везујући домен глукокортикоидног рецептора (GR-LVD), најважнијег рецептора за антиинфламаторне процесе. Испитивана једињења укључују оксиме, лактоне, лактаме, тетразоле, диеноне, C-24 алкохоле и амид холне киселине. Међу тестираним једињењима: оксим холне киселине, диенон деоксихолне киселине, 3-кето-24-алкохол и амид холне киселине показали су најбоље афинитете везивања за GR-LVD. Објашњење везивања поменутих деривата помогли су *in silico* доковање. Анализа односа структуре и активности је показала да експанзија B и C стероидних прстенова или везивање хетероцикла за C прстен није од користи за везивање; бочни ланац треба да садржи водоник-донорску групу; и GR-LVD добро толеришу различите функционалности на позицији C-3. Ови резултати пружају вредне информације за прављење нових антиинфламаторних молекула базираних на жучним киселинама.

(Примљено 12. септембра, ревидирано 22. септембра, прихваћено 28. септембра 2022)

REFERENCES

1. N. Sundahl, J. Bridelance, C. Libert, K. De Bosscher, I. M. Beck, *Pharmacol. Ther.* **152** (2015) 28 (https://doi.org/10.1016/j.pharmthera.2015.05.001)
2. F. Buttgereit, R. H. Straub, M. Wehling, G. R. Burmester, *Arthritis Rheumatol*. **50** (2004) 50 3408 (https://doi.org/10.1002/art.20583)
3. RECOVERY collaborative group*, *N. Engl. J. Med*. **384** (2021) 693 (https://doi.org/10.1056/NEJMoa2021436)
4. J. Souffriau, M. Eggermont, S. Van Ryckeghem, K. Van Looveren, L. Van Wyngene, E. Van Hamme, M. Vuylsteke, R. Beyaert, K. De Bosscher, C. Libert, *Sci. Rep.* **8** (2018) 12894. (https://doi.org/10.1038/s41598-018-31150-w)
5. J. Vandewalle, A. Luypaert, K. De Bosscher, C. Libert. *Trends Endocrinol. Metab*. **29** (2018) 42 (https://doi.org/10.1016/j.tem.2017.10.010)
6. A. Louw. *Front. Immunol.* **10** (2019) 1693 (https://doi.org/10.3389/fimmu.2019.01693)
7. E. Lontchi-Yimagou, E. Sobngwi, T. E. Matsha, A. P. Kengne. *Curr. Diab. Rep*. **13** (2013) 435 (https://doi.org/10.1007/s11892-013-0375-y)
8. P. S. Hench. *Br. Med. J.* **20** (1938) 394 (https://doi.org/10.1136/bmj.2.4050.394)
9. The Nobel Prize, https://www.nobelprize.org/prizes/medicine/1950/summary/ (20.06.2022.)
10. R. M. Gadaleta, M. Cariello, C. Sabbà, A. Moschetta, *Biochim. Biophys. Acta* **1851** (2015) 30 (https://doi.org/10.1016/j.bbalip.2014.08.005)
11. J. Hageman, H. Herrema, A. K. Groen, F. Kuipers, *Arterioscler. Thromb. Vasc. Biol.* **30** (2010) 1519 (https://doi.org/10.1161/ATVBAHA.109.197897)
12. A. Perino, K. Schoonjans, *Trends. Pharmacol. Sci.* **12** (2015) 847 (https://doi.org/10.1016/j.tips.2015.08.002)
13. B. Vasiljević, E. Petri, S. Bekić, A Ćelić, Lj. Grbović, K. Pavlović, *RSC Med. Chem.* **12** (2021) 278 (https://doi.org/10.1039/D0MD00311E)

* Complete list of collaborators in the RECOVERY trial is available at: https://www.nejm.org/doi/suppl/10.1056/NEJMoa2021436/suppl_file/nejmoa2021436_appendix.pdf

14. L. Li, C. Liu, W. Mao, B. Tumen, P. Li, *Molecules* **24** (2019) 4513. (https://doi.org/10.3390/molecules24244513)
15. T. Takigawa, H. Miyazaki, M. Kinoshita, N. Kawarabayashi, K. Nishiyama, K. Hatsuse, S. Ono, D. Saitoh, S. Seki, J. Yamamoto, *Am. J. Physiol. Gastrointest. Liver Physiol*. **305** (2013) G427 (https://doi.org/10.1152/ajpgi.00205.2012)
16. M. Poša, S. Bjedov, V. Tepavčević, M. Mikulić, M. Sakač, *J. Mol. Liq*. **303** (2020) 112634 (https://doi.org/10.1016/j.molliq.2020.112634)
17. M. N. Iqbal, W. H. Elliott, *Steroids* **53** (1989) 413 (https://doi.org/10.1016/0039-128X(89)90022-6)
18. R. Leppik, *Steroids* **41** (1983) 475 (https://doi.org/10.1016/0039-128X(83)90087-9)
19. R. Hüttenrauch, *Arch. Pharm. Pharm. Med. Chem*. **294** (1961) 366 (https://doi.org/10.1002/ardp.19612940608)
20. K. Tamaki, *J. Biochem*. **45** (1958) 299 (https://doi.org/10.1093/oxfordjournals.jbchem.a126869)
21. S. Bekić, M. Marinović, E. Petri, M. Sakač, A. Nikolić, V. Kojić, A. Ćelić, *Steroids* **130** (2018) 22 (https://doi.org/10.1016/j.steroids.2017.12.002)
22. S. Muddana, B. Peterson, *Chembiochem*. **4** (2003) 848 (https://doi.org/10.1002/cbic.200300606)
23. D. Gietz, A. St Jean, R. A. Woods, R. H. Schiestl, *Nucleic. Acids. Res*. **20** (1992) 1425. (https://doi.org/10.1093/nar/20.6.1425)
24. S. Dallakyan, A. J. Olson, *Methods. Mol. Biol*. **1263** (2015) 243 (https://doi.org/10.1007/978-1-4939-2269-7_19)
25. M. D. Hanwell, D. E. Curtis, D. C. Lonie, T. Vandermeerschd, E. Zurek, G. R. Hutchison, *J. Cheminform*. **17** (2012) (https://doi.org/10.1186/1758-2946-4-17)
26. R. K. Bledsoe, V. G. Montana, T. B. Stanley, C. J. Delves, C. J. Apolito, D. D. McKee, T. G. Consler, D. J. Parks, E. L. Stewart, T. M. Willson, M. H. Lambert, J. T. Moore, K. H. Pearce, H. E. Xu, *Cell* **110** (2002) 93 (https://doi.org/10.1016/s0092-8674(02)00817-6)
27. A. Pedretti, A. Mazzolari, S. Gervasoni, L. Fumagalli, G. Vistoli, *Bioinformatics* **37** (2021) 1174 (https://doi.org/10.1093/bioinformatics/btaa774)
28. PyMOL, http://www.pymol.org/pymol (15.09.2021.)
29. N. Meanwell, H. Roth, E. Smith, D. Wedding, and J. Kim Wright, *J. Org. Chem.* **56** (1991) 6897 (https://doi.org/10.1021/jo00024a036)
30. Y. Huang, J. Cui, S. Chen, C. Gan, Q. Yao, Q. Lin, *Bioorg. Med. Chem. Lett.* **23** (2013) 2265 (https://doi.org/10.1016/j.bmcl.2012.08.064)
31. H. H. Abdu-Allah, T. T. Chang, W. S. Li, *Steroids* **112** (2016) 54 (https://doi.org/10.1016/j.steroids.2016.04.013)
32. I. S. Zharinova, A. A. Bilyalova, S. I. Bezzubov, *Acta Crystallogr., E* **74** (2018) 816 (https://doi.org/10.1107/S2056989018007259)
33. M. I. Duran, C. González, A. Acosta, A. F. Olea, K. Díaz, L. Espinoza, *Int. J. Mol. Sci*. **8** (2017) 516 (https://doi.org/10.3390/ijms18030516)
34. M. Poša, V. Tepavčević, Lj. Grbović, M. Mikulić, K. Pavlović, *J. Phys. Org. Chem*. **34** (2021) e4133 (https://doi.org/10.1002/poc.4133)
35. D. Škorić, O. Klisurić, S. Jakimov, M. Sakač, J. Csanádi, *Beilstein J. Org. Chem.* **17** (2021) 2611 (https://doi.org/10.3762/bjoc.17.174)
36. D. Milijkovic, K. Kuhajda, J. Hranisavljevic, *J. Chem. Res.* **2** (1996) 106 (https://open.uns.ac.rs/handle/123456789/12941)
37. G. M. Morris, R. Huey, W. Lindstrom, M. Sanner, R. Belew, D. Goodsell, A. Olson, *J. Comput. Chem*. **16** (2009) 2785 (https://doi.org/10.1002/jcc.21256)

38. T. Mitić, S. Shave, N. Semjonous, I. McNae, D. Cobice, G. Lavarey, S. Webster, P. Hadkoe, B. Walker, R. Andrew, *Biochem. Pharmacol*. **86** (2013) 146 (https://doi.org/10.1016/j.bcp.2013.02.002)
39. U. Lind, P. Greenidge, M. Gillner, K. F. Koehler, A. Wright, J. Carlstedt-Duke, *J. Biol. Chem*. **275** (2000) 19041 (https://doi.org/10.1074/jbc.M000228200).

Journal of the Serbian Chemical Society
JSCS@tmf.bg.ac.rs • www.shd.org.rs/JSCS
J. Serb. Chem. Soc. 88 (2) S51–S59 (2023) *Supplementary material*

SUPPLEMENTARY MATERIAL TO

Screening the binding affinity of bile acid derivatives for the glucocorticoid receptor ligand-binding domain

SRĐAN BJEDOV[1]*#, SOFIJA BEKIĆ[2#], MAJA MARINOVIĆ[2], DUŠAN ŠKORIĆ[1#], KSENIJA PAVLOVIĆ[1#], ANĐELKA ĆELIĆ[2], EDWARD PETRI[2] and MARIJA SAKAČ[1#]

[1]*Department of Chemistry, Biochemistry and Environmental Protection, Faculty of Sciences, University of Novi Sad, Trg Dositeja Obradovića 3, 21000, Novi Sad, Serbia and* [2]*Department of Biology and Ecology, Faculty of Sciences, University of Novi Sad, Trg Dositeja Obradovića 2, 21000, Novi Sad, Serbia*

J. Serb. Chem. Soc. 88 (2) (2023) 123–139

(3EZ, 7Z, 12Z)-3,7,12-Trioximino-5β-cholan-24-oic acid (1)

^{1}H NMR (400 MHz, DMSO-d_6, δ) 10.30 and 10.28 (s, 1H, NOH on C-7), 10.19 and 10.18 (s, 1H, NOH on C-3), 10.14 (s, 1H, NOH on C-12), 1.13-1.12 (overlapping singlets, 3H, H-19), 0.89-0.88 (overlapping doublet (H-21) and singlet (H-18), 6H). ^{13}C NMR (101 MHz, DMSO-d_6, δ) 175.38 (C-24), 162.61(C-12), 157.41 (C-7), 156.87 (C-3), 156.67 (C-3), 53.57, 53.54, 49.23, 46.42, 45.21, 44.07, 43.94, 43.84, 41.52, 36.71, 36.67, 36.29, 35.72, 35.15, 32.76, 31.95, 30.96, 27.72, 27.44, 27.33, 26.39, 25.57, 25.42, 22.50 (C-19), 22.39 (C-19), 20.14, 19.86 (C-21), 19.32, 12.59 (C-18). (+)ESI-HRMS (*m*/*z*): calculated for $C_{24}H_{37}N_3O_5$ $[M+Na]^+$ 470.26309, found 470.26093.

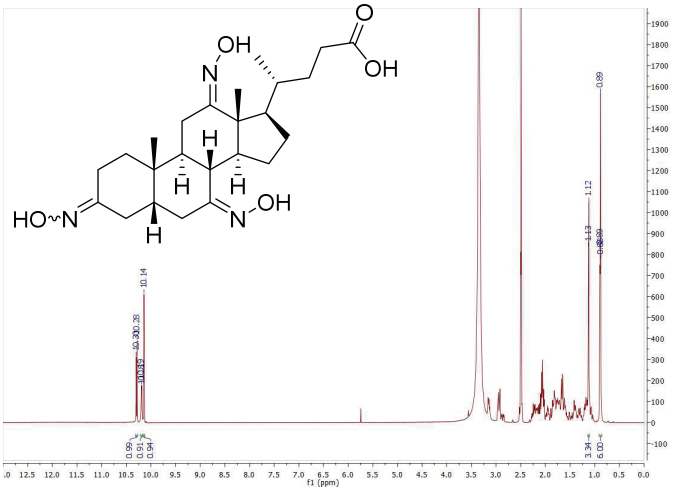

* Corresponding author. E-mail: srdjan.bjedov@dh.uns.ac.rs

Fig. S-1. Compound **1** ^{1}H NMR (400 MHz, DMSO-d_6) spectra.

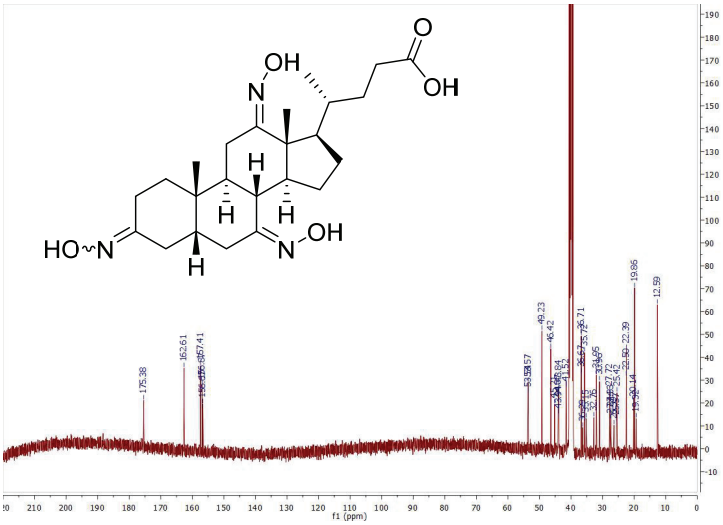

Fig. S-2. Compound **1** ^{13}C NMR (101 MHz, DMSO-d_6) spectra.

Methyl (7Z,12Z)-3,3-dimethoxy-7,12-dioximino-5β-cholan-24-oate (2)

^{1}H NMR (400 MHz, DMSO-d_6, δ) 10.21 (s, 1H, NOH on C-7), 10.11 (s, 1H, NOH on C-12), 3.56 (s, 3H, CH_3 ester), 3.01 (s, 3H, OCH_3), 3.00 (s, 3H, OCH_3), 1.09 (s, 3H, H-19), 0.87 (d, J = 6.8 Hz, 3H, H-21), 0.86 (s, 3H, H-18).^{13}C NMR (101 MHz, DMSO-d_6, δ) 174.17 (C-24), 162.71 (C-12), 157.75 (C-7), 100.07 (C-3), 53.68, 51.67 (CH_3 ester), 49.18, 47.32 (overlapping OCH_3 signals), 46.30, 44.00, 42.06, 41.56, 39.42, 36.16, 35.76, 33.97, 32.60, 31.50, 30.88, 27.80, 27.29, 25.40, 22.69 (C-19), 20.15, 19.75 (C-21), 12.50 (C-18). (+)ESI-HRMS (m/z): calculated for $C_{27}H_{44}N_2O_6$ $[M+Na]^+$ 515.30970, found 515.30725.

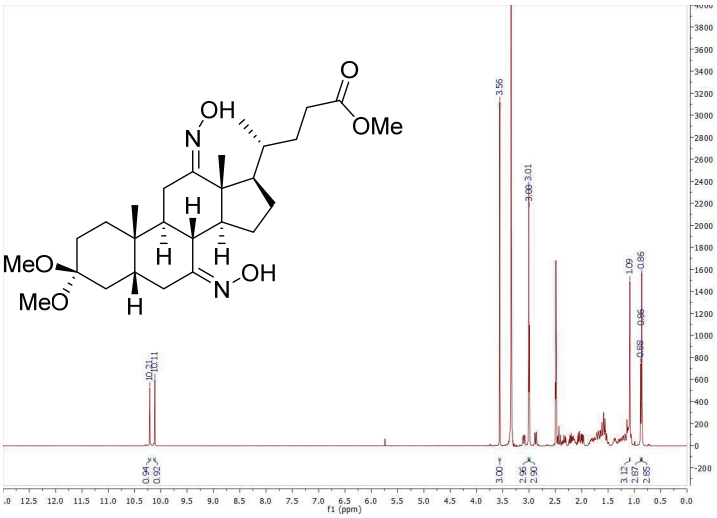

Fig. S-3. Compound **2** 1H NMR (400 MHz, DMSO-d_6) spectra.

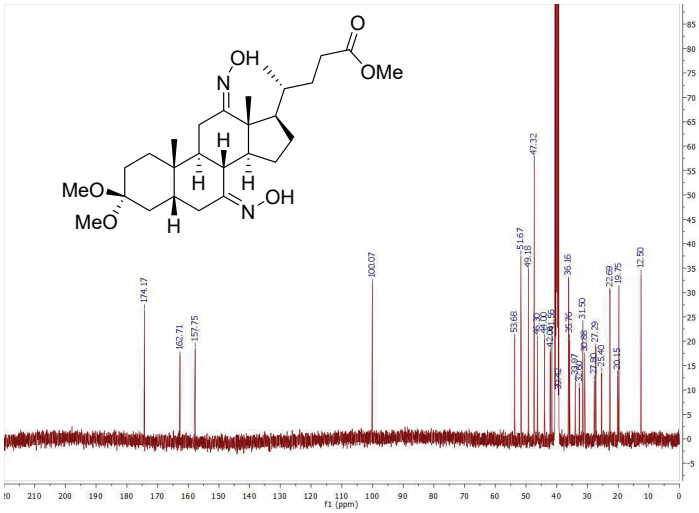

Fig. S-4. Compound **2** ^{13}C NMR (101 MHz, DMSO-d_6) spectra.

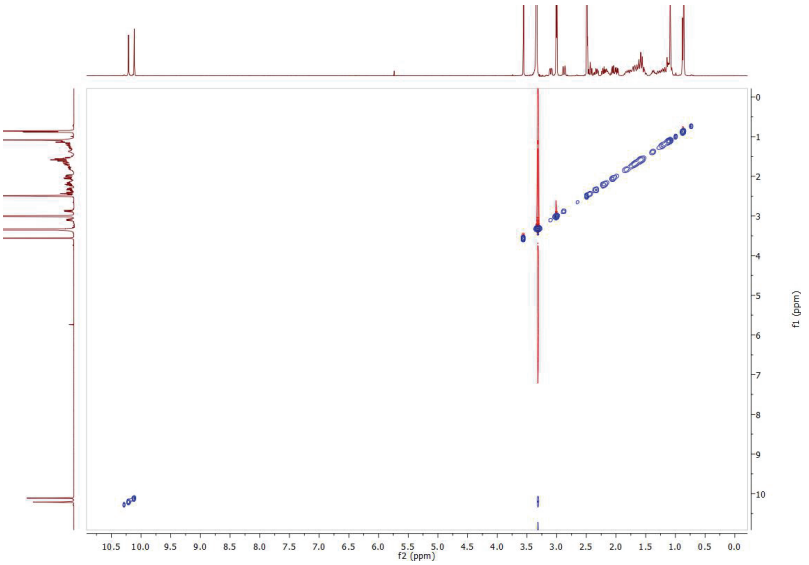

Fig. S-5. Compound **2** NOESY NMR spectra.

Methyl 3,3-dimethoxy-7,12-dioxo-5β-cholan-24-oate (3)

^{1}H NMR (400 MHz, $CDCl_3$, δ) δ 3.65 (s, 3H, CH_3 ester), 3.13 (s, 3H, OCH_3), 3.10 (s, 3H, OCH_3), 1.29 (s, 3H, H-19), 1.02 (s, 3H, H-18), 0.82 (d, J = 6.6 Hz, 3H, H-21).^{13}C NMR (101 MHz, $CDCl_3$, δ) 212.53 (C-12), 209.71 (C-7), 174.56 (C-24), 99.75 (C-3), 56.81, 51.80, 51.47 (CH_3 ester), 48.94, 47.64 (OCH_3), 47.41 (OCH_3), 45.55, 45.21, 45.09, 43.40, 38.55, 36.03, 35.53, 34.65, 31.89, 31.29, 30.46, 27.66, 26.60, 25.17, 22.35 (C-19), 18.61 (C-21), 11.79 (C-18). (+)ESI-HRMS (*m*/*z*): calculated for $C_{27}H_{42}O_6$ $[M+Na]^+$ 485.28791, found 485.28558.

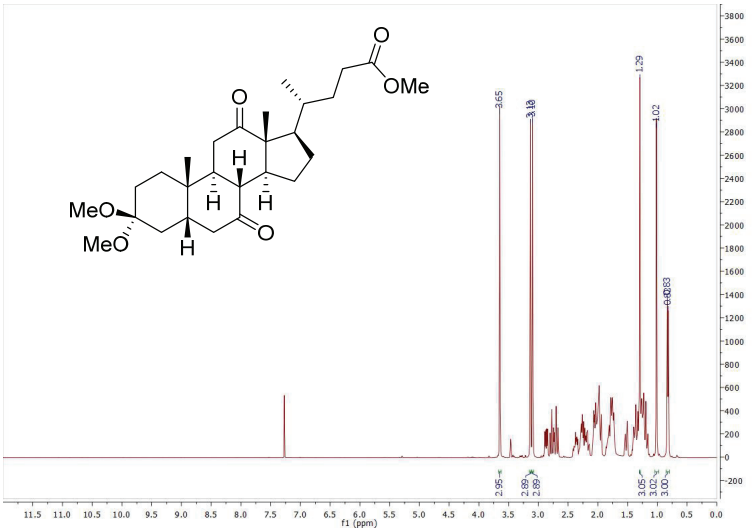

Fig. S-6. Compound **3** ^{1}H NMR (400 MHz, $CDCl_3$) spectra.

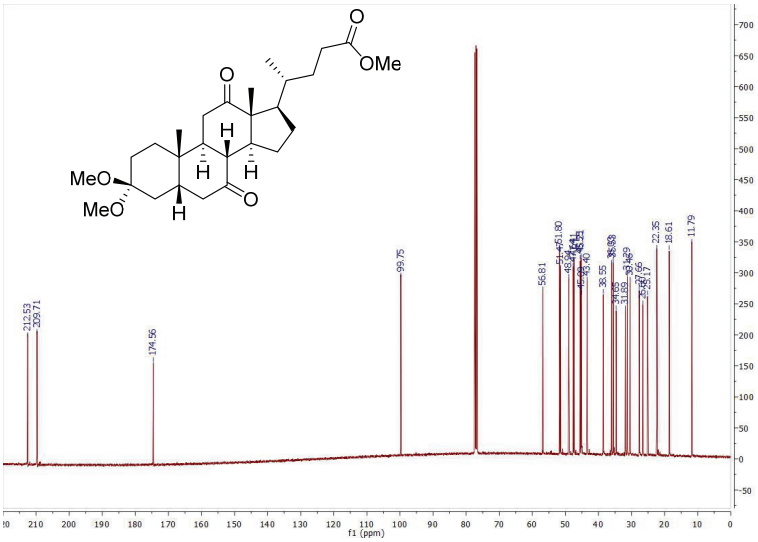

Fig. S-7. Compound **3** ^{13}C NMR (101 MHz, $CDCl_3$) spectra.

12α-Hydroxy-3-oxo-5β-chola-4,6-dien-24-oic acid (25)

^{1}H NMR (400 MHz, DMSO-d_6, δ) 11.95 (bs, 1H, H-24), 6.16 (s, 2H, H-4 and H-6), 5.61 (s, 1H, H-7), 4.31 (d, J = 3.6 Hz, 1H, OH), 3.87 (s, 1H, H-12), 1.04 (s, 3H, H-19), 0.94 (d, J = 6.5 Hz, 1H, H-21), 0.71 (s, 3H, H-18). ^{13}C NMR (101 MHz, DMSO-d_6, δ) δ 198.63 (C-3), 175.42 (C-24), 163.96 (C-5), 142.02 (C-4), 127.90 (C-6), 123.28 (C-7), 70.97 (C-12), 47.28, 46.54, 45.25, 43.71, 37.82, 35.55, 35.38, 34.02, 33.74, 31.31, 31.17, 28.67, 27.43, 23.31, 17.34 (C-21), 16.29 (C-19), 12.53 (C-18). IR (film, cm^{-1}): 3436, 2923, 1733, 1379, 1261. (+)ESI-HRMS (*m/z*): calculated for $C_{24}H_{34}O_4$ $[M-H]^-$ 387.25353, found 387.25246.

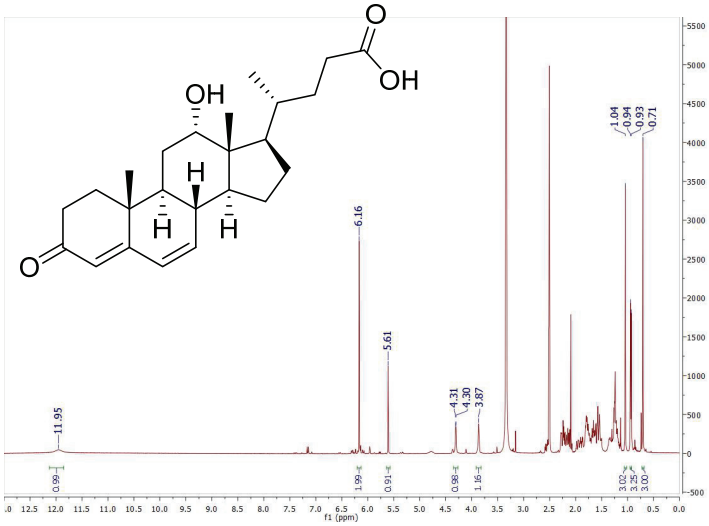

Fig. S-8. Compound **25** ^{1}H NMR (400 MHz, DMSO-d_6) spectra.

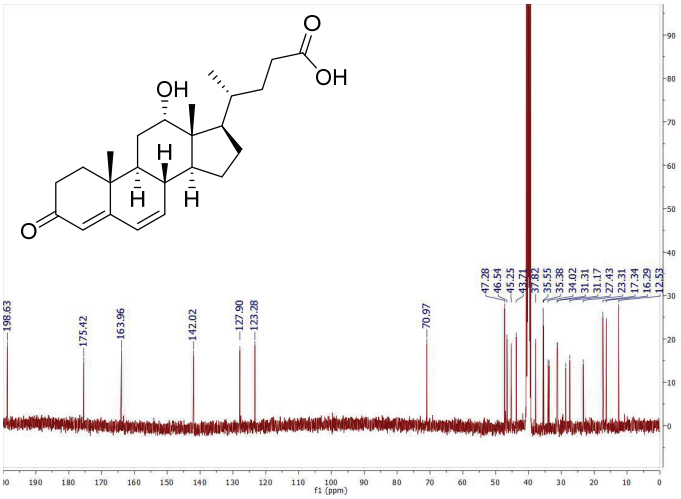

Fig. S-9. Compound **25** ^{13}C NMR (101 MHz, DMSO-d_6) spectra.

Ethyl 12α-hydroxy-3-oxo-5β-chola-4,6-dien-24-oate (26)

^{1}H NMR (400 MHz, DMSO-d_6, δ) 6.15 (s, 2H, H-4 and H-6), 5.59 (s, 1H, H-7), 4.29 (d, J = 4.0 Hz, 1H, OH), 4.03 (q, J = 6.9 Hz, 2H, CH_2 from Et), 3.85 (d, J = 3.1 Hz, 1H, H-12), 1.16 (t, J = 7.1 Hz, 3H, CH_3 from Et), 1.03 (s, 3H, H-19), 0.92 (d, J = 6.5 Hz, 3H, H-21), 0.69 (s, 3H, H-18). ^{13}C NMR (101 MHz, DMSO-d_6, δ) 198.59 (C-3), 173.74 (C-24), 163.92 (C-5), 141.97 (C-4), 127.91 (C-6), 123.29 (C-7), 70.95 (C-12), 60.09 (CH_2 from Et), 47.28, 46.49, 45.25, 43.69, 37.81, 35.54, 35.33, 34.02, 33.73, 31.17, 31.10, 28.66, 27.43, 23.30, 17.29 (C-21), 16.29 (C-19), 14.61 (CH_3 from Et), 12.49 (C-18). IR (film, cm^{-1}): 3457, 2943, 2871, 1734, 1649, 1615, 1447, 1268, 1180, 1034. (+)ESI-HRMS (*m/z*): calculated for $C_{26}H_{38}O_4$ [M-H]$^-$ 415.28483, found 415.28355.

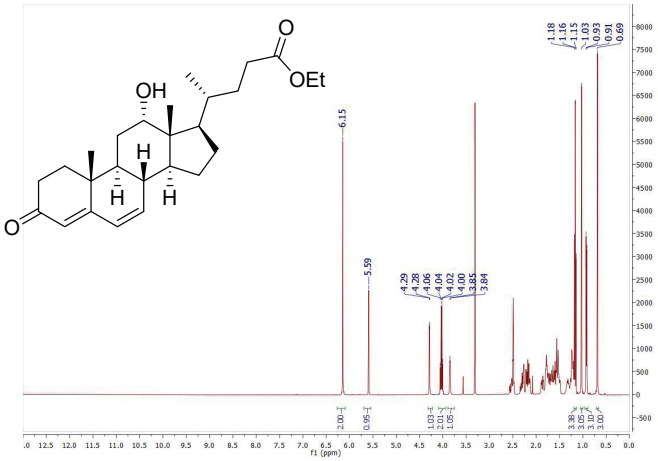

Fig. S-10. Compound **26** ^{1}H NMR (400 MHz, DMSO-d_6) spectra.

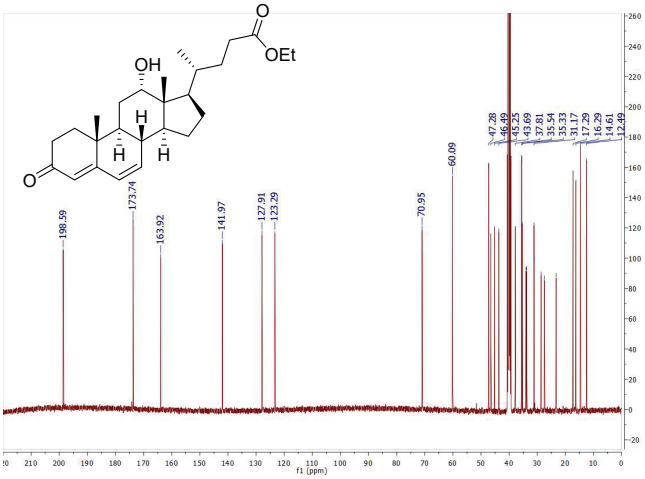

Fig. S-11. Compound **26** ^{13}C NMR (101 MHz, DMSO-d_6) spectra.

2-(5β-chol-3-ene-7α,12α,24-triol)-N-(1-hydroxy-2-methylpropan-2-yl)acetamide (30)

^{1}H NMR (400 MHz, DMSO-d_6, δ) 6.74 (s, 1H, NH), 5.41 (s, 1H, H-4), 4.05 (s, 1H, OH on C-12), 3.85 (s, 1H, OH on C-7), 3.79 (s, 1H, H-12), 3.60 (s, 1H, H-7), 3.46 and 3.37 (both are d, J_2 = 10.8 Hz, 1H, CH_2 from 1-hydroxy-2-methylpropan-2-yl), 3.35 (m, 2H, H-24), 2.79 and 2.54 (both are d, J_2 = 15.1 Hz, 1H, CH_2 from acetamide), 1.20 and 1.18 (s, 3H, CH_3 from 1-hydroxy-2-methylpropan-2-yl), 0.92 (d, J = 6.5 Hz, 3H, H-21), 0.89 (s, 3H, H-19), 0.61 (s, 3H, H-18). ^{13}C NMR (101 MHz, DMSO-d_6, δ) 170.57 (carbonyl from acetamide), 133.02 (C-4), 127.75 (C-3), 71.02 (C-12), 67.81 (CH_2 from 1-hydroxy-2-methylpropan-2-yl), 66.62 (C-7), 61.40 (C-24), 54.45, 46.33, 45.78, 41.64, 41.46, 39.21, 35.45, 34.82, 33.84, 32.84, 31.94, 29.41, 29.13, 27.46, 26.19, 24.28, 23.53, 23.29, 22.86, 21.97 (C-19), 21.17, 17.38 (C-21), 12.30 (C-18). (+)ESI-HRMS (*m/z*): calculated for $C_{30}H_{51}O_5$ $[M+Na]^+$ 528.36649, found 528.36477.

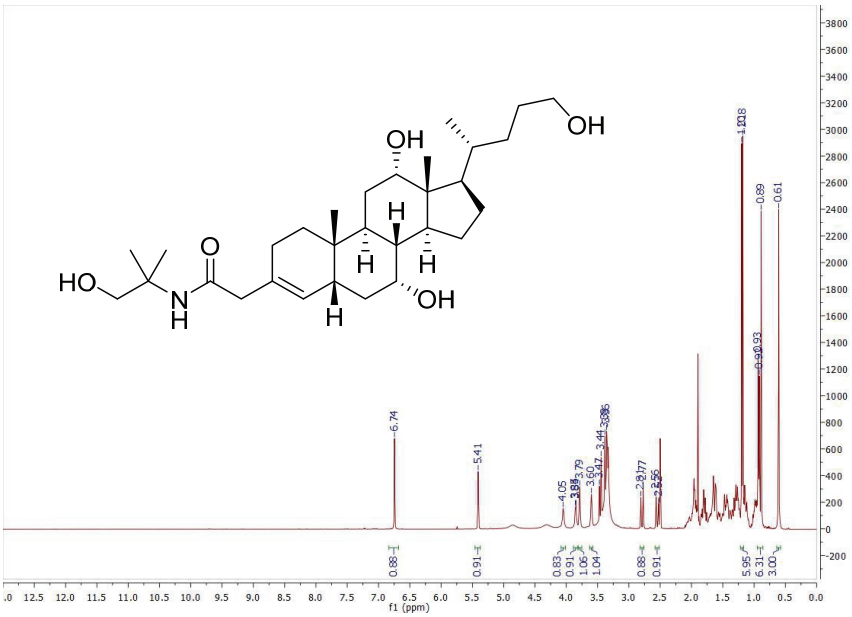

Fig. S-12. Compound **30** ^{1}H NMR (400 MHz, DMSO-d_6) spectra.

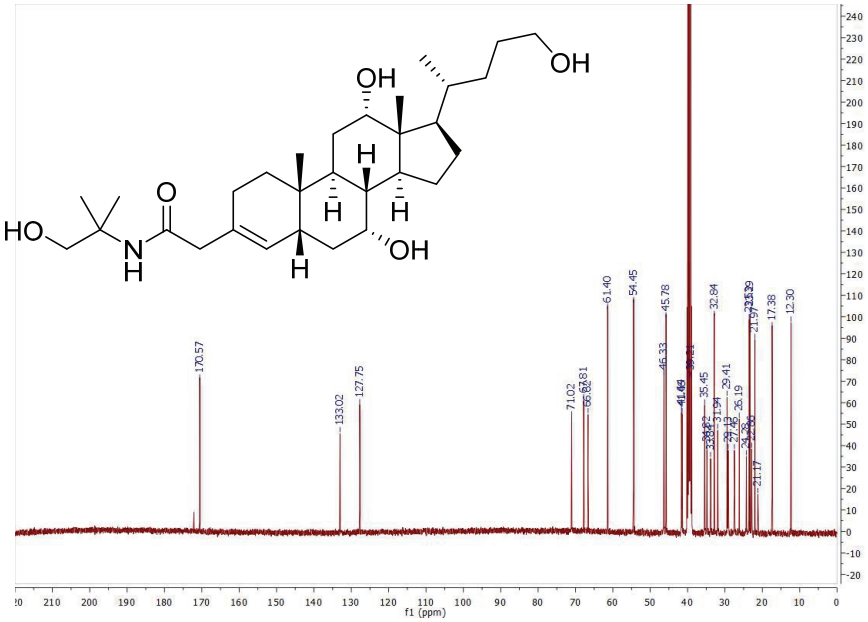

Fig. S-13. Compound **30** ^{13}C NMR (101 MHz, DMSO-d_6) spectra.

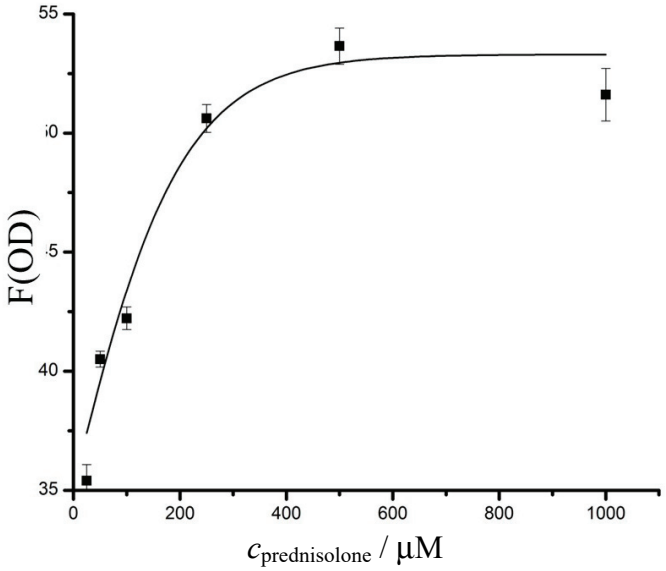

Fig. S-14. Dose-dependent changes in the fluorescence intensity normalized by optical density (F/OD) of yeast cells expressing GR LBD-YFP upon addition of the glucocorticoid receptor ligand, prednisolone, at six different concentrations (25, 50, 100, 250, 500 and 1000 μM) following 15 h exposure.

Journal of the Serbian Chemical Society
JSCS-info@shd.org.rs • www.shd.org.rs/JSCS
J. Serb. Chem. Soc. *88* (2) 141–152 (2023)
JSCS–5616
Original scientific paper
Published 18 November 2022

Dissociation of N_2 by electron impact in electric and magnetic RF fields

MIROSLAV RISTIĆ[1]*[#], RADOMIR RANKOVIĆ[1], MIRJANA M. VOJNOVIĆ[2], VIOLETA V. STANKOVIĆ[2] and GORAN B. POPARIĆ[2]

[1]*University of Belgrade, Faculty of Physical Chemistry, P. O. Box 47, 11000 Belgrade, Serbia and* [2]*University of Belgrade, Faculty of Physics, P. O. Box 44, 11000 Belgrade, Serbia*

(Received 10 July, revised 5 August, accepted 8 August 2022)

Abstract: Rate coefficients for electron impact dissociation of the N_2 molecule under the influence of crossed radio-frequency (RF) electric and magnetic fields were calculated for field frequencies of 13.56, 100 and 200 MHz and for root mean square values of the reduced electric field strength of 300 and 500 Td. The root mean square values of the reduced magnetic field were varied from 0 to 2000 Hx. The effects of the strength of the RF fields and their frequency on the rates for the dissociation to neutral fragments and for the dissociative ionization are discussed. The temporal evolution of the rate coefficients during one period of the RF field is shown and discussed.

Keywords: nitrogen molecule; neutral fragments; dissociative ionization.

INTRODUCTION

In addition to being the main component of the Earth's atmosphere, nitrogen is abundantly present in the atmospheres of Pluto, Titan and Triton, and in smaller quantities on Mars and Venus. Nitrogen is also used in many RF discharge-based technologies, such as nitriding of materials,[1] plasma polymerization,[2] production of nanomaterials,[3] medical sterilizations,[4] doping of graphene and many others.[5] In all these environments, the nitrogen molecules are exposed to collision with electrons. From the aspect of chemical reactivity of nitrogen plasma, one of the most important elementary processes in these collisions is certainly dissociation. Dissociation can occur to form two neutral nitrogen atoms and this reaction is known as the dissociation into neutral fragments:

$$e^- + N_2 \rightarrow N_2^* \rightarrow N + N + e^- \quad (1)$$

* Corresponding author. E-mail: ristic@ffh.bg.ac.rs
# Serbian Chemical Society member.
https://doi.org/10.2298/JSC220710066R

The threshold energy for reaction (1) is 9.75 eV* and the majority of the electronic states of the N_2 molecule lie above this energy. Excess energy during dissociation is transferred to atoms.

Zipf and McLaughlin recognized the importance of dissociation of excited N_2 molecules over radiative relaxation *via* a manifold of singlet valence and Rydberg states.[6] They came to the conclusion that nitrogen molecules that were excited to various $^1\Pi_u$ and $^1\Sigma_u^+$ states, whether by electron impact or UV photon absorption, mostly follow the predissociation path (*i.e.*, the radiationless transition of a molecule from a stable excited state to an unstable excited state that leads to dissociation). Photon relaxations from these singlet states *via* dipole-allowed transitions to the singlet ground state were expected to be dominant,[7] but it turned out that they last much longer than the dissociation. Namely, dissociation to neutrals occurs in a time interval of 10^{-13} s, while photon relaxation lasts 10^{-8} s.[8] The main contribution to reaction (1) for electron energies lower than 100 eV stems from a family of $^1\Pi_u$ states, which predissociate with almost 100 % efficiency. The contributions of $^1\Sigma_u^+$ states to dissociation vary depending on the vibrational level of the state.

At higher values of the electron energy (above 100 eV), the probability increases that the N atom and N^+ are formed during dissociation, instead in reaction of two N atoms. This process can be presented by the following reaction:

$$e^- + N_2 \rightarrow N_2^* \rightarrow N^+ + N + 2e^- \quad (2)$$

and it is called dissociative ionization. It is competitive with reaction (1) and it has a threshold value of 24.29 eV.[9]

In this manuscript, the rate coefficients for the dissociation to neutral fragments and for dissociative ionization, under the presence of crossed RF electric and RF magnetic field, which is a situation that corresponds to the one that exists in inductively coupled plasmas, are presented. The rate coefficients were calculated for values of fields frequencies of 13.56, 100 and 200 MHz and for different strength values of electric and magnetic fields. For this purpose, the electron energy distribution functions (EEDFs) that were obtained by Monte Carlo simulation, and the appropriate cross sections for processes (1) and (2) were used. The integral cross sections for dissociation into neutral fragments that were measured and rescaled by Cosby were adopted.[10] Cosby obtained integral cross section (ICS) by directly detecting the correlated fragment pair N + N, by a time and position sensitive detector.[10] The measured ICS were further adjusted by Cosby according to the results of Winters and as such are generally recommended and used in this work.[11,12] Cross sections for reaction (2) were taken from Straub *et al.*[13] In their experiment, a time-of-flight mass spectrometer was used to distinct charged particles according to their mass-to-charge ratios. For this reason, N^+

* 1 eV = 1.602×10^{-19} J

generated in the dissociative ionization process were detected together with N_2^{2+}, that can also be created by electron impact. However, N_2^{2+} can practically be produced only in trace amounts under the considered conditions, because the highest electron energies within this work were approximately 60 eV, while the threshold for the second ionization energy of N_2 is 42.88 eV.[9] The high-energy tail of the EEDF barely crosses the threshold for the second ionization energy of N_2 (even under conditions for which the highest energies are achieved) and very small amount of electrons are capable of performing the second ionization of the N_2 molecule. Therefore, it was consider appropriate to refer to the cross sections of Straub *et al.* as the cross sections for dissociative ionization within this work.[13] These cross sections were supplemented by including the threshold value for dissociative ionization of 24.29 eV.[9] The cross-section values between the threshold and the first electron energy reported by Straub *et al.*,[13] which was 30 eV, were linearly interpolated. The integral cross sections used for reactions (1) and (2) in the present manuscript are shown in Fig. 1.

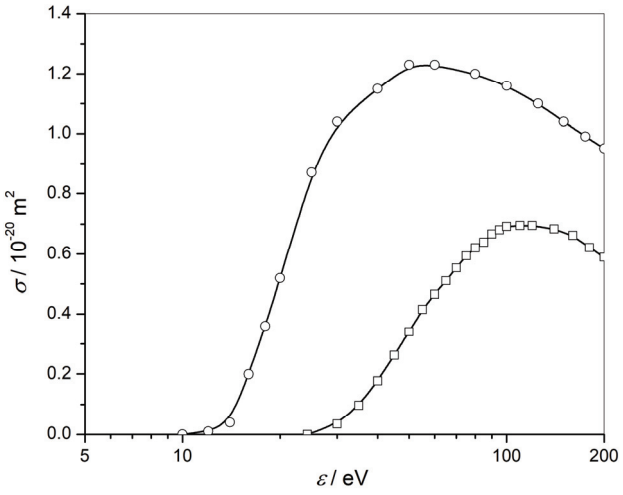

Fig. 1. Integral cross sections for the dissociation of N_2 to neutral fragments of Cosby[10] (circles) and for dissociative ionization of Straub *et al.*[13] (squares) *vs*. electron energy.

METHOD

Monte Carlo simulation

In order to simulate the motion of electrons through the N_2 gas under the presence of time-varying electric and magnetic fields, the Monte Carlo (MC) code used in earlier works of our group,[14,15] was modified and used.[16] The motion of the electron is described by the following differential equation:

$$m\frac{\mathrm{d}^2\mathbf{r}}{\mathrm{d}t^2} = e\left(\mathbf{E}(t) + \frac{\mathrm{d}\mathbf{r}}{\mathrm{d}t}\mathbf{B}(t)\right) \tag{3}$$

In Eq. (3), **r** is the radius vector of the electron, *m* and *e* are the mass and charge of the electron, **E** and **B** are the electric and magnetic field vectors, respectively, and *t* is time. The time-varying electric and magnetic field vectors periodically oscillate at fixed frequency are described by Eqs. (4) and (5):

$$\mathbf{E}(t) = \sqrt{2}E_{\mathrm{R}}\cos(2\pi ft)\mathbf{k} \quad (4)$$

$$\mathbf{B}(t) = \sqrt{2}B_{\mathrm{R}}\sin(2\pi ft)\mathbf{j} \quad (5)$$

where **k** and **j** are the unit vectors in the Cartesian coordinate system that characterize the direction of electric and magnetic fields, while *f* is the frequency of their oscillation. E_{R} and B_{R} are the root mean square values of the electric and magnetic field, respectively. Absolute values of electric and magnetic field within this work will be replaced with reduced electric field and reduced magnetic field, defined as quotients E_{R}/N and B_{R}/N, *N* being the gas number density. The electric and magnetic fields are mutually perpendicular, and phase shift among them is $\pi/2$ rad. The numerical solutions of the Eq. (3) were used to calculate the position and velocity of the electron in each small time step of the simulation (much smaller than the period of oscillation) by the numerical iterative Runge–Kutta method.[17]

Electrons were generated with a certain value of the kinetic energy and were simulated one by one under the defined conditions (E_{R}/N, B_{R}/N and *f* values specified). The simulation procedures follow every electron until it reaches the quasi-steady state, *i.e.*, the state where energy received from the electric field is balanced with the energy that is lost in non-elastic collisions with the N_2 molecules. When the quasi-steady state was reached, the ensemble of electrons obtains stable oscillations of mean electrons energy (ε_{m}) over time and at this point the EEDFs were sampled over one period of the fields oscillation. These EEDFs are essential for obtaining the rate coefficients, as shall be explained further.

The nitrogen gas in which the electrons were simulated was considered to be at 133.3 Pa ($N = 3.22\times10^{22}$ m^{-3}) and the zero-temperature gas approximation was used, meaning that every N_2 molecule was in its ground electronic, vibrational and rotational state. The procedures of the simulation included the possibilities of all real electron-molecule interactions under the conditions assumed: elastic collisions, non-elastic collisions (rotational, vibrational and electronic excitations) as well as ionization. The database of the simulations containing the cross sections for all relevant processes was carefully composed. The probability of a certain scattering process at a given electron energy ε depended on the corresponding effective cross section $\sigma(\varepsilon)$. The decision as to which collision process will occur was left to a pseudo-random generated number, as were the scattering angles of the electron after the collision. Electrons that were created in the ionization process were also simulated. The MC code was successfully tested on model gases,[18,19] by comparing the transport parameters of the electrons with the benchmark values from the literature.[20] For other details about the MC code, see Ristić *et al.* and Ristić *et al.*[15,16]

Cross-section database

Finding an optimal set of cross-sections for the electron-N_2 molecule interaction was crucial for a successful simulation. For elastic scattering, the recent cross-section data of Allan in the electron energy range from 0 to 5.5 eV was used.[21] For electron energies from 6 to 10 eV, the data of Sun *et al.* was used,[22] while in the energy region from 10 to 70 eV, the data of Gote and Ehrhardt was used.[23] In the high-energy region from 70 to 90 eV, the data of Nickel *et al*.[24] was used.

Cross-section values for rotational excitations were adopted from Itikawa and Mason for $J = 0 \rightarrow 2$ and $J = 0 \rightarrow 4$ excitations.[25] For vibrational excitations, the integral cross-sections

that were measured in our laboratory were used.[26] These measurements include excitations into the first ten vibrational levels of the ground electronic state of the N_2 molecule.

The cross-sections for $a'^1\Sigma_u^-$, $w^1\Delta_u$ and $a''^1\Sigma_g^+$ singlet electronic states were adopted from Itikawa,[27] compilation proposed by Brunger *et al*.,[28] based on the experiments of Trajmar *et al.* and Campbell *et al*.,[29,30] and the theoretical calculations of Ohmori *et al.* and Gillan *et al.*[31,32] The cross-section values were also taken from Brunger *et al*,[28] for the excitation of $a^1\Pi_g$ state on the basis of electron energy loss measurements of Finn and Doering,[33] direct detection of the excited molecule of Mason and Newell and swarm experiments.[34,35] For the $c_4'^1\Sigma_u^+$ and $b'^1\Sigma_u^+$ states, values from Ajello *et al.* were taken.[35] The $b^1\Pi_u$ state cross-section was adopted from James *et al.*,[36] and recent cross-section measurements of the $c_3^1\Pi_u$ and $o_3^1\Pi_u$ states were adopted from Malone *et al*.[37] The values of the cross sections for the excitations of the $A^3\Sigma_u^+$, $B^3\Pi_g$, $W^3\Delta_u$ and $B'^3\Sigma_u^-$ triplet electronic states were used from Itikawa,[27] which were recommended by Brunger *et al.* based on previously mentioned studies.[28-32] Cross-section proposed by Brunger *et al.*,[28] for $E^3\Sigma_g^+$ state (based on several beam experiments)[29,30,38,39] and for $C^3\Pi_u$ state (based also on beam experiments)[29,30,39,40] were used. $F^3\Pi_u$ and $G^3\Pi_u$ electronic state cross sections were used from Malone *et al.*[37] Ionization cross sections were adopted from Itikawa,[27] based on Lindsay and Mangan[41] and Straub *et al.* measurements.[13] Dissociation was included implicitly by taking into account all significant electronic states that contribute to it, as was explained in the Introduction section.

Validation of the present cross-section database for nitrogen was performed by comparing basic transport properties of electrons (drift velocities and diffusion coefficients) obtained by the present simulation with the experimentally measured ones. In a previous works we presented these comparisons for drift velocity, longitudinal diffusion coefficient and ionization coefficient, whereby excellent agreements were obtained.[14,42] Comparison was also made with the Boltzmann equation-based software BOLSIG+ (version 1.1).[43] By including the present cross-section database in both our Monte Carlo simulation and BOLSIG+ oscillating field routine, we obtained the agreement of period averaged mean electron energy within 2 % only.

Rate coefficient calculation

The EEDFs and corresponding mean electron energies were sampled within one phase of the electric field oscillation after the quasi-steady state was reached in the simulation. The EEDFs obtained were then normalized by the relation:

$$\int_0^\infty f_\varepsilon(\varepsilon_m,\varepsilon,t)\,\mathrm{d}\varepsilon = 1 \tag{6}$$

In Eq. (6), the normalized EEDF at the specific time t is denoted by $f_\varepsilon(\varepsilon_m, \varepsilon, t)$, while ε represents the actual kinetic energy of the electron. For every $f_\varepsilon(\varepsilon_m,\varepsilon,t)$ in the specific moment in time (that is, in the specific phase of the electric field oscillation), the corresponding rate coefficient, $k(\varepsilon_m, t)$ was calculated by the following relation:[44]

$$k(\varepsilon_m,t) = \sqrt{\frac{2}{m}}\int_{\varepsilon_{th}}^\infty \sigma(\varepsilon)\sqrt{\varepsilon} f_\varepsilon(\varepsilon_m,\varepsilon,t)\,\mathrm{d}\varepsilon \tag{7}$$

where $\sigma(\varepsilon)$ is the effective cross-section for a given process with a threshold energy ε_{th}.

RESULTS AND DISCUSSION

According to Eq. (7), the rate coefficients for dissociation processes (1) and (2) were calculated by implementing the EEDFs obtained after reaching the quasi-steady state by the MC code for given input parameters. The input parameters imply E_R/N values of 300 and 500 Td (1 Td = 10^{-21} V m^2), B_R/N values

of 0, 1000 and 2000 Hx (1 Hx = 10^{-27} T m^3) and values of frequency 13.56, 100 and 200 MHz. As stated earlier, the integral cross sections for the calculation of the rate coefficients for the dissociation of N_2 to neutral fragments were adopted from Cosby,[10] while the rates for dissociative ionization were calculated based on integral cross sections measured by Straub *et al.* with implemented energy threshold for process (2).[9,13] Background physics of electrons motion in crossed electric and magnetic RF fields is well known and will only be slightly addressed in this paper.[16,20]

Since the MC simulation records many EEDFs within one period of the field's oscillation, a fine time evolution of the rate coefficients on the nanosecond scale was obtained. The rate coefficients for dissociation of N_2 to neutral fragments are presented on Fig. 2. for all input parameters. First, it should be noticed that the rate coefficients are oscillating at twice the frequency of the applied RF fields. The reason is that the energy of the electron is independent of the absolute direction of the electric field. The rate coefficients depend on all the varied parameters. It should be noted that when discussing the dependence of the rate coefficient on one specific parameter, the other parameters are considered as constant.

By observing the coefficients at the lowest considered frequency of 13.56 MHz for given E_R/N and B_R/N, it was noticeable that the highest and lowest (zero) amplitude values of the coefficients were reached, which is expected because at that frequency, the electrons efficiently track the electric field changes and lag only slightly behind them. Therefore, when the electric field (which determines the energy of the electron) reaches a maximum or minimum, the EEDF also has the largest share of high-energy electrons (for given E_R/N and B_R/N) and consequently, the rate coefficient is the largest. On the other hand, when the electric field passes through the zero value, after which the electrons are slowed down, the share of fast electrons in the EEDF is the smallest and the rate coefficient reaches its lowest value. At 13.56 MHz, this lowest value is zero, as can be seen from Fig. 2.

At higher frequencies, the EEDFs have a narrowed oscillation range due to a more pronounced electron delay behind the electric field. For this reason, the rates also oscillate over a narrower range: they do not reach the maximum amplitude values they had at lower frequencies, but they do not fall to zero either. One of the characteristics of the time evolution of the rate coefficients is the existence of phase delay with respect to the electric field. This delay is also a consequence of the inertia of the motion of electrons through the N_2 gas and is more pronounced at higher frequencies.[14]

Regarding the influence of the strength of the electric and magnetic fields on the appearance of the rate coefficients, they are also noticeable in Fig. 2. Both electric and magnetic field strongly affect the value of the rates. At stronger electric fields, the share of high-energy tail of EEDF is higher, and thus the overlap

integral in Eq. (7) is higher, which leads to a higher values of the rate coefficients.

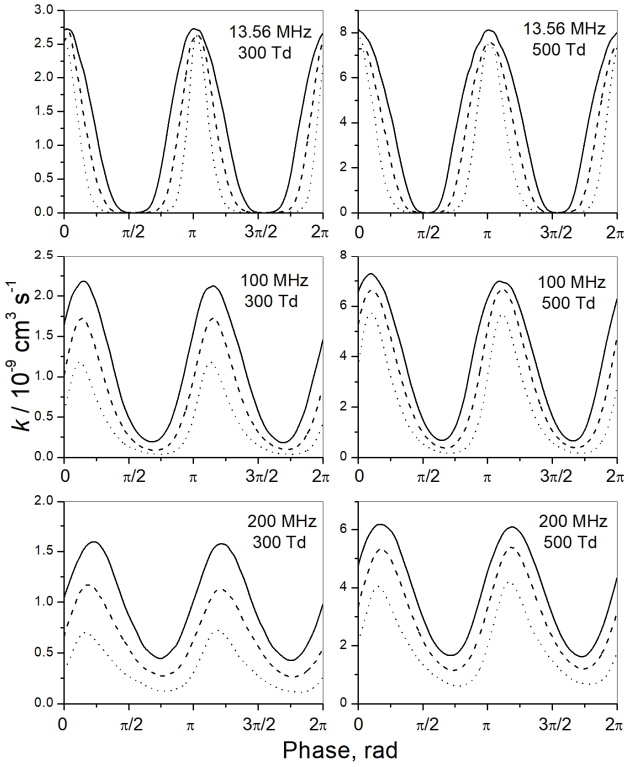

Fig. 2. Rate coefficients for the dissociation of N_2 to neutral fragments *vs.* the phase of the RF electric field at the indicated pair of f and E_R/N and for $B_R/N = 0$ Hx (full line), $B_R/N = 1000$ Hx (dashed line) and $B_R/N = 2000$ Hx (dotted line).

At higher B_R/N values, the profile of the rate coefficient with time is narrowed and at the same time reduced in height, due to the complex action of the magnetic field on the electrons. Hence the overall effect of increasing magnetic field on the rate coefficients shown here is their reduction.

For most practical applications in which nitrogen dissociation may be of interest in plasma chemistry and plasma technology of nitrogen-containing systems, an important fact is the time-averaged rate coefficient during one period of RF field oscillation. To this end, these period averaged rates for the dissociation of N_2 into neutral fragments are given Table I for all considered parameters. In the ranges of varied input parameters, the average rate coefficient changed its value from 0.341×10^{-9} to 3.929×10^{-9} cm^3 s^{-1}. By analyzing the data in Table I, it could be concluded that an increase of E_R/N leads to larger values of the rate coefficient, while an increase of B_R/N leads to their lowering. Increasing the fre-

quency does not have much effect on the value of the period averaged rate coefficients, nor can its effect be easily generalized.

TABLE I. Period averaged rates (10^{-9} cm^3 s^{-1}) for the dissociation of N_2 into neutral fragments under various conditions

f / MHz	E_R/N = 300 Td			E_R/N = 500 Td		
	(B_R/N) / Hx					
	0	1000	2000	0	1000	2000
13.56	1.156	0.786	0.492	3.929	2.828	1.972
100	1.064	0.693	0.391	3.778	2.871	1.926
200	0.971	0.641	0.341	3.796	2.948	1.923

The rate coefficients for dissociative ionization of N_2 are presented in Fig. 3. for all input parameters. Most of what has been said about the rate coefficients of dissociation into neutral fragments also applies here: E_R/N, B_R/N and f values

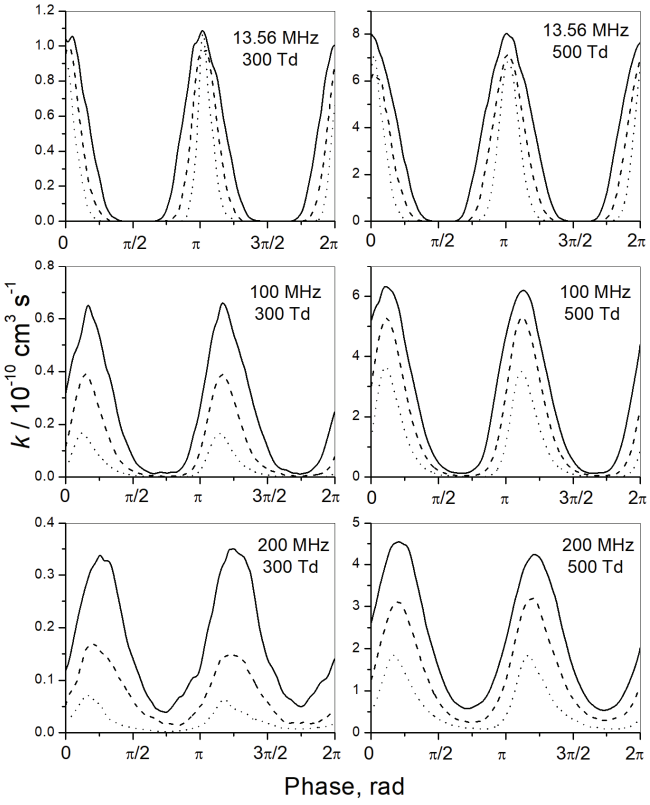

Fig. 3. Rate coefficients for dissociative ionization of N_2 *vs*. phase of the RF electric field at the indicated pair of f and E_R/N and for B_R/N = 0 Hx (full line), B_R/N = 1000 Hx (dashed line) and B_R/N = 2000 Hx (dotted line).

have qualitatively the same effect on the shape of the rates. The period averaged rates of the dissociative ionization for all considered parameters are given in Table II. However, in the case of dissociative ionization (unlike the previous case), the effect of frequency on the rates is evident. Raising the *f* significantly lowers the rate coefficients for dissociative ionization.

The rates for dissociative ionization were about 10 to 15 times lower than those for the dissociation into neutral fragments. This was expected since the cross-section for dissociative ionization is lower, while the energy threshold is higher. From Table II, it could be seen that the rate values ranged from 0.022×10^{-10} to 3.020×10^{-10} cm^3 s^{-1}. Nevertheless, dissociative ionization remains an important source of N^+ in plasmas, in addition to direct ionization of the N atom.

TABLE II. Period averaged rates (10^{-10} cm^3 s^{-1}) for dissociative ionization under various conditions

f / MHz	E_R/N = 300 Td			E_R/N = 500 Td		
	(B_R/N) / Hx					
	0	1000	2000	0	1000	2000
13.56	0.3493	0.2153	0.1275	3.020	1.939	1.271
100	0.2364	0.1112	0.0391	2.494	1.614	0.858
200	0.1699	0.0713	0.0225	2.181	1.309	0.604

Recently, Sode *et al.* developed a new model for the calculation of ion and radical densities in inductively coupled nitrogen plasmas.[45] They proposed the equations for the calculation rate coefficients for numerous elementary processes in plasma, among them the dissociation of N_2 to neutral fragments and for the dissociative ionization of N_2 (see Table II of their work, reactions 1.6 and 1.9). By implementing the mean electron energy obtained from the present MC simulation in their equations, significant difference in the values of the rate coefficients were obtained.

For example, at 13.56 MHz, 300 Td and 0 Hx, the mean electron energy obtained by the present MC code was 6.47 eV and the rate for dissociation to neutral fragments was 3.6×10^{-9} cm^3 s^{-1} (the present value was 1.1×10^{-9} cm^3 s^{-1}), while for dissociative ionization, the rate was 1.1×10^{-10} cm^3 s^{-1} (the present value was 0.35×10^{-10} cm^3 s^{-1}). Sode *et al.* stated that they assumed Maxwellian EEDF in their equations,[45] but here it could be seen that the dissociation rates in that case were roughly three times higher than the ones presented here, based on non-equilibrium EEDFs. In addition, the rates obtained in that way were independent of the magnetic field or frequency values. Note that the cross sections that Sode *et al.* used were practically the same as those used here. The described example shows that the dissociation coefficients presented here could significantly improve the kinetic calculations in nitrogen plasma chemistry.

CONCLUSIONS

The rate coefficients for electron impact dissociation of the N_2 molecule to neutral fragments, as well as for the dissociative ionization process were calculated under the presence of RF electric and magnetic fields. The choice of parameters included three frequencies: 13.56, 100 and 200 MHz, two E_R/N values: 300 and 500 Td and B_R/N values: 0, 1000 and 2000 Hx.

Therefore, the nitrogen molecule dissociation processes, as one of the most important processes in nitrogenous RF plasma chemistry, were quantified for the stated conditions. Fine temporal evolution of the dissociation rate coefficients within the RF field phase was presented with an adequate explanation. The time-averaged values of the rate coefficients were also shown. Dissociative ionization is by an order of magnitude a rarer process compared to dissociation into neutral fragments, which is expected due to its lower cross-section values and higher threshold.

Acknowledgements. This work was supported in part by the Ministry of Education, Science and Technological Development of the Republic of Serbia under contracts No. 451-03-68/2022-14/200146 and 451-03-9/2022-14/200162. The authors gratefully acknowledge the assistance of Muna Aoneas.

И З В О Д

ДИСОЦИЈАЦИЈА N_2 УДАРОМ ЕЛЕКТРОНА У ЕЛЕКТРОМАГНЕТНИМ RF ПОЉИМА

МИРОСЛАВ РИСТИЋ[1], РАДОМИР РАНКОВИЋ[1], МИРЈАНА М. ВОЈНОВИЋ[2], ВИОЛЕТА В. СТАНКОВИЋ[2] и ГОРАН Б. ПОПАРИЋ[2]

[1]*Универзитет у Београду – Факултет за физичку хемију, Студентски трг 12-16, Београд и* [2]*Универзитет у Београду – Физички факултет, Студентски трг 16, Београд*

Коефицијенти брзине дисоцијације молекула N2 ударом електрона под утицајем укрштеног радиофреквентног (RF) електричног и магнетног поља израчунати су за фреквенције од 13.56, 100 и 200 MHz и за средње квадратне вредности редукованог електричног поља од 300 и 500 Td. Средње квадратне вредности редукованог магнетног поља вариране су од 0 до 2000 Hx. Дискутовани су ефекти јачина RF поља и њихове фреквенције на коефицијенте брзине за дисоцијацију на неутралне фрагменте и за дисоцијативну јонизацију. Приказана је и продискутована временска еволуција коефицијената брзине у току једног периода RF поља.

(Примљено. 10. јула, ревидирано 5. августа, прихваћено 8. августа 2022)

REFERENCES

1. E. Guiberteau E, G. Bonhomme, R. Hugon, G. Henrion, *Surf. Coat. Technol.* **97** (1997) 552 (https://doi.org/10.1016/S0257-8972(97)00188-6)
2. D. D. Markushev, J. Jovanović-Kurepa, M. Terzić, *Rev. Sci. Instrum.* **74** (2003) 303 (https://doi.org/10.1063/1.1515900)
3. C. Zhang, L. Fu, N. Liu, M. Liu, Y. Wang, Z. Liu, *Adv. Mater.* **23** (2011) 1020 (https://doi.org/10.1002/adma.201004110)

4. S. Villeger, J. P. Sarrette, B. Rouffet, S. Cousty, A. Ricard, *Eur. Phys. J. Appl. Phys.* **42** (2008) 25 (http://dx.doi.org/10.1051/epjap:2007177)
5. A. S. Dobrota, I. A. Pašti, S. V. Mentus, B. Johansson, N. V. Skorodumova, *Appl. Surf. Sci.* **514** (2020) 145937 (https://doi.org/10.1016/j.apsusc.2020.145937)
6. E. C. Zipf, R.W. McLaughlin, *Planet. Space Sci.* **26** (1978) 449 (https://doi.org/10.1016/0032-0633(78)90066-1)
7. A. E. S. Green, C. A. Barth, *J. Geophys. Res.* **72** (1967) 3975 (https://doi.org/10.1029/JZ072i015p03975)
8. N. Itagaki, S. Iwata, K. Muta, A. Yonesu, S. Kawakami, N. Ishii, Y. Kawai, *Thin Solid Films* **435** (2003) 259 (https://doi.org/10.1016/S0040-6090(03)00395-X)
9. O. Dutuit, N. Carrasco, R. Thissen, V. Vuitton, C. Alcaraz, P. Pernot, N. Balucani, P. Casavecchia, A. Canosa, S. L. Picard, J. Loison, Z. Herman, J. Zabka, D. Ascenzi, P. Tosi, P. Franceschi, S. D. Price, P. Lavvas, *Astrophys. J. Suppl. Ser.* **204** (2013) 45 (https://doi.org/10.1088/0067-0049/204/2/20)
10. P. C. Cosby, *J. Chem. Phys.* **98** (1993) 9544 (https://doi.org/10.1063/1.464385)
11. H. F. Winters, *J. Chem. Phys.* **44** (1966) 1472 (https://doi.org/10.1063/1.1726879)
12. Y. Itikawa, *J. Phys. Chem. Ref. Data* **35** (2006) 31 (https://doi.org/10.1063/1.1937426)
13. H. C. Straub, P. Renault, B. G. Lindsay, K. A. Smith, R. F. Stebbings, *Phys. Rev., A* **54** (1996) 2146 (https://doi.org/10.1103/PhysRevA.54.2146)
14. M. P. Popović, M. M. Vojnović, M. M. Aoneas, M. Ristić, M. M. Vićić, G. B. Poparić, *Phys. Plasmas* **21** (2014) 063504 (https://doi.org/10.1063/1.4975312)
15. M. M. Ristić, M. Aoneas, M. M. Vojnović, G. B. Poparić, *Plasma Chem. Plasma Process.* **37** (2017) 1431 (https://doi.org/10.1007/s11090-017-9826-6)
16. M. M. Ristić, V. V. Stanković, M. M. Vojnović, G. B. Poparić, *Phys. Plasmas* **29** (2022) 093514 (https://doi.org/10.1063/5.0101931)
17. R. Morrow, *J. Comput. Phys*. **43** (1981) 1 (https://doi.org/10.1016/0021-9991(81)90108-X)
18. K. Maeda, T. Makabe, N. Nakano, S. Bzenić, Z. Lj. Petrović, *Phys. Rev., E* **55** (1997) 5901 (https://doi.org/10.1103/PhysRevE.55.5901)
19. H. T. Saelee, J. Lucas, *J. Phys., D* **8** (1975) 640 (https://doi.org/10.1088/0022-3727/10/3/014)
20. Z. Lj. Petrović, Z.M. Raspopović, S. Dujko, T. Makabe, *Appl. Surf. Sci.* **192** (2002) 1 (https://doi.org/10.1016/S0169-4332(02)00018-1)
21. M. Allan, *J. Phys., B* **38** (2005) 3655 (https://doi.org/10.1088/0953-4075/38/20/003)
22. W. Sun, M. A. Morrison, W. A. Isaacs, W. K. Trail WK, D. T. Alle, R. J. Gulley, M. J. Brennan, S. J. Buckman, *Phys. Rev., A* **52** (1995) 1229 (https://doi.org/10.1103/PhysRevA.52.1229)
23. M. Gote, H. Ehrhardt, *J. Phys., B* **28** (1995) 3957 (https://doi.org/10.1088/0953-4075/28/17/029)
24. J. C. Nickel, C. Mott, I. Kanik, D. C. McCollum, *J. Phys., B* **21** (1988) 1867 (https://doi.org/10.1088/0953-4075/21/10/018)
25. Y. Itikawa, N. Mason, *Phys. Rep.* **414** (2005) 1 (https://doi.org/10.1016/j.physrep.2005.04.002)
26. M. Ristić, G. B. Poparić, D. S. Belić, *Chem. Phys.* **331** (2007) 410 (https://doi.org/10.1016/j.chemphys.2006.11.012)
27. Y. Itikawa, *Phys. Chem. Ref. Data* **35** (2006) 31 (https://doi.org/10.1063/1.1937426)

28. M. J. Brunger, S. J. Buckman, M. T. Elford, *Photon and electron interactions with atoms, molecules and ions*, Springer, New York, 2003 (https://doi.org/10.1007/b83711)
29. S. Trajmar, D. F. Register, A. Chutjian *Phys. Rep.* **97** (1983) 219 (https://doi.org/10.1016/0370-1573(83)90071-6)
30. L. Campbell, M. J. Brunger, A. M. Nolan, L. J. Kelly, A. B. Wedding, J. Harrison, P. J. O. Teubner, D. C. Cartwright, B. McLaughlin, *J. Phys., B* **34** (2001) 1185 (https://doi.org/10.1088/0953-4075/34/7/303)
31. Y. Ohmori, M. Shimozuma, H. Tagashira, *J. Phys., D* **21** (1988) 724 (https://doi.org/10.1088/0022-3727/21/5/009)
32. C. J. Gillan, J. Tennyson, B. M. McLaughlin, P. G. Burke, *J. Phys., B* **29** (1996) 1531 (https://doi.org/10.1088/0953-4075/29/8/017)
33. T. G. Finn, J. P. Doering, *J. Chem. Phys.* **64** (1976) 4490 (https://doi.org/10.1063/1.432075)
34. N. J. Mason, W. R. Newell, *J. Phys., B* **20** (1987) 3913 (https://doi.org/10.1088/0022-3700/20/15/035)
35. J. M. Ajello, G. K. James, B. O. Franklin, D. E. Shemansky, *Phys. Rev., A* **40** (1989) 3524 (https://doi.org/10.1103/PhysRevA.40.3524)
36. G. K. James, J. M. Ajello, B. Franklin, D. E. Shemansky, *J. Phys., B* **23** (1990) 2055 (https://doi.org/10.1088/0953-4075/23/12/015)
37. C. P. Malone, P. V. Johnson, X. Liu, B. Ajdari, I. Kanik, M. A. Khakoo, *Phys. Rev., A* **85** (2012) 062704 (https://doi.org/10.1103/PhysRevA.85.062704)
38. M. J. Brunger, P. J. O. Teubner, S. J. Buckman, *Phys. Rev., A* **37** (1988) 3570 (https://doi.org/10.1103/PhysRevA.37.3570)
39. M. Zubek, G. C. King, *J. Phys., B* **27** (1994) 2613 (https://doi.org/10.1088/0953-4075/27/12/019)
40. G. Poparić, M. Vićić, D. S. Belić, *Chem. Phys.* **240** (1999) 283 (https://doi.org/10.1016/S0301-0104(98)00383-8)
41. B. G. Lindsay, M. A. Mangan, *Photon and electron interactions with atoms, molecules and ions. Interactions of photons and electrons with molecules*, Springer, New York, 2003 (https://doi.org/10.1007/b83711)
42. M. Vojnović, M. Popović, M. M. Ristić, M. D. Vićić, G. B. Poparić, *Chem. Phys.* **463** (2015) 38 (https://doi.org/10.1016/j.chemphys.2015.09.014)
43. G. J. M. Hagelaar, L. C. Pitchford, *Plasma Sources Sci. Technol.* **14** (2005) 722 (https://doi.org/10.1088/0963-0252/14/4/011)
44. D. S. Belić, *Chem. Phys.* **130** (1989) 141 (https://doi.org/10.1016/0301-0104(89)87043-0)
45. M. Sode, W. Jacob, T. Schwarz-Selinger, H. Kersten, *J. Appl. Phys.* **117** (2015) 083303 (http://dx.doi.org/10.1063/1.4913623).

Journal of the Serbian Chemical Society
JSCS-info@shd.org.rs • www.shd.org.rs/JSCS
J. Serb. Chem. Soc. *88* (2) 153–167 (2023)
JSCS–5617
Original scientific paper
Published 22 July 2022

Diagnostics of laser-induced plasma from a thin film of oil on a silica wafer

MILICA VINIĆ[1], MIROSLAV KUZMANOVIC[2#], JELENA SAVOVIC[3#] and MILIVOJE IVKOVIC[1]*

[1]*Institute of Physics, University of Belgrade, Belgrade, Serbia,* [2]*Faculty of Physical Chemistry, University of Belgrade, Belgrade, Serbia and* [3]*Vinča Institute of Nuclear Sciences, University of Belgrade, Belgrade, Serbia*

(Received 28 December 2021, revised 21 March, accepted 23 March 2022)

Abstract: In this study, plasma induced by a nanosecond Nd:YAG laser on thin oil films deposited on a silica wafer was characterized by evaluating the main plasma parameters. Spatially and temporally integrated spectral measurements were performed under experimental conditions optimized for elemental analysis of trace metals in oil. Time-resolved values of the spectral line intensities, electron number density, and plasma temperature were obtained from time-integrated measurements by subtracting averaged spectra recorded at different time delays. The electron number density was estimated using the Stark broadened profile of the hydrogen Balmer alpha line. Ionization temperatures were derived from Mg ionic to atomic line intensity ratios. The obtained apparent values of time-resolved plasma parameters were in the range of 1.1×10^{17} cm^{-3} (1.5 μs) to 1.5×10^{16} cm^{-3} (4 μs) and 9400 K (3 μs) to 7200 K (5 μs), depending on the delay time. Emission spectra of C_2 and CN molecules were used to evaluate the rotational and vibrational temperature.

Keywords: electron number density; plasma temperature; time-integrated; time-resolved.

INTRODUCTION

Laser-induced breakdown spectroscopy (LIBS) is a technique widely used for the multi-elemental analysis of complex samples by detecting spectrally resolved emission of plasma formed after laser ablation of the material. Advantages of the LIBS method include simple, or none sample preparation, fast measurements, capability to detect light elements, non-invasiveness, a possibility for *in-situ* measurements, and relatively high sensitivity.[1–4] While applying LIBS on solid materials is straightforward, analysis of liquid samples can be pretty com-

* Corresponding author. E-mail: ivke@ipb.ac.rs
# Serbian Chemical Society member.
https://doi.org/10.2298/JSC211228028V

plex due to experimental difficulties, such as laser-induced splashing and bubbling. This leads to reduced analytical capability of the LIBS technique, which could be improved by a proper experimental approach and sample preparation.[5–8] The choice of the sampling method is guided by the system complexity, the desired detection limits and precision, and the sample availability.

Laser ablation of a free liquid surface is the most straightforward approach, but the main problem is the production of splashes which require continuous cleaning of nearby optical elements.[6] Also, splashes rapidly consume liquid, so the necessary sample volume for analysis is above typically 1 mL. Liquid splashes can be reduced by analysing slowly flowing liquid[9,10] or almost eliminated by ablating the liquid jet.[11–13] Disadvantages of these approaches are the large, requested sample volumes (>10 mL) and the necessity of washing the circuit before introducing a new sample.

In this work, parameters of plasma formed by ablation of thin oil films deposited on a silica wafer substrate[8] were explored. The preferred oil film thickness was managed by controlling the speed of rotation of samples during the preparation phase. Hydrogen Balmer alpha line (H_α) was used to determine electron number density N_e. Spectral line intensity ratios of the successive ionization stages of the magnesium have been used to determine ionization temperature, T_{ion}. The temperature of heavy particles in the plasma (rotational temperature, T_{rot}, and vibrational temperature, T_{vib}) was estimated by comparing the experimental and simulated emission spectra of C_2 and CN molecules. In addition, time evolutions of the spectral intensities, electron number density, and temperature were deduced from time-integrated measurements by subtracting averaged spectra obtained at different time delays.[14] We must have in mind that all spectral measurements reported in this work were spatially integrated. Therefore, all plasma parameters (N_e, T_{ion}, T_{rot} and T_{vib}) determined in this work, including the calculated time-resolved values, are the apparent values of these parameters. For inhomogeneous spectrochemical sources such as laser-induced plasma, the parameters resulting from spatially integrated measurements represent population averages of the local temperature and electron number density values, *i.e.*, they describe the source but are different from the local values.[15] True plasma parameters, *i.e.*, spatial and temporal distribution of plasma parameters, were difficult to determine due to small plasma volume, large gradients of T and N_e, and the limited reproducibility of emission intensity measurements.

EXPERIMENTAL

Materials and methods

In this experiment, pure reference oil (Base Oil 75, further in the text referred to as Oil-0) and standard oil for spectroscopy measurements (SpexCertiPrep) containing 21 elements (Ag, Al, B, Ba, Ca, Cd, Cr, Cu, Fe, Mg, Mn, Mo, Na, Ni, P, Pb, Si, Sn, Ti, V and Zn) were analysed. The concentration of each element present in oil was of 100 ppm (further in the text

referred to as Oil-100). Oil samples were prepared in the form of thin films by placing a small drop of oil (0.3 μL) on a silica wafer (Graphene Supermarket, W-5P-300) cut into pieces with dimensions of 15 mm×15 mm. The silica wafer was glued on an aluminium disk that matched the spin-coater (Laurell Technologies, KL-SCI-20) and then rotated. When the maximum speed of rotation (150 rps) was used for 30 s, a minimal thickness of oil films (0.74 μm) was obtained. Detailed explanations about selecting optimal conditions for sample preparation can be found elsewhere.[8]

In the following, the substrate on the disk was transferred under the LIBS instrument and scanned.

LIBS system

Fig. 1 illustrates the experimental setup. Nd:YAG laser (Quantel, CFR Ultra) emitting 6.5 ns long pulses at 1064 nm was used to induce plasma. The laser beam with a diameter of 6 mm was guided utilizing two mirrors (M1, M2) and beam expander 2.7X (BE) placed between them. Plano-convex quartz lens (L) with focal length f = 100 mm and a 2" diameter was used to focus laser light perpendicularly to the sample, thus obtaining a spot diameter of 0.72 mm. The LIBS measurements were performed with the maximum incident laser energy of 165 mJ, corresponding to the laser fluence of 40.3 J cm^{-2} or 6.2 GW cm^{-2}.

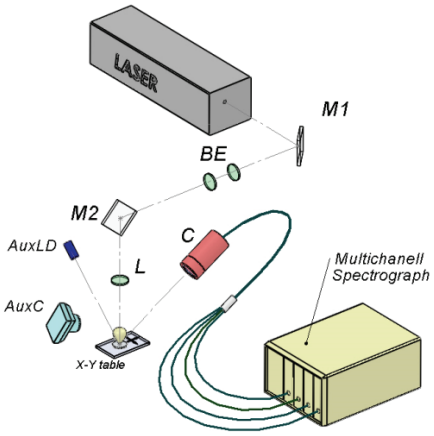

Fig. 1. Experimental setup. M1 and M2 are bending mirrors; BE is beam expander; L is focusing lens; AuxC is video-camera, AuxLD is pointing red diode laser (λ = 635 nm), and C is an optical system for the signal collection.

Plasma emission was then brought to four compact spectrometers (Avantes AvaSpec--ULS2048L), equipped with a grating with a groove density of 2400 or 3600 grooves mm^{-1}. The entrance slits of spectrometers were 10 μm. The spectrometer array covers the spectral range between 200 and 796 nm with the spectral resolution between 0.07 nm in the UV and 0.16 nm in NIR. A digital delay generator (Quantum Composer 9600+) was employed for the external triggering of the laser flash lamp and Q-Switch. DDG was also used for adjusting the acquisition delay from the laser pulse. The acquisition gate width was 1.050 ms. After each laser pulse, the spectra were recorded to monitor and exclude eventual anomalous shots.

RESULTS AND DISCUSSION

Temporal evolution of atomic, ionic and molecular lines

Depending on the characteristics of the laser pulse, the target, and the analyte of interest, it is convenient to optimize the delay time to obtain the best sig-

nal-to-background ratio. For the setup used in this research, it was shown that the optimal signal acquisition delay time in terms of the signal-to-noise ratio of the analytical lines was of 3 μs for the analysis of metal elements in oil.[8]

Fig. 2a shows the evolution of the spectral intensity of several atomic, ionic and molecular species with delay time, obtained by time-integrated measurements. Spectral emission of these species (H I, Mg I, Mg II, C_2 and CN) was used in this research for plasma diagnostics.

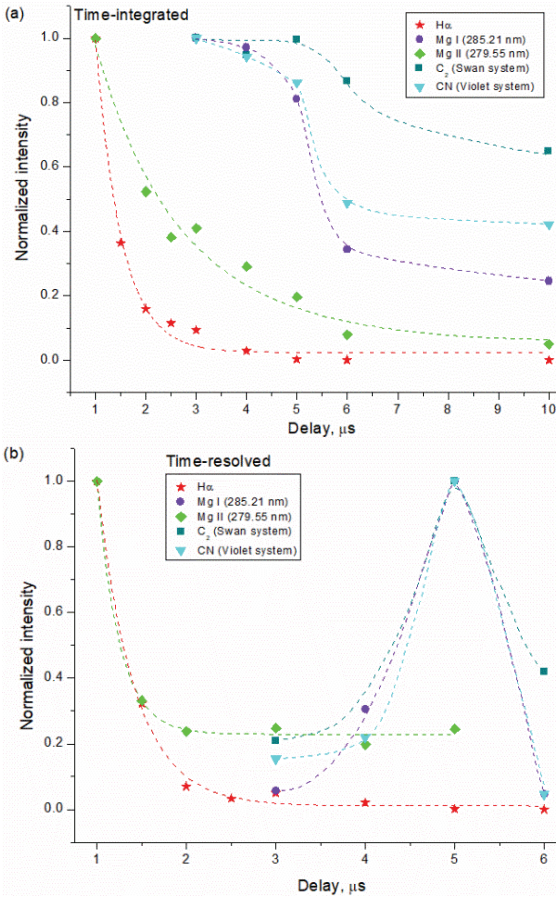

Fig. 2. Spectral line emission intensity of various species in plasma of Oil-100 as a function of time from the laser pulse: a) Time-integrated values and b) calculated time-resolved lines, equivalent to the integration time of 1 μs.

It can be seen in Fig. 2a that the H_α line intensity exponentially decays with the increase of acquisition delay time. The emission intensity of the Mg ionic line also decays exponentially but with the decay rate much slower than H_α. On the other hand, the emission intensity of the neutral Mg spectral line and C_2 and CN molecular emission retain high emission intensity up to around 5 μs and decays exponentially afterward.

The procedure proposed in reference[14] was used to extract time-resolved information from the time-integrated spectra. From a series of the time-integrated emission spectra measured at selected values of delay between the laser pulse and the data acquisition time, the time-resolved emission spectrum was calculated using the following expression:

$$I(t_i)n = \int_{t_i}^{\infty} I(t)\mathrm{d}t - \int_{t_i+n}^{\infty} I(t)\mathrm{d}t \quad (1)$$

where $I(t)$ represents the time-dependent spectral intensity of a given spectral line, t_i is the acquisition delay time, n is a delay interval equivalent to the gate time and $I(t_i)$ is the time-resolved intensity at the delay of t_i. In the present work, the acquisition delay time t_i was varied between 1 and 10 μs, with a step of n = 1 μs.

The calculated time-resolved variation of the spectral intensities as a function of delay time is shown in Fig. 2b. It can be seen that the H_α line emission is concentrated in the initial period of plasma evolution and rapidly exponentially decreases with time. The observed trend was expected because of the high excitation and ionization energies of non-metals. The same trend was observed for the atomic lines of nitrogen and oxygen (not shown in the figure). The Mg II spectral line follows the same trend but decreases more slowly. Due to recombination, which becomes increasingly important by plasma cooling, the intensity of the Mg ionic line decreases over time, while the Mg I line has a maximum at 5 μs and then decreases due to plasma cooling.

Significant emission of C_2 and CN molecular band sequences was registered at 3 μs. At earlier times, the plasma was too hot and did not favor the existence of molecules. Both bands achieve maximum emission at 5 μs and slowly decline afterward, in line with their low excitation energy.

As can be seen from Fig. 2, the calculated time-resolved intensities of the H_α and Mg ionic line (Fig. 2b) show similar profiles as those obtained by time-integrated measurements (Fig. 2a). The only difference is a faster decay of spectral line intensities in the time-resolved evolutions. By contrast, there is a substantial difference in the time-integrated and time-resolved line intensities for Mg I and molecular species. The possible explanation of this difference is as follows. The line profiles in Fig. 2a were obtained from spatially integrated measurements with gate time much longer than the plasma lifetime. Therefore, the measured intensity is composed of contributions from different spatial and time points of the plasma, in which the intensity values are very different. However, the main contribution to the time-integrated spectrum comes from a limited temporal window of the order of the decay time of the emission signal.[14] The emission of ions and high-energy excited atoms decreases faster than the emission signal of neutral atoms and molecules. Moreover, the emission maximum of ions and atoms with high excitation energy is concentrated in the hottest core region, while neut-

ral atoms and molecules populate mainly the plasma periphery. The plasma emission that enters the aperture of the optical fibre may comprise contributions both from the high and low T and N_e regions, whereby these contributions may differ for the short and long delay times. In other words, for short delays, the collected emission may be composed of both high and low T and N_e regions, while at longer delay times, mainly from the low-temperature and low-density regions.

The results presented in Fig. 2b are consistent with the expected behaviour of spectral line intensities due to the expansion and cooling of plasma and recombination processes. These results were further used to obtain the time evolution of the plasma parameters.

Determination of the electron number density

In this work, a standard deconvolution procedure was applied to the observed Voigt-type line profile (w_V) to determine the H_α line Stark width (w_S). The Gaussian fraction is assumed to be a combination of the instrumental and the Doppler broadening, while the Lorentzian component is due to Stark broadening. The Stark width w_S was calculated using the following expression:[16]

$$w_V = 0.5346\ w_L + \sqrt{0.2169\ {w_L}^2 + {w_G}^2}\ ;\ w_G = \sqrt{w_D^2 + w_i^2} \tag{2}$$

where w_V, w_L, w_G, w_D and w_i are the full width at half maximum (FWHM) of the Voigt, Lorentz, Gaussian, Doppler and instrumental profile (experimentally determined), respectively. The contribution of Doppler broadening was found to be negligible for T_g between 10000 and 20000 K.

An approximate formula was then used to calculate N_e / m^{-3}:[17,18]

$$N_e = 10^{23}\left(\frac{w_{SA}}{1.098}\right)^{1.47135} \tag{3}$$

where w_{SA} / nm is the half-width at half area (HWHA) of the H_α spectral line. The H_α line profile is close to Lorentzian, so it was justified to accept $w_{SA} = w_S = w_L$.[17] Finally, it should be pointed out that Eq. (3) differs from the original one,[18] where HWHA was used instead of the claimed.[19]

Fig. 3a shows the H_α line profile recorded at different delay times of the start of signal acquisition.

As expected, considering the high excitation energy of the H_α line, with the delay, both intensity and width of the spectral line profile decrease due to the plasma expansion and cooling. The electron number density calculated from the Stark-broadened H_α line profile (Eq. (3)) shows a rapidly decreasing trend, from 9.5×10^{16} cm^{-3} at gate delay of 1 μs, to 4.7×10^{15} cm^{-3} at a delay of 6 μs. By subtracting the spectra corresponding to different delay times, the temporal evolution of the emission signal and the corresponding electron number density was

roughly reconstructed,[14,20] as shown in Fig. 3b. Differences in time-integrated and time-resolved N_e values originate from different meanings of these values. While in the first case, they represent temporally and spatially averaged values of electron number density, in the second case, they correspond to a particular plasma evolution stage.

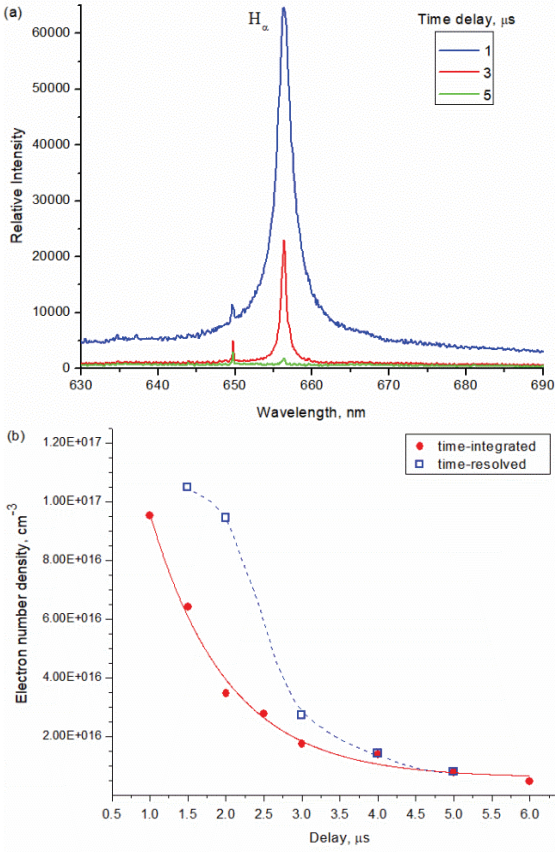

Fig. 3. a) Example of time-integrated H_α line profile at various delays for Oil-100 and b) electron number density at different delays for time-integrated and time-resolved spectra.

Evaluation of plasma temperature

In the oil samples analysed in this paper, the maximum concentration of individual elements was 100 ppm, which was insufficient for the appearance of spectral lines with higher excitation energy that would be suitable for determining T_{exc} using the Boltzmann plot method. Therefore, it was not possible to determine T_{exc} in the plasma of our samples.

Determination of the ionization temperature

The intensity ratio of the ionic and atomic spectral line of the same element is suitable for plasma diagnostics: with a predetermined temperature, the electron

number density can be calculated from it, or vice versa, if the electron number density is predetermined, this approach may be applied for evaluation of the ionization temperature.[21] By substituting the values for physical constants, the expression for the ratio of the integral intensities of the ionic (+) and atomic line (a) reads:

$$\frac{I^+}{I^a} = 4.83\times10^{15}\frac{g^+A^+\lambda^a}{g^aA^a\lambda^+}\frac{\sqrt{T^3}}{N_e}e^{-\frac{11605\left(E^+_{exc}+E_{ion}-E^a_{exc}-\Delta E_{ion}\right)}{T}} \quad (4)$$

where g^+ and g^a are the corresponding statistical weights of ions and atoms, A^+ and A^a are the transition probabilities, N_e the electron number density in cm^{-3}, T is the temperature in K, E^+_{exc} and E^a_{exc} are the excitation energies in eV*, and E_{ion} and ΔE_{ion} are the ionization energy and the reduction of E_{ion} due to Debye shielding, in eV.

Magnesium lines in the spectral region around 280 nm are very suitable for plasma diagnostics.[22,23] The transition probabilities for the Mg I 285.21 nm, Mg II 280.27 nm, and Mg II 279.55 nm lines were determined with accuracy better than 3 %.[24] By substituting the corresponding constants for the Mg I 285.21 nm and Mg II 279.55 nm lines into Eq. (4), the following expression was obtained:

$$\frac{I^+}{I^a} = 3.48\times10^{15}\frac{\sqrt{T^3}}{N_e}e^{-\frac{11605\left(7.734-\Delta E_{ion}\right)}{T}};\ \Delta E_{ion} = 9.96\times10^{-7}N_e^{1/3} \quad (5)$$

The intensity ratio of the corresponding atomic and ionic lines of Mg was measured at different delay times. Part of the LIBS spectrum in the interval 278 to 286 nm is shown in Fig. 4a. Three peaks fitting by the Gaussian function was applied on lines of interest, and peak area was used for further calculations.

The results presented in this work were obtained from the intensity ratio of the Mg II 279.55 nm and Mg I 285.21 nm emission lines. It should be noted that the same results were obtained utilizing the ratio of Mg II 280.27 nm and the Mg I 285.21 lines for plasma characterization.

These two Mg II lines have almost the same E_{exc} and values of transition probability A and differ only by the g values (4 and 2 for Mg II 279.55 nm and Mg II 280.27, respectively). Thus, to utilize data for the measured intensity ratio of Mg II 280.27 nm and Mg I 285.21 nm lines, it is sufficient to divide by 2 the constant ($3.48\cdot10^{15}$) from Eq. (5).

The obtained dependence of T_{ion} on the delay time shows that the temperature decreases from the value of ~8800 K corresponding to a delay of 2 μs to ~6900 K at 6 μs, Fig. 4b. The observed trend was expected considering the plasma expansion and cooling over time. Since they were estimated from time-

* 1 eV = 1.602×10^{-19} J

-integrated measurements, the obtained T_{ion} values represent the averaged values of this plasma parameter and differ from the calculated time-resolved values that characterize a particular plasma evolution stage.

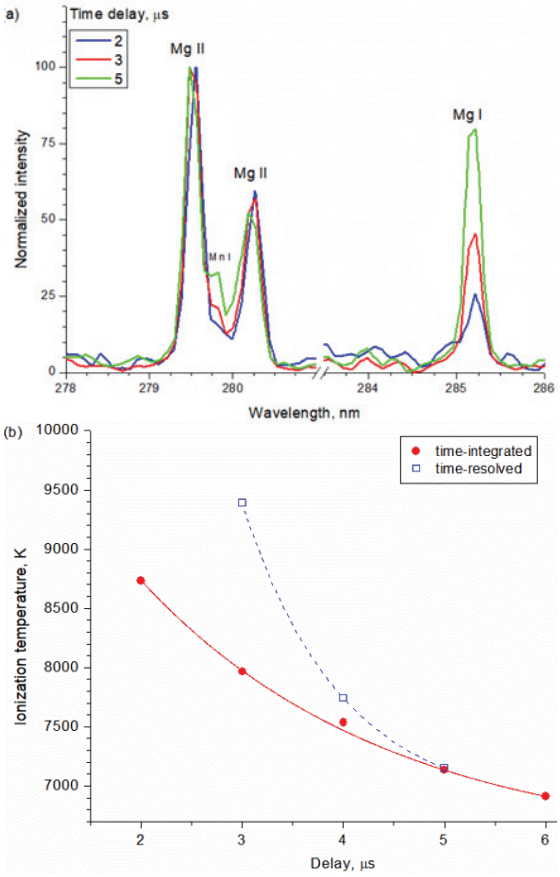

Fig. 4. a) Part of the LIBS spectrum of Oil-100 showing Mg emission lines; b) the ionization temperature as a function of the delay time for Oil-100.

Determination of rotational and vibrational temperatures

Apart from the atomic emission, LIBS spectra of the oil film deposited on a silicon substrate were dominated by high-intensity emission bands corresponding to CN and C_2 molecules. Due to the relatively high dissociation energies (7.72 eV for CN, and 6.27 eV for C_2),[25] low excitation potentials, and favourable transition probabilities, the CN violet system and C_2 Swan system bands can be readily observed in the LIBS spectra of carbon-containing materials. As it is seen in Fig. 5, intense CN molecular bands corresponding to $\Delta\nu$ 0, –1 and +1 sequence were registered. The figure also shows C_2 molecular bands corresponding to $\Delta\nu = 0$ and $\Delta\nu = +1$ sequence with (0-0) band head at 516.52 nm, and $\Delta\nu =$ $= +1$ with (1-0) band head at 473.71 nm, which were of somewhat lower int-

ensity. The $\Delta v = -1$ sequence with (0-1) band head at 563.55 nm, located in the spectral region 546–570 nm, could not be registered using the present setup.

The resolution of the used spectrometers was not high enough to provide a well-resolved rotational structure of the registered CN molecular bands. Therefore, these bands were unsuitable for the determination of the rotational temperature. Differently, vibrational band heads of the $\Delta v = 0$ and $\Delta v = -1$ sequences were sufficiently resolved, which allowed their use for the estimation of the vibrational temperature.

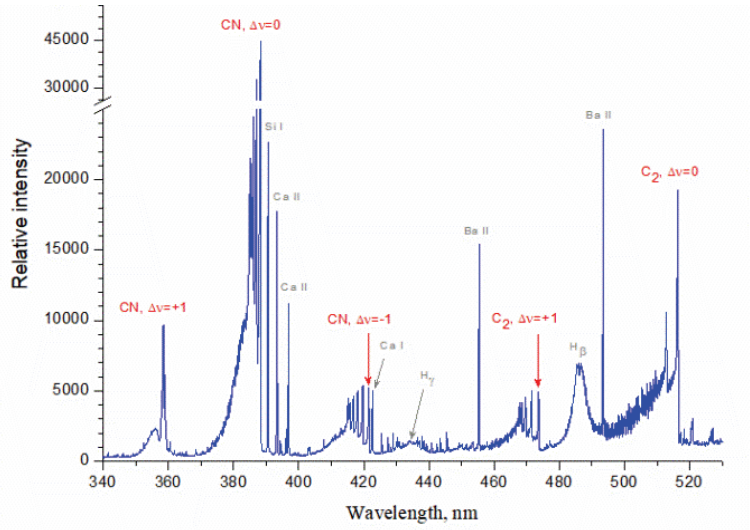

Fig. 5. Part of the time-integrated LIBS spectra of Oil-100 sample showing characteristic emission bands of C_2 and CN molecules.

Fig. 6a compares the experimental spectrum of the sample Oil-5 and synthetic spectra of the $\Delta v = -1$ sequence calculated for several different temperatures. The synthetic spectra were obtained using the program LIFBASE 2.1.1,[26] with a pure Gaussian line profile of 0.173 nm, as determined by deconvolution of the adjacent analyte (metal) spectral lines and assuming the rotational and vibrational temperature were equal. The instrumental profile estimated using the oil sample with a doped concentration of the analyte elements of 5 ppm was the same as that determined using the Argon spectral calibration lamp. All spectra were normalized to the intensity of the (0-1) band head. It is evident that the widths of the experimental and synthetic band heads were the same, implying an insignificant influence of self-absorption. The vibrational temperature was estimated at 5800 K with an error lower than 500 K. Approximately the same value for the rotational temperature could be estimated from the spectrum between the

(1-2) and (0-1) band heads (whose intensity entirely depends on the rotational temperature), although certainly with much lower accuracy.

In the $\Delta v = +1$ sequence of C_2 Swan system, five well-separated band heads were registered, suitable for determining the vibrational temperature because their relative intensity ratios are markedly dependent on temperature. Fig. 6b compares the normalized synthetic spectra for several temperatures (assuming that the vibrational and rotational temperatures are equal), with a pure Gaussian profile of 0.14 nm (determined experimentally) with an experimental spectrum of the Oil-0 sample. The synthetic spectra were obtained using the program PGOPHER 10.1.182.[27] As it can be seen in Fig. 6b, self-absorption can be neglected because the widths of the corresponding experimental and theoretical profiles coincide. The vibrational temperature was estimated at 4800 K, with an error lower than 300 K. An increase of the acquisition delay time, from 3 to 10 μs, showed a small but measurable trend of decreasing vibrational temperature. For a given delay time interval, the vibrational temperature decreased by approximately 700 K.

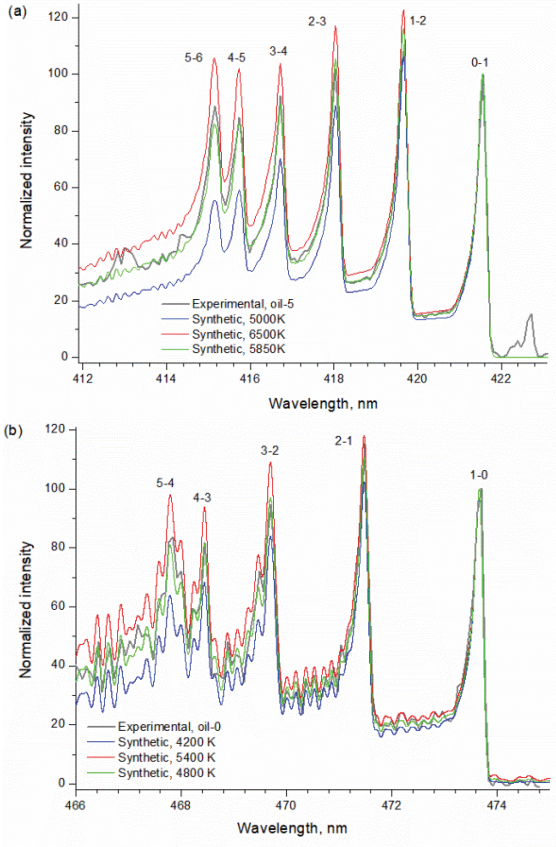

Fig. 6. Comparison of the experimental and synthetic spectra of the: a) CN violet system $\Delta v = -1$ sequence for Oil-5 and b) C_2 Swan system $\Delta v = +1$ sequence for Oil-0.

The difference in the temperatures estimated from the CN bands (5850 K) and C_2 bands (4800 K) indicates a different plasma zone from which CN and C_2 bands are predominantly emitted, which is partly related to a slightly higher excitation and dissociation energy of CN molecule (E_{exc} = 3.19 eV, E_{dis} = 7.8 eV) relative to the C_2 molecule (E_{exc} = 2.39 eV, E_{dis} = 6.2 eV).[28] Also, the difference may be due to the different time evolution of the emission bands, where the C_2 emission has a maximum at 5 μs and a slower decay time than CN (Fig. 2). Thus, the calculated temperatures for C_2 from the integrated spectra are characteristic for later stages of the plasma evolution. The difference may also be a consequence of different formation mechanisms for these two molecular species. Due to much smaller energy differences between adjacent vibrational, and especially rotational levels of molecules compared to differences in electronic states of free atoms, it is assumed that rotational and vibrational temperatures correspond to the temperature of heavy particles in the plasma (*i.e.*, the gas temperature).[29] The $\Delta v = 0$ sequences of both systems were not used for temperature estimation because they show significant self-absorption.

The difference between the temperatures determined from the molecular bands and using the emission of atomic and ionic lines is a consequence of the fact that plasma emission was registered spatially and temporally integrated. At the same time, molecules, atoms, and ions have their maximum emission intensity in plasma zones characterized by different temperatures.

The difference between the temperatures determined from the molecular bands and using the emission of atomic and ionic lines is a consequence of the fact that plasma emission was registered spatially and temporally integrated. At the same time, molecules, atoms, and ions have their maximum emission intensity in plasma zones characterized by different temperatures.

CONCLUSIONS

Time-integrated and time-resolved spectral line intensities imply that the emission of nonmetals and metal ions (H I and Mg II) are more intense in the earlier stages of plasma evolution. In contrast, the emission of atomic and molecular band lines occurs later, reaching maximum intensity at around 5 μs. Apparent values of electron number density (derived from time-integrated measurements of the H_α line profile) rapidly decrease from 9.5×10^{16} cm^{-3} at gate delay of 1 μs to 4.7×10^{15} cm^{-3} at a delay of 6 μs. The estimated time-resolved values for N_e show a similar declining trend. Ionization temperature (derived from Mg II/Mg I spectral line intensity ratio) also shows a declining trend with time. For time-integrated measurements, T_{ion} decreases from 8800 K at gate delay of 2 μs to 6900 K at a delay of 6 μs. Similar to the N_e values, the time-resolved values of T_{ion} have higher values and decrease faster than time-integrated values. The observed difference is understandable since time-integrated measurements represent

temporally and spatially averaged plasma parameters, while time-resolved values correspond to a particular plasma evolution stage.

Evaluation of the vibrational-rotational temperature from the molecular bands spectra gave different values for CN (5800 K) and C_2 molecules (4800 K), probably due to different formation mechanisms of these two molecular species and a difference in their dissociation and excitation energies. Increasing the detection delay time causes a slight decrease of the estimated temperature, about 700 K, for a delay time change from 3 to 10 μs.

Acknowledgments. The research was funded by the Ministry of Education, Science and Technological Development of the Republic of Serbia, Contract numbers: 451-03-9/2021-14/200024, 451-03-9/2021-14/200146, and 451-03-9/2021-14/200017. Milica Vinic acknowledges ENEA (Italy) for supporting her work on the collection of experimental data presented in this work. The authors acknowledge Dr. Violeta Lazić from ENEA (Italy) for providing the experimental data used in this work and for helpful scientific discussions.

ИЗВОД

ДИЈАГНОСТИКА ПЛАЗМЕ ИНДУКОВАНЕ ДЕЈСТВОМ ЛАСЕРСКОГ ЗРАЧЕЊА НА ТАНКИ ФИЛМ УЉА НА СУПСТРАТУ ОД СИЛИЦИЈУМА

МИЛИЦА ВИНИЋ[1], МИРОСЛАВ КУЗМАНОВИЋ[2], ЈЕЛЕНА САВОВИЋ[3] и МИЛИВОЈЕ ИВКОВИЋ[1]

[1]Институт за физику, Универзитет у Београду, Београд, [2]Факултет за физичку хемију, Универзитет у Београду, Београд и [3]Институт за нуклеарне науке "Винча", Универзитет у Београду, Београд

Тема овог рада је дијагностика плазме која се формира интеракцијом наносекундног Nd:YAG ласера са танким филмом уља нанешеним на супстрат од силицијума. Експериментални услови за спектрална мерења оптимизовани су у сврху елементне анализе метала присутних у траговима. Снимљени спектри су интегрални по простору и времену, али је временски разложене спектре могуће конструисати одузимањем усредњених спектара снимљених са различитим временима кашњења. Густина електрона процењена је из ширине Штарковог профила водоникове Балмер алфа линије. Температура јонизације рачуната је из односа интензитета јонске и атомске линије магнезијума. Процењена привидна вредност густине електрона креће се у опсегу од $1{,}07\times10^{17}$ cm^{-3} (за 1,5 μs) до $1{,}5\times10^{16}$ cm^{-3} (за 4 μs). Процењена привидна вредност температуре јонизације креће се у опсегу од 9400 K (за 3 μs) до 7200 K (за 5 μs). Из емисионих спектара C2 и CN молекула процењена је ротациона и вибрациона температура.

(Примљено 22. децембра 2021, ревидирано 21. марта, прихваћено 23. марта 2022)

REFERENCES

1. D. A. Cremers, R. C. Chinni, *Appl. Spectrosc. Rev.* **44** (2009) 457 (https://dx.doi.org/10.1080/05704920903058755)
2. R. Noll, *Laser-Induced Breakdown Spectroscopy*, Springer, Heidelberg, 2012 (https://dx.doi.org/10.1007/978-3-642-20668-9)
3. D. W. Hahn, N. Omenetto, *Appl. Spectrosc.* **64** (2010) 335A (https://dx.doi.org/10.1366/000370210793561691)

4. D. W. Hahn, N. Omenetto, *Appl. Spectrosc.* **66** (2012) 347 (https://dx.doi.org/10.1366/11-06574)
5. V. Lazic, in *Laser-Induced Breakdown Spectroscopy*, S. Musazzi, U. Perini (Eds.), Springer-Verlag, Berlin, 2014, p. 195 (https://doi.org/10.1007/978-3-642-45085-3_8)
6. V. Lazic, R. Fantoni, A. Palucci, M. Ciaffi, *Appl. Spectrosc.* **71** (2017) 670 (https://dx.doi.org/10.1177/0003702816685096)
7. N. Aras, Ş. Yalçın, *Talanta* **149** (2016) 53 (https://dx.doi.org/10.1016/j.talanta.2015.11.031)
8. M. Vinić, E. Aruffo, F. Andreoli, M. Ivković, V. Lazic, *Spectrochim. Acta, B* **164** (2020) 105765 (https://dx.doi.org/10.1016/j.sab.2020.105765)
9. K. Rifai, S. Laville, F. Vidal, M. Sabsabi, M. Chaker, *J. Anal. At. Spectrom.* **27** (2012) 276 (https://dx.doi.org/10.1039/c1ja10178a)
10. L. St-Onge, E. Kwong, M. Sabsabi, E.B. Vadas, *J. Pharm. Biomed. Anal.* **36** (2004) 277 (https://dx.doi.org/10.1016/j.jpba.2004.06.004)
11. P. Yaroshchyk, R. J. S. Morrison, D. Body, B. L. Chadwick, *Spectrochim. Acta, B* **60** (2005) 986 (https://dx.doi.org/10.1016/j.sab.2005.03.011)
12. N-H. Cheung, E. S. Yeung, *Anal. Chem.* **66** (1994) 929 (https://dx.doi.org/10.1021/ac00079a003)
13. N. K. Rai, A. K. Rai, *J. Hazard. Mater.* **150** (2008) 835 (https://dx.doi.org/10.1016/j.jhazmat.2007.10.044)
14. E. Grifoni, S. Legnaioli, M. Lezzerini, G. Lorenzetti, S. Pagnotta, V. Palleschi, *J. Spectrosc.* **2014** (2014) 1 (https://dx.doi.org/10.1155/2014/849310)
15. C. Aragón, J. A. Aguilera, *Spectrochim. Acta, B* **63** (2008) 893 (https://dx.doi.org/10.1016/j.sab.2008.05.010)
16. J. J. Olivero, R. L. Longbothum, *J. Quant. Spectrosc. Radiat. Transf.* **17** (1977) 233 (https://dx.doi.org/10.1016/0022-4073(77)90161-3)
17. N. Konjević, M. Ivković, N. Sakan, *Spectrochim. Acta, B* **76** (2012) 16 (https://dx.doi.org/10.1016/j.sab.2012.06.026)
18. M. A. Gigosos, M. A. González, V. Cardeñoso, *Spectrochim. Acta, B* **58** (2003) 1489 (https://dx.doi.org/10.1016/S0584-8547(03)00097-1)
19. M. A. Gonzalez, *private communication* (2012)
20. R. Ahmed, N. Ahmed, J. Iqbal, M. A. Baig, *Phys. Plasmas* **23** (2016) 083101 (https://dx.doi.org/10.1063/1.4959866)
21. P. W. J .M. Boumans, *Theory of Spectrochemical Excitation*, Hilger &Watts LTD, London, 1966
22. J. M. Mermet, *Anal. Chim. Acta* **250** (1991) 85 (https://dx.doi.org/10.1016/0003-2670(91)85064-Y)
23. E. Tognoni, M. Hidalgo, A. Canals, G. Cristoforetti, S. Legnaioli, A. Salvetti, V. Palleschi, *Spectrochim. Acta, B* **62** (2007) 435 (https://dx.doi.org/10.1016/j.sab.2007.05.006)
24. W. Ansbacher, Y. Li, E. H. Pinnington, *Phys. Lett., A* **139** (1989) 165 (https://dx.doi.org/10.1016/0375-9601(89)90353-8)
25. A. D. Pradhan, H. Partridge, C. W. Bauschlicher, *J. Chem. Phys.* **101** (1994) 3857 (https://dx.doi.org/10.1063/1.467503)
26. J. Luque, D. R. Crosley, *SRI Int. MP* **99** (1999) https://www.sri.com/engage/products-solutions/lifbase

27. C . M .Western, *J. Quant. Spectrosc. Radiat. Transf.* **186** (2017) 221 (https://dx.doi.org/10.1016/j.jqsrt.2016.04.010)
28. A. De Giacomo, J. Hermann, *J. Phys., D* **50** (2017) 183002 (https://dx.doi.org/10.1088/1361-6463/aa6585)
29. M. Venugopalan, *Reactions under plasma conditions*, John Wiley and Sons, Inc, New York, 1971.

Journal of the Serbian Chemical Society
JSCS@tmf.bg.ac.rs • www.shd.org.rs/JSCS
J. Serb. Chem. Soc. *88* (2) 169–182 (2023)
JSCS–5618
Original scientific paper
Published 30 September 2022

Anticorrosion action of the olive leaf compounds extracted under optimal parameters as determined with experimental design

SOUAD TOUAZI[1,2]*, MIHAEL M. BUČKO[3#], RADOUANE MAIZIA[2], SAMIRA SAHI[1], NADIA ZAIDI[2] and LAID MAKHLOUFI[2]

[1]Laboratoire de Valorisation des Energies Fossiles (LAVALEF), Ecole Nationale Polytechnique d'Alger, Algeria, [2]Laboratoire d'Electrochimie, Corrosion et de Valorisation Energétique (LECVE), Faculté de Technologie, Université de Bejaia, Algeria and [3]Military Academy, University of Defence, Veljka Lukića Kurjaka 33, Belgrade, Serbia

(Received 13 May, revised 6 July, accepted 1 August 2022)

Abstract: In this study, an agricultural waste product was used to prepare a green corrosion inhibitor based on olive leaves (*Olea europaea* var. *syslvestris*). Firstly, an optimization study of antioxidant activity of *O. europaea* leaves monitored by the DPPH free radical trapping method, was carried out using full factorial design. In the second step, the extract obtained under optimal conditions was tested as a green corrosion inhibitor for steel in 0.5 mol dm^{-3} HCl, using gravimetric and electrochemical methods. The results obtained by various techniques showed that the extract acted as a mixed-type inhibitor. The adsorption of the inhibitor was spontaneous (ΔG_{ads} = −12.443 kJ mol^{-1}), through the mechanism of physical adsorption, and it obeyed the Langmuir adsorption isotherm. The highest corrosion inhibition efficiency of 92 % was obtained for 2.8 10^{-3} g $cm^{-3}$of inhibitor, as measured by gravimetric method.

Keywords: antioxidant activity; extraction; green inhibitor.

INTRODUCTION

In industry, acid solutions are widely used, and the aggressiveness of these solutions causes metals degradation, either through chemical or electrochemical reactions. The most effective method of preventing or decreasing the bare metal dissolution in such acidic solutions, is the use of corrosion inhibitors, that are nowadays widely applied. Corrosion inhibitors are chemical compounds used to reduce the corrosion rate of metals and alloys in contact with aggressive environ-

* Corresponding author. E-mail: souad.touazi@g.enp.edu.dz
# Serbian Chemical Society member.
https://doi.org/10.2298/JSC220513064T

ments at low concentrations,[1] thereby delaying and minimizing the corrosion process and thus avoiding economic losses due to metallic corrosion.

Numerous synthetic compounds show good corrosion inhibiting action, but many of them are extremely toxic to humans and environment. Therefore, the development of non-toxic and biodegradable corrosion inhibitors is becoming a key issue as new global guidelines for industrial discharges are becoming increasingly ecologically strict.[2–6] Plants are one of the sources for these inexpensive and clean inhibitors. Plant parts contain many compounds that satisfy the required criteria.

In the Mediterranean coastal zone, olive leaves are one of the by-products in the olive grove farming; they occur in high quantities in olive oil industry. They are also collected during the pruning of the olive trees.[7] Olive leaves are a cheap raw material known for its antioxidant properties.[8] Following this line, our work focuses on the inhibitory action of the olive leaf-based, green and natural substance, from *Olea europaea* var. *sylvestris*, in the corrosion process of steel in 0.5 mol dm^{-3} HCl.

The present investigation was divided into two parts: in the first part, a full factorial design (FFD) optimization study of antioxidant activity of the extract from *O. europaea* leaves was conducted, using the DPPH free radical method. In the second part, the extract obtained under optimal conditions was tested for steel corrosion inhibition in hydrochloric acid by means of weight loss measurement, potentiodynamic polarization and impedance spectroscopy.

EXPERIMENTAL

Samples and reagents

Plant material consisting of leaves of *Olea europea* var. *sylvestris* was harvested in the Algiers region, situated in the north of Algeria, during the flowering period between February and March 2018. The collected samples were identified by the national High School of Agronomy. The leaves were washed in distilled water, dried at room temperature, and subsequently dried in an oven at 40 °C. They were grounded to obtain the powder, and then stored in a closed plastic box.

Methanol, ethanol, 2,2-diphenyl-1-picrylhydrazyl (DPPH) and HCl (37 %) of analytical grade, were purchased from Sigma–Aldrich.

Plant material extraction

The effects of different variables such as extraction temperature, solid/solvent ratio, water/ethanol ratio and extraction time, on the antioxidant activity, were studied using FFD. The conditions used in each experiment were settled according to the 2^4 FFD, as presented in Table I.

The powdered sample of *O. europea*, which had been previously weighed, was placed in a Bicol flask, in contact with the extracting solvent. The mixture was kept in a thermostatic water bath with shaking. After a determined extraction time, the mixture was cooled in an ice bath, and then separated. The obtained filtered extracts were stored in the dark for future use

for the determination of their antioxidant activity. The concentration of extracts (g cm^{-3}) was determined by evaporating 10 cm^3 of the filtrate and then weighing the obtained residue.[9]

TABLE I. Range of coded and actual values for FF

Independent variable	Coded variable	Level		
		(−1)	(0)	(+1)
Extraction temperature, °C	X_1	55	68	81
Solid/solvent ratio, g 100 cm^{-3}	X_2	08	12	16
Water/ethanol ratio, vol. %	X_3	25	50	75
Extraction time, min	X_4	45	60	75

Estimation of antioxidant activity

The effect of each antioxidant on DPPH-radical was estimated according to the procedure described by Brand-Williams *et al.*[10] Briefly, 1 cm^3 of the extract solution was added to 9 cm^3 of DPPH (40μg cm^{-3} prepared in methanol), and at the same time, a negative control (the blank) was prepared by mixing 1 cm^3 of methanol with 9 cm^3 of the methanol solution of DPPH. The samples were kept in the dark for 30 min. The absorbance measurements were carried out at the wavelength of 517 nm, using a UV–Vis spectrophotometer.

The antioxidant activity (AA / %) was calculated as:[11]

$$AA = (A_{\text{blank}} - A_{\text{sample}})/A_{\text{blank}} \quad (1)$$

where A_{blank} represents the absorbance of negative control and A_{sample} is the absorbance of the sample (diluted extract).

Experimental design

In this study, FFD methodology has been carried out to optimize the antioxidant activity of the samples. Two levels and four variables were used in this investigation, requiring 16 (2^4) experiments plus four experiments performed at the center point to evaluate the experimental error variance. The four selected factors were studied between a lower level coded (−1), a higher level coded (+1) and the center point coded (0). The actual and coded levels of the independent variables are presented in Table I.

The regression equation which includes all interaction terms was given by the following expression:

$$Y_i = b_0 + \sum_{i=1}^{4} b_i X_i + \sum_{i=3}^{3} \sum_{j=i+1}^{4} b_{ij} X_i X_j + \varepsilon \quad (2)$$

where Y_i is the predicted response, X_i represents the independent variables coded (1 or −1), b_0 is the average value of the response of sixteen assays, b_i represents the principal effect, whereas b_{ij} represents the interaction effect and ε is a random error.

Corrosion test

The working electrode used in the present study was steel, with the chemical composition presented in Table II. Prior to each experiment, the working electrode was polished with various emery paper grades (280, 360, 800 and 1000), degreased with acetone and rinsed in distilled water before being placed into the aggressive solution.

For weight loss measurements, the steel coupons with a surface area of 16.5 cm^2, were immersed in 100 cm^3 of 0.5 mol dm^{-3} HCl at 25 °C, without and with different concentrations of the olive leaf extract. Corrosion rate (C_R), inhibition efficiency (η) and the degree of sur-

face coverage (θ) were calculated from the weight loss measurements, determined at different immersion times for a total duration of 8 days, by using the equations:[12,13]

$$C_R = (W_b - W_A)/A \quad (3)$$

$$\eta = 100(C_R(\text{free}) - C_R(\text{inh}))/C_R(\text{free}) \quad (4)$$

$$\theta = \eta/100 \quad (5)$$

where W_b and W_a are the coupon weight measured before and after immersion in the aggressive solution, A is the exposed area, and C_R(free) and C_R(inh) are the corrosion rates of steel in the absence and presence of the inhibitor in the aggressive solution, respectively.

TABLE II. Composition of steel

Element	C	Si	Mn	P	S	Mo	Fe
Content, wt. %	0.15–0.26	<0.35	<1.5	<0.035	<0.040	0.4–0.6	97–98

Open circuit potential (OCP) and potentiodynamic polarization measurements were carried out using a Voltamaster software piloted potentiostat PGZ100. This potentiostat was connected to the three electrodes: steel panel as a working electrode, a platinum panel used as a counter electrode and K_2SO_4-saturated sulphate electrode (SSE) as the reference.

Tafel plots were obtained at a scan rate of 1 mV s^{-1}, over the respective OCP range between −250 and 250 mV (from cathodic to anodic end), after the constant OCP was established. The inhibition efficiency (η) was determined as:[14]

$$\eta = 100(j_{corr}(\text{free}) - j_{corr}(\text{inh}))/j_{corr}(\text{free}) \quad (6)$$

where j_{corr}(free) and j_{corr}(inh) are the corrosion current densities in free and inhibited acid solution, respectively.

Electrochemical impedance spectroscopy (EIS) tests were carried out at OCP in an aerated solution using an Autolab potentiostat/galvanostat (PGSTAT30) under FRA software. The response of the electrochemical system to AC excitation was measured with a frequency ranging from 100 kHz to 10 mHz and peak to peak AC amplitude of 10 mV.

For the electrochemical tests, the exposed area of the steel was 1 cm^2.

RESULTS AND DISCUSSION

Optimization of extraction parameters

Four variables and two levels were chosen to build the FFD in order to find the optimum combination of conditions for the extraction of active substances from the olive leaves. Variables such as extraction temperature (X_1), solid/solvent ratio (X_2), water/ethanol ratio (X_3) and extraction time (X_4) were selected as the independent variables, and antioxidant activity was taken as the response of the design experiments (Y). The results collected to build the FFD model are given in Table S-I of Supplementary material to this paper.

To obtain the mathematical model that represents the antioxidant activity with the first order polynomial (Eq. (2)), the regression analysis was applied on the experimental data using Statistica Software 7.0. Various effects of factors and their interactions were calculated using the analysis of variance (ANOVA) and other adequacy measures.

Fig. 1 shows the Pareto chart, which represents the analysis of the calculated standardized effects of the independent variables and their interactions, on the response value of antioxidant activity. As can be seen in the Pareto charts, the solid/solvent ratio (X_2) presented the most influencing parameter on the response. Whereas the interaction effects of extraction time with water/ethanol ratio (X_3, X_4) and extraction time with solid/solvent ratio (X_2,X_4) were insignificant, and therefore were eliminated from the regression equation. The negative value of the standardized effect indicates that the response decreases with increase of the value of this variable, and the opposite is the case for the positive value.

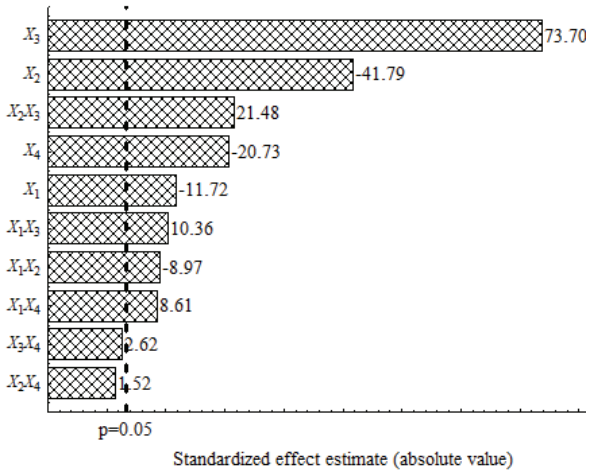

Fig. 1. Pareto chart of the response value of antioxidant activity on various independent variables and their interactions.

Table S-II of the Supplementary material shows the ANOVA analysis, used to verify the adequacy of the models at confidence level of 95 %. The regression *p*-value and *F*-value reveal that the model was highly significant and represented the data satisfactorily. In other words, the value of pure error is very low (0.84) suggesting strong data reproducibility.

A good adjustment of the regression equation to the experimental data was verified through the determination of coefficient value R^2 (0.954) which is close to 1, indicating that only 4.6 % of the variations in observed data could not be explained by the model (Fig. 2a). The value of the adjusted R^2 is equal to 0.905 which was also of very high importance to the model.

The comparison of experimental data and predicted values is shown in Fig. 2b. It can be seen that the predicted responses are in agreement with the experimental data and the difference between them does not exceed 0.055, indicating that the mathematical model is adequate. The final polynomial equation (Eq. (7))

representing the antioxidant activity as a function of the significant effects, was written as:

$$Y_i = 66.26 - 1.51X_i + 9.73X_3 - 2.74X_4 - 1.18X_1X_2 + 1.73X_1X_3 + \\ + 1.14X_1X_4 + 2.83X_2X_3 \quad (7)$$

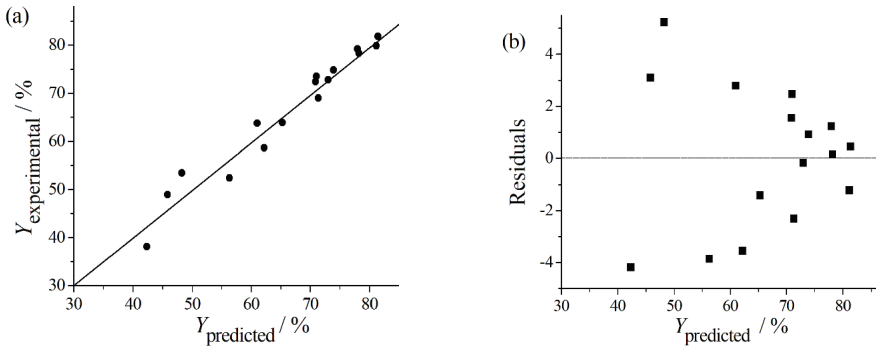

Fig. 2. Quality analysis of the model: a) experimental *versus* predicted responses, b) residual *versus* predicted value for antioxidant activity (Y_i).

The numerical optimization of the desirability function gave optimal conditions to obtain olive leaf extract with a maximum antioxidant activity. With the analysis of the prediction profiler at maximal desirability (Fig. S-1 in the Supplementary material), it can be deduced that the best response of antioxidant activity was obtained at the following conditions: extraction temperature (55 °C), solid/ /solvent ratio (8 g 100 cm^{-3}), water/ethanol ratio (75 %) and extraction time (45 min), with 0.99 as the value of desirability.

Corrosion tests

Weight loss measurements. Different concentrations of the olive leaf extract obtained under optimum conditions deduced from antioxidant capacity measurements, were added to 0.5 mol dm^{-3} HCl. Corrosion of steel in the solutions prepared in this manner, was monitored by weight loss experiments, *i.e.*, by measuring the mass of the metal converted into corrosion products per unit of surface area, per unit of time. Fig. 3a and b represent the variation in corrosion rate and inhibitory efficiency, calculated from the weight loss measurements.

The Fig. 3 inspection shows clearly that the rate of steel corrosion is significantly reduced, *i.e.*, the inhibition efficiency is increased, with the addition of olive leaf extract. This behavior represents the extract's inhibiting effect against the acid corrosion of steel. The maximum inhibition efficiency of 92 % was achieved for 2.8 10^{-3} g cm^{-3} of the added extract.

Open circuit potential measurements. It is well known that the formation of protective corrosion products or a surface protective film in general, can be eva-

luated by monitoring the OCP of the corroding electrode. The effect of various concentrations of olive leaf extract on the steel electrode OCP in 0.5 mol dm^{-3} HCl, is shown in Fig. 4.

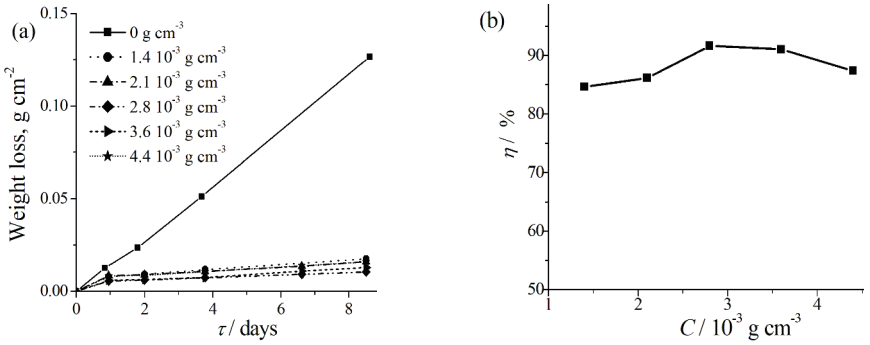

Fig. 3. a) Variation of the weight loss data with the immersion time recorded for steel electrode in 0.5 mol dm^{-3} HCl solution, in the absence and presence of various concentrations of extract; b) inhibition efficiency *versus* the concentration of the inhibitor, deduced from a).

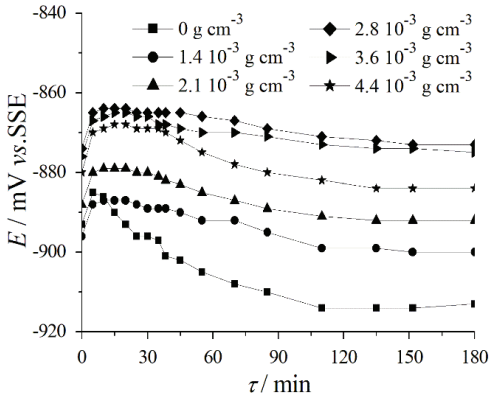

Fig. 4. OCP curves for steel in 0.5 mol dm^{-3} HCl solution as a function of time and inhibitor concentration.

The obtained results indicate that, as the immersion time increased, the OCP of the steel samples in the solution with the extract became more positive as compared to the OCP of the steel in the blank solution, which more rapidly shifted to negative values. The increase in the OCP, once the olive leaf extract was added, may be attributed to the adsorption of the inhibitor on the active metal sites.[15]

Potentiodynamic polarization curves. The inhibitive effect of olive leaf extract, on steel specimens immersed in 0.5 mol dm^{-3} HCl, was further studied by evaluating changes in cathodic and anodic behavior by recording the polarization curve from cathodic to anodic potential limit over the OCP at a scan rate of 1 mV s^{-1}.

Firstly, the effect of the extraction solvent (ethanol) on the typical anodic and cathodic polarization curves of steel in aggressive solution was studied as presented in Fig. 5a. The comparison of steel polarization in 0.5 mol dm^{-3} HCl blank solution and in 0.5 mol dm^{-3} HCl with ethanol, does not indicate any influence of ethanol. Therefore, the strong inhibitory activity of the extract observed at Tafel plots in Fig. 5b is primarily due to the presence of olive leaf compounds.

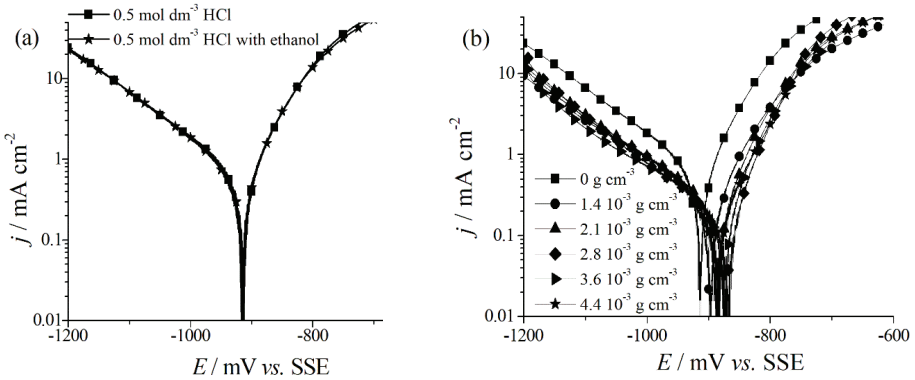

Fig. 5. Potentiodynamic polarization of steel in 0.5 mol dm^{-3} HCl blank solution and in the presence of: a) ethanol; b) different concentrations of olive leaf extract.

Steel corrosion parameters determined from polarization curves in 0.5 mol dm^{-3} HCl blank solution and in the solution containing olive leaves extract, are shown in Table III. Inspection of the obtained results revealed that the values of corrosion potential (E_{corr}) and corrosion current density (j_{corr}) were influenced by the presence of the inhibitor. As shown in Fig. 5b, the increase in the extract concentration results in lower current densities recorded from the potentiostatic polarization curves. Besides, the E_{corr} slightly shifts to a more positive value (noble direction of potential) in the presence of olive leaf extract.

TABLE III. Electrochemical parameters obtained from polarization curves at 25 °C.

C / mg cm^{-3}	E_{corr} / mV *vs.*SSE	j_{corr} / mA cm^{-2}	b_a / mV dec^{-1}	b_c / mV dec^{-1}	η / %
0	−932	1.13	65	143	–
1.4	−905	0.48	39	266	57.5
2.1	−898	0.40	58	159	64.6
2.8	−882	0.22	56	151	80.5
3.6	−884	0.29	63	166	74.3
4.4	−890	0.30	63	156	73.4

Since the difference between the E_{corr} of the steel electrode in the blank solution and in the solution containing inhibitor is lower than 85 mV, this behavior suggests that the extract functions as a mixed-type inhibitor.[16,17]

The highest inhibition efficiency of 80.53 % was obtained for the extract concentration value of 2.8×10^{-3} g cm^{-3}. As can be seen, the inhibition efficiency, both determined by gravimetric tests (Fig. 3) and polarization curves (Table III), increases with increasing the olive leaf extract concentration until reaching a peak value at optimal extract concentration.

The values of inhibition efficiency calculated by gravimetric measurements were higher than those calculated by the electrochemical method. A similar finding between the two approaches has previously been recorded.[18] The disparity observed may be due to the fact that the gravimetric method provides average corrosion rates, while electrochemical techniques give instantaneous corrosion rates. Indeed, the development of a protective film during the immersion time of 8 days, in the case of gravimetric measurement, may explain the difference between the obtained values.

Adsorption isotherms. The adsorption of the olive leaf extract compounds at the steel surface is assumed to be responsible for the inhibitory action of the extract against the corrosion of steel in acid solution. The adsorbed layer functions as a barrier between the steel surface and the aggressive solution, resulting in a reduction of the rate of corrosion.[19] Consequently, the inhibition efficiency (η) derived from the weight loss curves is directly proportional to the fraction of the surface covered by the adsorbed molecules (θ).[20] The mode of variation of (θ) with the extract concentration (C) determines the adsorption isotherm describing the system.[21] Several adsorption isotherms (Langmuir, Temkin and Frumkin) were evaluated to determine the effective adsorption isotherm, according to the following equations:[22,23]

$$\text{Langmuir: } C/\theta = 1/K + C \tag{8}$$

$$\text{Temkin: } e^{-2\alpha\theta} = KC \tag{9}$$

$$\text{Frumkin: } \frac{\theta}{1-\theta} e^{-2\alpha\theta} = KC \tag{10}$$

where α is the adsorbate interaction parameter and K the equilibrium constant of the adsorption process (L kg^{-1}), related to the adsorption free energy change (ΔG^0_{ads}) by the following equation:

$$\Delta G^0_{ads} = -RT \ln (55.5K) \tag{11}$$

where R is the gas constant (J $°K^{-1}mol^{-1}$) and T the temperature (K).

According to the experimental data, the relationship of (θ) *versus* C was observed to follow a linear pattern (Fig. 6), which can be described by Langmuir equation (Eq. (8)) with R^2-value equal to 0.99. The other equations (Eqs. (9) and (10)) were evaluated but did not indicate a good fit (for Temkin and Frumkin isotherms, the R^2-values obtained were 0.37 and 0.005 respectively).

The calculated values of adsorption equilibrium constant (K) and free energy change of adsorption (ΔG^0_{ads}) were found to be 2.73 L kg^{-1} and −12.443 kJ

mol^{-1}, respectively. The negative sign shows that the adsorption of olive leaf extract onto steel surface is a spontaneous process. The values of ΔG^0_{ads} of −20 kJ mol^{-1} or more positive, are well known to suggest physical adsorption, while values of −40 kJ mol^{-1} or more negative, involve charge sharing, *i.e.*, the charge transfer from the inhibitor molecules to the metal surface, to form the chemisorption related coordinate type of bond.[9,24] The acquired value of ΔG^0_{ads} in our work shows a strong physical adsorption of the olive leaf extract components onto the steel surface in 0.5 mol dm^{-3} HCl solution.

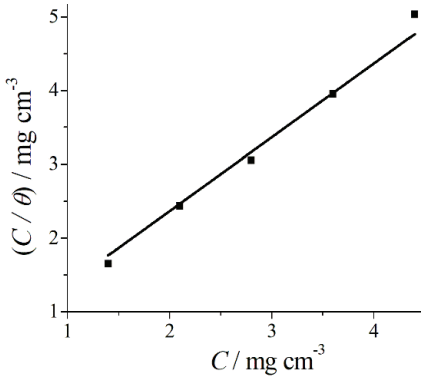

Fig. 6. Langmuir isotherm for adsorption of olive leaf extract onto steel surface in 0.5 mol dm^{-3} HCl solution at 25 °C. $R^2 = 0.99$.

Electrochemical impedance spectroscopy. The electrochemical impedance spectroscopy is used as a powerful technique to characterize the corrosion parameters at metal/electrolyte interface. Fig. 7 highlights the Nyquist plots of steel samples immersed in 0.5 mol dm^{-3} HCl solution in the absence and presence of various concentrations of the olive leaf extract at the OCP. The impedance plots obtained are similar in shape and consist of a single capacitive semicircle at high-to-medium frequency and an inductive loop at low frequency range. The capacitive loop is related to the charge transfer resistance process, while the appearance of the pseudo-inductive loop can be explained by the relaxation of adsorption species such as $(Cl^-)_{ads}$ and $(H^+)_{ads}$ on the surface of the electrode.[25] The inductive loop can also be related to the re-dissolution of the passivated surface.[26,27] Also, one can see that the addition of the olive leaf extract inhibitor, increases the size of the semi-circle in comparison to the blank solution, and the maximum circle diameter is obtained for 2.8×10^{-3} g cm^{-3} of inhibitor. This shows that there is an increase in the charge transfer resistance, which is in agreement with the literature,[25,26,28] and previous corrosion tests in this work. The improvement in the resistance by increasing the inhibitor concentration is due to an adsorption of inhibitor molecules on the surface of the steel, indicating the effective blocking of the surface.[29]

The impedance data were analyzed using ZSimpWin® software and fitted to the equivalent circuit model shown in Fig. 8. This equivalent circuit is exten-

sively reported in the literature.[30,31] The elements related to the circuit are: R_e representing the electrolyte resistance, R_{ct} as the charge transfer resistance, L as the inductance element, R_L as an inductive resistance, Q as the pseudocapacitance and CPE as the constant phase element.

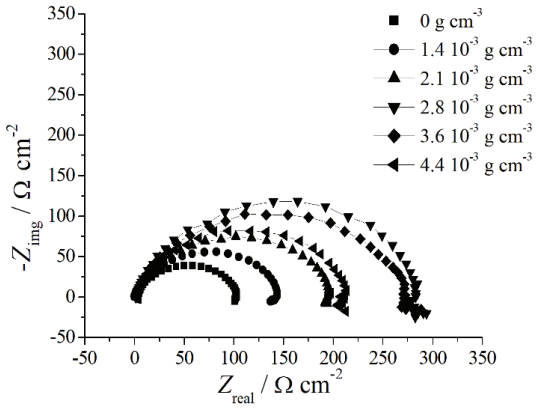

Fig. 7. Nyquist plots for mild steel in 0.5mol dm^{-3} HCl solution in the absence and presence of olive leaf extract at E_{corr} and T = 25 °C.

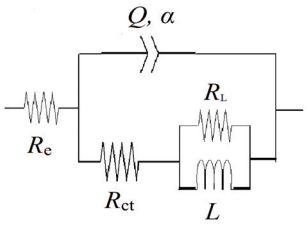

Fig. 8. Electrical equivalent circuit model used to fit the impedance parameters for steel electrode in 0.5 mol dm^{-3} HCl solution.

Due to the roughness and homogeneity of the metal surface, as well as adsorption effects, CPE can be used to replace the double-layer capacitance, C_{dl}.[26] The electrochemical impedance parameters obtained from the equivalent circuit are presented in Table IV.

TABLE IV. EIS parameters for the corrosion of steel immersed in 0.5 mol dm^{-3} HCl without and with different concentrations of olive leaf extract

C / mg cm^{-3}	R_e / Ω m^2	Q / 10^{-5} Ω^{-1} s^n cm^{-2}	n	R_{ct} / Ω cm^2	R_L / Ω cm^2	L / H cm^2
0	1.14	36.64	0.80	99.22	6.63	9.20
1.4	0.87	29.69	0.82	135.50	13.37	16.77
2.1	1.23	25.33	0.81	187.20	14.01	32.95
2.8	0.96	26.41	0.84	247.50	45.44	377.70
3.6	0.95	28.93	0.82	218.30	56.11	1552
4.4	1.44	20.48	0.87	208.20	2.37×10^{10}	0.10

From Table IV, a significant increase in the charge transfer resistance (R_{ct}) was observed in the presence of the inhibitor, providing a high anticorrosive efficiency. The largest effect was observed at 2.8×10^{-3} g cm^{-3} of olive leaf extract,

which gave R_{ct} value equal to 247 Ω cm^2. This behavior is due to an adsorption of inhibitor molecules on the metal surface, leaving less electroactive sites available for corrosion, *i.e.*, the inhibitor builds up a protective film on the metallic surface that isolates it from the corrosive environment, thereby impeding further charge and mass transfer.[31,32]

In addition, the increased n value after the addition of extract to the hydrochloric acid solution (0.82−0.87) when compared to that obtained in the blank solution (0.80), indicates the reduction in the surface in homogeneity due to the adsorption of inhibitor molecules on the active adsorption sites at steel surface.[32,33] Also, from Table IV, one can notice that the Q value is lower in the presence of olive leaf extract compared to the blank solution. The diminishing values of Q can be related to a lower local dielectric constant due to the replacement of water molecules with inhibitor molecules. This process increases the thickness of the electrical double layer and reduces the surface area exposed to the aggressive media, implying an adsorption of inhibitor molecules on the surface of the steel.[31,32]

CONCLUSION

In the present work, an optimization study of the antioxidative matter extraction from *Olea europaea* var. *syslvestris* leaves was performed using full factorial design. The statistical analysis of the experimental results showed that the final polynomial equation, representing the antioxidant activity as a function of the significant effect, gave a reasonably good fit with an R^2 value of 0.955. By response optimizer graph plot, the best response value of antioxidant activity was acquired at the following extraction parameters: extraction temperature 55 °C, solid/solvent ratio 8 g 100 cm^{-3}, water/ethanol ratio 75 %, and extraction time 45 min.

Afterwards, the olive leaf extract obtained under the final optimized conditions was tested as a green corrosion inhibitor for steel in 0.5 mol dm^{-3} HCl. Results of the electrochemical performance and weight loss analysis of steel samples, in HCl with the addition of *O. europaea* leaf extract, indicated that the extract:

– is a successful corrosion inhibitor for steel in 0.5 mol dm^{-3} HCl solution, with a maximum inhibition efficiency of 92 %, achieved at extract concentration of 2.8×10^{-3} g cm^{-3},

– acts as a mixed-type inhibitor and

– acts as an adsorption inhibitor, where the adsorption phenomenon is spontaneous, following the mechanism of physical adsorption related to the Langmuir adsorption isotherm.

SUPPLEMENTARY MATERIAL

Additional data and information are available electronically at the pages of journal website: https://www.shd-pub.org.rs/index.php/JSCS/article/view/11851, or from the corresponding author on request.

ИЗВОД

АНТИКОРОЗИОНО ДЕЈСТВО СУПСТАНЦИ ЕКСТРАХОВАНИХ ИЗ ЛИШЋА МАСЛИНЕ ПОД ОПТИМАЛНИМ ПАРАМЕТРИМА, ПРЕТХОДНО ОДРЕЂЕНИМ ПРИМЕНОМ МЕТОДОЛОГИЈЕ EXPERIMENTAL DESIGN

SOUAD TOUAZI[1,2], МИХАЕЛ М. БУЧКО[3], RADOUANE MAIZIA[2], SAMIRA SAHI[1], NADIA ZAIDI[2] и LAID MAKHLOUFI[2]

[1]*Laboratoire de Valorisation des Energies Fossiles (LAVALEF), Ecole Nationale Polytechnique d'Alger, Algeria,* [2]*Laboratoire d'Electrochimie, Corrosion et de Valorisation Energétique (LECVE), Faculté de Technologie, Université de Bejaia, Algeria и* [3]*Војна академија, Универзитет одбране, Ветка Лукића Курјака 33, Београд*

У овом истраживању, лишће маслине (*Olea europaea* var. *sylvestris)* је искоришћено за добијање зеленог инхибитора корозије. Прво су одређени оптимални параметри екстракције активних материја из лишћа, мерењем њихове антиоксидантне активности на слободним органским радикалима. Оптимизација параметара је извршена *full factorial design* методом. У другој фази истраживања, екстракт добијен при оптималним параметрима је испитиван као инхибитор корозије челика у 0,5 mol dm^{-3} HCl, гравиметријском и електрохемијским методама. Резултати показују да се екстракт понаша као мешовити инхибитор. Адсорпција инхибитора на супстрату је спонтана (ΔG^0_{ads} = −12,443 kJ mol^{-1}), одиграва се према механизму физичке адсорпције и може се описати Лангмировом адсорпционом изотермом. Највећи степен инхибирања корозије од 92 % мерено гравиметријском методом, се постиже при концентрацији инхибитора у киселини од $2{,}8\times10^{-3}$ g cm^{-3}.

(Примљено 13. маја, ревидирано 6. јула, прихваћено 1. августа 2022)

REFERENCES

1. D. Bouknana, B. Hammouti, H. Serghini Caid, S. Jodeh, A. Bouyanzer, A. Aouniti, I. Warad, *Int. J. Ind. Chem.***6** (2015) 233 (http://dx.doi.org/10.1007/s40090-015-0042-z)
2. A. Y. El-Etre, M. Abdallah, Z. E. El-Tantawy, *Corros. Sci.* **47** (2005) 385 (http://dx.doi.org/10.1016/j.corsci.2004.06.006)
3. A. Zaabar, R. Aitout, D. Amoura, R. Maizia, L. Makhloufi, B. Saidani, *Miner. Eng.* **142** (2019) 105 (http://dx.doi.org/10.1016/j.jcrusgro.2013.09.048)
4. A. Zaabar, R. Aitout, L. Makhloufi, K. Alilat, S. Maziz, B. Saidani, *Hydrometallurgy* **136** (2013) 58 (http://dx.doi.org/10.1016/j.hydromet.2013.03.004)
5. G. Salinas-Solano, J. Porcayo-Calderon, A. K. Larios-Galvez, J. G. Gonzalez-Rodriguez, *J. Electrochem. Sci. Eng.* **12** (2022) 373 (https://doi.org/10.5599/jese.1017)
6. S. E. Adeniji, B. A. Akindehinde, *J. Electrochem. Sci. Eng.* **8** (2018) 219 (https://doi.org/10.5599/jese.486)
7. J. Tabera, A. Guinda, A. Ruiz-Rodriguez, F. J. Senorans and E. Ibanez*, J. Agr. Food. Chem.* **52** (2004) 4774 (http://dx.doi.org/10.1021/jf049881+)
8. R. Briante, M. Patumi, S. Terenziani, E. Bismuto, F. Febbraio, J. *Agr. Food. Chem.* **50** (2002) 4934 (http://dx.doi.org/10.1021/jf025540p)
9. A. Zaabar, R. Aitout, L. Makhloufi, K. Belhamel, B. Saidani, *Pigment Resin Technol*. **43** (2014) 127 (http://dx.doi.org/10.1108/PRT-11-2012-0078)

10. W. Brand-Williams, M. E. Cuvelier, C. Berset, *Lwt-Food. Sci. Technol.* **28** (1995) 25 (http://dx.doi.org/10.1016/S0023-6438(95)80008-5)
11. Y. Carmona-Jiménez, M. V. García-Moreno, J. M. Igartuburu, C. G. Barroso, *Food Chem.* **165** (2014) 198 (http://dx.doi.org/10.1016/j.foodchem.2014.05.106)
12. A. A. Rahim, E. Rocca, J. M. Steinmetz, J. Kassim, R. Adnan, M. S. Ibrahim, *Corros. Sci.* **49** (2007) 402 (http://dx.doi.org/10.1016/j.corsci.2006.04.013)
13. N. A. Negm, N. G. Kandile, A. E. Badr, M. A. Mohammed, *Corros. Sci.* **65** (2012) 94 (http://dx.doi.org/10.1016/j.corsci.2012.08.002)
14. A. Y. El-Etre, *J. Colloid Interface Sci.* **314** (2007) 578 (http://dx.doi.org/10.1016/j.jcis.2007.05.077)
15. M. Keramatinia, B. Ramezanzadeh, M. Mahdavian, *J. Taiwan Inst. Chem. Eng.* **105** (2019) 134 (http://dx.doi.org/10.1016/j.jtice.2019.10.005)
16. N. Soltani, N. Tavakkoli, M. Khayatkashani, M. R. Jalali, A. Mosavizade, *Corros. Sci.* **62** (2012) 122 (http://dx.doi.org/10.1016/j.corsci.2012.05.003)
17. J. N. Asegbeloyin, P. M. Ejikeme, L. O. Olasunkanmi, A. S. Adekunle, E. E. Ebenso, *Materials* **8** (2015) 2918 (http://dx.doi.org/10.3390/ma8062918)
18. A. M. Al-Turkustani, S. T. Arab, L. S. S. Al-Qarni, *J. Saudi Chem. Soc*. **15** (2011) 73 (http://dx.doi.org/10.1016/j.jscs.2010.10.008)
19. M. A. Bidia, M. Azadia, M. Rassouli, Mater. *Today Commun.* **24** (2020) 100996 (http://dx.doi.org/10.1016/j.mtcomm.2020.100996)
20. R. Farahatia, S. M. Mousavi-Khoshdela, *Prog. Org. Coat.* **142** (2020) 105567 (http://dx.doi.org/10.1016/j.porgcoat.2020.105567)
21. Z. Bajić, D. Pamučar, J. Bogdanov, M. Bučko, Z. Veličković, *Milit. Tech. Courier* **67** (2019) 735 (http://dx.doi.org/10.5937/vojtehg67-21519)
22. A. Fateh, M. Aliofkhazraei, A. R. Rezvanian, *Arab. J. Chem.* **13** (2020) 481 (http://dx.doi.org/10.1016/j.arabjc.2017.05.021)
23. N.K. Gupta, C. Verma, R. Salghi, H. Lgaz, A. K. Mukherjee, M. A. Quraishi*, New J. Chem.* **41** (2017) 13114 (http://dx.doi.org/10.1039/C7NJ01431G)
24. A. K. Singh, M. A. Quraishi, *Corros. Sci.* **53** (2011) 1288 (http://dx.doi.org/10.1016/j.corsci.2011.01.002)
25. E. de B. Policarpi, A. Spinelli, J. Taiwan. *Inst. Chem. Eng.* **116** (2020) 215 (http://dx.doi.org/10.1016/j.jtice.2020.10.024)
26. T. Rabizadeh, S. K. Asl, *J. Mol. Liq.* **276** (2019) 694 (http://dx.doi.org/10.1016/j.molliq.2018.11.162)
27. H. Ashassi-Sorkhabi, E. Asghari, *Electrochim. Acta* **54** (2008) 162 (http://dx.doi.org/10.1016/j.electacta.2008.08.024)
28. F. E. Abeng, V. Anadebe, P. Y. Nkom, K. J. Uwakwe, E. G. Kamalu, *J. Electrochem. Sci. Eng.* **11** (2022) 11 (https://doi.org/10.5599/jese.1017)
29. M. A. Chidiebere, E. E. Oguzie, L. Liu, Y. Li, F. Wang, *J. Ind. Eng. Chem.* **26** (2015) 182 (http://dx.doi.org/10.1016/j.jiec.2014.11.029)
30. I. Danaee, P. Nikparsa, M. R. Khosravi-Nikou, H. Eskandari, S. Nikmanesh, *Prot. Met. Phys. Chem. Surf.* **55** (2019) 1001 (http://dx.doi.org/10.1134/S2070205119050289)
31. A. Sedik, D. Lerari, A. Salci, S. Athmani, K. Bachari, I.H. Gecibesler, R. Solmaz, *J. Taiwan Inst. Chem. Eng.* **107** (2020) 189 (http://dx.doi.org/10.1016/j.jtice.2019.12.006)
32. P. Mourya, S. Banerjee, M. M. Singh, *Corros. Sci.* **85** (2014) 352 (http://dx.doi.org/10.1016/j.corsci.2014.04.036)
33. H. Zarrok, A. Zarrouk, B. Hammouti, R. Salghi, C. Jama, F. Bentiss, *Corros. Sci.* **64** (2012) 243 (http://dx.doi.org/10.1016/j.corsci.2012.07.018).

Journal of the Serbian Chemical Society
JSCS@tmf.bg.ac.rs • www.shd.org.rs/JSCS
J. Serb. Chem. Soc. 88 (2) S60–S61 (2023) *Supplementary material*

SUPPLEMENTARY MATERIAL TO

Anticorrosion action of the olive leaf compounds extracted under optimal parameters as determined with experimental design

SOUAD TOUAZI[1,2]*, MIHAEL M. BUČKO[3#], RADOUANE MAIZIA[2], SAMIRA SAHI[1], NADIA ZAIDI[2] and LAID MAKHLOUFI[2]

[1]Laboratoire de Valorisation des Energies Fossiles (LAVALEF), Ecole Nationale Polytechnique d'Alger, Algeria, [2]Laboratoire d'Electrochimie, Corrosion et de Valorisation Energétique (LECVE), Faculté de Technologie, Université de Bejaia, Algeria and [3]Military Academy, University of Defence, Veljka Lukića Kurjaka 33, Belgrade, Serbia

J. Serb. Chem. Soc. 88 (2) (2023) 169–182

TABLE S-I. Experimental design table for independent variables and the antioxidant activity

Experiment	X_1	X_2	X_3	X_4	*AA* / %	Y_i / %
1	−1	−1	−1	−1	73.50	71.03
2	1	−1	−1	−1	63.88	65.30
3	−1	1	−1	−1	52.43	56.30
4	1	1	−1	−1	48.93	45.83
5	−1	−1	1	−1	81.84	81.39
6	1	−1	1	−1	79.90	81.12
7	−1	1	1	−1	79.22	77.99
8	1	1	1	−1	72.82	72.99
9	−1	−1	−1	1	58.64	62.19
10	1	−1	−1	1	63.79	61.00
11	−1	1	−1	1	53.50	48.26
12	1	1	−1	1	38.16	42.34
13	−1	−1	1	1	74.85	73.93
14	1	−1	1	1	78.35	78.21
15	−1	1	1	1	69.03	71.34
16	1	1	1	1	72.43	70.89
17	0	0	0	0	66.60	66.26
18	0	0	0	0	65.83	66.26
19	0	0	0	0	66.12	66.26
20	0	0	0	0	65.34	66.26

* Corresponding author. E-mail: souad.touazi@g.enp.edu.dz

TABLE S-II. ANOVA analysis

Source	DF	SS	MS	F	P
Regression	10	2362	236.2	19.16	0.000
Residual	9	110.94	12.33	-	-
Lack of fit	6	110.11	18.35	65.62	0.003
Pure error	3	0.84	0.28	-	-
R^2	0.955	-	-	-	-
R^2_{Adj}	0.905	-	-	-	-

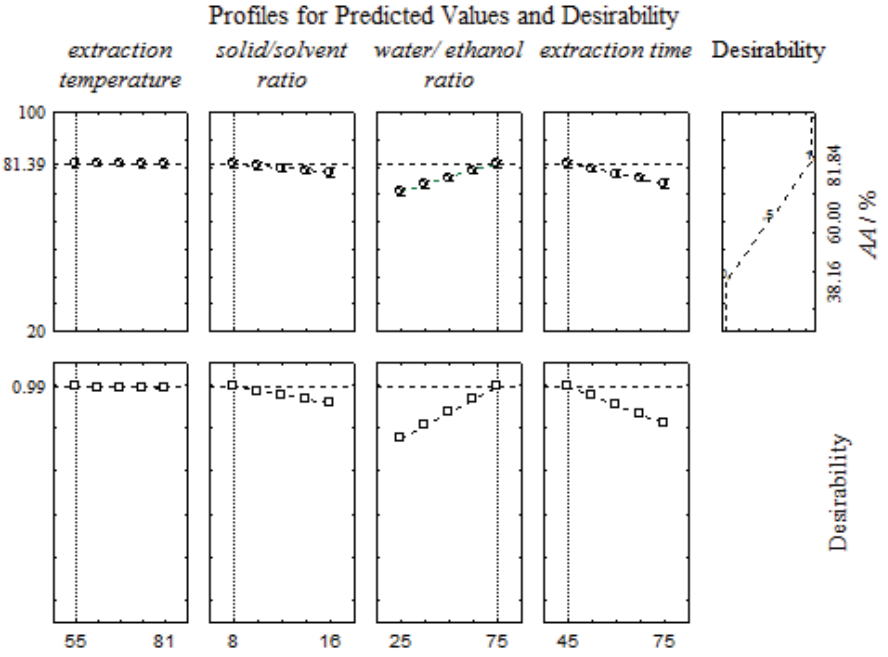

Fig S-1. Prediction profiler at maximal desirability.

Journal of the Serbian Chemical Society
JSCS@tmf.bg.ac.rs • www.shd.org.rs/JSCS
J. Serb. Chem. Soc. *88* (2) 183–197 (2023)
JSCS–5619
Original scientific paper
Published 18 November 2022

Influence of N doping on structural and photocatalytic properties of hydrothermally synthesized TiO_2/carbon composites

MARINA M. MALETIĆ[1]*#, ANA M. KALIJADIS[2], VLADIMIR LAZOVIĆ[3], SNEŽANA TRIFUNOVIĆ[4], BILJANA M. BABIĆ[3], ALEKSANDRA DAPČEVIĆ[5#], JANEZ KOVAČ[6] and MARIJA M. VUKČEVIĆ[5#]

[1]Innovation Center of the Faculty of Technology and Metallurgy, Karnegijeva 4, 11000 Belgrade, Serbia, [2]Department of Materials, „Vinča" Institute of Nuclear Sciences – National Institute of the Republic of Serbia, University of Belgrade, Mike Petrovića Alasa 12–14, 11000 Belgrade, Serbia, [3]Institute of Physics – National Institute of the Republic of Serbia, University of Belgrade, Pregrevica 118, 11080 Belgrade, Serbia, [4]Faculty of Chemistry, University of Belgrade, Studentski trg 12–16, 11000 Belgrade, Serbia, [5]Faculty of Technology and Metallurgy, University of Belgrade, Karnegijeva 4, 11000 Belgrade, Serbia and [6]Department of Surface Engineering, Institute Jožef Stefan, Jamova cesta 39, 1000 Ljubljana, Slovenia

(Received 8 June, revised 11 October, accepted 15 October 2022)

Abstract: N-doped TiO_2/carbon composites (TiO_2/CN) with different nitrogen content, were obtained starting from titanium isopropoxide and glucose, and by varying the amount of melamine, added to starting reaction mixture. For comparison, an undoped sample (TiO_2/C) was also prepared. Structural and surface characteristics were determined through scanning electron microscopy, thermogravimetric analysis, elemental analysis, Fourier transform infrared spectroscopy, X-ray photoelectron spectroscopy, X-ray diffraction and nitrogen adsorption–desorption isotherms. The photocatalytic activity of TiO_2/CN composites was examined via photocatalytic degradation of methylene blue and multiclass pharmaceuticals from water solution. It was found that N doping of TiO_2/carbon composites induced changes in structural and surface characteristics of TiO_2/CN composites, improving their adsorption, but decreasing photocatalytic efficiency. Nevertheless, $TiO_2/CN_{0.05}$ composite obtained by the hydrothermal synthesis in the presence of glucose and 0.05 g melamine showed the highest efficiency for removing selected pharmaceuticals and methylene blue from aqueous solutions through the combined processes of adsorption in the dark, and photocatalytic degradation under UV and visible irradiation.

* Corresponding author. E-mail: mvukasinovic@tmf.bg.ac.rs
# Serbian Chemical Society member.
https://doi.org/10.2298/JSC220608079M

Keywords: TiO_2/carbon composites; N-doping; surface properties; photocatalytic properties; pharmaceuticals.

INTRODUCTION

Photocatalysis represents a clean, green and sustainable technology that is constantly being studied and improved for its effective application in removing organic pollutants from the environmental water. Titanium dioxide is one of the most widely used photocatalytic materials in the fields of environmental purification, due to its advantages of good chemical stability, low cost and nontoxicity.[1] However, it is photocatalytically active only under UV light, due to its relatively high band gap energy.[2] Reduction of the band gap energy, which can be achieved by doping TiO_2 with non-metal elements, such as C, B, S and N,[2–6] spread the spectral response of TiO_2 into the visible region. Also, it was found[7] that N-doping of TiO_2 enhances the photocatalytic performance under UV irradiation by increasing the specific surface area of a photocatalyst.

To obtain highly reactive photocatalysts, in addition to TiO_2 doping with nitrogen, photocatalysts can be combined with different carbon materials that play the role of catalysts.[1,8–10] It was found that nitrogen doping combined with some carbon material as a carrier lead to an increase in the specific surface area of the material, as well as its photocatalytic activity under visible irradiation.[1]

Previously,[8] we have used a simple method of hydrothermal synthesis to obtain highly reactive TiO_2/carbon composites for photocatalytic degradation of selected organic pollutants, under UV irradiation. In this work, the hydrothermal method was applied to synthesize the material, photocatalytically active under visible light. N-doped TiO_2/carbon composites (TiO_2/CN), with different nitrogen content, were obtained starting from titanium isopropoxide and glucose, and by varying the amount of melamine, added to starting reaction mixture. Obtained composites were characterized by the means of structural and surface properties. Their photocatalytic activity was tested through the degradation of methylene blue (MB) and selected pharmaceuticals, belonging to classes of antibiotics, painkillers, sedatives and cardiovascular. Additionally, it is important to highlight that some of the examined pharmaceuticals (diclofenac, azithromycin, and erythromycin) were included in the watch list of substances for union-wide monitoring in the field of water policy,[11] since their presence may pose a significant risk to the aquatic environment.

EXPERIMENTAL

TiO_2/carbon composites doped with nitrogen (TiO_2/CN) were obtained by hydrothermal synthesis. Starting reaction mixture containing: 37 cm^3 glucose solution (30 g dm^{-3}), 3 cm^3 35 % hydrochloric acid, 6 cm^3 of titanium isopropoxide, and different amounts of melamine (0.05, 0.1 and 0.5 g), was placed in the Teflon lined stainless steel autoclave (50 cm^3), and carbonized at a temperature of 160 °C and self-generated pressure for 12 h. The resulting suspension, obtained after the carbonization, was filtered and the precipitate was washed with

distilled water and ethanol and dried at 60 °C overnight. Obtained samples were denoted as $TiO_2/CN_{0.05}$, $TiO_2/CN_{0.1}$ and $TiO_2/CN_{0.5}$, respectively, based on the amount of melamine used. For the purpose of comparison, the undoped sample (TiO_2/C) was prepared according to the same procedure, without melamine adding.

Scanning electron microscopy (Mira Tescan 3X, Tescan Orsay Holding, Czech Republic) was used to examine the structure and morphology of prepared carbon composites.

The thermogravimetric analysis (TGA, SDT Q600, TA Instruments) was performed in the O_2 atmosphere (flow rate: 100 cm^3 min^{-1}) from room temperature up to 800 °C, with a heating rate of 20 °C min^{-1}.

Elemental analysis (Vario EL III Element Analyzer, Elementar, Shimadzu Europe) was performed to determine the nitrogen content in the synthesized composite materials.

Fourier transform infrared spectroscopy (FTIR, Bomem MB-Series, Hartmann Braun) was used for qualitative analysis of surface functional groups. FTIR spectra were obtained in the wavenumber range from 400 to 4000 cm^{-1}.

X-Ray photoelectron spectroscopy (XPS) measurements were performed on the PHI--TFA XPS spectrometer produced by Physical Electronics Inc. and equipped with the monochromatic X-ray source with the Al anode. Wide energy range XPS spectra were taken with pass energy of 187 eV to identify present elements and high-energy resolution XPS spectra were taken with pass energy 29 eV to identify chemical bonds of elements on the surface. Low-energy electron gun was used for neutralization of possible charging effects.

The specific surface area and the pore size distribution (PSD) of carbon composites were analyzed using the Surfer (Thermo Fisher Scientific, USA). PSD was estimated by applying Barrett–Joyner–Halenda (BJH) method[12] to the desorption branch of isotherms and mesopore surface (S_{meso}) and micropore volume (V_{micro}) were estimated using the *t*-plot method.[13]

X-ray diffraction (XRD) patterns were performed by Philips PW1710 diffractometer with CuKα radiation at a scanning speed 1 °C min^{-1} in the range of 2θ of 20–60°. Based on obtained X-ray diffraction patterns, crystalline phases have been identified, and approximate share of the individual phases in the product and the crystallite size was calculated by computer program Powder Cell.[14]

The photocatalytic activity of TiO_2/CN composites, as well as undoped TiO_2/C composite, was evaluated by photocatalytic degradation of methylene blue (MB) and selected pharmaceuticals from multicomponent solution. Experiments were carried out at room temperature and atmospheric pressure with constant shaking on a magnetic stirrer. The starting concentration of the MB solution was 25 mg dm^{-3}, while the concentration of composite material was 2 g dm^{-3}. The suspension was held for 60 min in the dark until an adsorption–desorption equilibrium is reached, after which the suspension was exposed to UV irradiation. Process of photocatalytic degradation was monitored by periodic sampling (60, 75, 90, 105, 120, 150 and 180 min), and measuring of MB concentration. To compare the photocatalytic activity of examined samples under visible irradiation, MB solution with an initial concentration of 10 mg dm^{-3} was used. As a source of UV irradiation, 125 W high-pressure mercury lamp, Philips, HPLN was used, while visible irradiation was obtained by 150 W tungsten halogen lamp with a 400 nm cut off glass optical filter.

Also, TiO_2/CN composites were used as photocatalysts for degradation of the selected pharmaceuticals: diclofenac (painkillers); bromazepam (sedatives); atorvastatin, amlodipine, cilazapril and clopidogrel (cardiovascular); azithromycin, doxycycline and erythromycin (antibiotics). The initial concentration of each of the selected pharmaceuticals from the multicomponent solution was 5 mg dm^{-3}. The concentration of composite photocatalysts was 1 g

dm^{-3}, while experimental conditions were the same as for degradation of MB under UV irradiation. The solution samples were taken after 180 min of the removal process, which included 60 min of adsorption in the dark, followed by photocatalytic degradation. Samples were filtered through 0.45 μm PVDF syringe filters, and the concentration of selected pharmaceuticals was assessed by high-performance liquid chromatography–tandem mass spectrometry (LC–MS/MS Thermo Scientific). LC–MS/MS method conditions are given in the Supplementary material to this paper.

RESULTS AND DISCUSSION

The morphological characteristics of TiO_2/CN samples were examined by scanning electron microscopy (Fig. 1). Compared to the undoped sample (Fig. 1d), the addition of melamine in the reaction mixture does not lead to any important differences in the morphology of obtained composites. SEM photographs showed that all N-doped TiO_2/carbon composites were characterized by a similar and homogenous structure, regardless of the amount of melamine added to the reaction mixture.

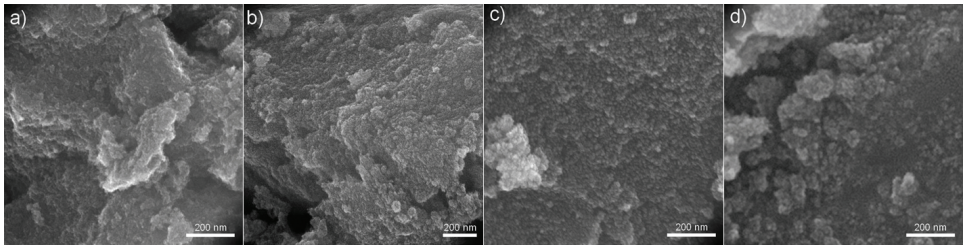

Fig. 1. SEM photographs of samples: a) $TiO_2/CN_{0.5}$; b) $TiO_2/CN_{0.1}$, c) $TiO_2/CN_{0.05}$ and d) TiO_2/C.

The contents of nitrogen, carbon phase and TiO_2 in examined composites were obtained by elemental and thermogravimetric analysis. The TGA, DTG, and DTA curves of the TiO_2/CN composites, as well as undoped TiO_2/C, are shown in Fig. 2a–c, respectively. For all examined samples, according to the DTG curves, the first mass loss was observed in the temperature range from 40 to 120 °C, which originates from physically and chemically adsorbed water. The second mass loss observed in the range 250–450 °C, is a consequence of hydrothermal carbon oxidation during TG analysis. Sample $TiO_2/CN_{0.05}$ has an additional mass loss in the temperature range 550–650 °C, which origin is not fully understood.

According to the literature[15] the mass loss in this region can be the consequence of the decomposition of residual melamine, which is unlikely because samples obtained with a higher amount of melamine do not display the mass loss in this temperature region. Also, it is suggested that the mass loss in the temperature region from 350–800 °C can be a result of carbon residue degradation, as well as TiO_2 crystal phase transformation.[16] The content of TiO_2, carbon

phase (obtained from TGA), and nitrogen (from elemental analysis) in examined composites are presented in Table I. Percentage contents of TiO_2 and carbon phase, shown in Table I, were calculated taking the content of hydrothermally obtained TiO_2 on 800 °C as 100 %.

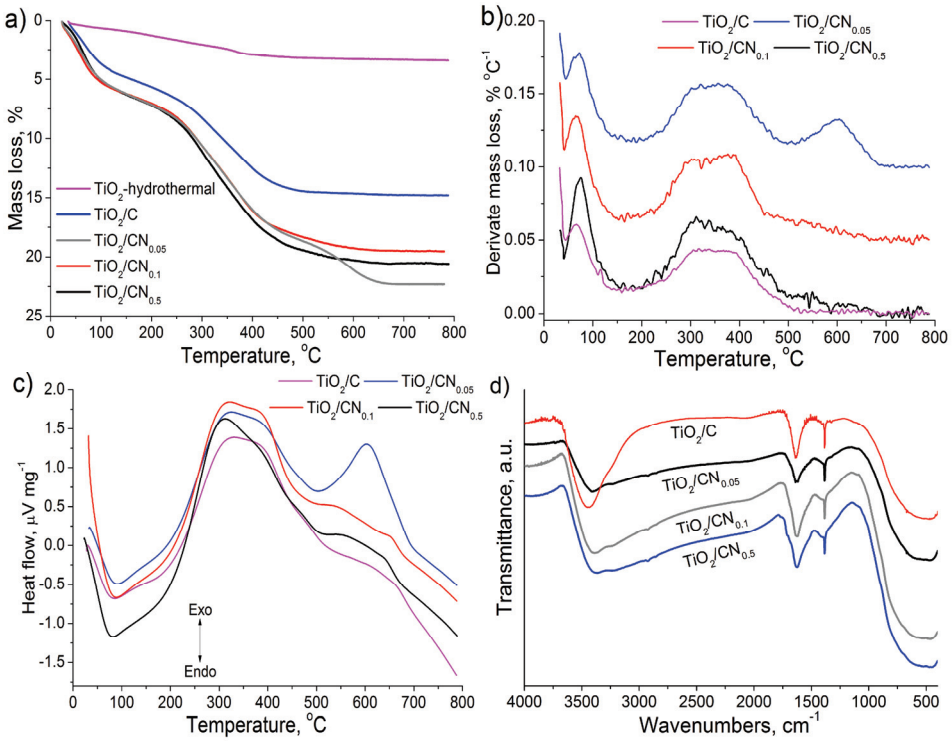

Fig. 2. TGA (a), DTG (b) and DTA (c) curves, and FTIR spectra (d) of TiO_2/C and TiO_2/CN composites.

Table I. TiO_2, carbon phase and nitrogen content in TiO_2/CN composites (wt. %)

Sample	Component		
	TiO_2	Carbon phase	N
TiO_2/C	88.17	11.83	0
$TiO_2/CN_{0.05}$	80.45	19.33	0.221
$TiO_2/CN_{0.1}$	83.27	16.61	0.156
$TiO_2/CN_{0.5}$	82.23	17.48	0.292

Obtained results showed that adding the melamine to the reaction mixture led to nitrogen incorporation into TiO_2/CN composites in the range from 0.156 to 0.292 wt. %. However, nitrogen content in TiO_2/CN composites is not directly dependent on the amount of melamine added to the reaction mixture since both, the lowest and the highest amount of melamine, led to similar nitrogen content in

the TiO_2/CN composites. It has been observed that the lowest concentration of melamine in the reaction mixture resulted in increased content of the organic carbonaceous phase at the expense of the TiO_2 inorganic phase.

FTIR spectra of undoped and doped composites are shown in Fig. 2d. The broad band in the range of 400–1000 cm^{-1} is derived from the stretch vibration of Ti–O and Ti–O–Ti bonds.[17,18] The peak at 3400 cm^{-1} originates from the stretching vibration of the OH bond in Ti–OH and in water adsorbed on the TiO_2 surface, indicating the presence of hydroxyl groups on the surface of the material.[18] Another peak that may correspond to bending vibrations of the O–H bond in water molecules appears around 1625 cm^{-1} for all tested samples.[18] Two weak peaks at 2850 and 2920 cm^{-1} can be ascribed to characteristic stretching vibrations of aliphatic C–H, which indicate the formation of carbon layers.[17] The addition of melamine leads to a broadening of the peak at 3400 cm^{-1}. It is necessary to highlight that there are no distinct differences between the FTIR spectra of TiO_2/CN composites. Nevertheless, a small shoulder at around 1715 cm^{-1}, was observed for sample $TiO_2/CN_{0.5}$. This peak may originate from stretching vibration of –C=O from carbonyl and carboxyl groups, indicating that N-doping with the highest amount of melamine induced their formation. Although the peak at 1385 cm^{-1} can be related to C=C and O–H bond,[19] it may also be induced by the C–N bond. However, this observation could not confirm the presence of nitrogen in obtained composite materials, since undoped TiO_2/C spectra displayed peaks at the same wavenumber.

XPS analysis was conducted to confirm the nitrogen incorporation into TiO_2/CN composites and to identify the valence state of the doping nitrogen. Fig. 3a shows the very similar spectra of undoped TiO_2/C and TiO_2/CN samples, doped with various nitrogen amounts, taken in the binding energy range from 0 to 1200 eV. In the high-resolution spectra of Ti 2p (Fig. 3b), peaks at 458.8 and 464.4 eV correspond to Ti $2p_{3/2}$ and Ti $2p_{1/2}$, respectively.[20] Binding energy difference between these two peaks is 5.6 eV. Binding energy 458.8 eV of Ti $2p_{3/2}$ confirms the presence of the Ti^{4+} states in TiO_2. Fig. 3c shows the high resolution XPS spectra of O 1s, deconvoluted in three peaks at 530.1, 531.7 and 532.8 eV that are ascribed to lattice oxygen (Ti–O–Ti), surface hydroxyl groups (Ti–O–H) and adsorbed water.[21,22]

The C 1s spectrum (Fig. 3d) was fitted with four peaks. The main peak at 284.8 eV corresponds to C–C and C–H bonds,[23] while the peak at 289.6 eV corresponds to O=C–O. Peaks at 286.4 and 288.4 eV can be assigned to nitrogen-doped sp^2 carbon (C–N) and nitrogen-doped sp^3 carbon (C=N),[20] although, these peaks may be related to the C–O, C–OH and C=O, due to much higher concentration of oxygen, compared to nitrogen. Furthermore, the high-resolution N 1s spectra display a peak of around 400 eV (Fig. 3e). Emission in the 399–400 eV region can originate from nitriles (N triple-bonded to only one carbon), graphitic

N (bonded to three carbons),[24] or adsorbed nitrogen, but also from the interstitial integration of nitrogen into TiO_2 lattice.

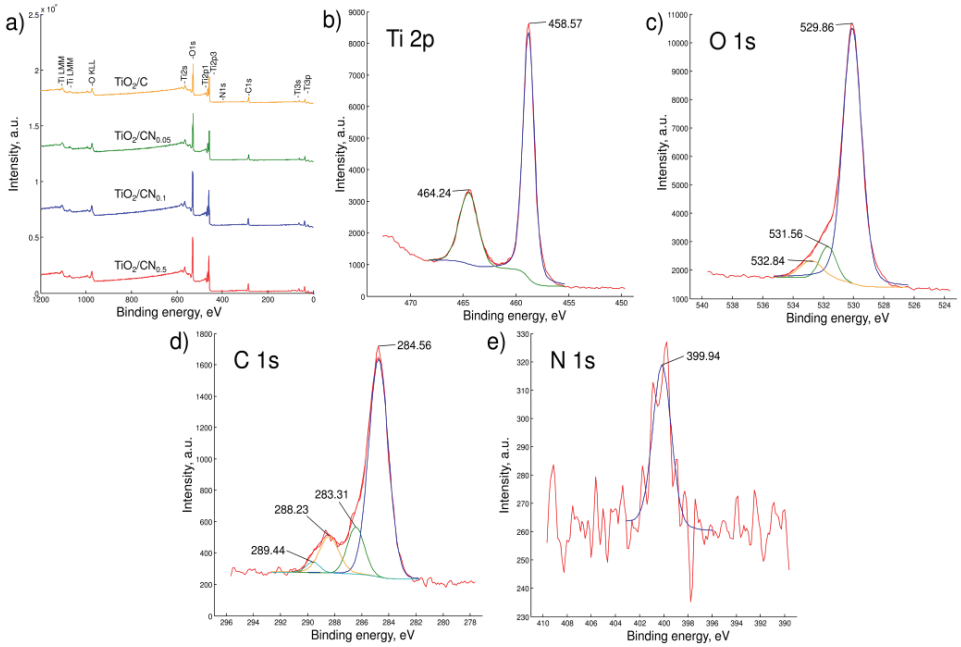

Fig. 3. XPS survey spectra of TiO_2/C and TiO_2/CN samples with various nitrogen content (a), the high-resolution spectra of Ti 2p (b), O 1s (c), C 1s (d) and N 1s (e) of $TiO_2/CN_{0.5}$.

Nitrogen adsorption isotherms obtained for undoped and TiO_2/CN samples are given in Fig. 4a, as the dependence of the adsorbed amount of N_2 (n / mmol g^{-1}) and relative pressure (P/P_0) at the temperature of liquid nitrogen. Obtained isotherms are type IV of IUPAC classification,[25] containing a hysteresis loop, which indicates a mesoporous material. The observed hysteresis loop of type H2 is typical for the pores of undefinable shape.

Additionally, non-limiting adsorption at high P/P_0, observed for N-doped samples indicates the presence of slit-shaped pores at non-rigid aggregates of plate-like particles.[26] Pore size distribution (Fig. 4b) for all samples is very narrow and close to the limiting value between micro and mesopores (2 nm). This means that these materials can be considered microporous with a small fraction of mesoporousness. Values for the average pore width (r_p), for all samples, along with the calculated porosity parameters (S_{BET}, S_{meso}, S_{mic}, V_{mic}) are given in Table II. The mesoporous TiO_2/C sample showed an S_{BET} of 174.08 m^2 g^{-1} and an average pore width of 3.78 nm.

On the other hand, all TiO_2/CN composites are mainly microporous, with a maximum pore radius of about 2.2 nm. Also, it was found that the S_{BET} of

N-doped samples, ranging from 186 to 239 m^2 g^{-1}, increase with nitrogen content. Consideration of the obtained results indicates that melamine addition in reaction mixture leads to the decrease of average pore width, and drastically increases the microporosity, as well as S_{BET} values of obtained TiO_2/CN samples. As it was reported previously,[27] these changes in specific surface area and average pore width may be the consequence of the substitution of carbon atoms, most likely located on the reactive edges, with nitrogen atoms during hydrothermal synthesis. These incorporated N atoms could act as a catalyst for porosity development.

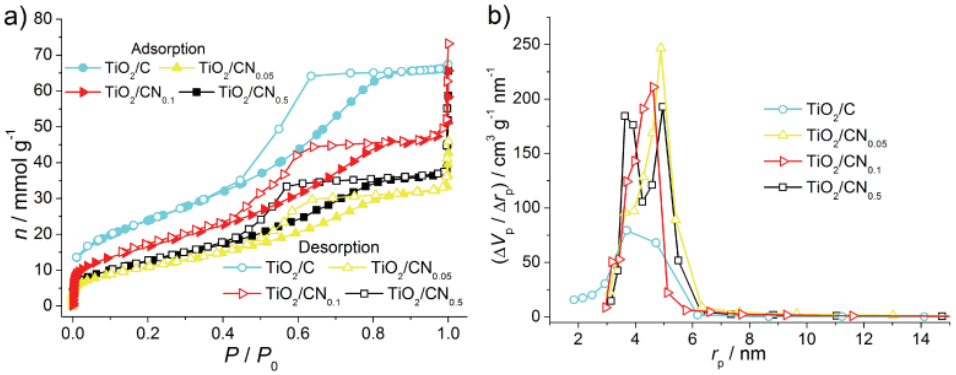

Fig. 4. Nitrogen adsorption isotherms (a) and pore size distribution (b) for TiO_2/C and TiO_2/CN samples.

TABLE II. Porous properties of TiO_2/CN samples

Sample	S_{BET} / m^2 g^{-1}	S_{meso} / m^2 g^{-1}	S_{mic} / m^2 g^{-1}	V_{mic} / cm^3 g^{-1}	r_p / nm
TiO_2/C	174	168	6	0.048	3.78
$TiO_2/CN_{0.05}$	231	32	199	0.231	2.37
$TiO_2/CN_{0.1}$	186	17	169	0.194	2.11
$TiO_2/CN_{0.5}$	239	22	217	0.246	2.38

XRD analysis was performed to determine the content of crystalline TiO_2 phases in TiO_2/C and TiO_2/CN composites, as well as the crystallite size. XRD diffraction pattern for all tested samples (Fig. 5) showed the presence of a characteristic peak for anatase (101) (2θ = 25.6°) crystalline phase, as well as peaks at 2θ 38.2 (112), 48.3 (200) and 54.6° (105) also arising from anatase crystalline modification.[10,28] The presence of a low-intensity peak at 2θ = 27.7° (110), originating from rutile crystal modification, was observed for the undoped sample TiO_2/C (Fig. 5).[28] However, no distinguish peaks characteristic for the rutile phase were displayed on XRD diffraction patterns of TiO_2/CN composites. A shoulder appearing at 2θ = 26° (110), visible on the XRD diffraction pattern of all TiO_2/CN composites, may originate from the photocatalytically inactive crys-

talline phase of brookite, as well as from titanium nitride.[29] The presence of these phases may affect the photocatalytic activity of the examined composites, especially of sample $TiO_2/CN_{0.5}$ which shows the shoulder of higher intensity. Although XPS analysis showed that nitrogen was most likely incorporated in carbon lattice, the addition of melamine to the starting reaction mixture affected the structure of N-doped composites by favoring the formation of the anatase phase and suppressing the formation of the rutile phase.

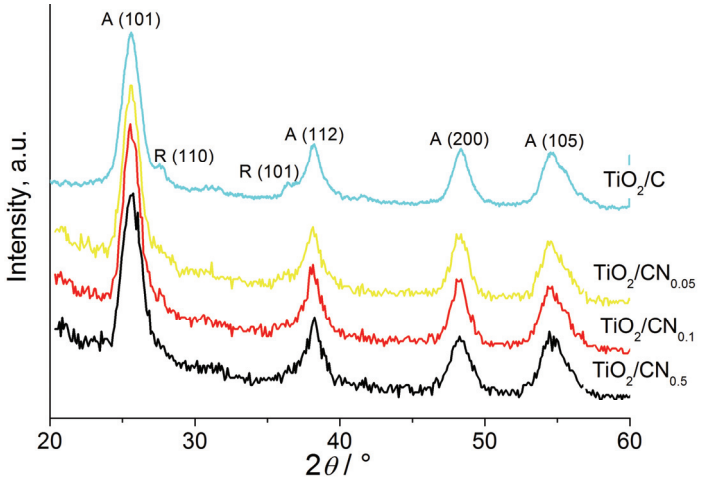

Fig. 5. XRD patterns of examined samples.

The calculated approximate values of the fraction of TiO_2 crystalline phases and the size of the crystallite are shown in Table III. The undoped sample, TiO_2/C, contains 24 % of the rutile phase, while N doping significantly decreased the content of the rutile phase. The observed increase of the anatase phase content should favorably affect the photocatalytic characteristics of TiO_2/CN composites. It can be noticed that N-doping leads to a decrease in the average grain size, which is dependable on nitrogen content in TiO_2/CN composites. The addition of melamine increases the content of amorphous carbon (Table I), which inhibits the growth of TiO_2 grains and thus N-doping leads to a decrease in the grain size. Obtained values for grain size and average pore width (Table II), suggest that these pores most likely represent interparticle spaces.

The photocatalytic activity of TiO_2/CN composites was investigated in the process of removing methylene blue from aqueous solutions under UV and visible irradiation. Fig. 6a shows the photocatalytic decomposition of MB as a decrease in the MB concentration during the time. The entire process of MB removal lasted 180 min and it was performed in two steps. The first step is related to the establishment of an adsorption/desorption equilibrium for 60 min in the dark, and the second step implied the degradation of organic pollutants in the

presence of UV or visible irradiation. Fig. 6b summarized the removal efficiency after the first adsorption step in the dark, the second step of photocatalytic degradation under UV irradiation, and total removal efficiency. At the end of the first step, TiO_2/CN samples showed higher adsorption capacity (removing 44–70 % of MB) than sample TiO_2/C, which adsorbed about 35 % of the initial amount of MB. According to the results shown in Fig. 6b and Table II, adsorption efficiency increases with specific surface area, although, a direct relationship between S_{BET} and the amount of MB adsorbed cannot be established. N-doped samples had higher adsorption capacity, but lower photocatalytic efficiency since N-doped samples showed lower removal efficiency during the irradiation step than the undoped sample. However, according to Fig. 6b, samples $TiO_2/CN_{0.5}$ and $TiO_2/CN_{0.05}$ showed the highest level of adsorption and total removal efficiency, due to the high specific surface area, which is the result of the highest content of carbon. Photocatalytic characteristics of examined materials are not directly influenced by nitrogen content. TiO_2/C showed better photocatalytic activity than N-doped samples, most likely because increased carbon content in N-doped samples had a negative effect on photocatalytic activity by preventing light penetration to the TiO_2.

TABLE III. Anatase and rutile phase content and grain sizes of TiO_2/C and TiO_2/CN composites

Sample	Crystallite size, nm	Phase content, wt. %	
		Anatase	Rutile
TiO_2/C	9.76	76.0	24.0
$TiO_2/CN_{0.05}$	7.15	98.0	2.0
$TiO_2/CN_{0.1}$	7.26	99.0	1.0
$TiO_2/CN_{0.5}$	6.52	95.0	5.0

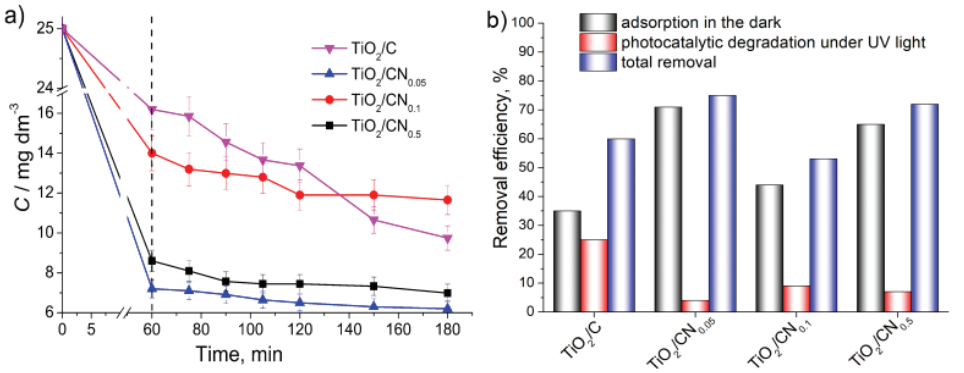

Fig. 6. Photocatalytic decomposition (a) and removal efficiency (b) of MB in the presence of TiO_2/C and TiO_2/CN composites.

Undoped and N-doped samples showed a similar trend in the photocatalytic activity in the process of methylene blue removal under visible irradiation (Fig. 7a). Samples obtained by adding a larger amount of melamine to the reaction mixture ($TiO_2/CN_{0.1}$, $TiO_2/CN_{0.5}$) show lower photocatalytic activity in the visible region than the undoped sample. Only the sample obtained with a small amount of melamine ($TiO_2/CN_{0.05}$) shows a better efficiency than the undoped sample. As was already mentioned, due to the large specific surface area and the highest carbon content, sample $TiO_2/CN_{0.05}$ displayed the best efficiency in the MB removal process. Also, its photocatalytic activity in the decomposition of MB under visible radiation ($\lambda > 400$ nm) was followed by the recording of the absorption spectra. According to the spectra shown (Fig. 7b), no new absorption bands appear in the visible or UV area, which confirms the disappearance of the dye chromophore structure.[30] Even though the absorption peak at 663 nm decreases with the increase in reaction time, the MB is not degraded after 24 h.

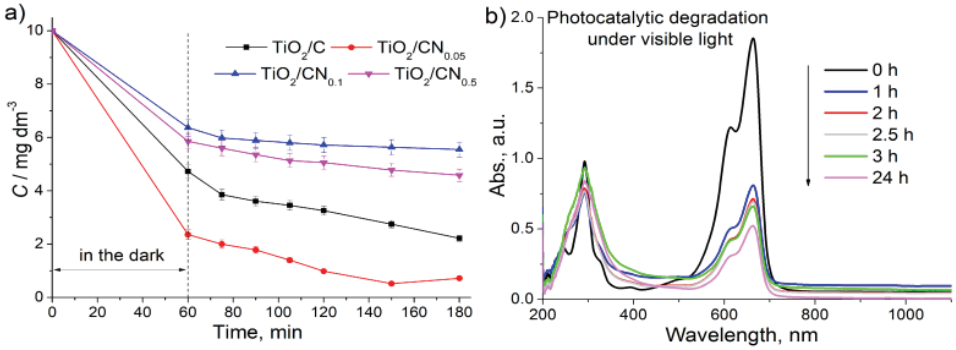

Fig. 7. Photocatalytic decomposition of MB in the presence of undoped and N-doped samples (a) and absorption spectraof MB on $TiO_2/CN_{0.05}$ (b).

The possibility of removing selected pharmaceuticals from a multi-component solution by TiO_2/CN composites under UV irradiation was also examined. For the purpose of comparison, results obtained by undoped TiO_2/C composite were also presented. Fig. 8 summarized the percentage of removed pharmaceuticals by adsorption in the dark, followed by the photocatalytic degradation under UV irradiation after 180 min, and total removal efficiency.

Generally, all tested materials better adsorb pharmaceuticals of decreased polarity (higher values of retention time in Table S-II of the Supplementary material), except in the case of doxycycline. The higher specific surface area of N-doped samples, compared to the undoped sample, positively affects the pharmaceutical adsorption, except for amlodipine adsorption where the undoped sample showed the highest removal efficiency in the dark. Samples $TiO_2/CN_{0.1}$ and $TiO_2/CN_{0.5}$ show a lower efficiency of pharmaceuticals removal under UV

irradiation (Fig. 8b), compared to the undoped sample and $TiO_2/CN_{0.05}$. Nevertheless, all tested composites demonstrate high efficacy in the total removal (Fig. 8c) of diclofenac, doxycycline, atorvastatin, amlodipine and clopidogrel, which were completely removed after the adsorption in the dark, followed by photocatalytic degradation under UV irradiation.

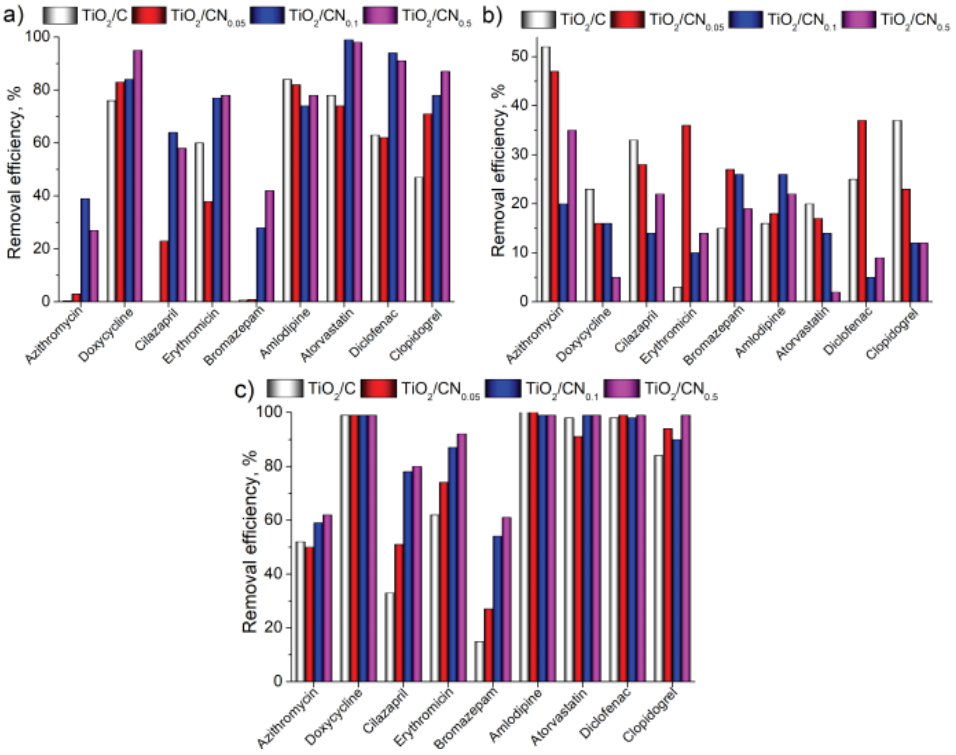

Fig. 8. Removal of pharmaceuticals from a multi-component solution by TiO_2/C and TiO_2/CN composites: a) adsorption in the dark, b) under UV irradiation and c) total removal.

The percentage of totally removed pharmaceuticals increases with the higher amount of melamine introduced in the starting reaction mixture, most likely due to the increased specific surface area and adsorption efficiency. In that way, the composite obtained with the highest amount of melamine, $TiO_2/CN_{0.5}$, showed the highest efficiency for removing selected pharmaceuticals from aqueous solutions.

CONCLUSION

N-doped TiO_2/carbon composites were obtained by hydrothermal synthesis using melamine, as a source of nitrogen, though the nitrogen content in TiO_2/CN composites was not directly proportional to the amount of melamine added to the

reaction mixture. The incorporation of nitrogen affected the structural and surface characteristics of composite photocatalysts, by increasing the specific surface area and microporosity, as well as the content of the photocatalytically active anatase phase. N-doping affected the efficiency of these composites to remove methylene blue and selected pharmaceuticals, by increasing their adsorption efficiency and decreasing photocatalytic activity under UV irradiation. Nevertheless, $TiO_2/CN_{0.05}$ composite, obtained by the hydrothermal synthesis in the presence of glucose and 0.05 g melamine, showed the highest efficiency for removing selected pharmaceuticals and methylene blue from aqueous solutions through the combined processes of adsorption in the dark and photocatalytic degradation under UV and visible irradiation.

SUPPLEMENTARY MATERIAL

Additional data and information are available electronically at the pages of journal website: https://www.shd-pub.org.rs/index.php/JSCS/article/view/11912, or from the corresponding author on request.

Acknowledgements. The research was funded by the Ministry of Education, Science and Technological Development of the Republic of Serbia (Contract Nos. 451-03-68/2022--14/200135, 451-03-68/2022-14/200287 and 451-03-9/2021-14/200017).

ИЗВОД

УТИЦАЈ ДОПИРАЊА АЗОТОМ НА СТРУКТУРНЕ И ФОТОКАТАЛИТИЧКЕ КАРАКТЕРИСТИКЕ ХИДРОТЕРМАЛНО СИНТЕТИСАНИХ TiO_2/КАРБОН КОМПОЗИТА

МАРИНА М. МАЛЕТИЋ[1], АНА М. КАЛИЈАДИС[2], ВЛАДИМИР ЛАЗОВИЋ[3], СНЕЖАНА ТРИФУНОВИЋ[4], БИЉАНА М. БАБИЋ[3], АЛЕКСАНДРА ДАПЧЕВИЋ[5], JANEZ KOVAČ[6] и МАРИЈА М. ВУКЧЕВИЋ[5]

[1]Иновациони Центар Технолошко–металуршког факултета, Карнегијева 4, 11000 Београд, [2]Лабораторија за материјале, Институт за нуклеарне науке Винча – Институт од националног значаја, Универзитет у Београду, Мике Петровића Аласа 12–14, 11000 Београд, [3]Институт за физику – Институт од националног значаја, Универзитет у Београду, Прегревица 118, 11080 Београд, [4]Хемијски факултет, Универзитет у Београду, Студентски трг 12–16, 11000 Београд, [5]Технолошко–металуршки факултет, Универзитет у Београду, Карнегијева 4, 11000 Београд и [6]Department of Surface Engineering, Institute Jožef Stefan, Jamova cesta 39, 1000 Ljubljana, Slovenia

TiO_2/карбон композити допирани азотом (TiO_2/CN) добијени су хидротермалном карбонизацијом смеше титан изопропоксида и глукозе, у присуству различитих количина меламина као прекурсора азота. Извршена је површинска и структурна карактеризација материјала, а добијени резултати су упоређени са карактеристикама недопираног TiO_2/карбон композита. Фотокаталитичка активност добијених композита испитана је фотокаталитичком разградњом метиленско плавог и лекова из мултикомпонентног воденог раствора. Утврђено је да допирање азотом TiO_2 карбон композита доводи до промена у структурним и површинским карактеристикама TiO_2/CN композита, побољшавајући њихову адсорпциону ефикасност, али смањујући фотокаталитичку активност. Показано је да се примењеном методом хидротермалне карбонизације могу добити ефикасни композити за уклањање одабраних лекова и метиленског плавог из водених раствора, применом процеса адсорпције у мраку, праћеног фотокаталитичком разградњом под UV и видљивим зрачењем.

(Примљено 8. јуна, ревидирано 11. октобра, прихваћено 15. октобра 2022)

REFERENCES

1. N. C. T. Martins, J. Ângelo, A.V. Girão, T. Trindade, L. Andrade, A. Mendes, *Appl. Catal., B* **193** (2016) 67 (http://dx.doi.org/10.1016/j.apcatb.2016.04.016)
2. B. Farkas, P. Heszler, J. Budai, A. Oszkó, M. Ottosson, Z. Geretovszky, *Appl. Surf. Sci.* **433** (2018) 149 (https://doi.org/10.1016/j.apsusc.2017.09.181)
3. R. Asahi, T. Morikawa, H. Irie, T. Ohwaki, *Chem. Rev.* **114** (2014) 9824 (https://dx.doi.org/10.1021/cr5000738)
4. Y.T. Lin, C.H. Weng, Y.H. Lin, C.C. Shiesh, F.Y. Chen, *Sep. Purif. Technol.* **116** (2013) 114 (http://dx.doi.org/10.1016/j.seppur.2013.05.018)
5. K. Siuzdak, M. Szkoda, A. Lisowska-Oleksiak, K. Grochowska, J. Karczewski, J. Ryl, *Appl. Surf. Sci.* **357** (2015) 942 (http://dx.doi.org/10.1016/j.apsusc.2015.09.130)
6. K. Pathakoti, S. Morrow, C. Han, M. Pelaez, X. He, D. D. Dionysiou, H. M. Hwang, *Environ. Sci. Technol.* **47** (2013) 9988 (https://dx.doi.org/10.1021/es401010g)
7. N. X. Qian, X. Zhang, M. Wangb, X. Sun, X. Y. Sun, C. Liu, R. Rao, Y. Q. Ma, *J. Photochem. Photobiol., A* **386** (2020) 112127 (https://doi.org/10.1016/j.jphotochem.2019.112127)
8. M. Maletić, M. Vukčević, A. Kalijadis, I. Janković-Častvan, A. Dapčević, Z. Laušević, M. Laušević, *Arab. J. Chem.* **12** (2019) 4388 (http://dx.doi.org/10.1016/j.arabjc.2016.06.020)
9. M. Maletić, M. Vukčević, A. Kalijadis, Z. Laušević, M. Laušević, *Adv. Mater. Sci. Eng.* (2015) 803492 (http://dx.doi.org/10.1155/2015/803492)
10. H. Belayachi, B. Bestani, N. Benderdouche, M. Belhakem, *Arab. J. Chem.* **12** (2019) 3018 (http://dx.doi.org/10.1016/j.arabjc.2015.06.040)
11. Commission implementing Decision (EU) 2015/495,*Off. J. Eur.n Union* **L78(58)** (2015) 40 (https://eur-lex.europa.eu/legal-content/EN/TXT/?uri=uriserv%3AOJ.L_.2015.078.01.0040.01.ENG&toc=OJ%3AL%3A2015%3A078%3ATOC)
12. E.P. Barrett, L.G. Joyner, P.P. Halenda, *J. Am. Chem. Soc.* **73** (1951) 373 (https://doi.org/10.1021/ja01145a126)
13. B.C. Lippens, B.G. Linsen, J.H. De Boer, *J. Catal.* **3** (1964) 32 (https://doi.org/10.1016/0021-9517(64)90089-2)
14. W. Kraus, G. Nolze, *Powder Cell for Windows*, V.2.4, Federal Institute for Materials Research and Testing, Berlin (https://powdercell-for-windows.software.informer.com/2.4/)
15. M. Sathish, B. Viswanathan, R. P. Viswanath, *Appl. Catal., .* **74** (2007) 307 (https://doi.org/10.1016/j.apcatb.2007.03.003)
16. J. Zhang, Y. Li, L. Li, W. Li, C. Yang, *ACS Sustain. Chem. Eng.* **6** (2018) 12893 (https://doi.org/10.1021/acssuschemeng.8b02264)
17. H. He, H. Wang, D. Sun, M. Shao, X. Huang, Y. Tang, *Electrochim. Acta* **236** (2017) 43 (http://dx.doi.org/10.1016/j.electacta.2017.03.104)
18. K. Kalantari, M. Kalbasia, M. Sohrabi, S. J. Royaee, *Ceram. Int.* **43** (2017) 973 (http://dx.doi.org/10.1016/j.ceramint.2016.10.028)
19. H. Safardoust-Hojaghan, M. Salavati-Niasari, *J. Clean. Prod.* **148** (2017) 31 (http://dx.doi.org/10.1016/j.jclepro.2017.01.169)
20. W. Ji, Y.G. Mei, M. Yang, H. Liu, S. Wang, Z. Shan, F. Ding, X. Liu, X. Gao, X. Li, *J. Alloys Compd.* **806** (2019) 946 (https://doi.org/10.1016/j.jallcom.2019.07.225)
21. Y. Li, H. Li, X. Lu, X. Yu, M. Kong, X. Duan, G. Qin, Y. Zhao, Z. Wang, D. D. Dionysiou, *J. Colloid Interface Sci.* **596** (2021) 384 (https://doi.org/10.1016/j.jcis.2021.03.140)

22. X. Chen, D. H. Kuo, D. Lu, *Chem. Eng. J.* **295** (2016) 192 (http://dx.doi.org/10.1016/j.cej.2016.03.047)
23. A. Kalijadis, J. Đorđević, T. Trtić-Petrović, M. Vukčević, M. Popović, V. Maksimović, Z. Rakočević, Z. Laušević, *Carbon* **95** (2015) 42 (http://dx.doi.org/10.1016/j.carbon.2015.08.016)
24. N. Hellgren, R.T. Haasch, S. Schmidt, L. Hultman, I. Petrov, *Carbon* **108** (2016) 242 (http://dx.doi.org/10.1016/j.carbon.2016.07.017)
25. K.S.W. Sing, D.H. Everett, R.A.W. Haul, L. Moscou, R.A. Pierotti, J. Rouquerol, T. Siemieniewska, *Pure Appl. Chem.* **57** (1985) 603 (https://doi.org/10.1351/pac198557040603)
26. S. Lowell, J.E. Shields, M.A. Thomas, M.Thommes, *Characterization of Porous Solids and Powders: Surface Area, Pore Size and Density*, Kluwer Academic Publishers, Dordrecht, 2004 (https://doi.org/10.1007/978-1-4020-2303-3)
27. A. Kalijadis, N. Gavrilov, B. Jokić, M. Gilić, A. Krstić, I. Pašti, B. Babić, *Mater. Chem. Phys.* **239** (2020) 122120 (https://doi.org/10.1016/j.matchemphys.2019.122120)
28. E. Kordouli, K. Bourikas, A. Lycourghiotis, C. Kordulis, *Catal. Today* **252** (2015) 128 (http://dx.doi.org/10.1016/j.cattod.2014.09.010)
29. A.D. Paola, M. Bellardita, L. Palmisano, *Catalysts* **3** (2013) 36 (http://doi:10.3390/catal3010036)
30. G. Dai, S. Liu, Y. Liang, H. Liu, Z. Zhong, *J. Mol. Catal., A* **368**–**369** (2013) 38 (http://dx.doi.org/10.1016/j.molcata.2012.11.014).

Journal of the Serbian Chemical Society
JSCS@tmf.bg.ac.rs • www.shd.org.rs/JSCS
J. Serb. Chem. Soc. 88 (2) S62–S64 (2022) *Supplementary material*

SUPPLEMENTARY MATERIAL TO

Influence of N doping on structural and photocatalytic properties of hydrothermally synthesized TiO_2/carbon composites

MARINA M. MALETIĆ[1]*#, ANA M. KALIJADIS[2], VLADIMIR LAZOVIĆ[3], SNEŽANA TRIFUNOVIĆ[4], BILJANA M. BABIĆ[3], ALEKSANDRA DAPČEVIĆ[5#], JANEZ KOVAČ[6] and MARIJA M. VUKČEVIĆ[5#]

[1]Innovation Center of the Faculty of Technology and Metallurgy, Karnegijeva 4, 11000 Belgrade, Serbia, [2]Department of Materials, „Vinča" Institute of Nuclear Sciences – National Institute of the Republic of Serbia, University of Belgrade, Mike Petrovića Alasa 12–14, 11000 Belgrade, Serbia, [3]Institute of Physics – National Institute of the Republic of Serbia, University of Belgrade, Pregrevica 118, 11080 Belgrade, Serbia, [4]Faculty of Chemistry, University of Belgrade, Studentski trg 12–16, 11000 Belgrade, Serbia, [5]Faculty of Technology and Metallurgy, University of Belgrade, Karnegijeva 4, 11000 Belgrade, Serbia and [6]Department of Surface Engineering, Institute Jožef Stefan, Jamova cesta 39, 1000 Ljubljana, Slovenia

J. Serb. Chem. Soc. 88 (2) (2023) 183–197

LC-MS/MS method

Surveyor HPLC system (Thermo Fisher Scientific) was used for the separation of the analytes on the reverse-phase Zorbax Eclipse XDB-C18 column, 75 mm long, 4.6 mm inner diameter (*i.d.)* and 3.5 μm particle size (Agilent Technologies). The mobile phase consisted of water (A), methanol (B) and 10 % acetic acid (C) and gradient changes are shown in Table S-I. An aliquot of 10 μl of the aqueous solution was injected into the HPLC system. Linear ion trap mass spectrometer, LTQ XL (Thermo Fisher Scientific), was used for the detection and quantification of pharmaceuticals. The electrospray ionization technique was used and all pharmaceuticals were analyzed in the positive ionization mode. The mass chromatogram of the pharmaceuticals is given in Fig. S-1. For quantification purposes, the selected reaction monitoring mode (SRM) was used. The selected precursor ion, the optimal collision energy, and the most abundant product ion, as well as its isolation width, for each analyte, are presented in Table S-II.

* Corresponding author. E-mail: mvukasinovic@tmf.bg.ac.rs

TABLE S-I. Gradient of mobile phase

Time, min	Content, %			Flow, ml min^{-1}
	A	B	C	
0	48	50	2	0,6
9.00	0	98	2	0,6
13.00	0	98	2	0,6
13.01	0	100	0	1
18.00	0	100	0	1
18.01	48	50	2	0,6
25.00	48	50	2	0,6

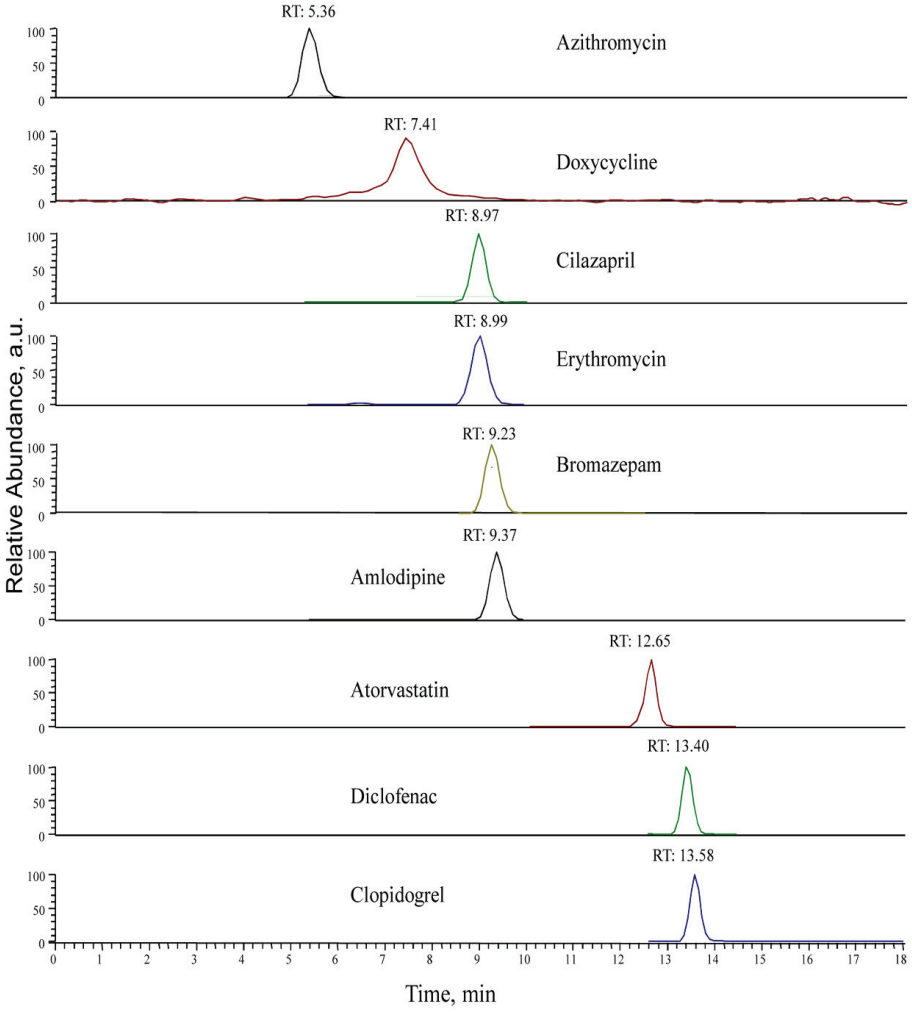

Fig. S-1. Mass chromatogram of selected pharmaceuticals.

TABLE S-II. LC/MS-MS quantification parameters for selected pharmaceuticals

Pharmaceutical	Retention time, min	Precursor ion, *m/z*	Collision energy, a.u.*	Product ion, *m/z*	Isolation width of product ion
Azithromycin	5.36	749	30	591	2
Doxycycline	7.41	445	25	428	2
Cilazapril	8.97	418	23	211	2
Erythromycin	8.99	734	26	576	2
Bromazepam	9.23	316	36	288	1
Amlodipine	9.37	408	25	237	2
Atorvastatin	12.65	559	25	466	2
Diclofenac	13.40	295	28	277	1
Clopidogrel	13.58	321	28	211	2

*arbitrary units defined by LCQ system

Journal of the Serbian Chemical Society
JSCS-info@shd.org.rs • www.shd.org.rs/JSCS
J. Serb. Chem. Soc. *88* (2) 199–209 (2023)
JSCS–5620
Original scientific paper
Published 30 September 2022

Experimental investigation on the influencing factors of preparing three-phase foam

BIN WANG[1,2], SHENG ZUO[1], XIXI ZUO[1] and XIANGMEI MA[1]*

[1]*School of Chemical Engineering, Anhui University of Science and Technology, Huainan, Anhui, 232001, China and* [2]*Disaster Prevention and Control in Deep Coal Mines, Anhui University of Science and Technology, Huainan, Anhui, 232001, China*

(Received 5 February, revised 10 July, accepted 26 July 2022)

Abstract: A three-phase foam is considered one of the promising advanced materials for fighting fires. However, the preparation conditions, cost and effect are key factors for industrial applications. In this study, new three-phase foam systems with fly ash and a complex surfactant are proposed. Five types of surfactants alcohol polyoxyethylene ether sodium sulfate, coconut oil diethanolamine, sodium lauryl sulfate, polyacrylamide and polyether-modified silicone resin emulsion were selected as foaming agents. Through laboratory experiments, the effect on the expansion ratio and foam stability of the surfactant type/concentration, fly ash particle concentration/size and pH were investigated. The foaming condition was determined by numerical optimization. The results of this study may serve as a reference for understanding the preparation of a novel three-phase foam. It is hoped that this work could provide useful guidance for the preparation of efficient three-phase fire-extinguishing foam for the safe guarding of process safety in the field of chemical production, transportation, and storage suitable for drug delivery than $Al_{12}P_{12}$ and $Al_{12}N_{12}$ based on their recovery times.

Keywords: fighting fire foam; expansion ratio; half-life; surfactant; fly ash; pH.

INTRODUCTION

Coal accounts for 60 % of the fuel used for power generation in China at present,[1] and for a long time into the future, the main body of China's energy consumption will remain coal.[2] However, a gradually expanding demand has brought more risks, such as coal field fire accidents,[3] this usually brings heavy losses and danger in the field of mining, transportation and storage. Therefore, effective and efficient fire-extinguishing material is particularly important in the process safety of firefighting and safeguarding. Foam mainly includes solidified

* Corresponding author. E-mail: wb6314005@126.com
https://doi.org/10.2298/JSC220205060W

foam, a type of dispersed gas-liquid/solid system and is an effective environmentally friendly and promising material in extinguishing fires, mineral floatation, and enhanced oil recovery.[4,5] Foam two-phase foam and three-phase foam, screening, cooling and insulating are the three main effects to extinguish fires.[6] Two-phase foam is a dispersion system composed of an aqueous surfactant solution and gas (air or nitrogen), which has an important role in fighting fires. Used properly, two-phase foam has previously effectively controlled mine fires.[7] However, its high specific surface area and surface energy lead to thermodynamic instability.[8,9] Moreover, the gravity and laplace pressure in the aqueous foam cause foam drainage to coalesce and coarsen, which leads to foam decay.[10] The efficiency of the fire extinguishing foam is mainly determined by its stability and heat insulation performance. Therefore, stabilized two-phase foams have limited applications in large-scale coal and oil fields.[11]

Three-phase foam is a system for dispersing gas and solid particles in a liquid phase,[12] in which particles stabilize the foam by adsorbing onto the gas/ /water interface.[13] Compared with a traditional gas-liquid two-phase foam, the addition of solid particles will inevitably affect the precipitation rate of water in the liquid film and the stability of the foam. Researchers have tried to add a burning-resistant powder to two-phase foam to form three-phase foam that was composed of water, air (or N_2) and solid.[14,15]

Fly ash (FA) is a massive waste residue produced as a by-product of coal combustion in power stations, out of nearly a billion tons produced in sample amount, not more than 25 % is utilized and the remaining is left untreated.[16,17] Using FA produced by coal-fired boilers as solid particles to form FA three--phase foam system could reduce the cost of the system. At the same time, it could reduce the pollution of solid waste by reducing FA discharge. Preground FA particles are commonly used to stabilize the three-phase foam and enhance oil recovery.[18] Previous studies have reported that FA particles produced by ball-milling could significantly improve the stability and resistance factor of the foam system. Although FA particles can effectively improve foam stability, grinding causes a significant increase in cost and work load. A water-based foam can produce an efficient fire prevention performance because it has good cooling and a filling effect in the fire extinction stage. Therefore, a water-based and non-ground FA stabilized foam system could promote the development of fire extinguishing materials. Currently, three-phase foams stabilized by unground FA have been applied to try and prevent and control spontaneous combustion in coal.[15,19,20]

The stability of three-phase foam is determined by the synergistic effect between surfactant and particles.[21–23] The synergistic effect is associated with the physicochemical properties, concentrations of surfactants and solid particles.[24] Mxed surfactants show a stronger synergistic interaction compared with a single surfactant.[25] However, whether it help to improve the properties of fire

fighting foam, and the influence of FA/surfactant on the stability and expansion ratio of three-phase foam still require clarification.[26]

In this study, because the used fly ash was negatively charged, cationic foam agents are unsuitable for the fly ash-based foam, anionic foamers, *i.e.*, fatty alcohol polyoxyethylene ether sodium sulfate (AES) and sodium lauryl sulfate (K12), and nonionic foamer, *i.e.*, polyacrylamide (PAM), coconut oil diethanolamine (6501), foam stabilizer: modified silicone resin polyether emulsion (FM-550), were first evaluated for the foaming agent system. Here air as gas phase and non-ground FA particles as solid phase were used to generate water-based three-phase foam. The formulation of foaming agent was optimized by orthogonal experiment. The effects of the FA particle size/content, pH on improving the expansion ratio and foam stability were investigated. As a result, the FA supported foam exhibited better stability and expansion ratio. The design in this work could be used to study the firefighting efficiency of different three-phase foams and serve as a prototype to develop better generators for both lab research and practical applications.

EXPERIMENTAL

Materials and instrumentations

All chemicals including AES, K12, 6501, PAM and FM-550 (active ingredient: 55 %) were industrial grade purchased from Lvsen Chemical Reagent Co., Ltd., China and used without further purification. Deionized water was used in all experiments. The FA used was obtained from Huainan Tianjiaan Power Co., Ltd., China. Air compressor (DET750-30 L, purchased from Shenba Compressor Manufacturing Co. Zhejiang, China): air pressure of 0.8 MPa, and air speed of 80 L min^{-1}. The foam gun delivered foam with a high-pressure spray by an air compressor.

Preparation of foam

The three-phase foam was prepared using a self-made designed system, which was mainly composed of an air compressor and a foam gun (shown in Fig. 1). First, a foam solution is prepared in a polyvinyl chloride (PVC) jar according to the ratio of ingredients, then FA particles were added as the solid phase, and fully stirred until a homogeneous slurry was obtained. The foam gun was provided with an air compressor to provide gas and pressure, then air was introduced through an air inlet on the tube and mixed with the slurry. The pressure then enables spray through the nozzle, whereby uniform and stable three-phase foams were jetted by the air through the outlet for fire extinguishing. After the foam was formed, the

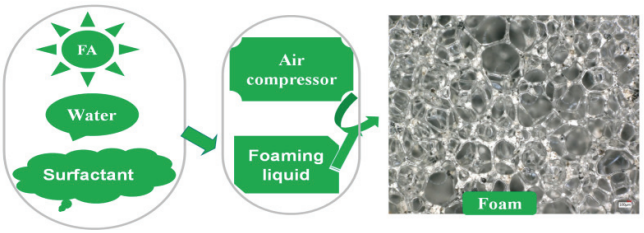

Fig. 1. Preparation process of the three-phase foam.

initial foam volume was immediately recorded, which was used to describe foaming capacity and stability. All the foam tests were performed at room temperature. A study of the properties of the foam in different foaming agent, different FA content/size and pH enabled the optimal parameters to be found.

Characterizations and calculation

The particle size distribution of FA sample was measured by a Laser Particle Sizer (Marvin Mastersizer 2000, UK). The FA was investigated by X-ray diffraction (XRD, Lab XRD, Shimadzu, Japan) test in the range of 10–60° with monochromatic CuKα radiation at 40 kV and 3 nm.

Foaming ability is one of the most fundamental properties of foam, which is expressed by the expansion ratio (F) and was calculated based on Eq. (1) according to the current Chinese national standards (GB/T 1966–1996):

$$F = \frac{\rho v}{m_2 - m_1} \quad (1)$$

ρ: the density of the foaming solution (assumed to be equal to the density of water, 1 kg dm^{-3}); v: volume of foam collector, dm^{-3}; m_1: the mass of the empty foam collector, kg; m_2: the mass of the foam collector was filled with foam, kg.

Every experiment was repeated 5 times, and three values of good precision were averaged as the measurement result. The relative change in foam volume as a function of time can be considered an indication of foam stability. Generally, foam stabilization performance is expressed by the defoaming time (decay half-life, $t_{1/2}$), $t_{1/2}$ for which the foam volume decreases by 50 %.

RESULTS AND DISCUSSION

Characterization of FA

FA is a highly heterogeneous material usually consisting of silicon dioxide and aluminum oxide as the major mineral components.[27] Laser particle analyzer is commonly used to measure the particle size distribution. As shown in Fig. 2a, the used FA particle size distribution range was 1–500 μm, and most FA diameter of particles were about 300 μm. The FA was also characterized by XRD, with Fig. 2b showing the spectra of the sample particles, the primary diffraction

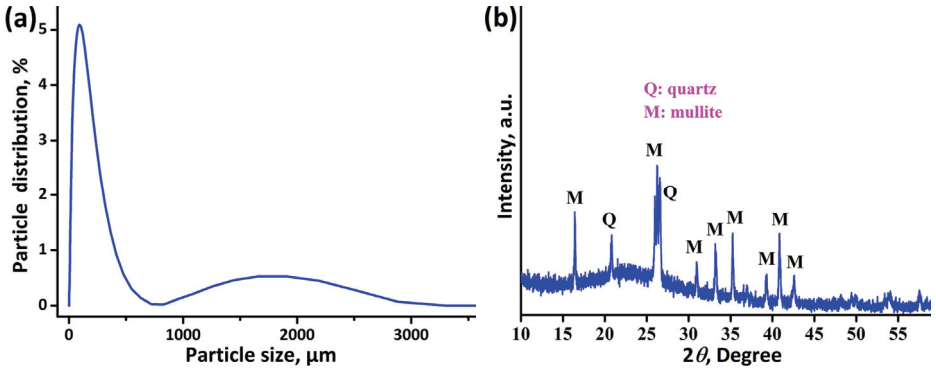

Fig. 2. Particle size distribution (a) and XRD analysis (b) of FA.

peaks at the 2θ values of the particles were located. These results indicate that the used FA contained mainly SiO_2 and Al_2O_3, the major absorptive capacity of water was low and was relatively resistant to dissolution.

Factors influencing of foam properties

Optimization of foaming agent. The surfactant in the foam could be adsorbed at the air/liquid interface to form and stabilize the foam. The orthogonal test is a method used in multiple factors analysis, which is the method of partial factor design by selecting the representative points from the comprehensive test. To determine the optimal foaming condition of the generator, the foaming agents were optimized by means of orthogonal experiment and extremum difference analysis. A five-factors four-levels including AES, 6501, K12, PAM and FM-550 were designed and a total of 16 tests were performed to analyze their foam expansion (F) and half-life ($t_{1/2}$).[28] In the experiment, the basic system was 200 g of water. Factor level values are shown in Table I and the scheme of the orthogonal test are shown in Table II. Each group of experiments was repeated five times, and the average value of the three with good precision was recorded.

TABLE I. Factors and levels of foaming agent compounding system

Level	Content, g				
	AES	6501	K12	PAM	FM-550
1	0.0	0.0	0.0	0.0	0.0
2	3.0	1.0	3.0	0.1	1.0
3	4.5	2.0	4.5	0.15	1.5
4	6.0	3.0	6.0	0.2	2.0

TABLE II. Orthogonal experiment of foaming agent compound system

Number	Content, g					F	$t_{1/2}$ / min
	AES	6501	K12	PAM	FM-550		
1	0.0	0.0	0.0	0.0	0.0	0.0	0.0
2	0.0	1.0	3.0	0.1	1.0	38.4	224
3	0.0	2.0	4.5	0.15	1.5	30.0	294
4	0.0	3.0	6.0	0.2	2.0	25.6	246
5	3.0	0.0	3.0	0.15	2.0	32.7	335
6	3.0	1.0	0.0	0.2	1.5	19.2	426
7	3.0	2.0	6.0	0.0	1.0	42.5	223
8	3.0	3.0	4.5	0.1	0.0	53.4	42
9	4.5	0.0	4.5	0.2	1.0	32.2	327
10	4.5	1.0	0.0	0.15	0.0	38.8	37
11	4.5	2.0	6.0	0.1	2.0	26.8	280
12	4.5	3.0	3.0	0.0	1.5	28.2	256
13	6.0	0.0	6.0	0.1	1.5	29.2	294
14	6.0	1.0	4.5	0.0	2.0	25.2	310
15	6.0	2.0	3.0	0.2	0.0	41.4	56
16	6.0	3.0	0.0	0.15	1.0	23.2	471

In order to systematically analyze the degree of influence of different foaming agents, the range analysis method was introduced according to the orthogonal test.

The results showed that the sequence of the influence of surfactant on the *F* and $t_{1/2}$ were as follows: K12>AES>PAM>6501>FM-550 (Table III), FM-550 >PAM>AES>K12>6501 (Table IV). The best array was $A_2B_3C_3D_2E_2$ and $A_4B_4C_4D_3E_3$, respectively. These results suggested that the surfactant plays the main role in the process of fire-retardant foam. Based on the range analysis, the best proportion of the foaming agent compounding system is AES:6501:K12: :PAM:FM-550 = 6:6:9:0.3:2 (mass ratio, 200 g water, which was recorded as the foaming agent in the follow-up experiments).

TABLE III. Analysis of foam expansion ratio range; *K* is the sum of the foaming multiples in parallel experiments, *k* is the average foaming multiples, *A* is the experimental results of AES, *B* is the experimental results of 6501, *C* the experimental results of K12, *D* the experimental results of PAM, *E* the experimental results of FM-550

Parameter	*F*				
	A (AES)	B (6501)	*C* (K12)	*D* (PAM)	*E* (FM-550)
*K*1	94.0	94.1	81.2	95.9	133.6
*K*2	147.8	121.6	140.7	147.8	136.3
*K*3	126.0	140.7	140.8	124.7	106.6
*K*4	119.0	130.4	124.1	118.4	110.3
*k*1	23.5	23.5	20.3	24.0	33.4
*k*2	37.0	30.4	35.2	37.0	34.1
*k*3	31.5	35.2	35.2	31.2	26.6
*k*4	29.8	32.6	31.0	29.6	27.6
Range	13.5	11.7	14.9	13.0	8.5
Primary and secondary sequence order *C*>*A*>*D*>***B***>*E*					
Optimization	A_2	B_3	C_3	D_2	E_2

TABLE IV. Analysis of foam half-life range

Parameter	$t_{1/2}$ / min				
	A (AES)	B (6501)	C (K12)	D (PAM)	E (FM-550)
*K*1	764	956	934	789	135
*K*2	1026	997	871	840	1245
*K*3	900	853	973	1137	1270
*K*4	1131	1015	1043	1035	1171
*k*1	191	239	233	197	34
*k*2	256	249	218	210	311
*k*3	225	213	243	284	318
*k*4	282	254	261	264	293
Range	91	41	43	87	284
Primary and secondary sequence order *E*>*D*>*A*>*C*>*B*					
Optimization	A_4	B_4	C_4	D_3	E_3

Foaming agent and water ratio (foaming liquid)

The best proportion of foaming agent were mixed with water in the mass ratio of 1:10, 1:15, 1:20, 1:25, 1:30 (recorded as the foaming liquid) to study the foaming capacity and foam stability. As shown in Fig. 3, with other condition remaining unchanged, the F and $t_{1/2}$ of the foam first increase and then decreases with decreaseing water, when 1:20 was added, both had the maximum at 34.2 and 7.5 h respectively, which depicts that the foaming agent and water ratio play other main roles for the foaming capacity and foam stabilization.

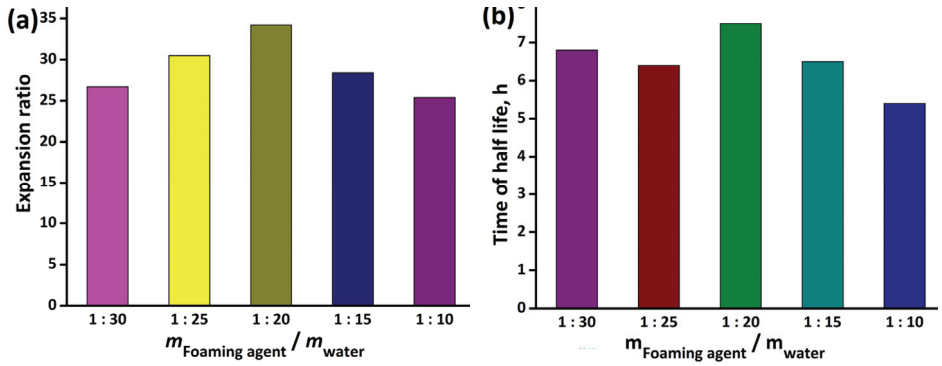

Fig. 3. Optimal ratio of foaming agent and water.

The ratio of foaming liquid/FA

FA particles are added to the foaming liquid (1:20 ratio of foaming agent and water) to form a three-phase foam system. Comparing the F and $t_{1/2}$, the performance of three-phase foam is evaluated under different solid–liquid ratios. As observed in Fig. 4, with increasing FA mass fraction, the $t_{1/2}$ values of the foam increased, but foam volume decreased continuously, thereby indicating that the FA can increase foam stability, but has an inhibitory effect on foam volume. The enhancement of foam stability of three-phase foam was attributed to the existence of FA particles. The attached particles decrease the pressure difference between the gas/liquid interface, slowing down the drainage process. Foam fire extinguishing mainly depends on covering the surface of burning objects to prevent them from contacting oxygen and continuing burning. Therefore, F has a greater impact on the foam extinguishing property than its $t_{1/2}$ period. According to experiment results, when the solid to liquid ratio is lower than 1:3, the expansion ratio below 10, limits its practical application as a fire extinguisher. When choosing the proportion with the solid to liquid ratio of 1:4 for the fire-retardant foam, not only ensures comprehensive properties such as F and stability are the best, but the use of stabilizer can also be reduced at the same time, and the F meets the current requirements of coal mine fire-extinguishing materials. By focusing on its F and $t_{1/2}$, a solid–liquid ratio of 1:4 was determined. Based on

this, the optimized FA three-phase foam system has excellent stability with a foam $t_{1/2}$ that can reach more than 28.7 h.

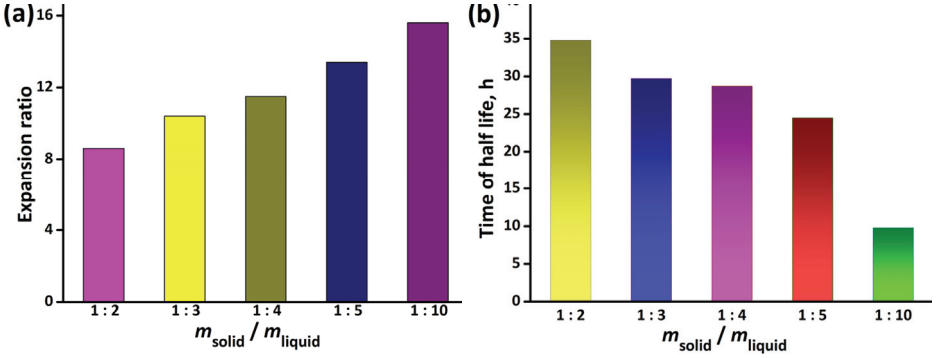

Fig. 4. Influence of solid-liquid ratio on the performance of three-phase foams.

FA particle size

FA particle is widely applied in the physical property test. To avoid particle size effect, specific graded particles were selected for physical parameter measurement experiments.[29] In lab research, there are some particle size distribution testing such as sieving, laser particle analyzer, *etc*. Sieving is the simplest powder particle size test method, the size of the lower and upper standard sieves as the lower and upper limits of the particle size. That is, broken FA samples can be separate by sieves of different sizes, and the FA particles after sieving were divided into different particle groups.: <38, 38–75, 75–106, 106–150 and 150––380 μm. Fig. 5 shows that with increasing particle size, the foam $t_{1/2}$ tends to stabilize and then decrease.

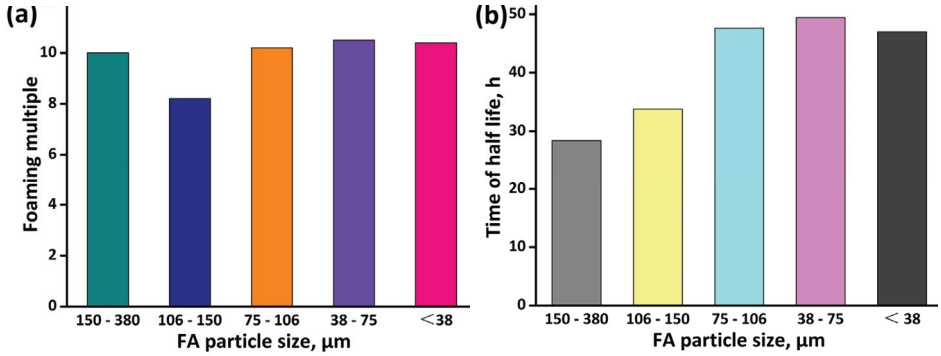

Fig. 5. Influence of particle size on the properties of three-phase foam.

No significant differences were observed in values of the F among smaller particle fractions (<75 μm). Thus, smaller particles can keep good dispersion in

the dispersion liquid, and hence the results can be grained large area. The larger particles are not suitable for stabilization because they are dispersed difficultly and the gravity in the aqueous foam leads to foam decay.

pH

In actual application in coal mines or oil fields, foam is often used in areas where coal or oil are prone to spontaneous combustion. In such places, the pH value differs from respective levels in the laboratory. Therefore, it is necessary to study the influence of pH value factors on the characteristics of the foam, and hence, the pH value of the foaming system was adjusted to about 4, 5, 6, 7, 8, 9, and 10. Fig. 6 shows that with increasing pH value, both the foaming ability and foam stabilization first increase and then decrease. This is mainly because at a low pH value, the foaming solution is acidic, and the H^+ in the solution will react with the anionic foaming agent (such as: $–SO_3^–$), resulting in a decreased effective content of the foaming agent and weakened foaming ability.

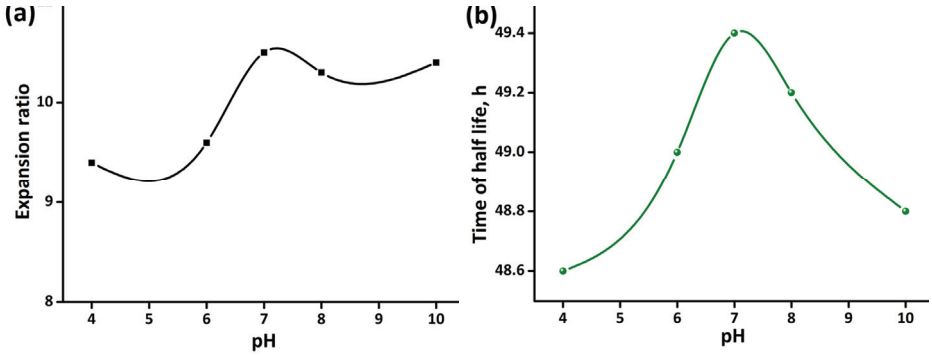

Fig. 6. Influence of pH on the performance of three-phase foam.

With increasing pH value, the relative effective content of the foaming agent increases, and foaming capacity is increased. When the pH value exceeds 7, the $OH^–$ combines with the hydrophilic group in the foaming agent, which affects the foaming effect. However, changes of the F and $t_{1/2}$ were not obvious, so they can be used for wider application fields.

CONCLUSIONS

This study combines the advantages of foam fire-extinguishing technologies, and a new type of mine fire-extinguishing foam was prepared. Firstly, the optimum ratio of foaming agents was obtained by orthogonal experiment and variance analysis for different factors and levels. Then, FA particles were used as the solid phase to generate three-phase foams. The effects of solid to liquid ratio, FA size distribution and the system pH on the foaming multiple and stabilization time of the foam were assessed. Under the optimized operating conditions of 1:4

solid–liquid ratio, smaller particle fractions (<75 μm) and from weak acid to weak base, the fly ash-based three-phase foam showed satisfactory stability and foaming ability. These investigations provided a novel route for preparing high--efficiency fire-extinguishing foams applicable in the confined space of underground coal mines.

Acknowledgment. The study was financially supported by the Key Research and Development Projects in Anhui Province (grant number 202004h07020022).

И З В О Д

ЕКСПЕРИМЕНТАЛНО ИСПИТИВАЊЕ ФАКТОРА КОЈИ УТИЧУ НА ПРИПРЕМУ ТРОФАЗНЕ ПЕНЕ

BIN WANG[1,2], SHENG ZUO[1], XIXI ZUO[1] и XIANGMEI MA[1]

[1]*School of Chemical Engineering, Anhui University of Science and Technology, Huainan, Anhui, 232001, China и* [2]*Disaster Prevention and Control in Deep Coal Mines, Anhui University of Science and Technology, Huainan, Anhui, 232001, China*

Трофазна пена се сматра једним од перспективних напредних материјала за гашење пожара. Међутим, услови припреме, цена и ефекат су кључни фактори за индустријску примену. У овој студији предложен је нови трофазни систем пене са летећим пепелом и комплексним сурфактантом. Пет типова сурфактаната: алкохол полиоксиетилен-етар, натријум-сулфат, диетаноламин кокосово уље, натријум-лаурил-сулфат, полиакриламид и емулзија силиконске смоле модификоване полиетаром су одабрани као средства за пењење. Кроз лабораторијске експерименте, испитан је утицај на степен експанзије и стабилност пене типа/концентрације сурфактанта, концентрације/величине честица летећег пепела и pH. Стање пене је одређено нумеричком оптимизацијом. Резултати ове студије могу послужити као референца за разумевање припреме нове трофазне пене. Надамо се да овај рад може да пружи корисне смернице за припрему ефикасне трофазне пене за гашење пожара за безбедно чување безбедности процеса у области хемијске производње, транспорта и складиштења.

(Примљено. 5. фебруара, ревидирано 10. јула, прихваћено 18. јула 2022)

REFERENCES

1. Y. Zheng, Q. Li, G. Zhang, Y. Zhao, P. Zhu, X. Ma, X. Liu, *Fuel Process Technol.* **208** (2020) 106510 (https://doi.org/10.1016/j.fuproc.2020.106510)
2. M. Wu, Y. Liang, Y. Zhao, W. Wang, X. Hu, F. Tian, Z. He, Y. Li, T. Liu, *Colloids Surfaces, A* **629** (2021) 127443 (https://doi.org/10.1016/j.colsurfa.2021.127443)
3. Z. Jelonek, A. Drobniak, M. Mastalerz, I. Jelonek, *Sci. Total Environ*. **747** (2020) 141267 (https://doi.org/10.1016/j.scitotenv.2020.141267)
4. X. Hu, Y. Li, X. He, C. Li, Z. Li, X. Cao, X. Xin, P. Somasundaran, *J. Phys. Chem., B* **116** (2012) 160 (https://doi.org/10.1021/jp205753w)
5. M. Simjoo, Q. P. Nguyen, P. L. J. Zitha, *Ind. Eng. Chem. Res.* **51** (2012) 10225 (https://doi.org/10.1021/ie202218z)
6. Q. Liu, S. Zhang, D. Sun, J. Xu, *Colloids Surfaces, A* **355** (2010) 151 (https://doi.org/10.1016/j.colsurfa.2009.12.003)

7. L. La Fosse, M. Cummins, *Coal Peat Fires: Global Perspect.* **1** (2011) 327 (https://doi.org/10.1016/B978-0-444-52858-2.00019-0)
8. Y. Li, G. Xiao, C. Chen, C. Chen, F. Li, F. Li, L. Lin, *Colloids Surfaces, A* **627** (2021) 127147 (https://doi.org/10.1016/j.colsurfa.2021.127147)
9. P. Sobolciak, A. Popelka, A. Tanvir, M. A. Al-Maadeed, S. Adham, I. Krupa, *Water* **13** (2021) 652 (https://doi.org/10.3390/w13050652)
10. R. Rafati, A. S. Haddad, H. Hamidi, *Colloids Surfaces, A* **509** (2016) 19 (https://doi.org/10.1016/j.colsurfa.2016.08.087)
11. W. P. Yang, T. F. Wang, Z. X. Fan, Q. Miao, Z. Y. Deng, Y. Y. Zhu, *Energy Fuels* **31** (2017) 4721 (https://doi.org/10.1021/acs.energyfuels.6b03217)
12. B. M. Mbama Gaporaud, P. Sajet, G. Antonini, *Chem. Eng. Sci.* **53** (1998) 735 (https://doi.org/10.1016/S0009-2509(98)00332-7)
13. N. P. Yekeen, M. A. Manan, A. K. Idris, E. Padmanabhan, R. Junin, A. Samin, A. O. Gbadamosi, *J. Petrol Sci. Eng.* **164** (2018) 43 (https://doi.org/10.1016/j.petrol.2018.01.035)
14. X. Xi, Q. L. Shi, *Fuel* **288** (2021) 119354 (https://doi.org/10.1016/j.fuel.2020.119354)
15. T. Wang, H. Fan, W. Yang, Z. Meng, *Fuel* **264** (2020) 116832 (https://doi.org10.1016/j.fuel.2019.116832)
16. K. Samvatsar, H. Dave, *Mater. Today: Proc.* **47** (2021) 2384 (https://doi.org/10.1016/j.matpr.2021.04.353)
17. M. R. Little, V. Adell, A. R. Boccaccini, C. R. Cheeseman, *Resour. Conserv. Recycl*. **52** (2008) 1329 (https://doi.org/10.1016/j.resconrec.2008.07.017)
18. B. Wei, H. Li, Q. Li, L. Lu, Y. Li, W. Pu, Y. Wen, *Fuel* **211** (2018) 223 (https://doi.org/10.1016/j.fuel.2017.09.054)
19. B. Qin, Y. Lu, Y. Li, D. Wang, *Adv. Powder Technol*. **25** (2014) 1527 (https://doi.org/10.1016/j.apt.2014.04.010)
20. Z. Shao, D. Wang, Y. Wang, X. Zhong, X. Tang, X. Hu, *China Nat. Hazard.* **75** (2015) 1833 (https://doi.org/10.1007/s11069-014-1401-3)
21. U. T. Gonzenbach, A. R. Studart, A. Elena Tervoort, L. J. Gauckler, *Langmuir* **22** (2006) 10983 (https://doi.org/10.1021/la061825a)
22. T. N. Hunter, R. J. Pugh, G. V. Franks, G. J. Jameson, *Adv. Colloid Interface Sci.* **137** (2008) 57 (https://doi.org/10.1016/j.foodhyd.2007.08.005)
23. D. T. Johnson, *J. Disper. Sci. Technol.* **25** (2005) 575 (https://doi.org/10.1081/DIS-200027307)
24. G. Zhao, C. Dai, D. Wen, J. Fang, *Colloid Surfaces, A* **497** (2016) 214 (https://doi.org/10.1016/j.colsurfa.2016.02.037)
25. N. Jiang, Y. J. Sheng, C. L. Li, S. X. Lu, *J. Mol. Liq*. **268** (2018) 249 (https://doi.org/10.1016/j.molliq.2018.07.055)
26. R. Zhou, X. Lang, X. Zhang, B. Tao, L. He, *Proc. Safety Environ. Prot.* **146** (2021) 360 (https://doi.org/10.1016/j.psep.2020.09.017)
27. M. Savić Biserčić, L. Pezo, I. Sredović Ignjatović, Lj. Ignjatović, A. Savić, U. Jovanović, V. Andrić, *J. Serb. Chem. Soc.* **81** (2016) 813 (https://doi.org/10.2298/JSC151222027B)
28. H. Zhu, C. Hu, J. Guo, X. Wang, B. Wu, *Coal Technol. (China)* **38** (2019) 45 (https://doi.org/10.13301/j.cnki.ct.2019.09.016)
29. Z. Lei, N. Aziz, T. Ren, J. Nemcik, S. Tu, *Arch. Min. Sci.* **59** (2014) 807 (https://dx.doi.org/10.2478/amsc-2014-0056).

Journal of the Serbian Chemical Society
JSCS@tmf.bg.ac.rs • www.shd.org.rs/JSCS
J. Serb. Chem. Soc. *88* (2) 211–221 (2023)
JSCS–5621
Original scientific paper
Published 18 November 2022

Remediation of chemistry teachers' misconceptions about covalent bonding using cognitive conflict interviews: A case study

SYAHRIAL SYAHRIAL[1], MASHFUFATUL ILMAH[1], YAHMIN YAHMIN[2], MUNZIL MUNZIL[2] and MUNTHOLIB MUNTHOLIB[2]*

[1]*Chemistry Education Program, Postgraduate Program, Universitas Negeri Malang, Indonesia and* [2]*Department of Chemistry, Universitas Negeri Malang, Indonesia*

(Received 17 January, revised and accepted 12 September 2022)

Abstract: Research has shown that most chemistry teachers have misconceptions about covalent bonding. This study investigates whether the cognitive conflict interview technique could persuade teachers to revise their possible misconceptions of covalent bonding. Eight chemistry teachers from different schools participated in this study. Two validated instruments, cognitive conflict technique interview guidelines and the open-ended covalent bonding test, were employed for the data collection. The results showed that the cognitive conflict interviews could facilitate respondents to overcome their misconceptions about covalent bonding. Five of the eight respondents experienced a conceptual change from misconceptions to scientific conceptions, and three others experienced a partial conceptual change. Six concepts which previously caused misconceptions were eliminated and turned into a scientific concept instead. Of the 46 cases of misconceptions, 41 cases turned into scientific conceptions. The result of this study serves as an initial perspective for exploring the effectiveness of cognitive conflict interviews more broadly.

Keywords: chemistry teacher; conceptual changes; contradicts phenomena.

INTRODUCTION

The concepts of covalent bonding underlie other chemistry concepts[1] such as molecular structure and chemical and physical properties of compounds.[2] However, various studies have shown that this subject generates many misconceptions.[3–6] Misconception refers to an individual concept different from the concept accepted by the scientific community,[7] that must be adequately addressed because it can cause learning problems.[8]

* Corresponding author. E-mail: muntholib.fmipa@um.ac.id
https://doi.org/10.2298/JSC220117073S

Various studies revealed that secondary school,[2] university students[9] and chemistry teachers demonstrated the misconception of covalent bonding.[10,11] Regardless of those results, limited evidence has been found regarding how to consider these misconceptions. How teachers explain chemical bonding may lead to students' difficulties with comprehending and learning.[12] Therefore, teachers' misconceptions must be corrected to avoid transferring their misconceptions to students. The effort to solve students' misconceptions must be initiated by ensuring that teachers hold clear scientific conceptions.

Cognitive conflict strategies emphasize the instability of people's beliefs in their existing conceptions through contradictory experiences. It then allows them to replace their misconception with scientifically accepted concepts.[13] This teaching strategy involves demonstrating phenomena in which students' observations contradict what they expected.[14] The contradiction causes a mental imbalance that encourages students to change their conceptions to fit the new facts they observe.[15] In other words, the cognitive conflict strategies facilitate the elimination of students' misconceptions after experiencing the counter-scientific conceptions.

The cognitive conflict strategies can be carried out in various ways or methods,[16] including cognitive conflict interviews.[17,18] The strategy of cognitive conflict interview allows researchers to ask in-depth questions to obtain broader and more profound answers.[19,20] The cognitive conflict interviews can also elaborate on students' cognitive structures[18] to uncover their misconceptions.[21] Studies have shown that the cognitive conflict interviews effectively revised students' misconceptions.[19,22] Various chemical phenomena of covalent bonding can be used to challenge the existing teachers' misconceptions, leading them to replace those with scientifically accepted conceptions.[13–15] For example, some respondents consider the electron configuration of an element in a molecule is simply the same as its configuration in a free atom. Presenting a configuration of Cl as a single atom and its configuration in HCl will challenge them to rethink of their initial conception.

EXPERIMENTAL

This study applied a case study and followed the interpretive paradigm[23] concerning the remediation of eight chemistry teachers' misconceptions about chemical bonding. This study was intended to explain the conceptual change phenomena occurring in chemistry teachers who held misconceptions about chemical bonding.[24] The uncovered misconceptions were corrected using the cognitive conflict interview technique.

Respondents

The respondents for this research were eight chemistry teachers from several schools in Banten Province, Indonesia. All respondents hold bachelor's degrees in chemical education with more than three years of teaching experience and offered their consent to participate.

Instruments

Two instruments, given in Supplementary material to this paper, cognitive conflict interview guidelines (Supplement 1) and an open-ended covalent bonding test (Supplement 2), were used for data collection. The cognitive conflict interview guidelines were used to correct the teachers' misconceptions. The open-ended test on covalent bonding consisting of 18 items was used to assess the changes in the teachers' conceptions.

The content validity and reliability of the instruments were assessed based on feedback from two experienced chemistry lecturers. Content validity describes how an instrument has an appropriate sample of items for the construct being measured,[25] whereas the reliability of the measurement result is its consistency and reproducibility.[26] The content validity was analyzed based on its content validity index (*CVI*), while the reliability was analyzed based on their inter-rater agreement (*IRA*).[25,27,28] The *CVI* was calculated by dividing the number of experts who gave a positive rating (*i.e.*, 3 or 4) and the total number of experts. The *IRA* was calculated by dividing the number of items with *IRA* items greater than 0.80 and the number of total items. The acceptable cut-off value for the *CVI* and the *IRA* was 0.80.[27-30] However, Landis and Koch[31] and Regier *et al.*[32] set *CVI* and *IRA* with different criteria, *i.e.*, poor if <0.00, low or unacceptable if 0.00–0.20, fair or questionable if 0.21–0.40, moderate or good if 0.41–0.60, substantial or very good if 0.61–0.80, and almost perfect or excellent if 0.81–1.00. The validity and the reliability of each secondary instrument are shown in Table I.

TABLE I. The CVI and IRA of secondary instruments used in this research

Secondary instrument	*CVI*		*IRA*	
	Value	Agreement strength	Value	Agreement strength
The cognitive conflict interview guide	1.0	Excellent	0.75	Very good
Open-ended test on covalent bonding	1.0	Excellent	0.69	Very good

Table I shows that all secondary instruments are feasible and can be used in data collection. In addition, this study also employed a tape recorder to record the interviews.

Procedure

The respondents were separately interviewed without a time limit. Respondents were free to use pictures or other schematic representations to express their opinions. The open--ended test on covalent bonding was carried out one week after the interview. This test was intended to identify teachers' understanding changes after interviews.

A cognitive conflict interview consists of 4 steps: 1) confirming the pre-conception, 2) creating cognitive conflicts by providing evidence, anomalies, and contradictions to promote mental imbalance that encourages teachers to change their conceptions,[15] 3) stimulating the equilibration process using the relevant questions to help them understand the new concept and 4) confirming the scientific concept.

Data analysis

The responses to the covalent bonding test were analyzed using descriptive analysis and categorized into six degrees of understanding. The degrees are sound understanding, partial understanding, partial understanding with misconceptions, misconceptions, lack of knowledge and no response.[33] This study simplified these six degrees of understanding into three categories (Table II).

TABLE II. The scoring criteria of teachers' responses (modified from Abraham *et al.*[33])

Scoring criteria	The degree of understanding	Category	Example from interviews
The response includes all components of the valid responses	Sound understanding	Sound understanding	Atoms bond to achieve a stable state or lower energy levels
The response includes at least one of the components of valid response, but not all components	Partial understanding		The atoms bond together to be stable, *i.e.*, obey the octet or duplet rule
The response shows understanding and consists of a statement that demonstrates a misconception	Partial understanding with misconception	Misconception	The bond polarity of HF > HCl > HBr is due to the atomic size of F < Cl < Br
The response includes illogical or incorrect information	Misconception		HF, HCl, and HBr have the same bond polarity
The response repeats questions only or is irrelevant or unclear	Lack of knowledge	Lack of knowledge	I don't know how the formal charge relates to stability
No responses or just stated "I have no idea"	No response		–

Partial understanding is an incomplete description of chemical phenomena. Example: They correctly explained that atoms bond each other to achieve stability. However, they explained, "obeying the octet or duplet rule is the root of stability." Partial understanding with misconceptions is a correct understanding but contains misconceptions. Example: bond polarity of HF > HCl > HBr. However, the respondents explained that the difference in the atomic size caused the difference in the bond polarity, where the atomic size of F < Cl < Br. The misconception implied by this statement is the difference in the bond polarity of HF > HCl > HBr is caused by the variability in the atomic size of F < Cl < Br only. The difference in atomic electronegativity causes the difference, F > Cl > Br, rather than the difference in atomic size, F < Cl < Br.

Each response was carefully read, compared, and tentatively assigned to one of the scoring criteria. The responses that were difficult to classify were separated and discussed in focus groups involving all research members until a consensus occurred.

RESULTS AND DISCUSSION

Our previous study showed that all respondents (before receiving cognitive conflict interviews) had misconceptions about the covalent bonding concepts.[11] The cognitive conflict interview guideline (Supplement 1) was developed based on the misconceptions identified through this preliminary research. After the intervention (cognitive conflict interview), only 3 of 8 respondents still demonstrated misconceptions in 2 concepts. The two misconceptions are: 1) the O–H bond of the water molecule resulting from the reaction of acid-base neutralization

is a covalent bond and 2) both N–O covalent bonds in the NO_2 molecule are double bonds or single bonds (Table III).

TABLE III. The two misconceptions identified after the intervention

Concept	Misconceptions	Respondent No.
The coordinate covalent bonding	The O–H bond of the H_2O molecule formed by the reaction of H^+ and OH^- are a covalent bonding because the electron pair between the H and O atoms are shared by the H and O atoms	1 3
Lewis structure	The Lewis structure of the NO_2 molecule is: 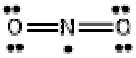 because both N–O covalent bonds are identical	1
	The Lewis structure of the NO_2 molecule is:  because both N–O covalent bonds are identical	3 7

Table III shows that after the intervention, the respondents who experienced misconceptions were 3, including respondents No. 1, No. 3 and No. 7. In contrast, the other five respondents understood the covalent bonding concepts well. Overall, the misconceptions about the covalent bonding concepts before and after the intervention are shown in Table IV.

TABLE IV. The respondents' misconceptions about the covalent bonding concepts before and after the intervention

No.	Concept	Number of respondents experiencing misconceptions	
		Before intervention	After intervention
1	The purpose of bond-forming atoms	8	0
2	The coordinate covalent bonding	2	2
3	Types of atoms that can form covalent bonds	7	0
4	Polar and nonpolar covalent bonds	4	0
5	The polarity order of covalent bonds	4	0
6	Lewis structure	8	3
7	Octet rule	8	0
8a	The length of C–C bonds in ethane, ethene, ethane	2	0
8b	The length of the covalent bonding in hydrogen halides	3	0
Total cases		46	5

Table IV shows that the cognitive conflict interviews: 1) decrease the number of respondents who experience misconceptions from 8 people to 3 people; 2) reduce the number of concepts in which respondents experience misconceptions from 8 to 2 concepts; 3) reduce the number of misconception cases from 46 to 5 cases.

Previous researchers have also reported the effectiveness of cognitive conflict interviews in correcting misconceptions.[19,22] Cognitive conflict is closely related to conceptual change.[13–15] Cognitive conflict helps a person realize that there is a problem with their conception by showing phenomena, data, or evidence that contradicts their initial conception. This awareness will lead them to replace their initial conception with the scientific one. Several factors could explain the effectiveness of this strategy in correcting misconceptions. Firstly, one-on-one interviews provide a convenient environment leading to a productive discussion between interviewer and respondent. Secondly, confirmation or supporting questions make respondents realize that their initial conception is scientifically incorrect. Confirmatory questions[22] can facilitate and describe the conceptual change process. Thirdly, respondents' prior knowledge was sufficient to recognize the phenomena, data, and/or evidence presented in the interviews. The plenty of experience in teaching covalent bonds leads them to quickly realize their misconceptions when facing the facts, phenomena, data, or evidence that contradicts their conceptions. However, the one-on-one interview approach is time-consuming.[34]

The following interview script illustrates the conceptual change regarding "atoms that form covalent bonds".

1. Researcher: What types of atoms are forming covalent bonds? Metal atoms? Non-metal atoms? Both of them?
2. Respondent: Non-metal atoms.
3. Researcher: Are metal atoms unable to form covalent bonds?
4. Respondent: Yes, right.
5. Researcher: If so, what type of bond is formed between the Be and the Cl in $BeCl_2$ and between the Al and the Br in $AlBr_3$?
6. Respondent: An ionic bond because Be and Al are metals while Cl and Br are non-metals.
7. Researcher: (Indicating a reference that for binary compounds, a covalent bond will be formed when the two atoms forming the bond have an electronegativity difference of <1.7 according to the Pauling scale) Now, pay attention to the following data! (Showing the data on the difference in electronegativity between Be with Cl and Al with Br) Count for a moment! What is the difference in electronegativity between Be and Cl and Al and Br? Smaller or greater than 1.7 on the Pauling scale?
8. Respondent: Smaller than 1.7 on the Pauling scale.
9. Researcher: Well, it is below 1.7 on the Pauling scale. Therefore, what kind of bond is formed between Be and Cl as well as between Al and Br?
10. Respondent: If, based on the data, both of the bonds are covalent.

11. Researcher: Well! Let's go back to the $BeCl_2$ and $AlBr_3$. Are these two compounds composed of non-metallic atoms only?
12. Respondent: No. Be and Al are metals, while Cl and Br are non-metals. Both compounds contain metal and non-metal atoms.
13. Researcher: What does it mean? Is the type of bond in a binary compound determined only by the type of atom that composes it?
14. Respondent: Ermmm ... It means that the kind of bond of binary compounds cannot be seen from the type of atoms composing it. Is it right?
15. Researcher: Yes, that's right. If so, what is your inference regarding the covalent bonding in binary compounds?
16. Respondent: Ummm ... The type of bond in binary compounds can't be seen from the type of atoms forming it, metal or non-metal. However, it can be seen from the difference in electronegativity of the two types of atoms forming it. If the difference in electronegativity of the two types of atoms on the Pauling scale is less than 1.7, the bond is covalent, but if it is greater than 1.7, the bond is ionic.

The interview script above shows that initially, the respondent highly believed that: 1) covalent bonds only formed between non-metal atoms and 2) Be–Cl bond in $BeCl_2$ and Al–Br bond in $AlBr_3$ were ionic bonds (lines 2, 4 and 6). This belief or conception raises a question for the respondent when the interviewer showed the Pauling scale parameter in determining the type of chemical bond, which led to a conclusion different from the respondent's conception (lines 7 and 8). This parameter made the respondent doubt their initial understanding when the interviewer pointed out that the difference in electronegativity between Be and Cl and Al and Br was below 1.7 on the Pauling scale, indicating a covalent bonding, not an ionic bond, as the respondents perceived before. This misconception changed after the interviewer asked the respondent to determine the type of atoms composing the $BeCl_2$ and $AlBr_3$ compounds (lines 11 and 12). At the end of the interview, the respondent believed that the type of bond (covalent or ionic) formed in binary compounds was not dependent on whether the atoms were metal or non-metal but on the difference in electronegativity between the atoms (line 16). This final script indicates a conceptual change from misconception to scientific conception.

Regardless of the positive conceptual change, as shown in the interview script example, three respondents still experienced two misconceptions (Table III). This implies that some misconceptions has persisted, as reported by previous researchers.[35]

The first persistent misconception is the coordinate covalent bonding in the water molecule produced by the acid-base neutralization reaction. The two respondents (No. 1 and 3) only considered the molecular structure of H_2O and

ignored how the water molecules were formed. They did not realize that in acid-base neutralization, OH^- acts as an electron-pair donor, and H^+ acts as an electron pair acceptor. Therefore, the bond is a coordinate covalent bonding. The lack of awareness regarding the formation of water molecules,[6,24] leads to the misconception.

The second persistent misconception is related to the Lewis structure of the molecule or polyatomic ion. The three respondents (No. 1, 3 and 7) keep determining the Lewis structure of a molecule according to the following steps: 1) determining the electron configuration of each atom; 2) determining the central atom; 3) drawing Lewis symbols for all atoms; 4) pairing the electrons of each atom until the octet or duplet rule was obeyed. This procedure makes them difficult when dealing with molecules that do not obey the octet rule. The correct steps to write the Lewis structure are identifying the central atom, calculating coordination numbers, bonding and lone pairs, writing a frame of Lewis structure, adding electrons to all the substituents to fulfil the octet or duplet rules, calculating the formal charges of all the atoms, and making the formal charge of all atoms equal to zero.[36]

The Lewis structure and coordinate covalent bonding concepts require a good understanding of the definitions and the rules associated with these definitions.[37] To write the Lewis structure of a species correctly, we need to understand the species well, the rules for writing Lewis structures, and the terms associated with these rules like coordination number, bonding electron pair, lone pair, formal charge, octet, duplet[36] and unpaired electrons.[38] A conventional example of a coordinate covalent bonding is $[Cu(H_2O)_6]^{2+}$, while an example of a coordinate covalent bonding that does not involve a transition element is NH_4^+. The lone pairs of the O atom of the neutral molecule H_2O and the N atom of the neutral molecule NH_3 are critical examples of a coordinate covalent bonding. The source of the electron pair in a coordinate covalent bonding does not always come from the lone pair of an atom of the neutral molecule,[39] for example, OH^- in an acid–base neutralization reaction. Lack of knowledge related to these concepts is a root of misconceptions about the concepts of coordinate covalent bonding and Lewis structure.

The issues of resistant misconceptions have been uncovered in the previous study.[40] According to Piaget, the incomplete conceptual change is caused by the inability to reach the equilibration phase in acquiring new concepts.[1]

CONCLUSION AND IMPLICATION

After applying the cognitive conflict interview, the number of misconception cases held by the teachers decreased. This phenomenon indicates that the cognitive conflict interviews can potentially encourage teachers to overcome misconceptions about the concepts of covalent bonding. Some persistent misconceptions

were still found, such as the O–H bond in the water molecule produced by the acid-base neutralization is a covalent bond. We realize that the sample size is insufficient to provide a robust conclusion. Still, the results of this study could be a pilot to implement the cognitive conflict interviews for overcoming misconceptions and establishing a conceptual understanding of chemical bonding and other chemical topics. Therefore, the effectiveness of this method in overcoming misconceptions needs to be proven by further research.

SUPPLEMENTARY MATERIAL

Additional data and information are available electronically at the pages of journal website: https://www.shd-pub.org.rs/index.php/JSCS/article/view/11570, or from the corresponding author on request.

Acknowledgements. We would like to express our deepest gratitude to our previous adviser, Prof. Effendy, PhD, for his guidance in conducting this research. Our prayers accompany him in the Barzakh realm. May Allah forgive his sins, have mercy on him and gather him with the souls of pious people. We also thank Habiddin, PhD, for restructuring the sentences and for valuable language feedback.

ИЗВОД

ОТКЛАЊАЊЕ ЗАБЛУДА О КОВАЛЕНТНОМ ВЕЗИВАЊУ КОД НАСТАВНИКА ХЕМИЈЕ ПОМОЋУ ИНТЕРВЈУА БАЗИРАНОГ НА КОГНИТИВНОМ КОНФЛИКТУ: СТУДИЈА СЛУЧАЈА

SYAHRIAL SYAHRIAL[1], MASHFUFATUL ILMAH[1], YAHMIN YAHMIN[2], MUNZIL MUNZIL[2] и MUNTHOLIB MUNTHOLIB[2]

[1]*Chemistry Education Program, Postgraduate Program, Universitas Negeri Malang, Indonesia* и [2]*Department of Chemistry, Universitas Negeri Malang, Indonesia*

Истраживања су показала да већина наставника хемије има неке погрешне представе о ковалентном везивању. У оквиру ове студије истражено је да ли техника интервјуа базирана на когнитивном конфликту може да подстакне наставнике да ревидирају те погрешне представе о ковалентном везивању. У истраживању је учествовало осам наставника хемије из различитих школа. За прикупљање података коришћена су два валидирана инструмента, упутство за интервју, технике базиране на когнитивном конфликту и тест с питањима отвореног типа о ковалентном везивању. Резултати су показали да примењени интервју може помоћи испитаницима да превазиђу своје заблуде о ковалентној вези. Пет од осам испитаника направило је концептуалну промену од мисконцепција (заблуда) ка научним појмовима, док је код три испитаника концептуална промена била делимична. Шест концепата који су претходно били извор заблуда елиминисани су и преведени у научне концепте. Од 46 случајева заблуда, 41 случај је преведен у научне концепте. Резултат ове студије служи као почетна перспектива за истраживање ефективности интервјуа базираног на когнитивном конфликту у ширем опсегу.

(Примљено 17. јануара, ревидирано и прихваћено 12. септембра 2022)

REFERENCES

1. H. S. Dhindsa, D. F. Treagust, *Chem. Educ. Res. Pract.* **15** (2014) 435 (https://doi.org/10.1039/C4RP00059E)

2. H. Özmen, *J. Sci. Educ. Technol.* **13** (2004) 147 (https://doi.org/10.1023/B:JOST.0000031255.92943.6d)
3. C. J. Luxford, S. L. Bretz, *J. Chem. Educ.* **91** (2014) 312 (https://doi.org/10.1021/ed400700q)
4. M. Vrabec, M. Prokša, *J. Chem. Educ.* **93** (2016) 1364 (https://doi.org/10.1021/acs.jchemed.5b00953)
5. M. M. Cooper, N. Grove, S. M. Underwood, M. W. Klymkowsky, *J. Chem. Educ.* **87** (2010) 869 (https://doi.org/10.1021/ed900004y)
6. E. Erman, *J. Res. Sci. Teach*. **54** (2017) 520 (https://doi.org/10.1002/tea.21375)
7. M. Kousathana, M. Demerouti, G. Tsaparlis, *Sci. Educ*. **14** (2005) 173 (https://doi.org/10.1007/s11191-005-5719-9)
8. E. J. Marsh, E. D. Eliseev, *Correcting student errors and misconceptions*, The Cambridge Handbook of Cognition and Education, Cambridge, 2019 (https://doi.org/10.1017/9781108235631.018)
9. W. C. Galley, *J. Chem. Educ.* **81** (2004) 523 (https://doi.org/10.1021/ed081p523)
10. D. Cheung, H. Ma, J. Yang, *Int J. Sci. Math. Educ*. **7** (2009) 1111 (https://doi.org/10.1007/s10763-009-9151-5)
11. M. Muntholib, M. Ilmah, Y. Yahmin, *J-PEK* **5** (2020) 108 (https://doi.org/10.17977/um026v5i22020p108)
12. A. Bergqvist, S. N. Chang Rundgren, *Res. Sci. Technol. Educ.* **35** (2017) 215 (https://doi.org/10.1080/02635143.2017.1295934)
13. H. Kang, L. C. Scharmann, S. Kang, T. Noh, *IJESE* **5** (2010) 383
14. R. B. Bucat, in *Chemistry Education: Best Practices, Opportunities and Trends*, J. García-Martínez, E. Serrano-Torregrosa, Eds., Wiley, NewYork, 2015 (https://doi.org/10.1002/9783527679300.ch18)
15. K. S. Taber, *Chem. Educ. Res. Pract.* **14** (2013) 156 (https://doi.org/10.1039/c3rp00012e)
16. E. Akpınar, D. Erol, B. Aydoğdu, *Procedia – Soc. Behav. Sci.* **1** (2009) 2402 (https://doi.org/10.1016/j.sbspro.2009.01.039)
17. Soeharto, B. Csapó, E. Sarimanah, F. I. Dewi, T. Sabri, *J. Pendidik. IPA Indones.* **8** (2019) 247 (https://doi.org/10.15294/jpii.v8i2.18649)
18. D. K. Gurel, A. Eryilmaz, L. C. McDermott, *Eurasia J. Math. Sci. Tech. Ed*. **11** (2015) 989 (https://doi.org/10.12973/eurasia.2015.1369a)
19. K. J. Linenberger, S. L. Bretz, *Chem. Educ. Res. Pract*. **13** (2012) 172 (https://doi.org/10.1039/C1RP90064A)
20. E. A. R. Adhabi, C. B. L. Anozie, *Int. J. Educ.* **9** (2017) 86 (https://doi.org/10.5296/ije.v9i3.11483)
21. U. T. Jankvist, M. Niss, *Educ. Sci.* **8** (2018) 53 (https://doi.org/10.3390/educsci8020053)
22. R. Zazkis, E. J. Chernoff, *Cognitive Conflict and Its Resolution Via Pivotal/Bridging Example*, PME-NA Org. 2, 2006
23. J. W. Creswell, J. D. Creswell, *Research design: qualitative, quantitative, and mixed methods approaches*, SAGE Publications, Los Angeles, CA, 2018 (ISBN 9781506386706)
24. E. Gudyanga, T. Madambi, *Int. J. Sec. Educ.* **2** (2014) 11 (https://doi.org/10.11648/j.ijsedu.20140201.13)
25. D. F. Polit, C. T. Beck, *Res. Nurs. Health* **29** (2006) 489 (https://doi.org/10.1002/nur.20147)
26. M. M. Cooper, S. Sandi-Urena, *J. Chem. Educ.* **86** (2009) 240 (https://doi.org/10.1021/ed086p240)

27. J. Lee, C. Lim, H. Kim, *Educ. Technol. Res. Dev.* **65** (2017) 427 (https://doi.org/10.1007/s11423-016-9502-1)
28. M. R. Lynn, *Nurs. Res.* **35** (1986) 382 (https://doi.org/10.1097/00006199-198611000-00017)
29. M. S. B. Yusoff, *Educ. Med. J.* **11** (2019) 49 (https://doi.org/10.21315/eimj2019.11.2.6)
30. L. L. Davis, *Appl. Nurs. Res.* **5** (1992) 194 (https://doi.org/10.1016/S0897-1897(05)80008-4)
31. J. R. Landis, G. G. Koch, *Biometrics* **33** (1977) 159 (https://doi.org/10.2307/2529310)
32. D. A. Regier, W. E. Narrow, D. E. Clarke, H. C. Kraemer, S. J. Kuramoto, E. A. Kuhl, D. J. Kupfer, *Am. J. Psychiatry* **170** (2013) 59 (https://doi.org/10.1176/appi.ajp.2012.12070999)
33. M. R. Abraham, E. B. Grzybowski, J. W. Renner, E. A. Marek, *J. Res. Sci. Teach*. **29** (1992) 105 (https://doi.org/10.1002/tea.3660290203)
34. J. W. Creswell, *Educational Research: Planning, Conducting, and Evaluating Quantitative and Qualitative Research*, Pearson, Boston, MA, 2012 (ISBN: 9780131367395)
35. P. Kowalski, A. K. Taylor, *Scholarsh. Teach. Learn. Psychol.* **3** (2017) 90 (https://doi.org/10.1037/stl0000082)
36. Effendy, *Ilmu Kimia untuk Siswa SMA dan MA Kelas X*, Indonesian Academic Publishing, Malang, 2016 (ISBN: 978-602-74830-2-6) (in Indonesian)
37. B. Jacka, *J Educ Res.* **78** (1985) 224 (https://doi.org/10.1080/00220671.1985.10885606)
38. A. B. P. Lever, *J. Chem. Educ.* **49** (1972) 819 (https://doi.org/10.1021/ed049p819)
39. A. K. Prodjosantoso, A. M. Hertina, Irwanto, *Int. J. Instr.* **12** (2019) 1477 (https://doi.org/10.29333/iji.2019.1219)
40. G. Nicoll, *Int. J. Sci. Educ.* **23** (2001) 707 (https://doi.org/10.1080/09500690010025012).

Journal of the Serbian Chemical Society
JSCS@tmf.bg.ac.rs • www.shd.org.rs/JSCS
J. Serb. Chem. Soc. 88 (2) S65–S67 (2023) *Supplementary material*

SUPPLEMENTARY MATERIAL TO

Remediation of chemistry teachers' misconceptions about covalent bonding using cognitive conflict interviews: A case study

SYAHRIAL SYAHRIAL[1], MASHFUFATUL ILMAH[1], YAHMIN YAHMIN[2], MUNZIL MUNZIL[2] and MUNTHOLIB MUNTHOLIB[2]*

[1]*Chemistry Education Program, Postgraduate Program, Universitas Negeri Malang, Indonesia and* [2]*Department of Chemistry, Universitas Negeri Malang, Indonesia*

J. Serb. Chem. Soc. 88 (2) (2023) 211–221

AN EXAMPLE OF COGNITIVE CONFLICT INTERVIEW

The misconception: An atom forms a bond to fulfill an octet or duplet structure

	Step	Cognitive conflict interview
1.	Identifying the pre-conception	Exploring and confirming respondent's misconceptions by using questions, for example: In a molecule, atoms form bonds. Why do these atoms form bonds one and another?
2.	Creating cognitive conflicts by providing the experimental facts, anomalies, and contradictions.	• Indicating atom(s) that in their compounds do not obey the octet or duplet rules, for example: • The Lewis structure of BF_3 is as follows: 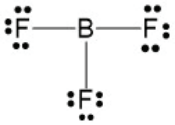 Does the B atom in BF_3 molecule obey the octet or duplet rules? • Showing that the energy level of a molecule in a gaseous state is lower than the energy level of its constituent atoms in the same state, for example: The energy level of 1 mole of CH_4 molecules gas is 1652 kJ lower than the energy level of 1 mole of C atoms and 4 moles of H atoms in the gaseous state.

* Corresponding author. E-mail: muntholib.fmipa@um.ac.id

Step	Cognitive conflict interview
3. Stimulating the equilibration process using the relevant questions	Asking guided questions to assist a respondent in realizing their misconceptions and overcoming those misconceptions, for example: • Consider the Lewis structure of BF_3. Does the B atom in the BF_3 molecule have an octet or duplet configuration? • Do atoms form bonds to obey the octet or duplet rule? • Which has higher stability, 1 C atom and 4 H atoms in the gaseous phase or one CH_4 molecule in the same phase? • Which has a lower energy level, 1 mole of C atoms and 4 moles of H atoms in the gaseous phase or 1 mole of CH_4 molecules in the same phase? • What is the relationship between the energy level of matter and its stability?
4. Confirming the scientific concept	Asking a question to confirm the respondent's understanding, for example: If so, why does an atom bond with the other(s)?

THE CONCEPTUAL UNDERSTANDING TEST OF COVALENT BONDING

Indicator	Problem	Item
Explaining the purpose of atoms forming bonds	An H atom and a Cl atom bond to form the HCl molecule, as shown in the following equation:  Why do these atoms bond? *Answer* : …	1
Determining the type(s) of bond in a molecule	What is the type of the bond formed in question number 1? *Answer* : … *Reason* : …	2
Determining the types of atoms that can form covalent bonds	Consider the following compounds formed through the covalent bonding: CH_4, PCl_5, $BeCl_2$, $B(CH_3)_3$, and CO_2. Based on these examples, what types of atoms form covalent bonds? *Answer* : … *Reason* : …	3
Distinguishing between a covalent bonding and a coordinate covalent bonding	H_2O compounds can be formed in the reaction between H^+ and OH^- ions as follows: 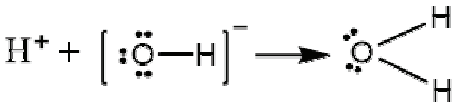 How many kinds of O-H bonds are there in the water molecule produced by the above reaction? Mention! *Answer* : … *Reason* : …	4
Estimating the polarity of a covalent bonding in a molecule	Predict the polarity of the covalent bonds in molecules of CCl_4, PCl_3, PBr_5, F_2, H_2, and SeF_6! *Answer* : … *Reason* : …	5
Ordering the degree of polarity of the covalent bonds in the molecules	Order the polarity of the covalent bonds of HF, HCl, and HBr molecules from the largest to the smallest! *Answer* : … *Reason* : …	6

Indicator	Problem	Item
Describing the Lewis structure of a molecule	Write down the Lewis structures of SF_2 and SF_4? *Answer* : …	7
	What is the formal charge of the atoms in question number 7? *Answer* : …	8
	Write down the Lewis structures of NO_2^- and NO_2 along with the formal charge of each atom! *Answer* : …	9
	Why is the formal charge on the atom N of one of the species in the problem No.9 not equal to zero? *Answer* : …	10
Determining the stability of a molecule or polyatomic ion based on their formal charge	Both carbon dioxide, CO_2, and azide ion, N_3^-, species have the same number of electrons, which is 22 electrons. The Lewis structure of both species is as follows: 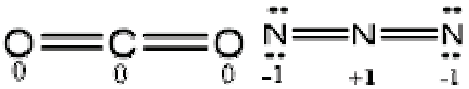 What is the stability of both species based on their formal charge? *Answer* : … *Reason* : …	11
Distinguishing between atoms that must obey the octet rule and those that do not need to obey the octet rule in the molecule	What atoms can have eight electrons or less in their valence shell, when acting as the central atom? Give an example! *Answer* : …	12
	What atoms tend to obey the octet rule when acting as the central atom? Give an example! *Answer* : …	13
	In which period atoms tend to have a formal charge of zero or can have more than eight electrons in their valence shell when acting as the central atom? Give an example! *Answer* : …	14
Ordering the covalent bonding lengths of several molecules	Draw the Lewis structure of ethane, ethene, and ethyne! *Answer* : …	15
	What is the bond order between the C atoms in ethane, ethene, and ethyne! *Answer* : … *Reason* : …	16
	Order the length of the covalent bonds between the C atoms in ethane, ethene, and ethyne molecules from the longest to the shortest! *Answer* : … *Reason* : …	17
	Order the length of the covalent bonds in the HF, HCl, and HBr molecules from the longest to the shortest! *Answer* : … *Reason* : …	18